

**Aims and Scope:** The "Cell Journal (Yakhteh)" is a peer review and monthly English publication of Royan Institute of Iran. The aim of the journal is to disseminate information through publishing the most recent scientific research studies on exclusively Cellular, Molecular and other related topics. **Cell J**, has been certified by the Ministry of Culture and Islamic Guidance since 1999 and also accredited as a scientific and research journal by HBI (Health and Biomedical Information) Journal Accreditation Commission since 2000 which is an open access journal. **This journal holds the membership of the Committee on Publication Ethics (COPE).**

### 1. Types of articles

The articles in the field of Cellular and Molecular can be considered for publications in **Cell J**. These articles are as below:

#### A. Original articles

Original articles are scientific reports of the original research studies. The article consists of English Abstract (structured), Introduction, Materials and Methods, Results, Discussion, Conclusion, Acknowledgements, Author's Contributions, and References (**Up to 40**).

#### B. Review articles

Review articles are the articles written by well experienced authors and those who have excellence in the related fields. The corresponding author of the review article must be one of the authors of at least three published articles appearing in the references. The review article consists of English Abstract (unstructured), Introduction, Conclusion, Author's Contributions, and References (**Up to 70**).

#### C. Systematic Reviews

Systematic reviews are a type of literature review that collect and critically analyzes multiple research studies or papers. The Systematic reviews consist of English Abstract (unstructured), Introduction, Materials and Methods, Results, Discussion, Conclusion, Acknowledgements, Author's Contributions, and References (**Up to 70**).

#### D. Short communications

Short communications are articles containing new findings. Submissions should be brief reports of ongoing researches. The short communication consists of English Abstract (unstructured), the body of the manuscript (should not hold heading or sub-heading), Acknowledgements, Author's Contributions, and References (**Up to 30**).

#### E. Case reports

Case reports are short discussions of a case or case series with unique features not previously described which make an important teaching point or scientific observation. They may describe novel techniques or use equipment, or new information on diseases of importance. It consists of English Abstracts (Unstructured), Introduction, Case Report, Discussion, Acknowledgements, Author's Contributions, and References (**Up to 30**).

#### F. Editorial

Editorials are articles should be written in relevant and new data of journals' filed by either the editor in chief or the editorial board.

#### G. Imaging in biology

Images in biology should focus on a single case with an interesting illustration such as a photograph, histological specimen or investigation. Color images are welcomed. The text should be brief and informative.

#### H. Letter to the editors

Letter to editors are welcome in response to previously published **Cell J** articles, and may also include interesting cases that do not meet the requirement of being truly exceptional, as well as other brief technical or clinical notes of general interest.

#### I. Debate

Debates are articles which show a discussion of the positive and negative view of the author concerning all aspect of the issue relevant to scientific research.

### 2. Submission process

It is recommended to see the guidelines for reporting different kinds of manuscripts here. This guide explains how to prepare

the manuscript for submission. Before submitting, we suggest authors to familiarize themselves with **Cell J** format and content by reading the journal via the website ([www.celljournal.com](http://www.celljournal.com)). The corresponding author ensures that all authors are included in the author list and agree with its order, and they must be aware of the manuscript submission.

### A. Author contributions statements

It is essential for authors to include a statement of responsibility in the manuscript that specifies the contribution of every one of them. This participation must include conception and design of the manuscript, data acquisition or data analysis and interpretation, drafting of the manuscript and/or revising it for critically important intellectual content, revision and final approval of the manuscript and statistical analysis, obtaining funding, administrative, technical, or material support, or supervision. Authors who do not meet the above criteria should be acknowledged in the **Acknowledgments section**.

### B. Cover letter and copyright

Each manuscript should be accompanied by a cover letter, signed by all authors specifying the following statement: "The manuscript has been seen and approved by all authors and is not under active consideration for publication. It has neither been accepted for publication nor published in another journal fully or partially (except in abstract form). Also, no manuscript would be accepted in case it has been pre-printed or submitted to other websites. I hereby assign the copyright of the enclosed manuscript to **Cell J**." Corresponding author must confirm the proof of the manuscript before online publishing. Also, it is needed to suggest three peer reviewers in the field of their manuscript.

### C. Manuscript preparation

Authors whose first language is not English encouraged to consult a native English speaker in order to confirm his manuscripts to American or British (not a mixture) English usage and grammar. It is necessary to mention that we will check the plagiarism of your manuscript by iThenticate Software. The manuscript should be prepared in accordance with the "International Committee of Medical Journal Editors (ICMJE)". Please send your manuscript in two formats word and PDF (including: title, name of all the authors with their degree, abstract, full text, references, tables and figures) and also send tables and figures separately in the site. The abstract and text pages should have consecutive line numbers in the left margin beginning with the title page and continuing through the last page of the written text. Each abbreviation must be defined in the abstract and text when they are mentioned for the first time. Avoid using abbreviation in the title. Please use the international and standard abbreviations and symbols

It should be added that an essential step toward the integration and linking of scientific information reported in published literature is using standardized nomenclature in all fields of science and medicine. Species names must be italicized (*e.g.*, *Homo sapiens*) and also the full genus and species written out in full, both in the title of the manuscript and at the first mention of an organism in a paper.

It is necessary to mention that genes, mutations, genotypes, and alleles must be indicated in italics. Please use the recommended name by consulting the appropriate genetic nomenclature database, *e.g.*, HUGO for human genes. In another words; if it is a human gene, you must write all the letters in capital and italic (*e.g.*, *OCT4*, *c-MYC*). If not, only write the first letter in capital and italic (*e.g.*, *Oct4*, *c-Myc*). **In addition, protein designations are the same as the gene symbol but are not italicized.**

**Of note, Cell J** will only consider publishing genetic association study papers that are novel and statistically robust. Authors are advised to adhere to the recommendations outlined in the STREGA statement (<http://www.strega-statement.org>). The following criteria must be met for all submissions:

1. Hardy-Weinberg Equilibrium (HWE) calculations must be carried out and reported along with the P-values if applicable [see Namipashaki et al. 2015 (Cell J, Vol 17, N 2, Pages: 187-192) for a discussion].
2. Linkage disequilibrium (LD) structure between SNPs (if multiple SNPs are reported) must be presented.
3. Appropriate multiple testing correction (if multiple independent SNPs are reported) must be included.

Submissions that fail to meet the above criteria will be rejected before being sent out for review.

Each of the following manuscript components should begin in the following sequence:

**Authors' names** and order of them must be carefully considered (full name(s), highest awarded academic degree(s), email(s), and institutional affiliation(s) of all the authors in English. Also, you must send mobile number and full postal address of the corresponding author).

**Changes to Authorship** such as addition, deletion or rearrangement of author names must be made only before the manuscript has been accepted in the case of approving by the journal editor. In this case, the corresponding author must explain the reason of changing and confirm them (which has been signed by all authors of the manuscript). If the manuscript has already been published in an online issue, an erratum is needed.

**Title** is providing the full title of the research (do not use abbreviations in title).

**Running title** is providing a maximum of 7 words (no more than 50 characters).

**Abstract** must include Objective, Materials and Methods, Results, and Conclusion (no more than 300 words).

**Keywords**, three to five, must be supplied by the authors at the foot of the abstract chosen from the Medical Subject Heading (MeSH). Therefore; they must be specific and relevant to the paper.

The following components should be identified after the abstract:

**Introduction:** The Introduction should provide a brief background to the subject of the paper, explain the importance of the study, and state a precise study question or purpose.

**Materials and Methods:** It includes the exact methods or observations of experiments. If an apparatus is used, its manufacturer's name and address should be stipulated in parenthesis. If the method is established, give reference but if the method is new, give enough information so that another author can perform it. If a drug is used, its generic name, dose, and route of administration must be given. Standard units of measurements and chemical symbols of elements do not need to be defined.

**Statistical analysis:** Type of study and statistical methods should be mentioned and specified by any general computer program used.

**Ethical considerations:** Please state that informed consent was obtained from all human adult participants and from the parents or legal guardians of minors and include the name of the appropriate institutional review board that approved the project. It is necessary to indicate in the text that the maintenance and care of experimental animals complies with National Institutes of Health guidelines for the humane use of laboratory animals, or those of your Institute or agency.

**Clinical trial registration:** All of the Clinical Trials performing in Iran must be registered in Iranian Registry of Clinical Trials ([www.irct.ir](http://www.irct.ir)). The clinical trials performed abroad, could be considered for publication if they register in a registration site approved by WHO or [www.clinicaltrials.gov](http://www.clinicaltrials.gov). If you are reporting phase II or phase III randomized controlled trials, you must refer to the CONSORT Statement for recommendations to facilitate the complete and transparent reporting of trial findings. Reports that do not conform to the CONSORT guidelines may need to be revised before peer-reviewing.

**Results:** They must be presented in the form of text, tables, and figures. Take care that the text does not repeat data that are presented in tables and/or figures. Only emphasize and summarize the essential features of the main results. Tables and figures must be numbered consecutively as appeared in the text and should be organized in separate pages at the end of the manuscript while their location should be mentioned in the main text.

**Tables and figures:** If the result of your manuscript is too short, it is better to use the text instead of tables & figures. Tables should have a short descriptive heading above them and also any footnotes. Figure's legend should contain a brief title for the whole figure and continue with a short explanation of each part and also the symbols used (no more than 100 words). All figures must be prepared based on cell journal's guideline in color (no more than 6 Figures and Tables) and also in GIF or JPEG format.

**Of Note: Please put the tables & figures of the result in the results section not any other section of the manuscript.**

**Supplementary materials** would be published on the online version of the journal. This material is important to the understanding and interpretation of the report and should not repeat material within the print article. The amount of supplementary material should be limited. Supplementary material should be original and not previously published and will undergo editorial and peer review with the main manuscript. Also, they must be cited in the manuscript text in parentheses, in a similar way as when citing a figure or a table. Provide a legend for each supplementary material submitted.

**Discussion:** It should emphasize the present findings and the variations or similarities with other researches done by other researchers. The detailed results should not be repeated in the discussion again. It must emphasize the new and important aspects of the study.

**Conclusion:** It emphasizes the new and important aspects of the study. All conclusions are justified by the results of the study.

**Acknowledgements:** This part includes a statement thanking those who contributed substantially with work relevant to the study but does not have authorship criteria. It includes those who provided technical help, writing assistance and name of departments that provided only general support. You must mention financial support in the study. Otherwise; write this sentence "There is no financial support in this study".

**Conflict of interest:** Any conflict of interest (financial or otherwise) and sources of financial support must be listed in the Acknowledgements. It includes providers of supplies and services from a commercial organization. Any commercial affiliation must be disclosed, regardless of providing the funding or not.

**References:** The references must be written based on the Vancouver style. Thus the references are cited numerically in the text and listed in the bibliography by the order of their appearance. The titles of journals must be abbreviated according to the style

used in the list of Journals Indexed in PubMed. Write surname and initials of all authors when there are six or less. In the case of seven or more authors, the names of the first six authors followed by "et al." must be listed. You can download Endnote file for Journal references style: endnote file

The reference of information must be based on the following order:

**Article:**

Surname(s) and first letter of name & middle name(s) of author(s) .Manuscript title. Journal title (abbr).publication date (year); Volume & Issue: Page number.

Example: Manicardi GC, Bianchi PG, Pantano S, Azzoni P, Bizzaro D, Bianchi U, et al. Presence of endogenous nicks in DNA of ejaculated human spermatozoa and its relationship to chromomycin A3 accessibility. Biol Reprod. 1995; 52(4): 864-867.

**Book:**

Surname(s) and first letter of name & middle name(s) of author(s).Book title. Edition. Publication place: publisher name; publication date (year); Page number.

Example: Edelman CL, Mandle CL. Health promotion throughout the lifespan. 2nd ed. ST Louis: Mosby; 1998; 145-163.

**Chapter of book:**

Surname(s) and first letter of name & middle name(s) of author(s).Chapter title. In: Surname(s) and first letter of name & middle name(s) of editor(s), editors. Book title. Edition. Publication place: publisher name; publication date (year); Page number.

Example: Phillips SJ, Whisnant JP. Hypertension and stroke. In: Laragh JH, Brenner BM, editors. Hypertension: pathophysiology, diagnosis, and management. 2nd ed. New York: Raven Press; 1995; 465-478.

**Abstract book:**

Example: Amini rad O.The antioxidant effect of pomegranate juice on sperm parameters and fertility potential in mice. Cell J. 2008;10 Suppl 1:38.

**Thesis:**

Name of author. Thesis title. Degree. City name. University. Publication date (year).

Example: Eftekhari Yazdi P. Comparison of fragment removal and co-culture with Vero cell monolayers on development of human fragmented embryos. Presented for the Ph.D., Tehran. Tarbiyat Modarres University. 2004.

**Internet references**

**Article:**

Example: Jahanshahi A, Mirnajafi-Zadeh J, Javan M, Mohammad-Zadeh M, Rohani M. Effect of low-frequency stimulation on adenosineA1 and A2A receptors gene expression in dentate gyrus of perforant path kindled rats. Cell J. 2008; 10 (2): 87-92. Available from: <http://www.celljournal.org>. (20 Oct 2008).

**Book:**

Example: Anderson SC, Poulsen KB. Anderson's electronic atlas of hematology.[CD-ROM]. Philadelphia: Lippincott Williams & Wilkins; 2002.

**D. Proofs** are sent by email as PDF files and should be checked and returned within 72 hours of receipt. It is the authors' responsibility to check that all the text and data as contained in the page proofs are correct and suitable for publication. **We are requested to pay particular attention to author's names and affiliations as it is essential that these details be accurate when the article is published.**

**E. Pay for publication:** Publishing an article in Cell J requires Article Processing Charges (APC) that will be billed to the submitting author following the acceptance of an article for publication. For more information please see [www.celljournal.org](http://www.celljournal.org).

**F. Ethics of scientific publication:** Manuscripts that have been published elsewhere with the same intellectual material will refer to duplicate publication. If authors have used their own previously published work or work that is currently under review, as the basis for a submitted manuscript, they are required to cite the previous work and indicate how their submitted manuscript offers novel contributions beyond those of the previous work. Research and publication misconduct is considered a serious breach of ethics.

The Journal systematically employs iThenticate, plagiarism detection and prevention software designed to ensure the originality of written work before publication. Plagiarism of text from a previously published manuscript by the same or

another author is a serious publication offence. Some parts of text may be used, only where the source of the quoted material is clearly acknowledged.

### 3. General information

**A.** You can send your manuscript via online submission system which is available on our website. If the manuscript is not prepared according to the format of **Cell J**, it will be returned to authors.

**B.** The order of article appearance in the Journal is not demonstrating the scientific characters of the authors.

**C.** **Cell J** has authority to accept or reject the manuscript.

**D.** The received manuscript will be evaluated by associate editor. **Cell J** uses a single-blind peer review system and if the manuscript suits the journal criteria, we select the reviewers. If three reviewers pass their judgments on the manuscript, it will be presented to the editorial board of **Cell J**. If the editorial board has a positive judgment about the manuscript, reviewers' comments will be presented to the corresponding author (the identification of the reviewers will not be revealed). The executive member of journal will contact the corresponding author directly within 3-4 weeks by email. If authors do not receive any reply from journal office after the specified time, they can contact journal office. Finally, executive manager will respond promptly to authors' request.

### The Final Checklist

The authors must ensure that before submitting the manuscript for publication, they have to consider the following parts:

1. Title page should contain title, name of the author/coauthors, their academic qualifications, designation & institutions they are affiliated with, mailing address for future correspondence, email address, phone, and fax number.
2. Text of manuscript and References prepared as stated in the "guide for authors" section.
3. Tables should be on a separate page. Figures must be sent in color and also in JPEG (Jpg) format.
4. Cover Letter should be uploaded with the signature of all authors.
5. An ethical committee letter should be inserted at the end of the cover letter.

*The Editor-in-Chief: Ahmad Hosseini, Ph.D.*

*Cell Journal* (Yakhteh)

*P.O. Box: 16635-148, Iran*

*Tel/Fax: + 98-21-22510895*

*Emails: [Celljournal@royaninstitute.org](mailto:Celljournal@royaninstitute.org)*

*[info@celljournal.org](mailto:info@celljournal.org)*





## IN THE NAME OF GOD

### Gone But not Forgotten

In the memory of the late Director of Royan Institute, Founder of Stem Cells Research in Iran and Chairman of *Cell Journal* (Yakhteh). May he rest in peace.

**Dr. Saeed Kazemi Ashtiani**

### OWNED:

Royan Institute, Iranian Academic Center for Education Culture and Research (ACECR)

### CHAIRMAN:

Hamid Gourabi, Ph.D., (Professor, Royan Institute, Tehran, Iran)

### EDITOR IN CHIEF:

Ahmad Hosseini, Ph.D., (Professor, Shahid Beheshti Medical University, Tehran, Iran)

### EDITOR ASSOCIATE:

Saeid Abroun, Ph.D., (Associate Professor, Tarbiat Modares University, Tehran, Iran)

### EDITORIAL BOARD:

Saeid Abroun, Ph.D., (Associate Professor, Tarbiat Modares University, Tehran, Iran)  
Kamran Alimoghadam, M.D., (Associate Professor, Tehran Medical University, Tehran, Iran)  
Alireza Asgari, Ph.D., (Professor, Baghyatallah University, Tehran, Iran)  
Mohammad Kazem Aghaee Mazaheri, D.D.S., (Assistant Professor, ACECR, Tehran, Iran)  
Gila Behzadi, Ph.D., (Professor, Shahid Beheshti Medical University, Tehran, Iran)  
Hossein Baharvand, Ph.D., (Professor, Royan Institute, Tehran, Iran)  
Mary Familiari, Ph.D., (Senior Lecturer, University of Melbourne, Melbourne, Australia)  
Hamid Gourabi, Ph.D., (Professor, Royan Institute, Tehran, Iran)  
Jurgen Hescheler, M.D., (Professor, Institute of Neurophysiology of University Zu Koln, Germany)  
Ghasem Hosseini Salekdeh, Ph.D., (Assistant Professor, Agricultural Biotechnology Research Institute, Karaj, Iran)  
Esmail Jabbari, Ph.D., (Associate Professor, University of South Carolina, Columbia, USA)  
Suresh Jesuthasan, Ph.D., (Associate Professor, National University of Singapore, Singapore)  
Bahram Kazemi, Ph.D., (Professor, Shahid Beheshti Medical University, Tehran, Iran)  
Saadi Khochbin, Ph.D., (Professor, Inserm/Grenoble University, France)  
Ali Khademhosseini, Ph.D., (Associate Professor, Harvard Medical School, USA)  
Kun Ping Lu, M.D., Ph.D., (Professor, Harvard Medical School, Boston, USA)  
Navid Manuchehrabadi, Ph.D., (Angio Dynamics, Marlborough, USA)  
Hosseinali Mehrani, Ph.D., (Professor, Baghyatallah University, Tehran, Iran)  
Marcos Meseguer, Ph.D., (Clinical Embryology Laboratory IVI Valencia, Valencia, Spain)  
Seyed Javad Mowla, Ph.D., (Professor, Tarbiat Modares University, Tehran, Iran)  
Mohammad Hossein Nasr Esfahani, Ph.D., (Professor, Royan Institute, Tehran, Iran)  
Toru Nakano, M.D., Ph.D., (Professor, Osaka University, Osaka, Japan)  
Donald Newgreen, Ph.D., (Professor, Murdoch Children Research Institute, Melbourne, Australia)  
Mojtaba Rezazadeh Valojerdi, Ph.D., (Professor, Tarbiat Modares University, Tehran, Iran)  
Mohammad Hossein Sanati, Ph.D., (Associate Professor, National Institute for Genetic Engineering and Biotechnology, Tehran, Iran)  
Eimei Sato, Ph.D., (Professor, Tohoku University, Sendai, Japan)  
Andreas Serra, M.D., (Professor, University of Zurich, Zurich, Switzerland)  
Abdolhossein Shahverdi, Ph.D., (Professor, Royan Institute, Tehran, Iran)  
Michele Catherine Studer, Ph.D., (Institute of Biology Valrose, IBV University of Nice Sophia-Antipolis, France)  
Peter Timashev, Ph.D., (Sechenov University, Moscow, Russia)  
Daniela Toniolo, Ph.D., (Head, Unit of Common Disorders, San Raffaele Research Institute, Milano, Italy)  
Christian van den Bos, Ph.D., Managing Director MARES Ltd, Greven, Germany  
Catherine Verfaillie, Ph.D., (Professor, Katholie Universiteit Leuven, Leuven, Belgium)  
Gianpaolo Zerbin, M.D., Ph.D., (San Raffaele Scientific Institute, Italy)  
Shubing Zhang, Ph.D., (Associate Professor, Central South University, China)  
Daniele Zink, Ph.D., (Institute of Bioengineering and Nanotechnology, Agency for Science Technology & Science, Singapore)

**EXECUTIVE MANAGER:**

Farideh Malekzadeh, M.Sc., (Royan Institute, Tehran, Iran)

**EXECUTIVE BOARD:**

Parvaneh Afsharian, Ph.D., (Royan Institute, Tehran, Iran)  
Reza Azimi, B.Sc., (Royan Institute, Tehran, Iran)  
Reza Omani-Samani, M.D., (Royan Institute, Tehran, Iran)  
Elham Amirchaghmaghi, M.D., Ph.D., (Royan Institute, Tehran, Iran)  
Leila Daliri, M.Sc., (Royan Institute, Tehran, Iran)  
Mahdi Lottfipannah, M.Sc., (Royan Institute, Tehran, Iran)

**ENGLISH EDITOR:**

Saman Eghtesad, Ph.D., (Royan Institute, Tehran, Iran)  
Vahid Ezzatizadeh, Ph.D., (Royan Institute, Tehran, Iran)  
Jane Elizabeth Ferrie, Ph.D., (University College of London, London, UK)  
Ramin Rezaee, Pharm.D., Ph.D., (Mashhad University of Medical Sciences, Mashhad, Iran)  
Kim Vagharfard, M.Sc., (Royan Institute, Tehran, Iran)

**GRAPHICS:**

Laleh Mirza Ali Shirvani, B.Sc., (Royan Institute, Tehran, Iran)

**PUBLISHED & SPONSORED BY:**

Publication of Royan Institute (ACECR)

**Indexed in:**

1. Thomson Reuters (ISI)
3. PubMed Central (PMC)
4. National Library Medicine (NLM)
5. Biosis Preview
6. Index Medicus for the Eastern Mediterranean Region (IMEMR)
7. Regional Information Center for Sciences and Technology (RiCeST)
8. Index Copernicus International
9. Cambridge Scientific Abstract (CSA)
10. EMBASE
11. Scopus
12. Cinahl Database
13. Google Scholar
14. Chemical Abstract Service (CAS)
15. Proquest
16. Directory of Open Access Journals (DOAJ)
17. Open Academic Journals Index (OAJI)
18. Directory of Research Journals Indexing (DRJI)
19. Scientific Information Database (SID)
20. Iranmedex
21. Islamic World Science Citation Center (ISC)
22. Magiran
23. Science Library Index
24. Biological Abstracts
25. Essential Science Indicators
26. EuroPub

**ACECR****Copyright and license information:**

The **Cell Journal** <sup>(Yakhteh)</sup> is an open access journal which means the articles are freely available online for any individual author to download and use the providing address. The journal is licensed under a Creative Commons Attribution-Non Commercial 3.0 Unported License which allows the author(s) to hold the copyright without restrictions that is permitting unrestricted use, distribution, and reproduction in any medium provided the original work is properly cited.

**Editorial Office Address (Dr. Ahmad Hosseini):**

Royan Institute, P.O.Box: 16635-148,  
Tehran, Iran  
Tel & Fax: (+9821)22510895  
Website: [www.celljournal.org](http://www.celljournal.org)  
Emails: [info@celljournal.org](mailto:info@celljournal.org)  
[celljournal@royaninstitute.org](mailto:celljournal@royaninstitute.org)

**Printing Company:**

Naghsh e Johar Co.  
No. 103, Fajr alley, Tehranpars Street,  
Tehran, Iran.



CONTENTS

Original Articles

- **An Integrative Analysis of The Micro-RNAs Contributing in Stemness, Metastasis and B-Raf Pathways in Malignant Melanoma and Melanoma Stem Cell**  
 Parisa Sahranavardfard, Zahra Madjd, Amirnader Emami Razavi, Alireza Ghanadan, Javad Firouzi, Pardis Khosravani, Saeid Ghavami, Esmacel Ebrahimie, Marzieh Ebrahimi ..... 261
- **A Novel Insight into Endothelial and Cardiac Cells Phenotype in Systemic Sclerosis Using Patient-Derived Induced Pluripotent Stem Cell**  
 Sedigheh Gholami, Zahra Mazidi, Sara Pahlavan, Fariba Moslem, Mahya Hosseini, Adeleh Taei, Mahdi Hesaraki, Maryam Barekat, Nasser Aghdami, Hossein Baharvand ..... 273
- **Isolation and Differentiation of Adipose-Derived Stem Cells into Odontoblast-Like Cells: A Preliminary *In Vitro* Study**  
 Saber Khazaei, Abbasali Khademi, Mohammad Hossein Nasr Esfahani, Mozafar Khazaei, Mohammad Hossein Nekoofar, Paul M. H. Dummer ..... 288
- **Mir-106b Cluster Regulates Primordial Germ Cells Differentiation from Human Mesenchymal Stem Cells**  
 Sadaf Mahboudi, Kazem Parivar, Zohreh Mazaheri, Shiva Irani ..... 294
- **Neuroprotective Effects of Normobaric Hyperoxia and Transplantation of Encapsulated Choroid Plexus Epithelial Cells on The Focal Brain Ischemia**  
 Maesumeh Eslami, Shahrbanoo Oryan, Mehdi Rahnema, Mohammad Reza Bigdeli ..... 303
- **Association between rs11614913 Polymorphism of The *MiR-196-a2* Gene and Colorectal Cancer in The Presence of Departure from Hardy-Weinberg Equilibrium**  
 Ali Reza Soltanian, Bistoon Hosseini, Hossein Mahjub, Fatemeh Bahreini, Ehsan Nazemalhosseini Mojarad, Mohammad Ebrahim Ghaffari ..... 313
- **Astaxanthin Protects Human Granulosa Cells against Oxidative Stress through Activation of NRF2/ARE Pathway and Its Downstream Phase II Enzymes**  
 Mojtaba Eslami, Sahar Esfandyari, Marzieh Aghahosseini, Zahra Rashidi, Shirzad Hosseinishental, Samane Brenjian, Aligholi Sobhani, Fardin Amidi ..... 319
- **MiR-221 Expression Level Correlates with Insulin-Induced Doxorubicin Resistance in MCF-7 Breast Cancer Cells**  
 Parisa Kheradmand, Sadeq Vallian Boroogeni, Saeed Esmaeili-Mahani ..... 329
- **The Effect of Contrast Enhanced Abdominopelvic Magnetic Resonance Imaging on Expression and Methylation Level of *ATM* and *AKT* Genes**  
 Amir Hossein Jalali, Hossein Mozdarani, Hossein Ghanaati ..... 335
- **MicroRNA and Hemophilia-A Disease: Bioinformatics Prediction and Experimental Analysis**  
 Halimeh Rezaei, Majid Motovali-Bashi, Seyed Javad Mowla ..... 341
- **Spermatozoa Induce Maternal Mononuclear Cells for Production of Antibody with Cytotoxic Activity on Paternal Blood Mononuclear Cells**  
 Nasrin Sereshki, Alireza Andalib, Mohadeseh Toghiani, Hossein Motedayyen, Mohammad Sadegh Hesamian, Abbas Rezaei, David Wilkinson ..... 349
- **Neuroprotective Effects of Isoquercetin: An *In Vitro* and *In Vivo* Study**  
 Qingxiao Yang, Zhichen Kang, Jingze Zhang, Fuling Qu, Bin Song ..... 355
- **Correction** ..... 366
- **Front page of Cell Journal<sup>(Yakhteh)</sup>: Figure 1A, B, Page: 298**

# An Integrative Analysis of The Micro-RNAs Contributing in Stemness, Metastasis and B-Raf Pathways in Malignant Melanoma and Melanoma Stem Cell

Parisa Sahranavardfard, Ph.D.<sup>1</sup>, Zahra Madjd, M.D., Ph.D.<sup>2</sup>, Amirnader Emami Razavi, M.D.<sup>3</sup>, Alireza Ghanadan, M.D.<sup>3,4</sup>, Javad Firouzi, M.Sc.<sup>1</sup>, Pardis Khosravani, M.Sc.<sup>1</sup>, Saeid Ghavami, Ph.D.<sup>5,6,7,8\*</sup>, Esmail Ebrahimie, Ph.D.<sup>9,10\*</sup>, Marzieh Ebrahimi, Ph.D.<sup>1\*</sup>

1. Department of Stem Cells and Developmental Biology, Cell Science Research Center, Royan Institute for Stem Cell Biology and Technology, ACECR, Tehran, Iran
2. Department of Pathology, Iran University of Medical Sciences, Tehran, Iran
3. Iran National Tumor Bank, Cancer Institute of Iran, Tehran University of Medical Sciences, Tehran, Iran
4. Department of Dermatopathology, Razi Skin Hospital, Tehran University of Medical Sciences, Tehran, Iran
5. Department of Human Anatomy and Cell Sciences, University of Manitoba, Manitoba, Canada
6. Biology of Breathing, Children Hospital Research Institute of Manitoba, University of Manitoba, Winnipeg, Canada
7. Autophagy Research Center, Shiraz University of Medical Sciences, Shiraz, Iran
8. Research Institute in Oncology and Hematology, Cancer Care Manitoba, University of Manitoba, Winnipeg, Canada
9. School of Animal and Veterinary Sciences, The University of Adelaide, Adelaide, Australia
10. Genomics Research Platform, School of Life Sciences, College of Science, Health and Engineering, La Trobe University, Melbourne, Australia

\*Corresponding Addresses: Department of Human Anatomy and Cell Sciences, University of Manitoba, Manitoba, Canada  
School of Animal and Veterinary Sciences, The University of Adelaide, Adelaide, Australia  
Department of Stem Cells and Developmental Biology, Cell Science Research Center, Royan Institute for Stem Cell Biology and Technology, ACECR, Tehran, Iran  
Emails: saeid.ghavami@umanitoba.ca, esmaeil.ebrahimie@adelaide.edu.au, mebrahimi@royaninstitute.org

Received: 08/December/2019, Accepted: 14/April/2020

## Abstract

**Objective:** Epithelial-mesenchymal transition (EMT) and the stemness potency in association with *BRAF* mutation are indispensable to the progression of melanoma. Recently, microRNAs (miRNAs) have been introduced as the regulator of a multitude of oncogenic functions in most of tumors. Therefore identifying and interpreting the expression patterns of these miRNAs is essential. The present study sought to find common miRNAs regulating all three important pathways in melanoma development.

**Materials and Methods:** In this experimental study, 18 miRNAs that importantly contribute to EMT and have a role in regulating self-renewal and the *BRAF* pathway were selected based on current literature and cross-analysis with available databases. Subsequently, their expression patterns were evaluated in 20 melanoma patients, normal tissues, serum from patients and control subjects, and melanospheres. Pattern discovery and integrative regulatory network analysis were used to find the most important miRNAs in melanoma progression.

**Results:** Among 18 selected miRNAs, miR-205, -141, -203, -15b, and -9 were differentially expressed in tumor samples than normal tissues. Among them, miR-205, -15b, and -9 significantly expressed in serum samples and healthy donors. Attribute Weighting and decision trees (DT) analysis presented evidence that the combination of miR-205, -203, -9, and -15b can regulate self-renewal and EMT process, by affecting *CDH1*, *CCND1*, and *VEGF* expression.

**Conclusion:** We suggested here that miR-205, -15b, -203, -9 pattern as the key miRNAs linked to melanoma status, the pluripotency, proliferation, and motility of malignant cells. However, further investigations are required to find the mechanisms underlying the combinatory effects of the above mentioned miRNAs.

**Keywords:** Epithelial-Mesenchymal Transition, Melanoma, MicroRNA, Network Analysis

Cell Journal (Yakhteh), Vol 23, No 3, August 2021, Pages: 261-272

**Citation:** Sahranavardfard P, Madjd Z, Emami Razavi AN, Ghanadan AR, Firouzi J, Khosravani P, Ghavami S, Ebrahimie E, Ebrahimi M. An integrative analysis of the micro-RNAs contributing in stemness, metastasis and B-Raf pathways in malignant melanoma and melanoma stem cell. Cell J. 2021; 23(3): 261-272. doi: 10.22074/cellj.2021.7311.

This open-access article has been published under the terms of the Creative Commons Attribution Non-Commercial 3.0 (CC BY-NC 3.0).

## Introduction

Epithelial to mesenchymal transition (EMT) is that major mechanism involved in increasing the mortality and morbidity of malignancies including melanoma (1). The induction of EMT requires key transcription factors, including snail family transcriptional repressor (SNAIL), zinc finger E-box binding homeobox (ZEB), and twist family bHLH transcription factor (TWIST), that promote

epithelial cell reprogramming to repress expression of adhesion molecules, particularly E-cadherin, to initiate migration and invasion (2). The association between the EMT process and stem cell properties in cancer cells has been reported in various tumor cells (3). Studies on malignant tumors, such as melanoma, have reported the involvement of cancer stem cells (CSCs) in tumor initiation, drug resistance, metastasis, and their possible

role in cancer recurrence (4). Moreover, based on genome-wide analyses, the mutation in the 600<sup>th</sup> codon of the *BRAF* gene which is the substitution of glutamic acid for valine, is present in about 52% of patients with melanoma and in nearly 15% of all human cancers (5). *BRAF* encodes a protein belonging to the mitogen-activated protein kinases (MAPK) pathway (6), which mediates a significant role in the regulation of cell division, cell differentiation, and drug resistance (7). On the other hand, through cross talk with the PI3K signaling pathway, the oncogenic *BRAF* induces EMT and facilitates cell invasion and metastasis (8) and contributing in self renewal potency of melanoma stem cells (9). Therefore these three key pathways; EMT, stemness and *BRAF* play important role in melanoma progression and targeting them has been proposed as the main strategy for successful treatment of melanoma (10).

miRNAs are an evolutionarily conserved group of small regulatory noncoding RNAs with an approximate length of 22 nucleotides (11). They regulate gene expression by promoting target degradation or translational repression not only during normal development, but also under condition of various diseases, such as cancers (12). Each miRNA can regulate several mRNAs expression. Therefore, miRNAs play key roles in the development of several cancer-related hallmarks (13) and could be considered as prognostic and diagnostic marker, tumorigenicity inducer, migration and even invasion regulator (14), in most of cancers including melanoma.

Based on various investigations on the regulatory role of miRNAs in melanoma, this study was designed to find miRNAs that can simultaneously target multiple processes, which involved in melanoma progression including EMT, stemness, and *BRAF* pathway. To this end, we used a combination of experimental and computational methods to illustrate the miRNAs and their effect in regulating melanoma progression.

## Materials and Methods

### Clinical specimens and human ethics

The present experimental study was conducted with the approval of the Ethical Committee of the Royan Institute (code: IR ACECR ROYAN REC.1394.111). In order to perform this experimental study, melanoma specimens were sampled from January 2007 to May 2014 upon the approval of the Iranian National Tumor Bank (INTB) of the Cancer Institute of Iran, obtained based on INTB regulations. The Ethics Committee of INTB had obtained patients' approval according to local authorities. All contributors signed a written form of consent to enroll in this study. Patients histopathological information, including tumor size and depth, lymph-vascular and perineural invasion, grade and the clinical tumor/node/metastasis was recorded and pathologically staged using the tumor-nodes metastasis (TNM) staging method (15). All specimens were frozen within 20 minutes after surgery, using nitrogen vapor based on Tumor Bank standard operating protocols.

Twenty patients with malignant melanoma who underwent surgery at the Cancer Institute of Iran were malignancies were excluded from the study. Normal adjacent biopsies were collected from included in this research. The malignant melanoma was confirmed based on histopathological examination in patients. None of the patients had been treated with radio- or chemotherapy prior to surgery. Subjects with chronic or acute inflammatory diseases, other skin cancers, and/or any other all twenty patients as negative controls. In addition, serum samples were taken from 11 patients and 5 healthy donors.

### Culture conditions and melanosphere formation

Three human melanoma cell lines (A375, D10, and NA8) with *BRAF* V600E mutation were kindly provided by Prof. Giulio Spagoli (University of Basel, Switzerland). Cells were cultured in Dulbecco's Modified Eagle's Medium (DMEM) supplemented with 10% fetal bovine serum (FBS), 1% non-essential amino acids (NEAA), 2 mM L-glutamine, and 1% penicillin/streptomycin (Gibco, Germany). Cell culture was performed in an incubator operating at 37°C and 5% CO<sub>2</sub>.

The formation of melanospheres was established based on a previously published protocol (16). Briefly, 10<sup>4</sup> cells/ml were grown in six-well plates coated with 12 mg/ml poly 2-hydroxyethyl methacrylate (Sigma, Germany). Serum-free DMEM containing 1% NEAA, 2 mM L-glutamine, 1% penicillin/streptomycin, 1x B-27 supplement (Gibco, Germany), 20 µg/ml epidermal growth factor (EGF, Royan, Iran), and 20 µg/ml basic fibroblast growth factor (bFGF, Royan, Iran) was used for culturing melanospheres. Every 48 hours, fresh B27, bFGF, and EGF were added to the culture medium. Melanospheres were passaged three times in total, once every seven days.

### MiRNA selection based on literature and database mining

To identify possible miRNAs associated with EMT in melanoma, we first performed a systematic search on PubMed and Scopus using "microRNA" and "melanoma" as keywords in the title of papers published between 2007 and 2016. Then we excluded manuscripts if there were no correlations with "epithelial-mesenchymal transition", "metastasis", and "invasion". Parallel database mining was performed by using the Kyoto Encyclopedia of Genes and Genomes (KEGG) Pathway Database to find genes associated with EMT signaling, the *BRAF* pathway, and stemness. Subsequently, further analysis was conducted using miRNA databases, which were available in miRTarBase (<http://mirtarbase.mbc.nctu.edu.tw/>), TargetScanHuman ([www.targetscan.org/](http://www.targetscan.org/)), and miRCancer (<http://mircancer.ecu.edu/>) (17-19), to find miRNAs that directly regulate these genes. Finally, potent miRNAs in the regulation of self-renewal, invasion, migration, and metastasis in malignant melanoma were selected by cross-analysis of the results of literature and database mining.

## Quantification of miRNAs and mRNA by real-time quantitative reverse transcription polymerase chain reaction

Trizol® Reagent (Invitrogen, USA) was used to extract total RNA from melanoma cells, melanospheres, and tissues. Total RNA extraction from serum was performed using miRNAeasy kit (Qiagen, USA). All procedures were conducted according to the manufacturer's instructions. Reverse transcription of 2 µg of miRNAs and mRNAs was carried out using MiR-Amp kit (PARSGENOME, Iran) and Thermoscript (TaKaRa, China), respectively. Next, real-time quantitative reverse transcription polymerase chain reaction (qRT-PCR) using Power SYBR® Green (Applied Biosystems®, UK) was applied to quantify the expression levels of miRNAs and mRNAs in duplicate (7500 Fast qRT-PCR System, Applied Biosystems, CA). The qRT-PCR was performed in three steps: 30 seconds at 95°C as hold time, 40 cycles of denaturation at 95°C for 5 seconds, annealing at 60°C for 20 seconds, and 30 seconds extension at 72°C. Melting curves were determined from 55 to 99°C. The expression level of each miRNA was normalized against U6 snRNA expression and *GAPDH* was used to normalize mRNAs. The quantitative  $2^{-\Delta Ct}$  method was adopted for calculating the individual expression levels of patients' miRNAs in tumor and normal samples. The relative quantitative approach ( $2^{-\Delta\Delta Ct}$ ) was used to demonstrate relative expression of target genes of miRNAs, and miRNAs and mRNAs levels in melanospheres. GraphPad Prism 6 was used for data analysis and graph preparation.

## Univariate statistical analysis

Categorical variables were assessed using proportion tests including Z-test and Fisher's exact test. t tests were applied to compare numerical data (presented as mean ± standard error of the mean). The statistical comparisons were performed using R software (version 3.0.2), Minitab17, and GraphPad Prism version 7 (San Diego, USA).

## MiRNA pattern recognition based on data mining

In an attempt to i. Identify the major miRNAs distinguishing between tumor and normal samples, ii. Determine the combination and hierarchy of miRNAs which had the highest accuracy in predicting tumor development, and iii. Calculate the predictive power of the created model using cross-validation, a comprehensive data mining analysis was applied. For this purpose, 10 different attribute weighting models and 176 combinational decision tree (DT) models were developed.

## Attribute weighting

Ten different attribute weighting algorithms were applied to determine the main miRNAs that could accurately discriminate between melanoma and normal samples (Table S1, See Supplementary Online Information at [www.celljournal.org](http://www.celljournal.org)). Following attribute weighting, the weights were normalized and miRNA attributes received

a value between 0 and 1. Values, which were closer to 1, showed higher importance of that particular miRNA in the discrimination between normal and tumor samples according to the employed models. Variables weighted as  $\geq 0.9$  were then selected and with tree induction algorithms were used to predict the cancer development.

## Decision tree and random forest models

As the most popular supervised learning methods for data exploration, DT classifiers facilitate easy interpretation by summarizing and transforming data into more compact forms with the same essential characteristics as the original data. As described earlier, 10-fold cross-validation was adopted to identify the DT models most accurately predicting cancer development.

## Enrichment analysis for signaling pathways using fisher's exact test

Enrichment analysis was employed to find the significant regulatory mechanisms of differentially expressed miRNAs using Pathway Studio Web tool (18).

The statistical significance (P values) of enriched annotation terms was determined using Fisher's exact test. Lower P values indicated greater enrichment,  $P \leq 0.05$  were considered significant.

## Interaction network database

We used the Mammalian+ChemEffect+DiseaseFx Database (Elsevier), which is a comprehensive dataset of proteins, small molecules, diseases, Gene Ontology, and functions collected by a natural language processing (NLP) tool (19). The relations were collected from PubMed, KEGG, Science Signaling, GO Consortium, and Prolexys HyNet protein-protein interaction databases as well as full texts of relevant papers in both Elsevier and non-Elsevier journals. The database contains 284400 entities, 7151512 relationships, and 2023 pathways. Pathway Studio was used to build networks and pathways from relationships of Mammalian+ChemEffect+DiseaseFx Database.

## Common targets common regulators algorithms

Pathway Studio Web tool (19) was used for 'common targets' and 'common regulators' analysis. A component (gene /miRNA) is regarded as a common regulator when it has a high number of upstream interactions with the differentially expressed miRNAs. We optimized this parameter and set a threshold of three interactions. Likewise, a component is considered as a common target if it has a high number of downstream interactions with the differentially expressed miRNAs. After the evaluation of various values, a threshold of three interactions was set for the analysis.

Differentially expressed miRNAs were used as the input of common targets and common regulators algorithms. The common targets algorithm identified the targets/mechanisms, which were activated/ inactivated

by the altered miRNAs, i.e. it sought to clarify the goal/consequence of the determined miRNAs modulation pattern. However, the common regulators algorithm determined the regulators with the maximum number of regulation/expression relationships with the altered miRNAs, i.e. it sought to identify the managers/commanders/regulators of the altered miRNAs.

### Survival analysis and definition of miRNA-related prognostic signature

For assessment of overall survival implications for significant miRNAs, the PROGmiR tool (20) was used as a publicly available dataset (<http://www.compbio.iupui.edu/progmir>). The melanoma expression data comes from the TCGA dataset (<https://cancergenome.nih.gov>), including 163 cases of skin cutaneous melanoma.

### Construction of the tissue microarray

A total of 12 archival tissue samples of melanoma (Shohada-e-Tajrish Hospital, Iran) were used for tissue microarray analysis (TMA). Medical records were reviewed to collect the clinicopathological data (Table S2, See Supplementary Online Information at [www.celljournal.org](http://www.celljournal.org)). The study protocol was approved by the Research Ethics Committee of Iran University of Medical Sciences.

For TMA, 12 melanoma and 7 adjacent normal tissues of hematoxylin and eosin-stained slides were reviewed to determine the best pathological area from each specimen. The slides were then prepared by placing duplicate samples (0.6 mm in diameter) from each specimen using a manual tissue-arraying instrument (Minicore; ALPHELYS, Plaisir, France). These slides were used for immunohistochemical staining.

### Immunohistochemistry

The expression of CDH1 and SOX2 were immunohistochemically evaluated using the manufacturer's protocol. After initial preparation, the sections were incubated overnight at 4°C with rabbit polyclonal E-cadherin antibody recognizing the extracellular domain of E-cadherin (1:300 dilution, H-108, Santa Cruz Biotechnology, USA), and specific antibody against rabbit monoclonal anti-human SOX2 (1:250 dilution, cat. 3579, Cell Signaling, USA). The sections were washed the next day and incubated with the anti-rabbit/anti-mouse EnVision reagent (Dako, Denmark), as the secondary antibody, for 60 minutes. The sections were then stained with 3, 3'-diaminobenzidine (DAB, Dako) substrate as chromogen for two minutes in the dark and at room temperature. Subsequently, the sections were counterstained with hematoxylin (Dako, Denmark), dehydrated through graded ethanol followed by xylene, and mounted. Normal human brain tissue and ovarian carcinoma were used as positive control for SOX2 and E-cadherin antibodies respectively. The negative control was incubated only with Tris-buffered saline (TBS).

### Immunohistochemical evaluation and scoring

Two independent observers used a multi-headed microscope to evaluate the stained slides based on a semi-quantitative scoring system. The scoring was executed without previous knowledge of clinicopathological data. The intensity of staining was scored as 1+ (weak), 2+ (moderate), or 3+ (intense) and the percentage of positive tumor cells was scored as 1 (positive tumor cells <25%), 2 (positive tumor cells: 25-50%), 3 (positive tumor cells: 50- 75%), and 4 (positive tumor cells >75%). The histochemical score (H-score) was ultimately calculated as the product of staining intensity and the percentage of positive tumor cells by multiplying the intensity of staining and the percentage of positive tumor cells.

## Results

### Patient demography

Specimens obtained from 20 patients with cutaneous malignant melanoma were evaluated in this study.

Patients' age varied between 38 and 83 years, with 60% of the subjects being older than 65 years. In nine patients (45%), the primary tumor site was at the lower limb and hip and 50% of all patients had ulcerations. According to the TNM classification of malignant melanoma, 65% of patients had stage II melanoma (Tables S3, S4, See Supplementary Online Information at [www.celljournal.org](http://www.celljournal.org)).

### miRNA selection

To gain further insight into miRNAs that simultaneously control EMT, stemness, and the BRAF pathway, literature mining and cross-analysis with available databases were performed, as described in the Methods section. Literature mining resulted in 141 articles that were published between 2007 and 2016, and contained the predetermined keywords "microRNA" and "melanoma" in the title. Of those, 99 articles were excluded as they did not meet our selection criteria (correlation to EMT, metastasis, invasion and stemness features) and also because of data duplication. Finally, 45 miRNAs were selected from 42 articles. Parallel database search resulted in a total of 626 miRNAs (including 33 target genes) contributing to the EMT process. Interestingly, 85 and 161 of these also targeted stemness modulators (including four target genes) and BRAF pathway factors (including four target genes), respectively. Finally, 73 miRNAs were identified to target all three processes of EMT, stemness, and metastasis. However, only 18 miRNAs (miR-9, -10b, -15b, -18b, -21, -22, -34a, -141, -146a, -155, -200a, -200c, -203, -205, -211, -221, -222, and -429) were ultimately selected following the cross-analysis of the miRNAs extracted from literature and database mining (Fig.1, Supplementary Excel 1, See Supplementary Online Information at [www.celljournal.org](http://www.celljournal.org)).

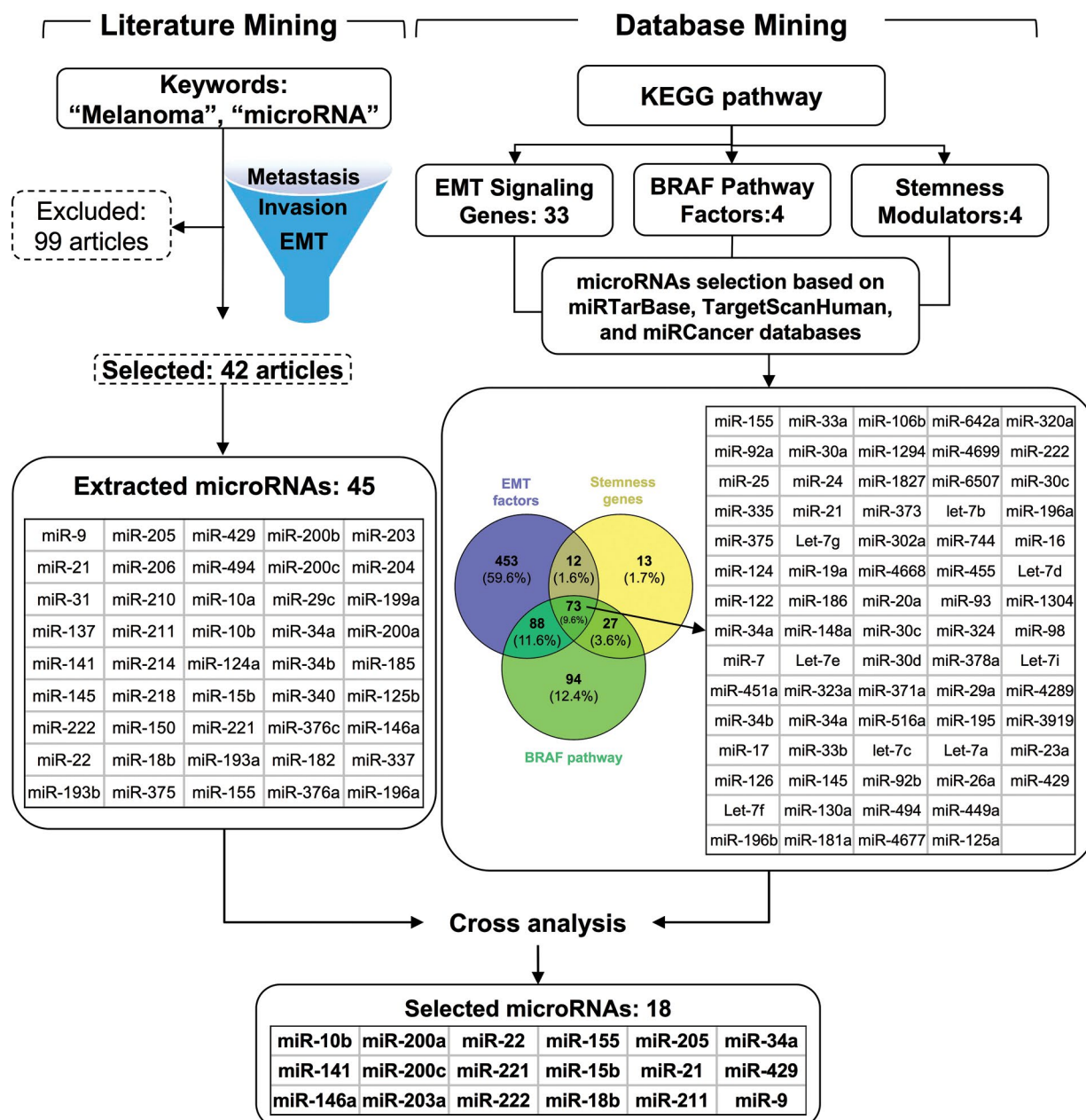


**Fig.1:** Schematic illustration of miRNA selection procedure. MiRNAs were selected using literature and database mining. Ultimately, 18 miRNAs were selected following cross-analysis.

### Differential expression of miRNAs in melanoma, normal adjacent tissue, and serum

Among 18 selected miRNAs, the expression of 5 of them (miR-205, -141, -203, -15b, and -9) was significantly different between groups. The expression of miR-205, -203, -141 and -15b was decreased in tumor samples in comparison with normal adjacent tissues, and the expression of miR-9 was significantly higher in tumor samples as compared to the normal group ( $P < 0.05$ , Fig.2).

According to validated data (miRTarBase 6.0: Sept. 15, 2015), all of these 5 miRNAs had at least one target in the EMT pathway: miR-205 and miR-141 target *ZEB*; miR-

203 targets *ZEB*, *SNAIL*, and *SMAD2*; miR-15b targets *SMAD2*; miR-9 targets *CDH1* and *SNAIL*. Moreover, with regards to stemness genes, miR-141 inhibits *POU5F1* and miR-9 directly targets *SOX2*. In addition, miR-9, -15b, and -203 are involved in the BRAF pathway by directly targeting *BRAF* or one of its downstream factors, like *ERK*, *MEK* or *CCND1* (Fig.S1, See Supplementary Online Information at [www.celljournal.org](http://www.celljournal.org)). Comparison of the expression of miR-205, -141, -203, -15b, and -9 in the serum of patients and healthy donors revealed significant differences for miR-205, -15b, and -9 ( $P < 0.05$ , Fig.3). The expression patterns of miR-205 and miR-9 in serum from patients were similar to those of tumor samples.

However, in contrast to tumor samples, serum obtained from patients showed increased expression of miR-15b as compared to serum from control subjects.

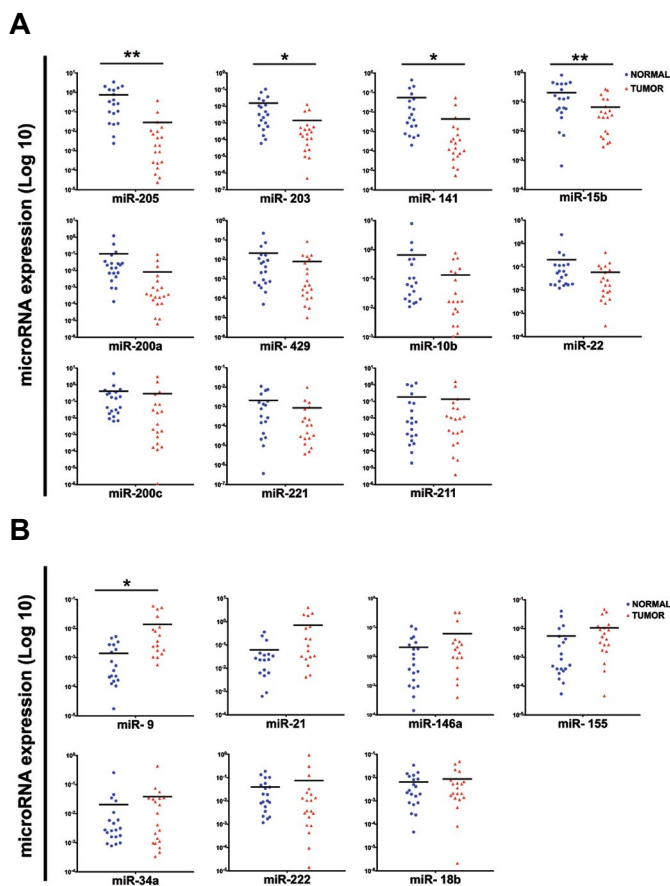


**Fig.2:** The expression pattern of selected miRNAs in melanoma and normal adjacent tissue. **A.** The significant down regulation of miR-205, -141, -203, -15b was observed in melanoma tissues (n=20, Log 10, \*, P<0.05, \*\*, P<0.01) and **B.** Scatter-plots of the expression levels of the selected miRNAs show a significant higher expression of miR-9 (n=20, Log 10, \*, P<0.05) in melanoma samples compared with normal adjacent tissues.

**Predicting the most important melanoma-linked miRNAs and developing predictive models using attribute weighting and decision tree by random forest**

MiR-205, -15b, and -141 were selected as the key miRNAs linked to tumor/normal status using four-attribute weighting models with different statistical backgrounds (Table S5, See Supplementary Online Information at [www.celljournal.org](http://www.celljournal.org)). MiR-205 received the highest weight of 1 by information gain ratio, information gain, and Gini index. It was also weighted as 0.9 by the uncertainty model (Supplementary Excel 2, See Supplementary Online Information at [www.celljournal.org](http://www.celljournal.org)).

In order to identify the best combination of miRNAs that distinguished between healthy and malignant status, extensive computational biology analysis was applied to test DT based on expression of miRNAs. Distinguished capability decision-tree classifier in highly accurate identification of cancer origin based on miRNA profile has been documented (21). Also, DT models have shown high applicability for accurate classification of kidney cancer subtypes using miRNAs signature (22). Therefore, we used DT model for finding the hierarchical combination of miRNAs as a biomarker for melanoma. On the other hand, 10 attribute weighting algorithms were applied with various statistical backgrounds to determine the main miRNAs that could accurately discriminate between melanoma and normal samples. We selected miRNAs based on the intersection/agreement of different models where miRNA receiving high weights by most of models were announced as important ones. Applying these models increased our confidence about the selected miRNAs. The accuracy of each model was evaluated and presented in Supplementary Excel 3 (See Supplementary Online Information at [www.celljournal.org](http://www.celljournal.org)). The highest accuracy was obtained by the Random Forest Gain Ratio and Random Forest Info Gain models, which were able to accurately predict tumor/normal status of 90% of the samples (based on cross-validation).

Following attribute weighting on expression of microRNAs (miRNAs) in normal and tumour, the weights were normalized and miRNA attributes received a value between zero and one. Values closer to one showed higher importance of that particular miRNA in discrimination between normal and tumor samples according to the employed model. Variables weighted as  $\geq 0.9$  were then selected. For example, in the following Table S5 (See Supplementary Online Information at [www.celljournal.org](http://www.celljournal.org)), miR-205 is selected based on statistics of 4 models including Weight\_Info Gain Ratio, Weight\_Info Gain, Weight\_Uncertainty, and Weight\_Gini Index to be important in discriminating tumour from normal sample.

MiR-205 emerged as the key indicator of healthy and malignant status and the combination of high miR-205 expression with low miR-200c expression indicated a healthy status. In contrast, low miR-205 and -141 expression was associated with malignancy (Fig.4A, Right panel). Moreover, the low expression of both miR-

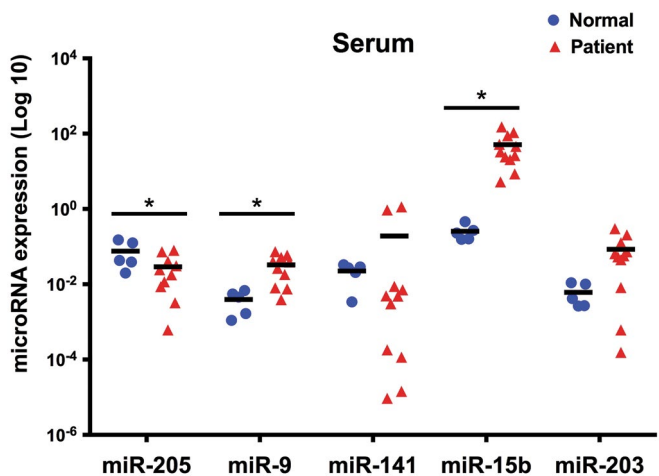


**Fig.3:** The expression pattern of selected miRNAs in serum obtained from melanoma patients and healthy donors. Among five miRNAs, miR-205, -15b, and -9 showed significant differences (Log 10, \*, P<0.05) between serum obtained from melanoma patients (n=11) and control subjects (n=5).

205 and miR-15b could be indicative of the malignant state (Fig.4A, Left panel). To determine the commonality between miRNAs, they were clustered by hierarchical clustering methods, as previously described (23). Our results revealed that the expression patterns of miR-205, -200c, and -222 in melanoma tissue samples were over 95% similar to those of miR-200a, -155, and -10b, respectively (Fig.4B). As the miRNAs with the similar expression pattern may be regulated by the similar set of transcription factors (common regulators), therefore, we suggested the same transcription factors might regulate these miRNAs. As shown in Figure 4C, tumor samples had high diversity and negative amount of second principal component analysis (PCA).

### Regulatory network in progression to malignant melanoma

A 'regulatory network' sustaining the progress toward malignancy was designed by combining the statistically significant sub-networks of significant miRNAs in Gene Set Enrichment Analysis using Pathway Studio Web tool (Elsevier, Supplementary Excel 4, See Supplementary Online Information at [www.celljournal.org](http://www.celljournal.org)). The selected miRNAs were subject to regulation by most intracellular components, including the nucleus, Golgi apparatus, and the cell membrane (Fig.S2A, B, See Supplementary Online Information at [www.celljournal.org](http://www.celljournal.org)).

org). The common regulatory factors were TGF $\beta$ 1, TP53, and histone deacetylase that regulated six of the seven indicator miRNAs: miR-9, -200a, -200c, -141, -15b and -205 (Fig.S3, Supplementary Excel 5, See Supplementary Online Information at [www.celljournal.org](http://www.celljournal.org)).

Analysis of common targets revealed that MET proto-oncogene (*MET*), *CDH1*, vascular endothelial growth factorA (*VEGFA*), and tumor necrosis factor (*TNF*) were the key targets of these six miRNAs. Also, it seems that miR-200c was the upstream of most important cancer regulators like *ZEB*, *CDH1*, and *CCND1* as common targets (Fig.5A).

In order to validate the targets, qRT-PCR was performed to assess the mRNA expression of *CDH1*, *CCND1*, *SOX2*, *VIM*, *BRAF*, *TNFA* and *VEGF*. According to Figure 5A all of these genes are common targets for miR-205, -203, -9 and -15b. TMA using 12 samples from malignant patients and 7 normal/control tissues showed the higher expression of SOX2 at protein level in melanoma tissues, in comparison with normal skin biopsies. CDH1 protein was highly expressed both in melanoma and normal skin biopsies ( $P < 0.01$ , Fig.5B, C). Although, at mRNA level, *CCND1* expression was significantly lower in tumor samples ( $P < 0.001$ , Fig.5D), *SOX2*, *BRAF*, *TNFA*, and *VEGF* expression was increased in malignant tissues compared with normal adjacent samples ( $P < 0.05$ , Fig.5D).

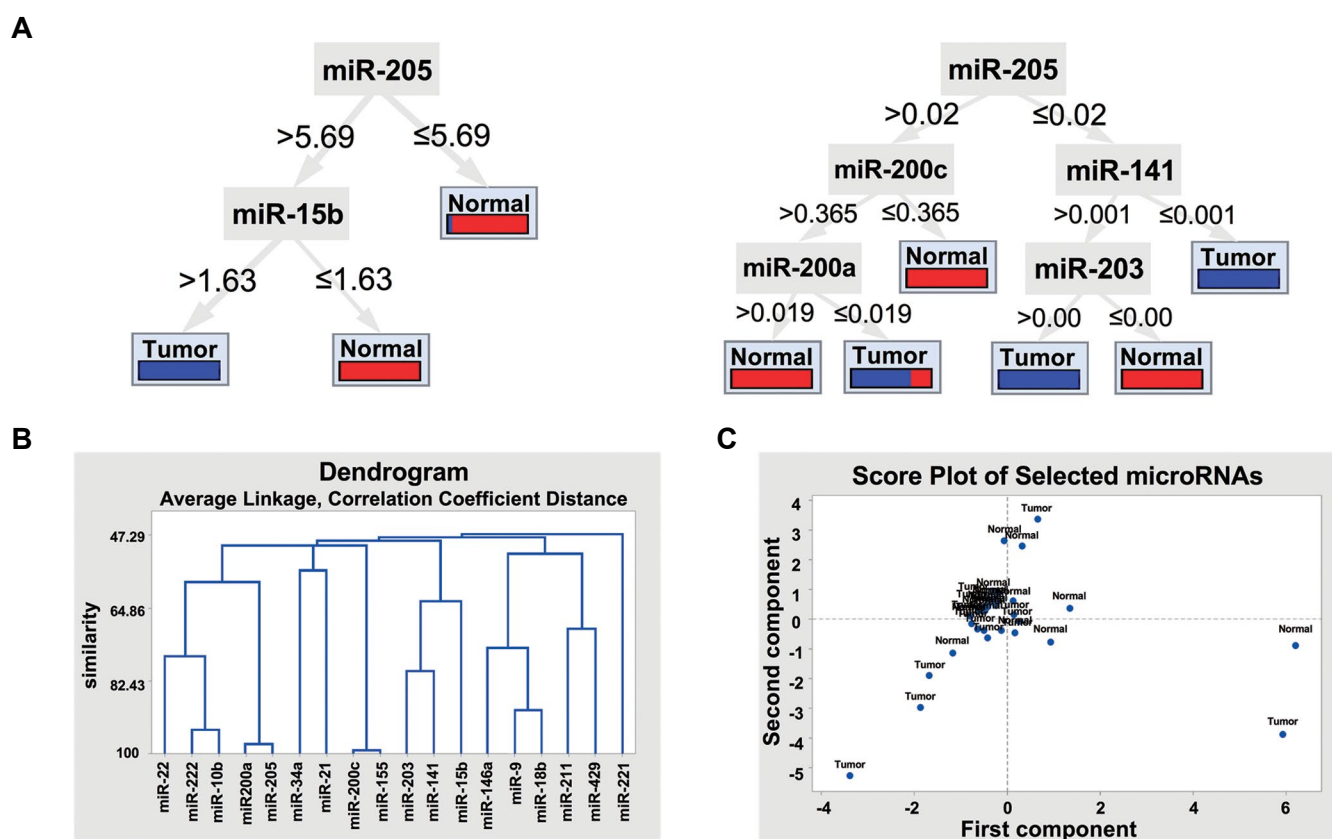


**Fig.4:** Pattern discovery distinguishing tumor from normal samples using machine learning and multivariate analytical models. **A.** Decision tree (DT) model of Random Forest Gain Ratio predicts normal/tumor status based on miRNA expression levels. Random Forest is able to find the threshold in expression of each miRNA. As shown in the results, miR-205 was the key regulator of healthy and malignant status, **B.** Clustering of miRNAs, based on their expression levels, indicates that the expression patterns of miR-205/ miR-200a, miR-200c/ miR-155, and miR-222/ miR-10b in cancer samples were over 95% similar, and **C.** PCA analysis of expression of miRNAs in relation to tumor/normal status exhibited high diversity in tumor samples.

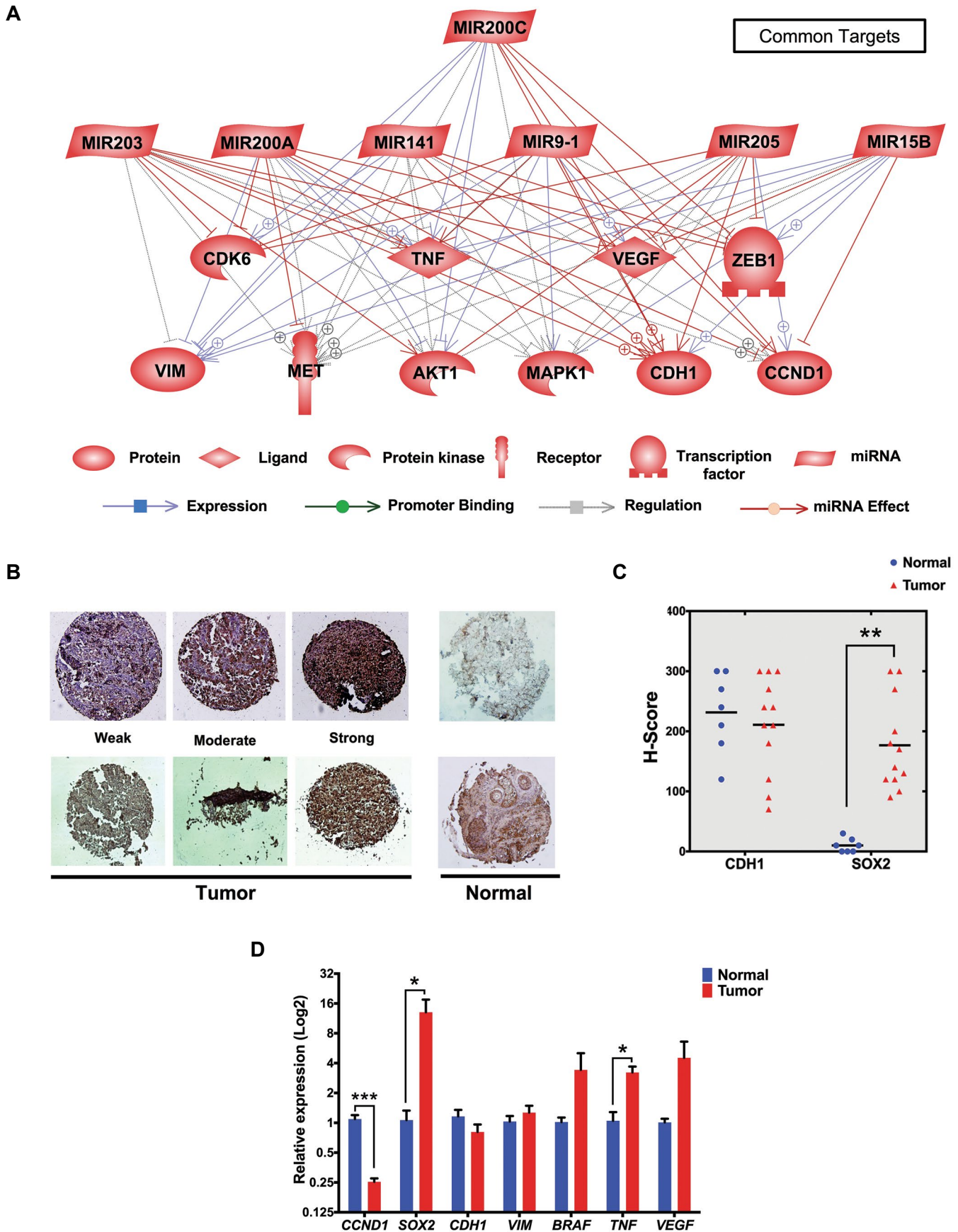


**Fig.5:** Validation of the most important common regulators and targets of differentially expressed miRNAs. **A.** Analysis of common targets revealed that MET, CDH1, VEGFA, TNF, ZEB, CDH1, and CCND1 represent the key targets of differentially expressed miRNAs, **B, C.** The protein expression levels of SOX2 and CDH1 obtained from Tissue Micro Array data and presented as H-Score. SOX2 expression was elevated in melanoma tissues (n=12) despite of normal skin (n=7), and **D.** mRNA expression levels of *CCND1*, *SOX2*, *CDH1*, *VIM*, *BRAF*, *TNF*, *VEGF*. *CCND1* was significantly lower expressed in tumor samples, whereas *SOX2*, *BRAF*, *TNF*, and *VEGF* were overexpressed in malignant tissues compared with normal samples (n≤15, \*, P<0.05, \*\*, P<0.01, \*\*\*, P<0.001).

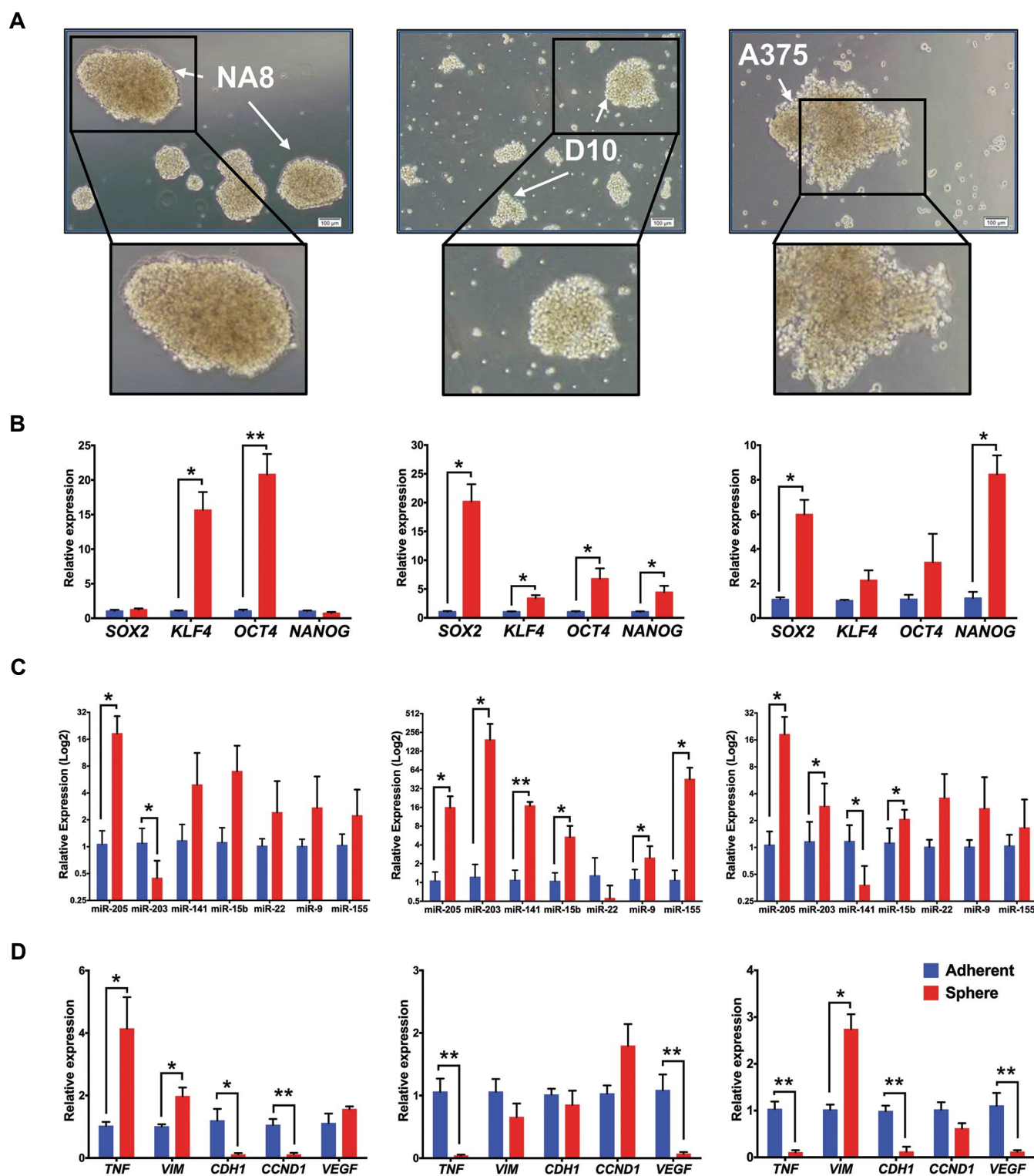


**Fig.6:** The expression analysis of stemness transcripts, selected miRNAs, and their target genes in melanospheres by quantitative reverse transcription polymerase chain reaction (qRT-PCR). **A.** The morphology of melanospheres derived from NA8 (left), D10 (middle), and A375 (right) revealed that, NA8-melanospheres were compact with defined borders. However, D10 and A375 formed loose, grapelike melanospheres. **B.** Relative expression levels of *SOX2*, *KLF4*, *OCT4* and *NANOG* transcripts in NA8-, D10- and A375-melanospheres compared to adherent cells. There were significant upregulations in *KLF4* and *OCT4* expression in NA8-melanospheres. D10 showed upregulation in *SOX2*, *KLF4*, *OCT4* and *NANOG* levels and significant upregulation was observed in *SOX2* and *NANOG* in melanosphere derived from A375 cells ( $n=3$ , \*,  $P<0.05$ , \*\*,  $P<0.01$ ), **C.** The expression of miR-205, -203, -141, -15b, -22, -9, and -155 in melanospheres originating from all three cell lines. The expression of miR-205 was upregulated in all melanospheres compared with parental cells. MiR-203 was significantly upregulated in D10 and A375 melanospheres, unlike in spheres derived from NA8 cells. MiR-15b expression was significantly increased in D10 and A375 melanospheres compared to parental cells. MiR-141 was upregulated in D10 and downregulated in A375. Although miR-9 showed significantly higher expression in D10 melanospheres in comparison with parental cells ( $n=3$ , log 2, \*,  $P<0.05$ , \*\*,  $P<0.01$ ), and **D.** Relative expression of *CDH1*, *VIM*, *TNFA*, *VEGF* and *CCND1* transcript in three cell lines. *TNFA* was significantly downregulated in D10- and A375- and upregulated in NA8-melanospheres compared to parental cells. *VIM* shows higher and *CDH1* lower expression in NA8- and A375-melanospheres. *CCND1* was significantly downregulated only in NA8-melanospheres. Expression of *VEGF* was markedly lower in D10 and A375 spheres ( $n=3$ , \*,  $P<0.05$ , \*\*,  $P<0.01$ ).

### The combined expression of miR-203, -205, -15b, and -9 is associated with survival rates

Based on the PROGmiR database, the individual expression levels of miR-205, -15b, or -9 alone did not significantly correlate with the survival rates of melanoma patients. In contrast, higher expression of miR-203 was significantly associated with reduced survival rate ( $P < 0.05$ , Fig.S4A, See Supplementary Online Information at [www.celljournal.org](http://www.celljournal.org)). On the other hand, the combined expression of them, appears to severely effect overall survival ( $P = 0.0192$ ) in melanoma patients (Fig.S4B, See Supplementary Online Information at [www.celljournal.org](http://www.celljournal.org)).

### EMT-miRNAs expression pattern in melanospheres as a cancer stem cell model

To determine if the six selected miRNAs were expressed in melanospheres (melanoma stem like cells), we assessed the expression pattern of those by qRT-PCR. The melanospheres were derived from three different melanoma cell lines. Morphologically, melanospheres derived from NA8 were dense, compact with defined borders; conversely, the D10 and A375 cells formed loose, grapelike melanospheres (Fig.6A). Melanospheres derived from different melanoma cell lines revealed differential expression patterns for stemness genes. Levels of *KLF4* and *OCT4* mRNA were significantly increased in NA8-melanospheres, while D10-melanospheres showed elevated expression of *SOX2*, *KLF4*, *OCT4* and *NANOG*, and A375- melanospheres displayed enhanced expression of *SOX2* and *NANOG* ( $P < 0.05$ ,  $P < 0.01$ , Fig.6B). In all melanospheres, overall the expression levels of miR-205, -203 and -9 were higher than in their parental cells; of note, the expression of miR-203 was significantly decreased in NA8-melanospheres and miR-9 just significantly expressed in D10-melanosphere ( $P < 0.05$ , Fig.6C). MiR-15b expression was significantly increased in D10 and A375 melanospheres, whereas miR-141 was differentially expressed, upregulated in D10 ( $P < 0.01$ , Fig.6C) and downregulated in A375 ( $P < 0.05$ , Fig.6C). Among the main common targets, *TNF* expression was higher in NA8-melanospheres; conversely, it was reduced in D10- and A375-melanospheres. The level of *VIM* was increased and that of *CDH1* reduced in melanospheres derived from NA8 and A375. NA8-melanospheres had lower levels of *CCND1* expression. Lastly, the expression pattern of *VEGF* was reduced in D10- and A375-melanospheres in comparison with parental cells ( $P < 0.05$ ,  $P < 0.01$ , Fig.6D).

### Discussion

Alterations in the EMT process and BRAF signalling pathway play a key role in melanoma progression (24, 25), and affect stemness properties involved in metastatic competence and tumor regrowth (26). Nevertheless, further research is required to determine exactly which factors can simultaneously regulate these processes. For this, a systematic analysis based on literature and

databases' mining was performed, and 18 miRNAs were identified. However, the expression of miR-205, -141, -203, -15b, and -9, was significantly different between malignant melanoma and adjacent normal tissues. Expression levels of miR-205, -141, -203, and -15b were lower, whereas expression of miR-9 was higher in melanoma tissue. Interestingly, miR-9, -15b, and -203 are documented to contribute to BRAF pathways by direct targeting of *RAF*, *MEK*, and *ERK*. Moreover, miR-9 and -141 are associated with stemness properties by targeting *SOX2* and *OCT4*.

In order to distinguish a unique expression pattern of miRNAs, 10 attribute weighting models and DT models were used. Based on these models, we suggested miR-205, -203, -9, and -15b as common regulators of EMT, self-renewal, and BRAF pathways in melanoma. Therefore, we evaluated expression of these miRNAs in patients' serum and melanospheres derived from NA8, D10, and A375 cell lines. Interestingly, among them miR-205 had a similar expression pattern (low expression) in tumor biopsies and serum of patients in comparison with normal control groups, but showed an increased expression in all groups of cell line melanospheres. Machine learning analysis revealed the reduction of miR-205 level as a key regulator of the malignant state in melanoma, which is in accordance with previous reports in melanoma (27) and gastric cancer (28). Although, its increased expression in melanoma stem cells is still ambiguous, it had positive correlation with *OCT4* in all types of melanospheres and with *NANOG* in melanospheres derived from D10. Therefore, it may be connected to the pluripotent state of melanoma cells. Similar to our results, miR-205 has been reported to be associated with the EMT process, stemness traits of cancer stem cell (CSC) fate, tumorigenicity, and chemoresistance in breast cancer (29) and non-small cell lung cancer (30). The elevated expression of miR-205 in mouse mammary epithelial stem-like cells led to expansion of the progenitor cell population through the suppression of phosphatase and tensin homologue (PTEN) (31). Additionally, the overexpression of miR-205 resulted in high proliferation of endometrial and ovarian cancer (32).

MiR-9 displayed a similar expression pattern in patients' melanoma biopsies, serum, and melanospheres (higher expression as compared to control). According to common regulator analysis, we found that *SOX2* can regulate miR-9 expression, as a *SOX2*-binding site has been detected in the promoter region of miR-9 (33). Based on our results, enhancement of *SOX2* at the mRNA and protein level in tumor tissues as well as melanospheres, can enhance the expression of miR-9, which results in an increased motility of melanoma cells through reduction of *CDH1* level (34). Moreover, its overexpression increases *VIM* in hepatocellular carcinoma (34), and squamous cell carcinoma CSCs (35).

Interestingly, the expression of miR-15b was higher in patients' serum and melanospheres than in the control group. However, in patient samples, its expression in

melanoma biopsies was lower than normal tissues. This difference in the pattern of expression may be associated with recurrent-free survival in patients (36).

A combination of ingenuity analysis for potential regulators and target genes and examination of biological pathways targeted by the deregulated miRNAs, indicated that the regulatory network around miR-205, -9, -203, and -15b was most prominent in our data. The significant association of combined expression of these miRNAs with overall survival of melanoma patients was confirmed through the TCGA data. Among all target genes, negative correlation between miR-205, -203 and -15b expression and *VEGF* was observed in melanospheres. Also, our results provide evidence for negative correlation between these miRNAs and *TNF* by miR-205, -203 and -15b in tumors. Whereas, miR-9 shows a positive regulatory effect on *TNF* expression in D10 and A375 melanospheres and melanoma patient samples. In fact, in patients' samples, *TNF* expression was increased concomitant with a high expression of miR-9 and low expression of miR-203. This data was verified by the expression patterns in melanospheres, in which reduced *TNF* expression coincided with higher expression of miR-203 (D10- and A375-melanospheres). These data can confirm the important role of miR-203 in regulating the expression of the pro-inflammatory cytokine *TNF*. Importantly, treatment of melanoma cells with *TNF* suppresses CSCs differentiation through PI3K/AKT-signaling (37). However, the role of *TNF* as an intrinsic factor in melanoma stem cell fate requires further studies. *VEGF* is another factor that can affect the growth and metastasis of melanoma (38). We suggested here that miR-205, -203, and -15b could negatively regulate *VEGF* expression. Although we could not find an explanation for the observed lowered expression of *VEGF* in melanospheres, but it plays an important role in the *VEGF*-CSC axis in a variety of tumors, including melanoma (39).

## Conclusion

Based on our findings, miR-205, -15b, -203, -9 were selected as the key miRNAs linked to tumor/normal status, which can regulate the pluripotency, proliferation, and motility of malignant cells. However, further studies are required to find the exact mechanisms underlying the combinatory effects of the abovementioned miRNAs.

## Acknowledgments

This study received grants from the Royan Institute (ID No: 91000426) and an external fund from Iran National Science Foundation (Grant #90003728). We also thank Elham Kalantari, Dedmer Schaafsma, Yashar Abbasnejad, Bahareh Fasihpour, Foroogh Sayyehpour, Azam Samadian, Fatemeh Ganji, Sara Pahlevan, and Ali Jahanbin for their technical assistance. The authors declare no conflicts of interest.

## Authors' Contributions

P.S.; Carried out the experiments, wrote the manuscript

with support from all authors. Z.M.; Helped and supervised project, verified analytical methods in TMA and immunohistochemistry experiments. A.E.R.; Helped in collection of fresh frozen melanoma and normal tissue biopsies from Iran National Tumor Bank. A.Gh.; Contributed in pathological diagnosis of the samples from Iran National Tumor Bank. J.F., P.Kh.; Contributed in cellular lab and help in data analysis. S.Gh.; Contributed in final editing of manuscript, help for designing the figures and writing the manuscript. E.E.; Verified the analytical methods, performed the bioinformatics and statistics analysis of data. M.E.; Conceived of the presented idea, developed idea, supervised the findings of this work. All authors discussed the results and contributed to the final manuscript and approved it.

## References

- Alizadeh J, Shojaei S, Sepanjnia A, Hashemi M, Eftekharpour E, Ghavami S. Simultaneous detection of autophagy and epithelial to mesenchymal transition in the non-small cell lung cancer cells. *Methods Mol Biol.* 2019; 1854: 87-103.
- Sun T, Jiao L, Wang Y, Yu Y, Ming L. SIRT1 induces epithelial-mesenchymal transition by promoting autophagic degradation of E-cadherin in melanoma cells. *Cell Death Dis.* 2018; 9(2): 136.
- Kong J, Leteurtre F, Goislard M, Biard D, Morel-Altmeier S, Vaurijoux A, et al. Breast cancer stem cell-like cells generated during TGFbeta-induced EMT are radioresistant. *Oncotarget.* 2018; 9(34): 23519-23531.
- Wickremesekera AC, Brasch HD, Lee VM, Davis PF, Woon K, Johnson R, et al. Expression of cancer stem cell markers in metastatic melanoma to the brain. *J Clin Neurosci.* 2019; 60: 112-116.
- Cancer Genome Atlas Network. Genomic classification of cutaneous melanoma. *Cell.* 2015; 161(7): 1681-1696.
- Tusa I, Gagliardi S, Tubita A, Pandolfi S, Urso C, Borgognoni L, et al. ERK5 is activated by oncogenic BRAF and promotes melanoma growth. *Oncogene.* 2018; 37(19): 2601-2614.
- Paudel BB, Harris LA, Hardeman KN, Abugable AA, Hayford CE, Tyson DR, et al. A nonquiescent "idling" population state in drug-treated, BRAF-mutated melanoma. *Biophys J.* 2018; 114(6): 1499-1511.
- Pal HC, Diamond AC, Strickland LR, Kappes JC, Katiyar SK, Elmets CA, et al. Fisetin, a dietary flavonoid, augments the anti-invasive and anti-metastatic potential of sorafenib in melanoma. *Oncotarget.* 2016; 7(2): 1227-1241.
- Lee CH, Yu CC, Wang BY, Chang WW. Tumorsphere as an effective in vitro platform for screening anti-cancer stem cell drugs. *Oncotarget.* 2016; 7(2): 1215-1226.
- O'Brien J, Hayder H, Zayed Y, Peng C. Overview of microRNA biogenesis, mechanisms of actions, and circulation. *Front Endocrinol (Lausanne).* 2018; 9: 402.
- Islas JF, Moreno-Cuevas JE. A microRNA perspective on cardiovascular development and diseases: an update. *Int J Mol Sci.* 2018; 19(7): 2075.
- Tuna M, Machado AS, Calin GA. Genetic and epigenetic alterations of microRNAs and implications for human cancers and other diseases. *Genes Chromosomes Cancer.* 2016; 55(3): 193-214.
- van Laar RK, Lincoln MT, van Laar BJ. A plasma microRNA biomarker of melanoma as a personalised assessment of treatment response. *Melanoma Res.* 2019; 29(1): 19-22.
- Fomeshi MR, Ebrahimi M, Mowla SJ, Khosravani P, Firouzi J, Khayatizadeh H. Evaluation of the expressions pattern of miR-10b, 21, 200c, 373 and 520c to find the correlation between epithelial-to-mesenchymal transition and melanoma stem cell potential in isolated cancer stem cells. *Cell Mol Biol Lett.* 2015; 20(3): 448-465.
- Chou CH, Chang NW, Shrestha S, Hsu SD, Lin YL, Lee WH, et al. miRTarBase 2016: updates to the experimentally validated miRNA-target interactions database. *Nucleic Acids Res.* 2016; 44(Database issue): D239-D247.
- Agarwal V, Bell GW, Nam JW, Bartel DP. Predicting effective microRNA target sites in mammalian mRNAs. *Elife.* 2015; 4: e05005.
- Xie B, Ding Q, Han H, Wu D. miRCancer: a microRNA-cancer association database constructed by text mining on literature. *Bioin-*

- form. 2013; 29(5): 638-644.
18. Nikitin A, Egorov S, Daraselia N, Mazo I. Pathway studio--the analysis and navigation of molecular networks. *Bioinform.* 2003; 19(16): 2155-2157.
  19. Yuryev A, Kotelnikova E, Daraselia N. Ariadne's chemeffect and pathway studio knowledge base. *Expert Opin Drug Discov.* 2009; 4(12): 1307-1318.
  20. Goswami CP, Nakshatri H. PROGmiR: a tool for identifying prognostic miRNA biomarkers in multiple cancers using publicly available data. *J Clin Bioinform.* 2012; 2(1): 23.
  21. Rosenfeld N, Aharonov R, Meiri E, Rosenwald S, Spector Y, Zepeniuk M, et al. MicroRNAs accurately identify cancer tissue origin. *Nat Biotechnol.* 2008; 26(4): 462-469.
  22. Youssef YM, White NM, Grigull J, Krizova A, Samy C, Mejia-Guerrero S, et al. Accurate molecular classification of kidney cancer subtypes using microRNA signature. *Eur Urol.* 2011; 59(5): 721-730.
  23. Mahdi LK, Deihimi T, Zamansani F, Fruzangohar M, Adelson DL, Paton JC, et al. A functional genomics catalogue of activated transcription factors during pathogenesis of pneumococcal disease. *BMC Genomics.* 2014; 15:769.
  24. De Craene B, Berx G. Regulatory networks defining EMT during cancer initiation and progression. *Nat Rev Cancer.* 2013; 13(2): 97-110.
  25. Zhou L, Yang K, Dunaway S, Abdel-Malek Z, Andl T, Kadekaro AL, et al. Suppression of MAPK signaling in BRAF-activated PTEN-deficient melanoma by blocking beta-catenin signaling in cancer-associated fibroblasts. *Pigm Cell Melanoma Res.* 2018; 31(2): 297-307.
  26. Faiao-Flores F, Smalley KSM. Get with the program! stemness and reprogramming in melanoma metastasis. *J Invest Dermatol.* 2018; 138(1): 10-13.
  27. Noguchi S, Iwasaki J, Kumazaki M, Mori T, Maruo K, Sakai H, et al. Chemically modified synthetic microRNA-205 inhibits the growth of melanoma cells in vitro and in vivo. *Mol Ther.* 2013; 21(6): 1204-1211.
  28. Yin WZ, Li F, Zhang L, Ren XP, Zhang N, Wen JF. Down-regulation of microRNA-205 promotes gastric cancer cell proliferation. *Eur Rev Med Pharmacol Sci.* 2014; 18(7): 1027-1032.
  29. Chao CH, Chang CC, Wu MJ, Ko HW, Wang D, Hung MC, et al. MicroRNA-205 signaling regulates mammary stem cell fate and tumorigenesis. *J Clin Invest.* 2014; 124(7): 3093-3106.
  30. Yeh DW, Chen YS, Lai CY, Liu YL, Lu CH, Lo JF, et al. Downregulation of COMMD1 by miR-205 promotes a positive feedback loop for amplifying inflammatory- and stemness-associated properties of cancer cells. *Cell Death Differ.* 2016; 23(5): 841-852.
  31. Greene SB, Gunaratne PH, Hammond SM, Rosen JM. A putative role for microRNA-205 in mammary epithelial cell progenitors. *J Cell Sci.* 2010; 123(Pt 4): 606-618.
  32. Li J, Li L, Li Z, Gong G, Chen P, Liu H, et al. The role of miR-205 in the VEGF-mediated promotion of human ovarian cancer cell invasion. *Gynecol Oncol.* 2015; 137(1): 125-133.
  33. Vencken SF, Sethupathy P, Blackshields G, Spillane C, Elbaruni S, Sheils O, et al. An integrated analysis of the SOX2 microRNA response program in human pluripotent and nullipotent stem cell lines. *BMC Genomics.* 2014; 15: 711.
  34. Drakaki A, Hatzia Apostolou M, Polytaichou C, Vorvis C, Poultsides GA, Souglakos J, et al. Functional microRNA high throughput screening reveals miR-9 as a central regulator of liver oncogenesis by affecting the PPARA-CDH1 pathway. *BMC Cancer.* 2015; 15(1): 542.
  35. White RA, Neiman JM, Reddi A, Han G, Birlea S, Mitra D, et al. Epithelial stem cell mutations that promote squamous cell carcinoma metastasis. *J Clin Invest.* 2013; 123(10): 4390-4404.
  36. Fleming NH, Zhong J, da Silva IP, Vega-Saenz de Miera E, Brady B, Han SW, et al. Serum-based miRNAs in the prediction and detection of recurrence in melanoma patients. *Cancer.* 2015; 121(1): 51-59.
  37. Ostyn P, El Machhour R, Begard S, Kotecki N, Vandomme J, Flamenco P, et al. Transient TNF regulates the self-renewing capacity of stem-like label-retaining cells in sphere and skin equivalent models of melanoma. *Cell Commun Signal.* 2014; 12: 52.
  38. Ayubi E, Safiri S. Lymphatic vessel density and VEGF-C expression as independent predictors of melanoma metastases: Methodological issues. *J Plast Reconstr Aesthet Surg.* 2018; 71(4): 604-605.
  39. Calvani M, Bianchini F, Taddei ML, Becatti M, Giannoni E, Chiarugi P, et al. Etoposide-bevacizumab a new strategy against human melanoma cells expressing stem-like traits. *Oncotarget.* 2016; 7(32): 51138-51149.
-

# A Novel Insight into Endothelial and Cardiac Cells Phenotype in Systemic Sclerosis Using Patient-Derived Induced Pluripotent Stem Cell

Sedigheh Gholami, Ph.D.<sup>1,2</sup>, Zahra Mazidi, M.Sc.<sup>1</sup>, Sara Pahlavan, Ph.D.<sup>1</sup>, Fariba Moslem, M.Sc.<sup>1</sup>, Mahya Hosseini, M.Sc.<sup>1</sup>, Adeleh Taei, Ph.D.<sup>1</sup>, Mahdi Hesaraki, M.Sc.<sup>1</sup>, Maryam Barekat, M.D.<sup>3</sup>, Nasser Aghdami, M.D., Ph.D.<sup>3\*</sup>, Hossein Baharvand, Ph.D.<sup>1,2\*</sup>

1. Department of Stem Cells and Developmental Biology, Cell Science Research Center, Royan Institute for Stem Cell Biology and Technology, ACECR, Tehran, Iran
2. Department of Developmental Biology, University of Science and Culture, Tehran, Iran
3. Department of Regenerative Medicine, Cell Science Research Center, Royan Institute for Stem Cell Biology and Technology, ACECR, Tehran, Iran

\*Corresponding Addresses: P.O.Box: 16635-148, Department of Regenerative Medicine, Cell Science Research Center, Royan Institute for Stem Cell Biology and Technology, ACECR, Tehran, Iran  
P.O.Box: 16635-148, Department of Stem Cells and Developmental Biology, Cell Science Research Center, Royan Institute for Stem Cell Biology and Technology, ACECR, Tehran, Iran  
Emails: nasser.aghdami@royaninstitute.org, baharvand@royaninstitute.org

Received: 03/November/2019, Accepted: 26/January/2020

## Abstract

**Objective:** Systemic sclerosis (SSc) is a connective tissue disease associated with vascular damage and multi organ fibrotic changes with unknown pathogenesis. Most SSc patients suffer from defective angiogenesis/vasculogenesis and cardiac conditions leading to high mortality rates. We aimed to investigate the cardiovascular phenotype of SSc by cardiogenic differentiation of SSc induced pluripotent stem cells (iPSC).

**Materials and Methods:** In this experimental study, we generated iPSC from two diffuse SSc patients, followed by successful differentiation into endothelial cells (ECs) and cardiomyocytes (CMs).

**Results:** SSc-derived EC (SSc-EC) expressed KDR, a nearly EC marker, similar to healthy control-EC (C1-EC). After sorting and culturing KDR+ cells, the resulting EC expressed CD31, a late endothelial marker, but vascular endothelial (VE)-cadherin expression markedly dropped resulting in a functional defect as reflected in tube formation failure of SSc-EC. Interestingly, upregulation of SNAI1 (snail family transcriptional repressor 1) was observed in SSc-EC which might underlie VE-cadherin downregulation. Furthermore, SSc-derived CM (SSc-CM) successfully expressed cardiac-specific markers including ion channels, resulting in normal physiological behavior and responsiveness to cardioactive drugs.

**Conclusion:** This study provides an insight into impaired angiogenesis observed in SSc patients by evaluating *in vitro* cardiovascular differentiation of SSc iPSC.

**Keywords:** Angiogenesis, Cardiomyocyte, Induced Pluripotent Stem Cells, Systemic Sclerosis, VE-Cadherin

Cell Journal (Yakhteh), Vol 23, No 3, August 2021, Pages: 273-287

**Citation:** Gholami S, Mazidi Z, Pahlavan S, Moslem F, Hosseini M, Taei A, Hesaraki M, Barekat M, Aghdami N, Baharvand H. A novel insight into endothelial and cardiac cells phenotype in systemic sclerosis using patient-derived induced pluripotent stem cell. Cell J. 2021; 23(3): 273-287. doi: 10.22074/cellj.2021.7244. This open-access article has been published under the terms of the Creative Commons Attribution Non-Commercial 3.0 (CC BY-NC 3.0).

## Introduction

Systemic sclerosis (SSc) develops as a chronic connective tissue disease which involves multiple organs; however, its etiology remains unknown. It is characterized by vascular injury, immune dysregulation and extensive fibrosis of several organs including the skin (1). The complex pathogenesis of SSc remains unclear, however it is known that genetic, epigenetic and environmental factors contribute to its development (2). Endothelial cell (EC) injury is one of the first phases in pathogenesis of SSc. The damaged endothelium upregulates the expression of adhesion molecules and chemokines resulting in recruitment of inflammatory cells. Multiple cytokines and growth factors, secreted by inflammatory and immune cells, promote activation and differentiation of resident fibroblasts into myofibroblasts, which cause excessive

extracellular matrix (ECM) proteins production leading to fibrosis. Thus, suggested pathogenesis of SSc includes a complex interplay between vascular abnormality, inflammation and autoimmunity, as well as fibrosis (3).

Clinical and *in vitro* studies demonstrated an impaired angiogenesis in SSc. Moreover, several studies suggested that ECs might be the origin of a subset of activated fibroblasts or myofibroblasts. Furthermore, endothelial-mesenchymal transition (EndoMT) and their differentiation into collagen-producing cells are likely to represent an additional source of extra collagen (4).

In addition to vascular complications, many cases of heart phenotypes have been reported in SSc which accounts for 11-36% mortality in these patients (5). Cardiac manifestation of SSc can be caused directly

by a myocardial involvement developing to myocardial fibrosis or indirectly by pulmonary arterial hypertension or systemic hypertension as the possible outcome of pulmonary and renal involvements (6). Not only the heart wall including epicardium, myocardium and endocardium, but also coronary arteries, cardiac valves and nervous system may be affected in SSc leading to heart failure (7). A meta-analysis done by Komócsi et al. (8), confirmed that cardiopulmonary manifestation is the main cause of mortality in SSc patients. Despite cohort studies suggesting a decline in mortality risk of SSc, a meta-analysis of cohort studies, conducted by Elhai et al. (9) reported no substantial changes in standardized mortality ratio (SMR) over 40 years.

Over the last decade, molecular studies-based clinical trials provided more knowledge on the pathogenesis of scleroderma (10), however, further investigations are still needed. Such molecular studies require appropriate animal or cell-based models recapitulating scleroderma phenotype. Patient-specific induced pluripotent stem cells (iPSCs) allow us to examine the disease phenotype in target tissue as well as other cell types of body (11). In the present study, we produced iPSC from skin biopsies of two SSc patients and characterized them followed by cardiogenic differentiation into cardiomyocytes (CMs) and ECs and their characterization.

## Materials and Methods

### Generation of patient-specific induced pluripotent stem cells

In this experimental study, human dermal fibroblasts of SSc patients were digested using 0.1% collagenase I (Sigma, USA) and cultured in fibroblast medium (Dulbecco's modified Eagle's medium [DMEM, Gibco, USA]) enriched with 10% fetal bovine serum (FBS, Gibco, USA) and 1% penicillin and streptomycin (Gibco, USA), as previously described (12). Institutional review board approval by Royan Institute Ethics Committee's general principles in compliance with the declaration of Helsinki (IR ACECR, ROYAN REC, 1395 175) and consent from patients for iPSC derivation, were obtained. The clinical features of the SSc patients are shown in Table S1 (See Supplementary Online Information at [www.celljournal.org](http://www.celljournal.org)). To generate patient-specific iPSC, dermal fibroblasts were reprogrammed by four Yamanaka factors (*OCT4*, *SOX2*, *KLF4*, and *c-MYC*) delivered by retrovirus in serum- and feeder-free conditions based on a previously reported protocol (12). On transduction day 6, fibroblast medium was exchanged with human embryonic stem cell (hESC) medium supplemented with 100 ng/ml basic fibroblast growth factor (bFGF, Royan Biotech, Iran). hESC medium was comprised of DMEM/F12 (Gibco, USA) supplemented with 20% Knockout serum replacement (KOSR, Gibco, USA), 1% non-essential amino acids (Gibco, USA), 1% penicillin and streptomycin, 2 mM L-glutamine (Gibco, USA) and 0.1 mM  $\beta$ -mercaptoethanol (Sigma, USA). At day 14-20 of re-plating, embryonic stem cells (ES)-

like colonies were observed (Fig. 1A). For each patient, three iPSC clones were established for subsequent analyses. Due to same characteristics, we followed our experiment on one clone for each patient. Two control iPSC lines, one derived from a healthy Iranian 40-year-old male (iPSC4 abbreviated as C1) (12) and the other obtained from a healthy Iranian 32-year-old female (B-iPSC11 abbreviated as C2) (13) were acquired from the Stem Cell Bank of Royan Institute. Following thawing, iPSC was cultured on mitomycin C-treated mouse embryonic fibroblast (MEF) feeder cells in hESC medium supplemented with 5 ng/ml bFGF. For expansion, iPSCs were passaged on ECM Gel (Sigma, USA, 1:30) using collagenase IV (0.5 mg/ml, Gibco, USA): dispase (1 mg/ml, Gibco, USA) at the ratio of 1:2.

### Karyotype analysis

Karyotyping was performed at cytogenetic laboratory of the Institute for Human Genetics (Royan Institute, Iran) according to a standard procedure described previously (14). Briefly, 70% confluent human iPSC (hiPSC) colonies were treated with 0.66  $\mu$ M thymidine (Sigma-Aldrich, USA) at 37°C overnight. Then, cells were washed and rested for 5 hours before being exposed to colcemid (Gibco, USA, 0.15  $\mu$ g/ml) for 30 minutes. Afterwards, trypsinized cells were treated with 0.075 M KCl and fixed. Karyotyping was performed using standard G-band staining.

### In vitro spontaneous differentiation of human induced pluripotent stem cells

To evaluate the spontaneous differentiation capacity of the above-noted derived hiPSC lines into three embryonic germ layers, we generated embryoid body (EB). Briefly, hiPSC colonies were dispersed into single cells using Accutase (Sigma, USA) and transferred into non-adhesive bacterial plates (Greiner Bio-One, Germany) containing DMEM/F12 medium supplemented with 20% KOSR, 1% non-essential amino acids, 2 mM L-glutamine, and 0.1 mM  $\beta$ -mercaptoethanol without bFGF. After 12 days, the generated EBs were plated on ECM Gel-coated culture dishes for another 8 days. On day 21 of spontaneous differentiation, EB samples were collected and ectoderm, mesoderm and endoderm differentiation were evaluated with respect to transcriptional expression of each germ layer's specific genes using quantitative real-time polymerase chain reaction (qRT-PCR).

### Teratoma formation

SSc iPSC ( $2 \times 10^6$ ) were suspended in phosphate-buffered saline (PBS) and injected into the subrenal capsule of 8-week-old NOD/SCID mice (BioLASCO) using a 26-gauge syringe (BD Biosciences, USA). Eight weeks after injection, tumors were harvested, weighed and fixed in 10% formalin. After fixation, tumors underwent histological analyses for ectoderm, mesoderm and endoderm formation.

## Immunofluorescence and alkaline phosphatase staining

Cells were fixed in 4% paraformaldehyde at room temperature (RT) for 25 minutes, washed with PBS/0.05% Tween 20 and permeabilized using 0.5% Triton X-100 in PBS for 30 minutes at RT. Thereafter, cells were washed and blocked in blocking solution (1% bovine serum albumin [BSA, Life Technology] in PBS) for 1 hour at RT. Primary antibodies were diluted in blocking solution and added to the cells overnight at 4°C. Cells were then washed three times with PBS/0.05% Tween 20, each time for 5 minutes, and incubated with appropriate secondary antibodies in blocking solution for 45 minutes at RT. Lastly, cells were washed three times with PBS/0.05% Tween 20 and nuclei were counterstained with 4',6-diamino-2-phenylindole (DAPI, Sigma, USA). Images were captured using a fluorescent microscope (IX71, Olympus, Japan). Antibodies used in the present study are mentioned in Table S2 (See Supplementary Online Information at [www.celljournal.org](http://www.celljournal.org)).

We performed Alkaline phosphatase (ALP) staining based on the manufacturer's instructions (Sigma, USA).

## Cardiac and endothelial differentiation of human induced pluripotent stem cells

hiPSC colonies were dispersed into single cells by 4-5 minutes treatment with Accutase (Sigma-Aldrich, USA) at 37°C and incubated in non-adhesive bacterial plates (Greiner Bio-One, Germany) at the density of  $2 \times 10^5$  cells/ml in hESC medium. After aggregate formation, the directed cardiogenic differentiation of hiPSC was performed in static suspension culture using a cocktail of small molecules (SM) as previously described (15). Briefly, hiPSC aggregates with average diameter of  $175 \pm 25 \mu\text{m}$  were treated with 12  $\mu\text{M}$  of SM CHIR99021 (CHIR, Stemgent, USA) in differentiation medium (RPMI 1640 (Gibco, USA) supplemented with 2% B27 without retinoic acid (Gibco, USA), 2 mM L-glutamine (Gibco, USA), 0.1 mM  $\beta$ -mercaptoethanol (Sigma, USA), 1% nonessential amino acids (Gibco, USA), 1% penicillin and streptomycin). After 24 hours, aggregates were washed with Dulbecco's PBS (DPBS, Gibco, USA) and maintained in fresh differentiation medium for 24 hours. On differentiation day 2, the medium was changed with new differentiation medium containing 5  $\mu\text{M}$  IWP2 (Tocris Bioscience, UK), 5  $\mu\text{M}$  SB431542 (Sigma-Aldrich, USA) and 5  $\mu\text{M}$  purmorphamine (Pur, Stemgent, USA) for 48 hours. On day 4, the aggregates were washed with DPBS and cultured in fresh differentiation medium which was refreshed every 2 or 3 days. In order to determine the efficiency of cardiac differentiation, we counted the number of beating spheroids on a daily basis, starting with the first beating observation, using an inverted cell culture microscope (Olympus, Japan). For CM immunostaining, the 30-day-post-differentiation beating spheroids were subjected to enzymatic digestion by 4-5 min treatment with Accutase at 37°C followed by gentle pipetting and plated at the density of  $8 \times 10^4$  cell/

$\text{cm}^2$  on ECM-Gel (Sigma, USA, 1:30) coated 4-well tissue-culture plate in differentiation medium. After adequate cell attachment, CM were fixed and all steps of immunofluorescence staining were taken as described in supplementary material.

For endothelial differentiation, we used a previously reported protocol with some modifications (16). hiPSC aggregates with average diameter of 200-250  $\mu\text{m}$  were treated with 12  $\mu\text{M}$  of CHIR99021 in RPMI medium supplemented with B27 without retinoic acid for 24 hours. Cells were then incubated in RPMI/B27 without SM for another 24 hours. On day 2 of differentiation, cells were treated with 25 ng/ml BMP4 (R&D), 10  $\mu\text{M}$  Purmorphamine, 10  $\mu\text{M}$  SB431542 and 50 ng/ml VEGF-A (Royan-Biotech, Iran) in RPMI/B27 medium for 48 hours. Next, the medium was exchanged with EGM-2 (Lonza, Switzerland) supplemented with 50 ng/ml VEGF-A and cells were incubated for another 48 hours. On day 6, differentiated aggregates were dispersed into single cells using Accutase and sorted based on KDR expression (R&D, USA). KDR<sup>+</sup> sorted cells were sub-cultured on collagen type I-coated plates (10  $\mu\text{g}/\text{cm}^2$ , Sigma-Aldrich, USA) in EGM-2 medium containing 50 ng/ml VEGF-A until reaching appropriate confluency.

## Gene expression analyses

Total RNA was extracted using TRIzol reagent (Sigma-Aldrich, USA). To prevent DNA contamination, extracted RNA was treated with RNase-free DNase I (Takara, Japan). cDNA synthesis was performed using a PrimeScript™ RT Reagent Kit (Perfect Real Time) (Takara, Japan) based on the manufacturer's instructions and qRT-PCR was performed using a SYBR Premix Ex Taq Kit (Takara Bio, Inc, Japan) and a Rotor Gene Corbett System (Corbett Life Science, Australia). Results were analyzed by Rotor-Gene 6000 analysis software (Corbett Life Science, Australia, version 1.7). All experiments were done in triplicate. The relative gene expression level of the desired genes was calculated by  $\Delta\Delta\text{CT}$  method and normalized against the housekeeping gene, glyceraldehyde 3-phosphate dehydrogenase (*GAPDH*). All primer sequences used in the present work, are listed in Table S3 (See Supplementary Online Information at [www.celljournal.org](http://www.celljournal.org)).

## Flow cytometry and cell sorting

Differentiated hiPSC aggregates were collected at particular time-points of differentiation and dissociated into single cells using Accutase solution and 0.05% trypsin/ ethylenediaminetetracetic acid (Gibco, USA) for hiPSC-CM and hiPSC-EC, respectively. Then, single cells were fixed by treatment with 4% paraformaldehyde for 20 minutes at 4°C. After washing with PBS/0.05% Tween 20, the fixed cells were permeabilized by 0.2% Triton X-100 in PBS for 30 minutes at RT, blocked in serum and stained, either 1 hour for surface markers or overnight for cytoplasmic markers, with appropriate primary antibodies at 4°C. Cells were then washed and

incubated with appropriate secondary antibody for 1 hour at RT. Cells were analyzed using a BD FACS Calibur flow cytometer (BD Biosciences, USA). Data analysis was done by Flowing Software (version 2.5.1, Turku Centre for Biotechnology, Finland).

For sorting, cells were dissociated into single cells using 0.05% trypsin/EDTA on day 6 of endothelial differentiation. Cells were then washed in PBS containing 2% FBS (FACS buffer) and incubated with anti-human KDR for 1 hour at 4°C. After washing, KDR-positive cells were sorted using FACS Calibur.

### **Uptake of acetylated low-density lipoprotein (Dil-ac-LDL)**

ECs were incubated with 10 µg/ml of acetylated low-density lipoprotein (Dil-Ac-LDL, Biomedical Technology, UK) for 4 hours at 37°C. Then, cells were fixed by treatment with 4% paraformaldehyde for 10 minutes at RT. After washing with PBS, nuclei were counterstained with DAPI (DAPI, Sigma, USA) and visualized using a fluorescence microscopy (IX71; Olympus, Japan).

### **Tube formation assay**

ECMatrix™ (*In Vitro* Angiogenesis Assay Kit, Chemicon, USA) was aliquoted into all wells of a 96-well plate (50 µl/well) and incubated for 1-2 hour at 37°C to polymerize. Thereafter, 10<sup>4</sup> cells/well were seeded onto the matrix in 150 µl of EGM-2 medium and incubated for 2 hours at 37°C with 5% CO<sub>2</sub>. Tube formation was assessed using Olympus CKX41 inverted microscope and analyzed using “Image J” software.

### **Multielectrode array recording**

A multielectrode array (MEA) data acquisition system (Multi Channel Systems, Reutlingen, Germany) was used to record the extracellular field potential (FP) of hiPSC-CM. The MEA plate is composed of 60 titanium nitride electrodes with an inter-electrode space of 200 µm. Beating spheroids were plated on ECM Gel-coated MEA plates and allowed to attach for 48-72 hours before recording. Baseline FP recording and drug testing were performed 30 ± 5 days post-differentiation. On the day of the experiment, the MEA plates were connected to a head stage amplifier. FP was acquired at 2 kHz, and all recordings were performed at 37°C. Signals were recorded for 60 seconds at baseline and 5 minutes after drug application. All drugs were purchased from Sigma-Aldrich, otherwise stated. Stock solutions were prepared daily in appropriate solvent and used at desired concentrations made in RPMI/B27 medium. Data were analyzed by Cardio2D software (version 2.2.2.0, Multi-channel system MCS GmbH). FP durations (FPD) was normalized to beating rate using the Bazett correction formula (corrected FPD [cFPD]=FPD/<sup>√</sup>(RR interval)). Drugs used in pharmacological studies are listed in Table S4 (See Supplementary Online Information at [www.celljournal.org](http://www.celljournal.org)).

### **Whole cell patch-clamp recording**

Action potential (AP) was recorded from spontaneously beating hiPSC-CM using the current-clamp mode of the whole cell patch-clamp configuration. On differentiation day 30, beating spheroids were dissociated into single cells by Accutase accompanied by gentle pipetting. Single beating CM were plated onto ECM-Gel coated glass coverslips and incubated at 37°C overnight. Then, the cover slips were transferred to a recording chamber mounted on the stage of an Olympus inverted microscope (Olympus, Japan). The bath solution within the chamber contained 135 mM NaCl, 5.4 mM KCl, 10 mM HEPES, 10 mM D-glucose, 1 mM MgCl, and 1.8 mM CaCl<sub>2</sub> and the pH was adjusted to 7.4 using NaOH. Recording pipettes were pulled from borosilicate glass capillaries (Harvard Apparatus, Holliston, MD) by a P-97 horizontal puller (Sutter Instrument, Novato) to a tip resistance of 3-6 MΩ. The pipette solution contained 135 mM KCl, 10 mM NaCl, 1 mM EGTA, 10 mM HEPES, and 5 mM MgATP, and the pH was adjusted to 7.2 using KOH.

Data were acquired using a multiclamp 700B amplifier (Axon Instruments, Molecular Devices Corp., Union City, CA, USA), a Digidata 1440 analog-to-digital board and pClamp 10 software (Axon Instruments), at a sampling frequency of 10 kHz and low-pass filtered at 2 kHz. Data analysis was performed using Clampfit 10 (Axon Instruments) and Prism 6 (GraphPad Software, La Jolla, CA, USA) software.

### **Ca<sup>2+</sup> imaging**

In order to record Ca<sup>2+</sup> transients in hiPSC-CM, beating spheroids were incubated with 1 µM Fura-2 AM (Sigma-Aldrich, USA) for 30 minutes at 37°C, 30-day post-differentiation. Then, beating spheroids were washed with RPMI/B27 medium for 15 minutes at 37°C. Afterwards, Ca<sup>2+</sup> imaging was performed using a fluorescent microscope (IX71, Olympus, Japan) equipped with a DP72 digital camera (Olympus, Japan) and analyzed in a custom-made Matlab macro. Calcium transient amplitude and calcium transient duration at 80% decay (CTD80) were calculated. In order to study the Ca<sup>2+</sup> content of sarcoplasmic reticulum (SR), rapid puffs of 10 mM caffeine were applied and Ca<sup>2+</sup> release was imaged. Fractional Ca<sup>2+</sup> release (FCR) from the stores was calculated as the ratio of the amplitude of Ca<sup>2+</sup> transient to the amplitude of the caffeine-induced Ca<sup>2+</sup> release.

### **Statistical methods**

All data are presented as mean ± SEM from at least three independent biological replicates for each hiPSC line. Comparisons were made by analysis of variance (ANOVA, one-way and two way) or unpaired t test when appropriate, using GraphPad Prism version 6.01 (GraphPad Software, La Jolla California, USA) and considered significant when P<0.05.

### **Data availability**

The datasets generated during and/or analysed during the current study are available from the corresponding author on reasonable request.

## Results

### Systemic sclerosis fibroblasts were successfully reprogrammed to pluripotency *in vitro*

To generate SSc iPSC, primary fibroblasts were obtained from skin biopsy of each patient following receiving an informed written consent. Cells were reprogrammed with Yamanaka factors using retroviral vectors. After 20 days, hESC-like colonies were picked and expanded for characterization (Fig.1A). Both SSc iPSC lines revealed strong ALP activity (Fig.1A) and expressed major hESC-specific markers (OCT4, NANOG, TRA-1-60, and TRA-1-81, Fig.1B). Furthermore, a normal karyotype was determined for both SSc iPSC lines (S1-iPS2 and S2-iPS3) indicating chromosomal stability during iPSC generation (Fig.1C). To further confirm reprogramming to pluripotency, the expression of *OCT4* and *NANOG* was evaluated which revealed that both S1-iPS2 and S2-iPS3 expressed endogenous *OCT4* and *NANOG* (Fig.1D). In addition, qRT-PCR analysis showed silencing of exogenous genes (*OCT4*, *c-MYC*, *KLF4* and *SOX2*) in derived S1-iPS2 and S2-iPS3 (Fig. S1, See Supplementary Online Information at [www.celljournal.org](http://www.celljournal.org)). Differentiation potency of S1-iPS2 and S2-iPS3 into embryonic germ layers was evaluated by EB formation. To achieve that, iPSC were cultured in suspension for 12 days to form EB in the absence of bFGF and then transferred to ECM Gel-coated dishes for another 8 days. RT-PCR analyses demonstrated that ectoderm (*PAX6* and *TAU*), mesoderm (*Brachyury*) and endoderm (*ALB* and *FOXA2*) specific markers were only expressed in differentiated S1-iPS2 and S2-iPS3 but not in undifferentiated state (Fig.1E). Furthermore, spontaneous differentiation of iPSC lines resulted in the development of ectoderm, mesoderm and endoderm cells as reflected by upregulation of *SOX1/PAX6*, *MESP1/Brachyury* and *FOXA2/AFP* genes as specific markers of each germ layer, respectively (Fig.S2, See Supplementary Online Information at [www.celljournal.org](http://www.celljournal.org)). Moreover, SSc iPSC were transplanted into the subrenal capsule of 5-week-old NOD mice. After about 7 weeks, teratoma was formed, harvested and subjected to immunohistochemistry analyses. Our results demonstrated the presence of cartilage (mesoderm), gut-like epithelium (endoderm) and neural rosette (ectoderm) tissues in teratoma which further confirmed stemness of iPSC (Fig.1F). Altogether, these data showed that SSc fibroblasts were successfully reprogrammed to pluripotency.

### Systemic sclerosis induced pluripotent stem cells were successfully differentiated into endothelial progenitor cells

hiPSC lines were differentiated to ECs by a cocktail of growth factors and SMs (Fig.2A). Cells were collected on days 0, 1, 4, 6 and 8 of differentiation in order to evaluate the expression of endothelial genes and proteins. The highest level of *Brachyury* transcriptional expression was observed on day 1 (Fig.2B). The expression of *KDR* was substantially increased on day 6 of differentiation in

iPSC lines ( $40.3 \pm 7$ ,  $26.4 \pm 8$  and  $15.9 \pm 0.6$  fold increase compared to undifferentiated state in C1-EC, S1-EC and S2-EC, respectively, Fig.S3A, See Supplementary Online Information at [www.celljournal.org](http://www.celljournal.org)). Flow cytometry analyses indicated that almost 30% of cells were KDR-positive (Fig.2C) implicating their identical potential for endothelial progenitor cells (EPC) generation. Although the percentage of KDR expressing cells was similar in C1-EC and both SSc iPSC lines-derived EC, the levels of expression were reduced in SSc-ECs (Fig.S3B, See Supplementary Online Information at [www.celljournal.org](http://www.celljournal.org)).

### Systemic sclerosis induced pluripotent stem cells-derived endothelial cells showed defective angiogenesis

KDR-positive cells were sorted on day 6 and cultured in VEGF-A supplemented media on collagen I-coated plates to confluency (Fig.2A). Expression of *CD31* (*PECAM-1*) as a late endothelial marker was substantially upregulated on differentiation day 8 ( $60.5 \pm 10$ ,  $79.2 \pm 11$  and  $63.4 \pm 6$  fold increase compared to undifferentiated state in C1-EC, S1-EC and S2-EC, respectively) which was followed by a fairly similar protein expression pattern ( $90.5 \pm 1\%$ ,  $93.5 \pm 1\%$  and  $87.7 \pm 4\%$  in C1-EC, S1-EC and S2-EC, respectively) (Fig.2D, E). Relative expression of *CD31* on differentiation day 8 was similar in iPSC lines-derived EC (Fig.S3B, See Supplementary Online Information at [www.celljournal.org](http://www.celljournal.org)). In contrast, while *VE-cadherin* (*CD144*) expression in C1-EC peaked on differentiation day 8, neither S1-EC nor S2-EC showed upregulation of this endothelial specific marker (Fig.2F, G). C1-EC exhibited 87-fold rise in *VE-cadherin* expression during differentiation and 91.7% of C1-EC were positive for VE-cadherin. However, no more than 8.6 and 3.9% of differentiated S1-iPS2 and S2-iPS3 were CD144<sup>+</sup>, respectively. Immunostaining for CD31 and CD144 showed a similar pattern to that for gene expression and further confirmed the protein expression results obtained from flow cytometry analyses. Furthermore, ECs derived from both C1- and SSc iPSC, expressed endothelial marker vWF (von Willebrand factor) in a similar manner (Fig.2H). To evaluate the functional characteristics of differentiated ECs, the ability to uptake acetylated low-density lipoprotein (AcLDL) as well as tube formation potential was examined. Both SSc iPSC-derived EC (SSc-EC) revealed strong AcLDL uptake capacity when incubated with these lipoprotein particles (Fig.3A). However, these ECs failed to form tubes (Fig.3B). While C1-EC developed vessel-like tubes with around  $70 \pm 5$  tubes/field, 134.3 branch points/field and mean tube area of  $0.12 \text{ mm}^2$  (Fig.3C-E, respectively), the number of well-formed tubes were substantially decreased to  $10 \pm 7$  and  $13 \pm 3$  tubes/field in S1- and S2-EC, respectively (Fig.3C). This characteristic was also projected into a marked reduction in the number of branch points as well as smaller tube areas when tube formation ability of SSc-EC was assessed (Fig.3D, E). These results suggested a defective angiogenic capacity for SSc-EC.

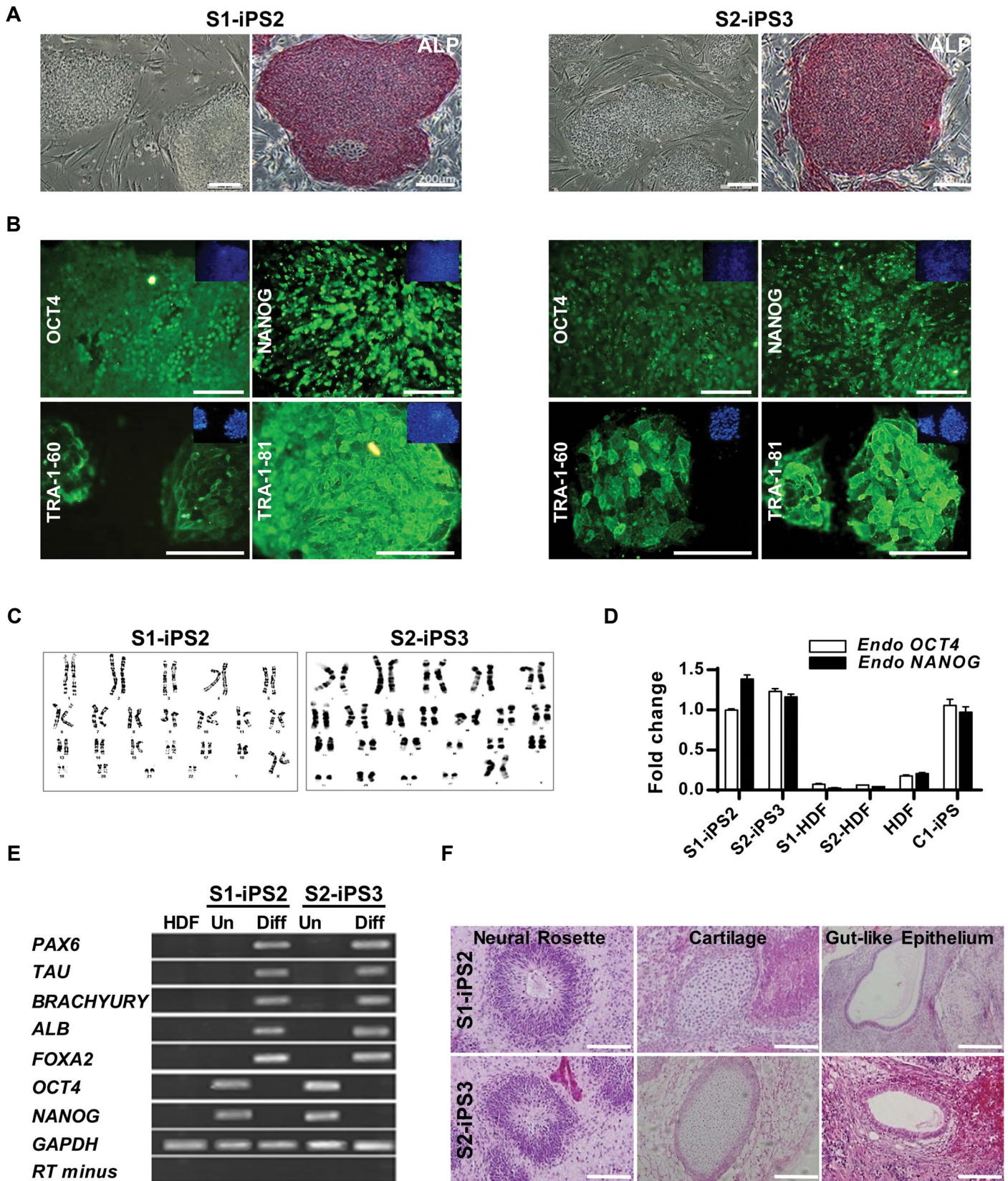


**Fig.1:** Characterization of established SSC iPSC. **A.** Phase contrast microscopy of established SSC iPSC clones [S1-iPS2 (patient 1) and S2-iPS3 (patient 2)] and ALP staining of derived iPSC (scale bar: 200  $\mu$ m). **B.** Immunofluorescence staining demonstrated the expression of pluripotency markers (OCT4, NANOG, TRA-1-60 and TRA-1-81) in derived iPSC. Nuclei were counterstained with DAPI (scale bar: 100  $\mu$ m). **C.** Both S1-iPS2 and S2-iPS3 lines maintained normal karyotype. **D.** qRT-PCR analysis showed endogenous *OCT4* and *NANOG* expression in SSC iPSC to levels similar to those of healthy control-iPSC (C1-iPSC) while were silent in the HDF. Fold change was calculated by  $\Delta\Delta$ Ct method and expression of each gene was normalized against *GAPDH*. **E.** RT-PCR analyses indicated the expression of differentiation markers for the three germ layers by EB-mediated differentiation (Diff) in comparison with undifferentiated state (Un), and **F.** Tissue morphology of teratoma derived from SSC iPSC (scale bar: 100  $\mu$ m). Data are represented as mean  $\pm$  SEM, n=3 (biological replicate). SSC; Systemic sclerosis, iPSC; Induced pluripotent stem cells, ALP; Alkaline phosphatase, qRT-PCR; Quantitative real-time polymerase chain reaction, HDF; Human dermal fibroblasts, and EB; Embryoid body.

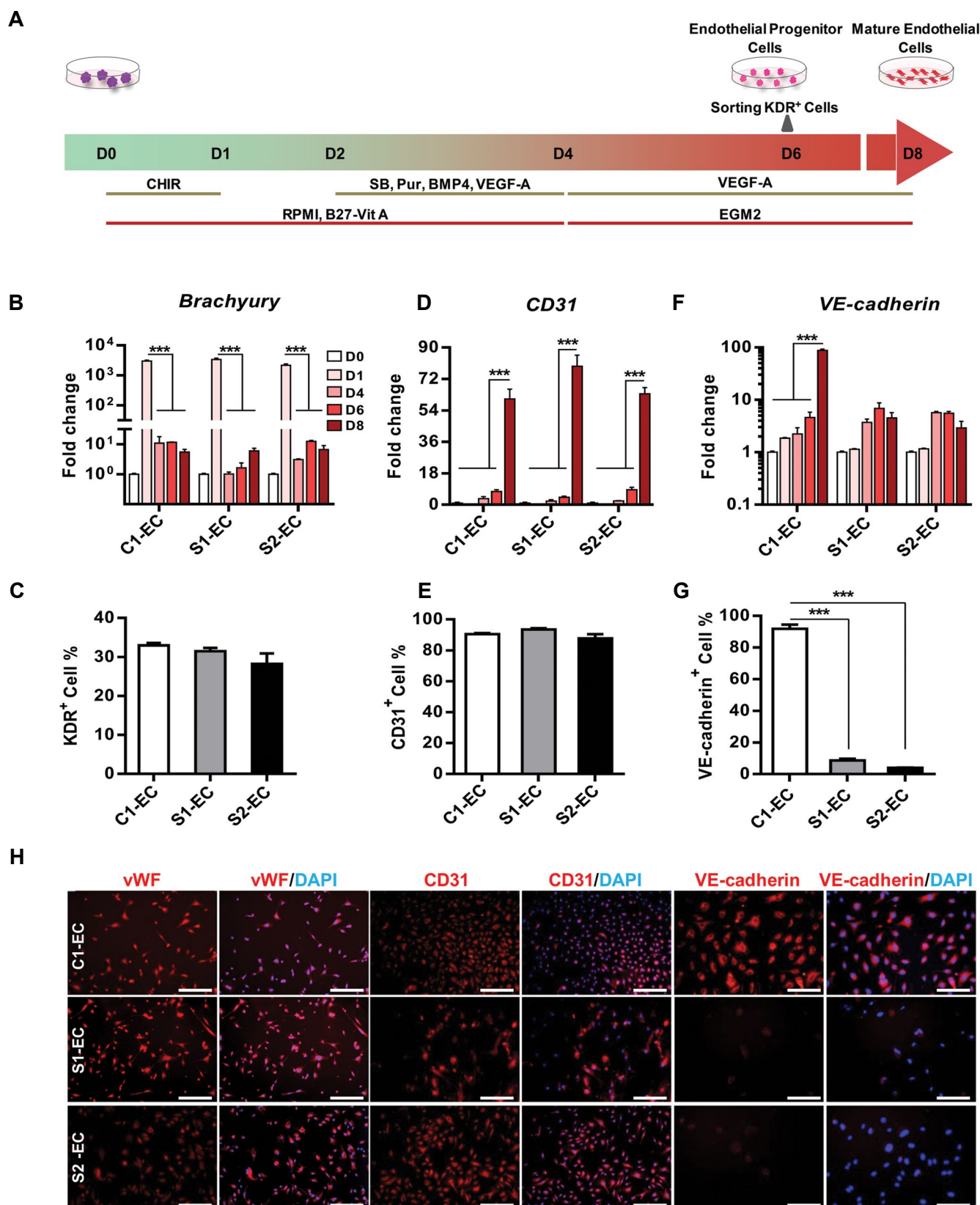


**Fig. 2:** Differentiation of SSc iPSC toward endothelial lineage. **A.** A schematic diagram illustrating the endothelial differentiation protocol in which growth factors and small molecules were used, **B.** The relative expression of *Brachyury* gene during differentiation as assessed by qRT-PCR, **C.** Flow cytometry analysis of KDR expression on differentiation day 6 demonstrated no significant difference between SSc-EC and C1-EC, **D.** Similar expression of *CD31* at mRNA and E. At protein levels in iPSC-derived EC, **F.** qRT-PCR analysis demonstrated that *VE-cadherin* was significantly downregulated in SSc-EC compared to C1-EC. The expression of each gene was normalized against *GAPDH*. The relative expression was calculated by  $\Delta\Delta Ct$  method (undifferentiated state "D0" was set at 1), **G.** Expression level of VE-cadherin protein was measured by flow cytometry, and **H.** Immunofluorescence staining demonstrated the expression of vWF, CD31 and VE-cadherin in iPSC-derived EC. Nuclei were counterstained with DAPI (scale bar: 100  $\mu$ m). All data are represented as mean  $\pm$  SEM. Comparisons were made by one-way and two-way analysis of variance (\*\*\*,  $P < 0.001$ ). SSc; Systemic sclerosis, iPSC; Induced pluripotent stem cells, qRT-PCR; Quantitative real-time polymerase chain reaction, VE; Vascular endothelial, EC; Endothelial cells, C1-EC; Healthy control iPSC-EC, S1-EC; SSc1 iPSC2-EC, and S2-EC; SSc2 iPSC3- EC.  $n \geq 3$  (biological replicate) for all experiments.

Downregulation of VE-cadherin and inability to form tubular network in SSc-derived ECs led us to examine VE-cadherin signaling and regulation. VE-cadherin/ $\beta$ -catenin signaling regulates the expression of matrix metalloproteinases (MMPs) in ECs during angiogenesis (17). The importance of MMPs in angiogenesis as well as possible angiogenesis-related changes in the expression of MMPs and VE-cadherin, was reported previously (18). In our *in vitro* differentiated SSc-ECs, while the expression of *MMP1* was 2.4-fold upregulated in S1-EC, *MMP9* expression showed 12-fold decrease compared to C1-EC, suggesting a dysregulation of *MMP1* and *MMP9* expression in S1-EC (Fig.3F). Scleroderma vessels have abnormal ECs which express regulator of G protein signaling 5 (*RGS5*), a protein associated with vascular rarefaction, but lack normal VE-cadherin expression (19). Interestingly, relative expression of *RGS5* was similar in C1- and S1-EC characterized in this study (Fig.3F). Moreover, the relative expression of *endothelin 1* (*EDN1*), which is involved in vascular remodeling of SSc (20), showed similar pattern in S1- and C1-EC (Fig.3F).

Multiple mechanisms are involved in regulation of VE-cadherin including mammalian target of rapamycin (MTOR) and phosphoinositide-3 kinase (PI3K) signaling (21). In order to address the mechanism involved in the downregulation of VE-cadherin in S1-EC, the expression of PI3KCA (PI3K catalytic subunit alpha) and MTOR was assessed in iPSC-derived EC. Transcriptional analyses showed significant upregulation of *MTOR* and *PI3KCA* in S1-EC compared to C1-EC. Furthermore, the expression of *SNAIL*, a transcriptional repressor of VE-cadherin, was markedly increased in SSc-EC, indicating the possible role of *SNAIL* in downregulation of *VE-cadherin* (Fig.3F).

### Systemic sclerosis induced pluripotent stem cells could generate functional cardiomyocytes

iPSC lines were subjected to cardiomyocyte differentiation in static suspension culture using a SM-based protocol (Fig.4A) which resulted in generation of spontaneously beating spheroids on day 7 that expanded to about 90% of spheroids on differentiation day 10. The ratio of beating spheroids was calculated daily and plotted for all three hiPSC lines (Fig.4B); this ratio peaked on day 10 ( $93.6 \pm 1$ ,  $89.6 \pm 0.9$  and  $90 \pm 1.1\%$  for healthy control iPSC-derived cardiomyocytes [C2-CM], S1-CM and S2-CM, respectively) showing their similar cardiac differentiation potency. The efficiency of cardiogenic differentiation was evaluated in C2 and SSc iPSC by assessing the gene and protein expression of cardiac specific markers (Fig.4C-E). All C2-iPSC, S1-iPSC2 and S2-iPSC3 derived CM expressed cardiac specific genes encoding cardiac structural proteins namely; *TNNT2* (cardiac type of troponin), *MYL2* (myosin light chain 2) and *MYH* (myosin heavy chain), encoding calcium handling proteins; *SERCA* (sarco/endoplasmic reticulum  $Ca^{2+}$ -ATPase), *SLC8A1* (solute carrier family 8 of member A1), *CACNA1C* (calcium voltage-gated channel), *RYR2* (ryanodine receptor), *TRDN* (Triadin) and *CASQ* (calsequestrin), and encoding ion channels; *KCNH2* (potassium voltage-gated channel). While *MYL2*, *MYH6* and *MYH7* were upregulated in S1-CM, relative

expression of these contractile apparatus-related genes were similar in S2-CM and C2-CM (Fig.4C). Furthermore, *MYH6/MYH7* ratio was decreased by 4- and 2-fold in S1-CM and S2-CM, respectively compared to C2-CM. While expression of *CASQ2* and *KCNH2* was substantially higher in S1-CM, *RYR2* expression was markedly elevated in both S1- and S2-CM. On the other hand, expression levels of other genes encoding calcium handling proteins (*CACNA1C*, *TRDN*, *SERCA*, and *SLC8A1*) were similar in all three hiPSC-derived CM. Protein expression of cTNT showed a similar pattern to that of its gene expression as reflected in immunostaining images; also, both SSc and C2 iPSC lines generated similar abundance of cTNT<sup>+</sup> CM (Fig.4D, E). Altogether, these results indicated that SSc iPSC and healthy control iPSC have the same cardiogenic differentiation potential.

### Systemic sclerosis induced pluripotent stem cells-derived CM revealed normal excitation-contraction coupling

To evaluate the functional properties of differentiated CM, two components of excitation-contraction coupling were studied. FPs generated by spontaneously beating spheroids were recorded to study the electrophysiological properties of SSc and C2-CM (Fig.5A). All differentiated CM derived from either SSc iPSC or control iPSC, showed a normal beating frequency of about 65 beats per minute (bpm) (Fig.5B). FP duration (FPD) which provides information on the repolarization phase of cardiomyocytes' excitation and has been reported to be well correlated with AP duration obtained from a single cardiomyocyte (22), did not differ between SSc- and C2-derived cardiac spheroids (Fig.5C). Furthermore, single spontaneously beating CM were evaluated for their AP. Two types of AP, one specific for working CM and the other specific for nodal-like cells, were observed in C2-CM, S1-CM and S2-CM (Fig.5D). Various AP parameters such as maximal diastolic potential (MDP), upstroke velocity ( $V_{max}$ ) and AP duration at different time-points of repolarization ( $APD_x$ ) as well as  $APD_{90}/APD_{50}$  ratio were used for AP classification (23). Analysis of AP parameters showed that working CM were highly frequent in both C2- and SSc iPSC-derived CM (Fig.5E-K). Electrophysiological characteristics of iPSC-derived CM are summarized in Tables S5 and S6 (See Supplementary Online Information at [www.celljournal.org](http://www.celljournal.org)).

$Ca^{2+}$  transients as another component of excitation-contraction coupling was characterized in C2-CM, S1-CM and S2-CM.  $Ca^{2+}$  transient amplitude (Fig. S4A,B, See Supplementary Online Information at [www.celljournal.org](http://www.celljournal.org)) and CTD80 did not significantly differ between patient-specific and healthy CM (Fig. S4C, See Supplementary Online Information at [www.celljournal.org](http://www.celljournal.org)). Furthermore, fractional  $Ca^{2+}$  release which represents the ratio of active intracellular  $Ca^{2+}$  bulk to whole intracellular  $Ca^{2+}$ , did not vary between C1-CM, S1-CM and S2-CM (Fig.S4D, See Supplementary Online Information at [www.celljournal.org](http://www.celljournal.org)). Fractional  $Ca^{2+}$  release is basically defined as the ratio of the excitation-induced  $Ca^{2+}$  release to caffeine-induced  $Ca^{2+}$  release which depletes all intracellular  $Ca^{2+}$  stores.

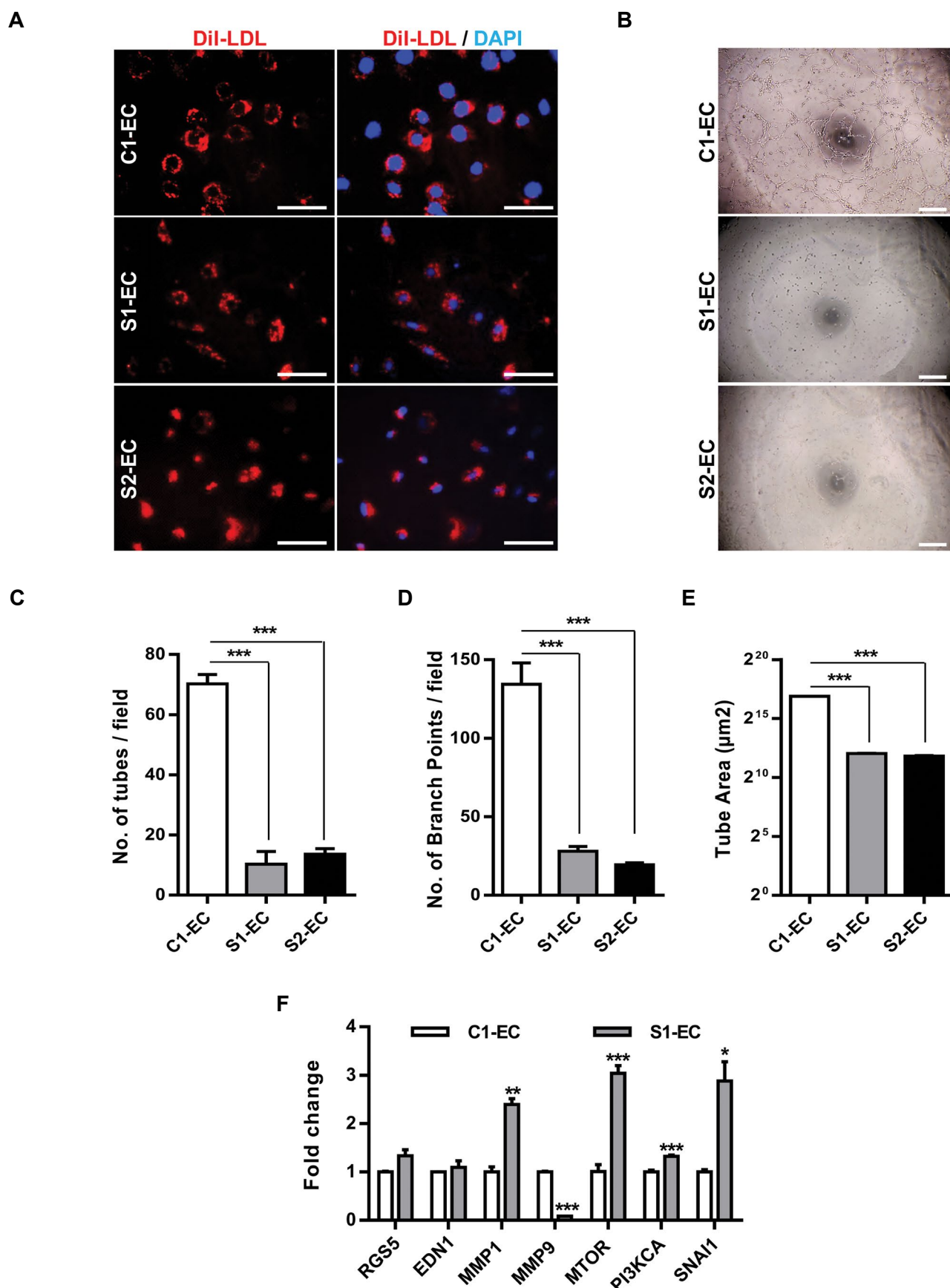


**Fig.3:** Functional analyses of SSc-EC. **A.** Immunofluorescence staining of C1-EC, S1-EC and S2-EC demonstrated DiI-LDL uptake by iPSC-derived EC. Nuclei were counterstained with DAPI (blue) (scale bar: 50 μm), **B.** SSc-EC did not form tube-like structures *in vitro* (scale bar: 500 μm), **C-E.** Analyses of tube-like structures demonstrated that SSc-EC lacked angiogenic properties, and **F.** Gene expression analysis in iPSC-derived EC. All data are represented as mean ± SEM. Comparisons were made by one-way analysis of variance or unpaired t test when appropriate (\*; P<0.05, \*\*; P<0.01, and \*\*\*; P<0.001). SSc; Systemic sclerosis, EC; Endothelial cells, iPSC; Induced pluripotent stem cells, C1-EC; Healthy control iPSC-EC, S1-EC; SSc1 iPSC-EC, and S2-EC; SSc2 iPSC-EC. n≥3 (biological replicate) for all experiments.

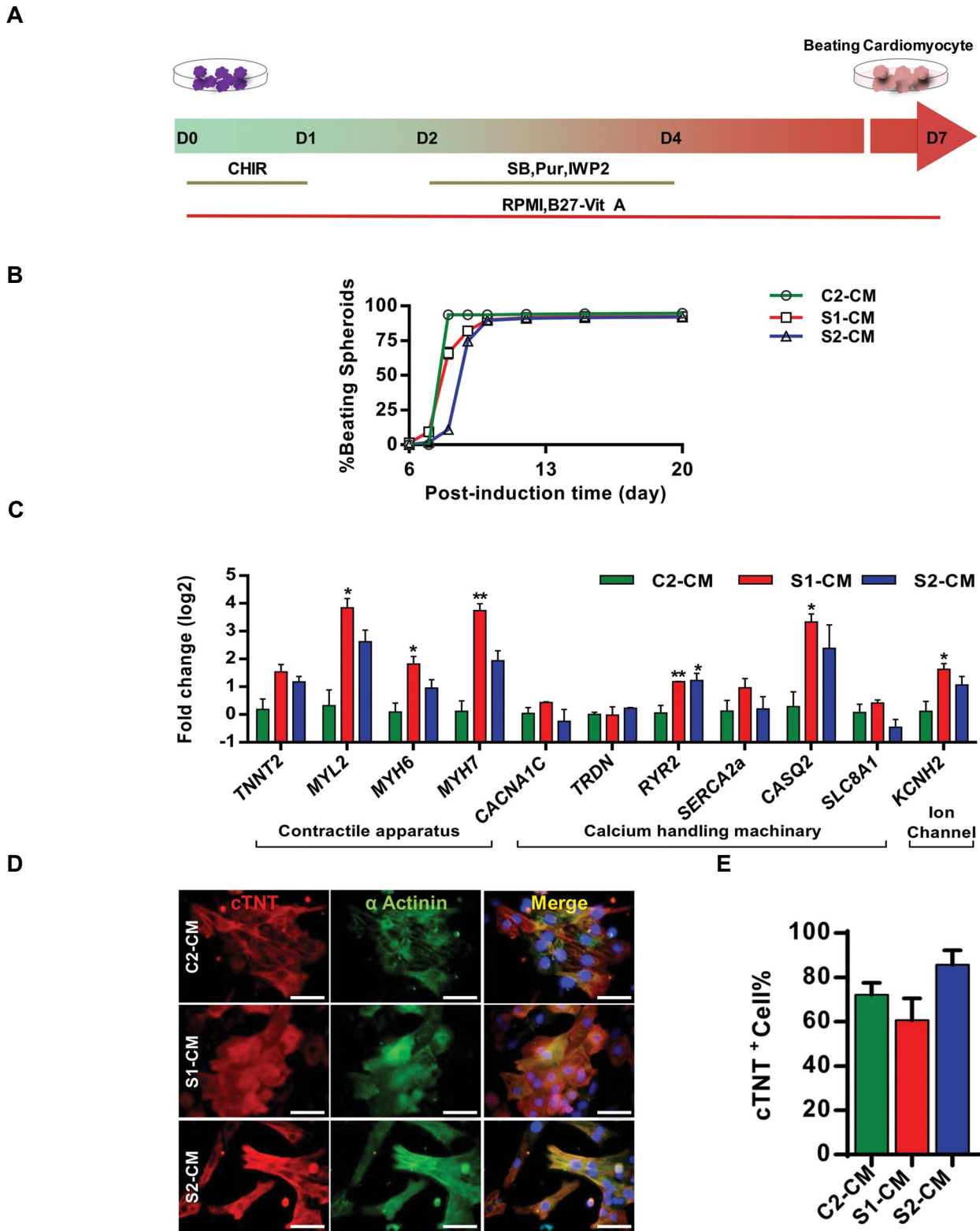


**Fig.4:** Generation and characterization of SSc iPSC-derived CM. **A.** A schematic diagram of the static suspension culture system used to induce cardiac differentiation of hiPSC lines. Five days after expansion in hESC medium, hiPSC aggregates (average size,  $175 \pm 25 \mu\text{m}$ ) were transferred to low-attachment dishes containing differentiation medium and treated with  $12 \mu\text{M}$  CHIR99021 for 1 day. After 1-day rest, the aggregates were treated with IWP2, SB431542, and purmorphamine ( $5 \mu\text{M}$  each) for 2 days, after which the media was exchanged every 2-3 days. **B.** The percentage of beating spheroids over the experimental period ( $n=3$ , biological replicate). **C.** Expression of cardiac markers in iPSC-derived CM on differentiation day 30 as measured by qRT-PCR. Fold change was calculated by  $\Delta\Delta\text{Ct}$  method and expression of each gene was normalized against *GAPDH* ( $n=3$ , biological replicate). **D.**  $\alpha$ -actinin (green) and troponin T (red) immunostaining of iPSC-derived CM on day 30 of cardiac differentiation. Nuclei were counterstained with DAPI (blue) (scale bar:  $50 \mu\text{m}$ ), and **E.** Flow cytometry analysis of cTnT<sup>+</sup> cells showed same cardiac differentiation efficiency for SSc iPSC and control iPSC ( $n=3$ , biological replicate). All data are represented as mean  $\pm$  SEM. Comparisons were made by one-way analysis of variance or unpaired t test when appropriate (\*;  $P<0.05$  and \*\*;  $P<0.01$  shows significant differences versus healthy control). SSc; Systemic sclerosis, iPSC; Induced pluripotent stem cells, CM; Cardiomyocytes, hiPSC; Human induced pluripotent stem cells, hESC; Human embryonic stem cells, qRT-PCR; Quantitative real-time polymerase chain reaction, C2-CM; Healthy control iPSC-CM, S1-CM; SSc1 iPSC-CM, and S2-CM; SSc2 iPSC-CM.

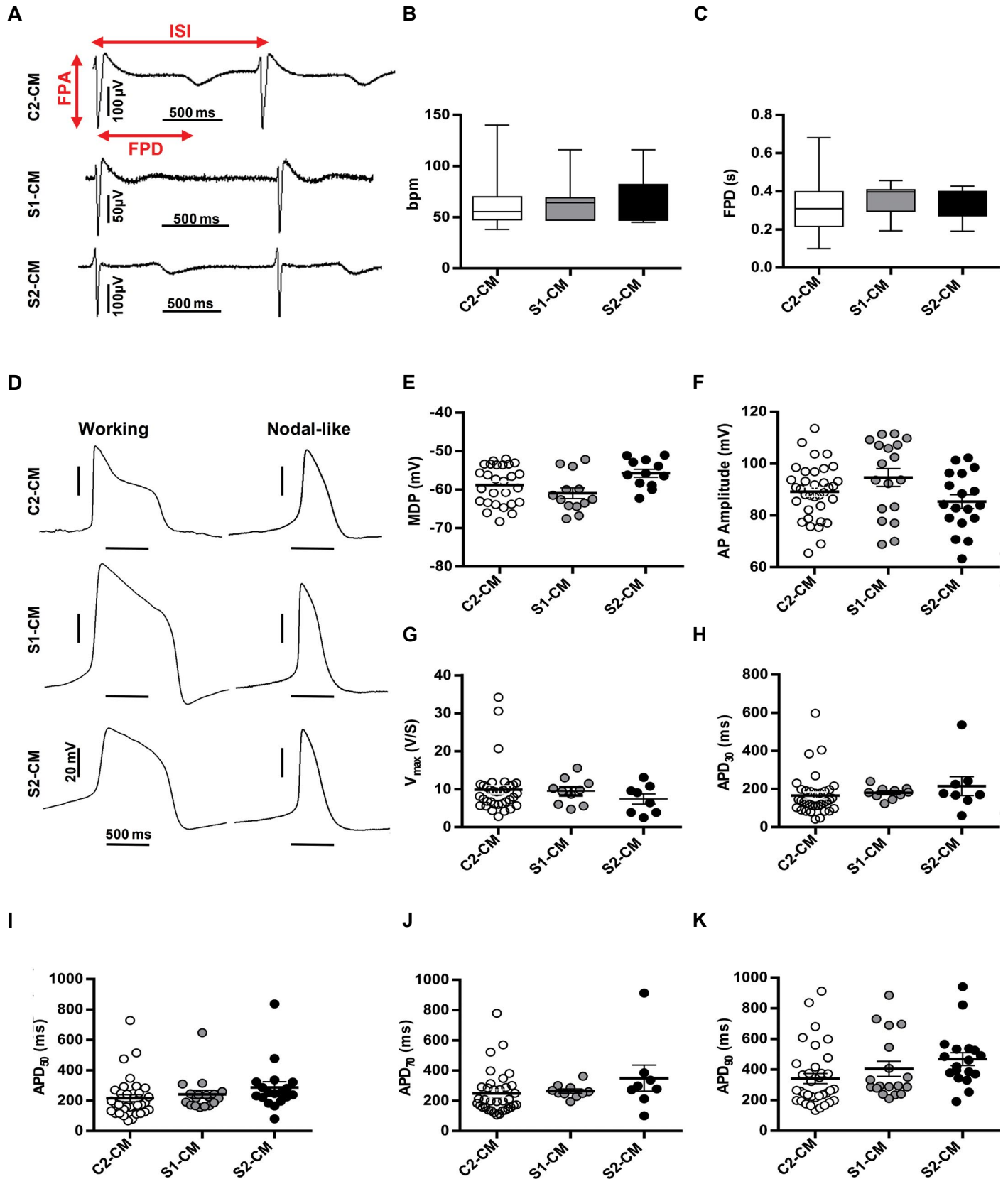
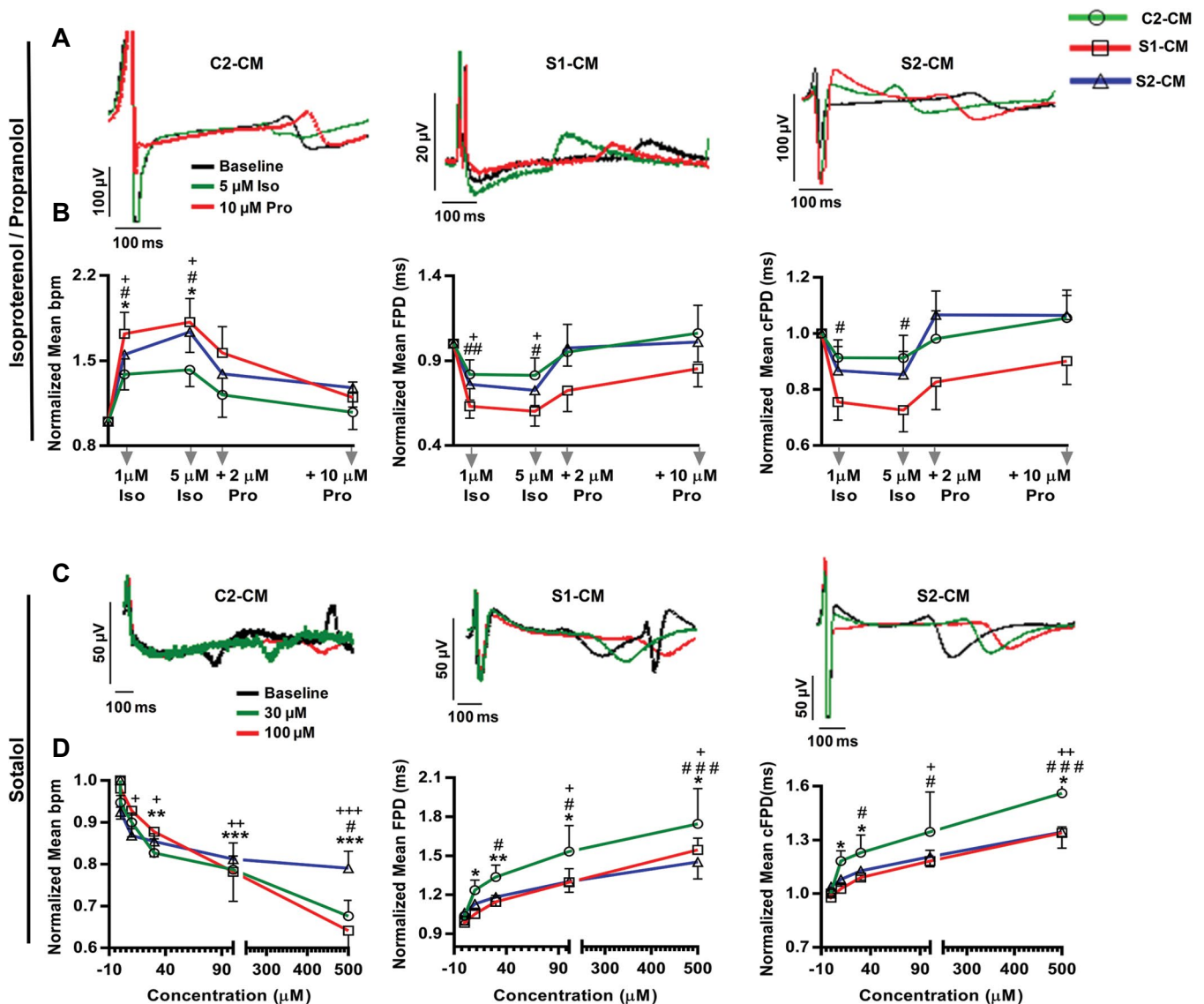


**Fig.5:** Electrophysiological properties of SSc iPSC-derived CM. **A.** Representative extracellular FP recorded from iPSC-derived beating spheroids using MEA at baseline, **B, C.** Electrophysiological features of cardiomyocytes as assessed by MEA revealed similarities in spontaneous beating rate (bpm) and FPD between SSc iPSC-derived CM and C2-CM, **D.** Representative AP recorded from single CM using whole-cell mode of patch-clamp technique, and **E-K.** Statistical analyses of action potential characteristics showed no significant differences between C2- and SSc iPSC-derived CM. All data are presented as mean  $\pm$  SEM. Comparisons were made by one-way analysis of variance (ANOVA). SSc; Systemic sclerosis, iPSC; Induced pluripotent stem cells, CM; Cardiomyocytes, FP; Field potential, MEA; Multielectrode array, FPD; Field potential duration, AP; Action potential, ISI; Inter spike Interval, FPA; Field potential amplitude, MDP; Maximal diastolic potential, AP; Action potential amplitude,  $V_{max}$ ; Maximal upstroke velocity, APD<sub>30-70</sub>; Action potential duration measured at 30-90% of repolarization, C2-CM; Healthy control iPSC-CM, S1-CM; SSc1 iPSC2-CM, and S2-CM; SSc2 iPSC3-CM. ( $n \geq 7$  in MEA experiments and  $n \geq 18$  in patch-clamp experiments).

### Systemic sclerosis induced pluripotent stem cells-derived CM were responsive to cardioactive drugs

Heart rate and contractility are regulated by the autonomic nervous system (22). To study the responsiveness of differentiated CM to neurohormonal regulation, the effects of a  $\beta$ -stimulant and a  $\beta$ -blocker agent (isoproterenol and propranolol, respectively) on C2-CM, S1-CM and S2-CM were assessed. Baseline extracellular FP was recorded for each spontaneously beating spheroid mounted on the electrodes of a MEA plate followed by recordings in the presence of serial concentrations of isoproterenol (Iso). The FP recording was performed 300 seconds after Iso application and antagonized by serial concentrations of propranolol (Pro). Iso and Pro concentrations were chosen based on previous studies (22).  $\beta_1$ -adrenergic stimulation by Iso substantially increased the spontaneous beating frequencies of iPSC-derived CM (5  $\mu$ M Iso vs. baseline; 1.4-, 1.8- and 1.7 fold in C2-CM, S1-CM and S2-CM, respectively) which were antagonized by Pro as reflected by substantial reduction of beating rates to values approaching baseline frequencies.

Furthermore, Iso administration caused significant shortening of FPD and cFPD which were reversed by Pro treatment (Fig.6A, B). Thus, SSc iPSC-derived CM responded to  $\beta$ -adrenergic agonist and antagonist in a similar manner to C2-CM. Also, the effect of sotalol as a cardioactive drug that blocks hERG channel was assessed on SSc iPSC-derived CM. Serial concentrations of sotalol (100 nM, 10  $\mu$ M, 30  $\mu$ M, 100  $\mu$ M, and 500  $\mu$ M) caused a gradual reduction of beating frequencies which accompanied by significant concentration-dependent FPD prolongation (Fig.6C, D). Verapamil as an L-type calcium channel blocker, was also added to CM differentiated from SSc iPSC. While serial concentrations of verapamil (50, 100, and 200 nM) induced a dose-dependent reduction of beating frequencies in C2-CM, it produced no effects on beating cycles of S1- and S2-CM. However, verapamil at concentrations  $\geq$  100 nM caused a significant reduction of FPD and cFPD in both patient-specific and control iPSC-derived CM (Fig.6E, F). Drug concentrations were chosen based on previous works (24). Altogether, these results indicated that SSc iPSC-derived CM, are responsive to some important cardioactive drugs.



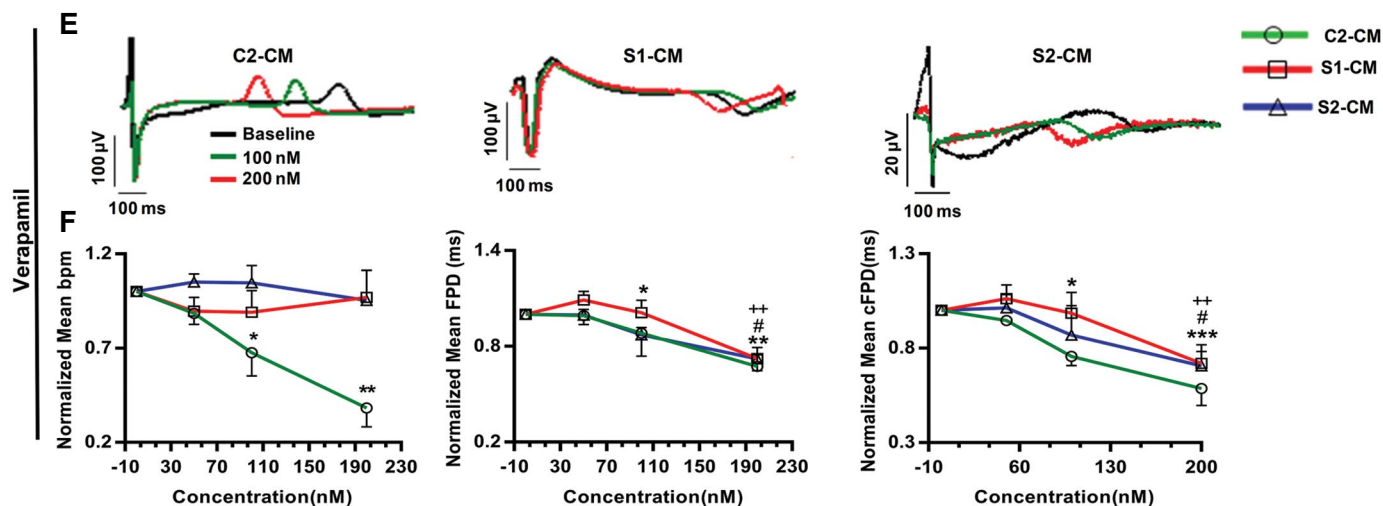


**Fig. 6:** Response of SSc iPSC-derived CM to cardioactive drugs. **A.** Representative MEA traces showing FP shortenings induced by Iso treatment followed by FP prolongation after Pro administration, **B.** Iso significantly increased the beating frequency of CM derived from both SSc and control iPSC, but this increment was reversed by Pro. Iso reduced cFPD which was prolonged by Pro in hiPSC-derived CM, **C.** The prolongation of FP caused by sotalol, **D.** Reducing effect of sotalol on beating frequency. Treatment with sotalol prolonged the FPD and cFPD in iPSC-derived CM. All data are represented as mean  $\pm$  SEM. Comparisons were made by one-way analysis of variance (ANOVA) or unpaired t test when appropriate ( $n \geq 3$ , biological replicate). \*; Shows significant differences of C2-CM, #; Significant differences of S1-CM and +; Significant differences of S2-CM following drug application (+, #, \*;  $P < 0.05$ , ##, ++, \*\*;  $P < 0.01$ , ###, +++, \*\*\*;  $P < 0.001$ ), SSc; Systemic sclerosis, iPSC; Induced pluripotent stem cells, MEA; Multielectrode array, FP; Field potential, CM; Cardiomyocyte, C2-CM; Healthy control iPSC-CM, S1-CM; SSc1 iPSC-CM, S2-CM; SSc2 iPSC-CM, Iso; Isoproterenol, Pro; Propranolol, bpm; Beats per minute, FPD; Field potential duration, and cFPD; Corrected FPD (corrected according to the Bazett Formula).

## Discussion

Here, we reported the generation of iPSC lines from two patients with SSc and their endothelial and cardiac differentiation. ECs were successfully derived from iPSC using a cocktail of growth factors and SMs that target signaling pathways involved in vascular system development, *in vivo*. Although SSc iPSC possessed the same pluripotency characteristics as their healthy counterparts, they showed different EC differentiation potentials. Furthermore, we found that angiogenic activity was significantly reduced in SSc-EC. Although there were no alterations at the primary stages of endothelial differentiation as reflected in similar expression of KDR, maturation phase of ECs was altered as presented in downregulation of VE-cadherin and loss of tube formation. Consistent with our results, Fleming et al. (25) stained endothelium and showed loss of VE-cadherin from some vessels of SSc patients. In contrast, Wang et al. (26) did not observe alterations in VE-cadherin protein expression in SSc iPSC-derived EC. Moreover study, Cipriani et al. (27) characterized CD31<sup>+</sup> sorted EC isolated from SSc patients and did not report impaired VE-cadherin expression.

The important role of VE-cadherin in ECs' tube formation is known so as anti-VE cadherin significantly decreased the number of tube structures in human umbilical vein ECs (HUVEC) (28). Importantly, VE-cadherin knockout resulted in defective EC maturation in animal models (29). Furthermore, Montero-Balaguer et al. (30) studied VE-cadherin function by making a knockdown of VE-cadherin in zebrafish using morpholino. They

showed that partial VE-cadherin inactivation leads to vascular fragility, thus total amount of expressed protein is essential for vascular stability.

The role of MTOR in vascular development was previously reported (31). Bieri et al. (21) reported the regulatory effect of MTOR and PI3K signaling in VE-cadherin expression of HUVEC. Despite their report, we did not observe a similar pattern for PI3K, MTOR and VE-cadherin expression in SSc-EC suggesting there might be another mechanism involved in VE-cadherin regulation in SSc-ECs. It should be noted that in fibroblasts obtained from SSc patients, the expression of MTOR is elevated and it is involved in fibrotic response. Indeed, blockade of MTOR pathway is being studied as a potential therapeutic approach for scleroderma (32, 33).

Multiple mechanisms are involved in VE-cadherin regulation including Twist/Slug/Snail family which are transcriptional repressors of VE-cadherin gene (34). Lopez et al. (34) investigated the cause of VE-cadherin downregulation in ECs exposed to breast cancer cells-conditioned media and found direct repression of VE-cadherin promoter by Twist/Slug/Snail family. In the current study, we also observed upregulation of snail1 which might be one of the regulatory mechanisms underlying VE-cadherin downregulation in SSc-EC.

Absence of VE-cadherin expression and subsequent defective angiogenic activity of SSc-EC motivated us to assess the effect of VE-cadherin signaling on MMPs expression, which play multiple roles in angiogenesis (35). Kiran et al. (18) reported a reciprocal relationship between

VE-cadherin and MMPs during angiogenesis. There are conflicting data on MMPs expression in scleroderma. While some researchers reported downregulation of MMP1 in scleroderma patients with increases in the levels of tissue inhibitor of MMP (TIMPs) (36), other studies reported the increased expression of MMP1 in SSc fibroblasts compared to healthy fibroblasts (37). Moreover, Kim et al. (38) investigated the expression of MMP9 in 42 SSc patients and observed elevated levels of MMP9. In contrast, Fuzii et al. (39) found decreased expression of MMP9 in dermal fibroblasts of SSc patients. In the present study, we also observed alterations in MMP1 and MMP9 expression in patients' iPSC-derived EC; however, no reciprocal relation between MMP9 and VE-cadherin expression was found.

As majority of SSc patients suffer from cardiac involvements (6), we also investigated the cardiac differentiation of SSc iPSC and found similar cardiogenic potential when comparing these cells and the healthy control iPSC. A substantial percentage of differentiated CM was positive for the cardiac marker cTNT, in all three hiPSC-derived CM indicating the successful cardiac differentiation of SSc iPSC. The time course required for generation of beating CM from SSc iPSC and the efficiency of cardiogenesis were similar to those observed for healthy control. A similar pattern for cardiac specific markers and ion channels expression was observed in SSc iPSC-derived CM and C2-CM. Also, key components of the excitation-contraction complex were similarly expressed in patients and healthy differentiated CM. Notably, the expression level of MYH6, MYH7 and MYL2 was increased in S1-CM and the MYH6/MYH7 ratio was lower in both patient-derived CM compared to C2-CM which may indicate more mature phenotype of SSc iPSC-derived CM; however, the similar functional properties were found in all cardiomyocytes. SSc-derived CM also exhibited functional ion channels resulting in appropriate response to pharmacologically active compounds.

## Conclusion

The present study reports the successful differentiation of SSc iPSC into endothelial and functional cardiac cells that would provide a unique opportunity for mechanistic studies of scleroderma pathogenesis and possible targeted drug discovery.

## Acknowledgements

The authors would like to thank Dr. Gharibdoost for introducing SSc patients. We are grateful to the patients who contributed to this research project. This work was supported by a grant from Royan Institute, the Iran National Science Foundation (INSF, grant no. 96001316), and Iran Science Elites Federation to H.B as well as Iran National Science Foundation (INSF, grant no. 95849387) to SP. The authors declare no competing interests in this study.

## Authors' Contributions

S.G.; Generated cardiomyocytes from iPSC lines

(control and SSc iPSC) and performed cellular and molecular characterization of iPSC-CM, prepared beating spheroids for electrophysiological studies and performed MEA analysis by cardio2D. F.M.; Contributed in cardiac differentiation and characterization. Z.M., M.Ho.; Performed endothelial differentiation and cellular and molecular characterization of EC. S.P.; Performed electrophysiological studies including multielectrode array and patch clamp techniques. A.T., M.He.; Generated SSc iPSC from patient's fibroblasts. M.B.; Performed echocardiography. S.G., S.P.; Wrote the manuscript. N.A., H.B.; Supervised the project. H.B; Revised the manuscript and approved the final manuscript. All authors read and approved the final manuscript.

## References

1. Angiolilli C, Marut W, van der Kroef M, Chouri E, Reedquist KA, Radstake TR. New insights into the genetics and epigenetics of systemic sclerosis. *Nat Rev Rheumatol*. 2018; 14(11): 657-673.
2. Broen JCA, Radstake TRDJ, Rossato M. The role of genetics and epigenetics in the pathogenesis of systemic sclerosis. *Nat Rev Rheumatol*. 2014; 10(11): 671-681.
3. Allanore Y, Simms R, Distler O, Trojanowska M, Pope J, Denton CP, et al. Systemic sclerosis. *Nat Rev Dis Primers*. 2015; 1: 15002.
4. Cantatore FP, Maruotti N, Corrado A, Ribatti D. Angiogenesis dysregulation in the pathogenesis of systemic sclerosis. *Biomed Res Int*. 2017; 2017: 5345673.
5. Plastiras SC, Toumanidis ST. Systemic sclerosis: the heart of the matter. *Hellenic J Cardiol*. 2012; 53(4): 287-300.
6. Cannarile F, Valentini V, Mirabelli G, Alunno A, Terenzi R, Luccioli F, et al. Cardiovascular disease in systemic sclerosis. *Ann Transl Med*. 2015; 3(1): 8.
7. Meune C, Vignaux O, Kahan A, Allanore Y. Heart involvement in systemic sclerosis: evolving concept and diagnostic methodologies. *Arch Cardiovasc Dis*. 2010; 103(1): 46-52.
8. Komócsi A, Vorobcsuk A, Faludi R, Pintér T, Lenkey Z, Költő G, et al. The impact of cardiopulmonary manifestations on the mortality of SSc: a systematic review and meta-analysis of observational studies. *Rheumatology (Oxford)*. 2012; 51(6): 1027-1036.
9. Elhai M, Meune C, Avouac J, Kahan A, Allanore Y. Trends in mortality in patients with systemic sclerosis over 40 years: a systematic review and meta-analysis of cohort studies. *Rheumatology (Oxford)*. 2012; 51(6): 1017-1026.
10. Giusti B, Fibbi G, Margheri F, Serrati S, Rossi L, Poggi F, et al. A model of anti-angiogenesis: differential transcriptome profiling of microvascular endothelial cells from diffuse systemic sclerosis patients. *Arthritis Res Ther*. 2006; 8(4): R115.
11. Medvedev S, Shevchenko AI, Zakian SM. Induced pluripotent stem cells: problems and advantages when applying them in regenerative medicine. *Acta Naturae*. 2010; 2(2): 18-28.
12. Totonchi M, Taei A, Seifinejad A, Tabebordbar M, Rassouli H, Farrokhi A, et al. Feeder-and serum-free establishment and expansion of human induced pluripotent stem cells. *Int J Dev Biol*. 2010; 54(5): 877-886.
13. Seifinejad A, Taei A, Totonchi M, Vazirinasab H, Hassani SN, Aghdami N, et al. Generation of human induced pluripotent stem cells from a Bombay individual: moving towards "universal-donor" red blood cells. *Biochem Biophys Res Commun*. 2010; 391(1): 329-334.
14. Mollamohammadi S, Taei A, Pakzad M, Totonchi M, Seifinejad A, Masoudi N, et al. A simple and efficient cryopreservation method for feeder-free dissociated human induced pluripotent stem cells and human embryonic stem cells. *Hum Reprod*. 2009; 24(10): 2468-2476.
15. Fonoudi H, Ansari H, Abbasalizadeh S, Rezaei Larijani M, Kiani S, Hashemizadeh S, et al. A universal and robust integrated platform for the scalable production of human cardiomyocytes from pluripotent stem cells. *Stem Cells Transl Med*. 2015; 4(12): 1482-1494.
16. Patsch C, Challet-Meylan L, Thoma EC, Urich E, Heckel T, O'Sullivan JF, et al. Generation of vascular endothelial and smooth muscle cells from human pluripotent stem cells. *Nat Cell Biol*. 2015; 17(8): 994-1003.
17. Athira AP, Kiran MS, Sudhakaran PR. Reciprocal relationship between VE-cadherin and matrix metalloproteinases expression in

- endothelial cells and its implications to angiogenesis. In: Sudhakaran PR, editor. Perspectives in cancer prevention-translational cancer research. New Delhi: Springer; 2014; 113-120.
18. Kiran MS, Viji RI, Kumar SV, Prabhakaran AA, Sudhakaran PR. Changes in expression of VE-cadherin and MMPs in endothelial cells: Implications for angiogenesis. *Vasc Cell*. 2011; 3(1): 6.
  19. Fleming JN, Nash RA, Mahoney WM, Schwartz SM. Is scleroderma a vasculopathy? *Curr Rheumatol Rep*. 2009; 11(2): 103-110.
  20. Jimenez SA, Piera-Velazquez S. Endothelial to mesenchymal transition (EndoMT) in the pathogenesis of systemic sclerosis-associated pulmonary fibrosis and pulmonary arterial hypertension. Myth or reality? *Matrix Biol*. 2016; 51: 26-36.
  21. Bieri M, Oroszlan M, Zuppinger C, Mohacsi PJ. Biosynthesis and expression of VE-cadherin is regulated by the PI3K/mTOR signaling pathway. *Mol Immunol*. 2009; 46(5): 866-872.
  22. Blazeski A, Zhu R, Hunter DW, Weinberg SH, Zambidis ET, Tung L. Cardiomyocytes derived from human induced pluripotent stem cells as models for normal and diseased cardiac electrophysiology and contractility. *Prog Biophys Mol Biol*. 2012; 110(2-3): 166-177.
  23. Ma J, Guo L, Fiene SJ, Anson BD, Thomson JA, Kamp TJ, et al. High purity human-induced pluripotent stem cell-derived cardiomyocytes: electrophysiological properties of action potentials and ionic currents. *Am J Physiol Heart Circ Physiol*. 2011; 301(5): H2006-H2017.
  24. Navarrete EG, Liang P, Lan F, Sanchez-Freire V, Simmons C, Gong T, et al. Screening drug-induced arrhythmia using human induced pluripotent stem cell-derived cardiomyocytes and low-impedance microelectrode arrays. *Circulation*. 2013; 128(11 Suppl 1): S3-S13.
  25. Fleming JN, Nash RA, McLeod DO, Fiorentino DF, Shulman HM, Connolly MK, et al. Capillary regeneration in scleroderma: stem cell therapy reverses phenotype? *PLoS One*. 2008; 3(1): e1452.
  26. Wang Z, Nakamura K, Jinnin M, Kudo H, Goto M, Era T, et al. Establishment and gene expression analysis of disease-derived induced pluripotent stem cells of scleroderma. *J Dermatol Sci*. 2016; 84(2): 186-196.
  27. Cipriani P, Di Benedetto P, Ruscitti P, Capece D, Zazzeroni F, Liakouli V, et al. The endothelial-mesenchymal transition in systemic sclerosis is induced by endothelin-1 and transforming growth factor- $\beta$  and may be blocked by macitentan, a dual endothelin-1 receptor antagonist. *J Rheumatol*. 2015; 42(10): 1808-1816.
  28. Yang S, Graham J, Kahn JW, Schwartz EA, Gerritsen ME. Functional roles for PECAM-1 (CD31) and VE-cadherin (CD144) in tube assembly and lumen formation in three-dimensional collagen gels. *Am J Pathol*. 1999; 155(3): 887-895.
  29. Gavard J. Endothelial permeability and VE-cadherin: a wacky comradeship. *Cell Adh Migr*. 2014; 8(2): 158-164.
  30. Montero-Balaguer M, Swirsding K, Orsenigo F, Cotelli F, Mione M, Dejana E. Stable vascular connections and remodeling require full expression of VE-cadherin in zebrafish embryos. *PLoS One*. 2009; 4(6): e5772.
  31. Yang Z-Z, Tschopp O, Di-Poi N, Bruder E, Baudry A, Dümmler B, et al. Dosage-dependent effects of Akt1/protein kinase Balpha (PK-Balpa) and Akt3/PKBgamma on thymus, skin, and cardiovascular and nervous system development in mice. *Mol Cell Biol*. 2005; 25(23): 10407-10418.
  32. Zhu X, Chu H, Jiang S, Liu Q, Liu L, Xue Y, et al. Sirt1 ameliorates systemic sclerosis by targeting the mTOR pathway. *J Dermatol Sci*. 2017; 87(2): 149-158.
  33. Mitra A, Luna JI, Marusina AI, Merleev A, Kundu-Raychaudhuri S, Fiorentino D, et al. Dual mTOR inhibition is required to prevent TGF- $\beta$ -mediated fibrosis: implications for scleroderma. *J Invest Dermatol*. 2015; 135(11): 2873-2876.
  34. Lopez D, Niu G, Huber P, Carter WB. Tumor-induced upregulation of Twist, Snail, and Slug represses the activity of the human VE-cadherin promoter. *Arch Biochem Biophys*. 2009; 482(1-2): 77-82.
  35. Jabłońska-Trypuć A, Matejczyk M, Rosochacki S. Matrix metalloproteinases (MMPs), the main extracellular matrix (ECM) enzymes in collagen degradation, as a target for anticancer drugs. *J Enzyme Inhib Med Chem*. 2016; 31 Suppl 1: 177-183.
  36. Frost J, Ramsay M, Mia R, Moosa L, Musenge E, Tikly M. Differential gene expression of MMP-1, TIMP-1 and HGF in clinically involved and uninvolved skin in South Africans with SSc. *Rheumatology (Oxford)*. 2012; 51(6): 1049-1052.
  37. Kim M-W, Park JT, Kim JH, Koh S-J, Yoon H-S, Cho S, et al. Periostin in mature stage localized scleroderma. *Ann Dermatol*. 2017; 29(3): 268-275.
  38. Kim WU, Min SY, Cho ML, Hong KH, Shin YJ, Park SH, et al. Elevated matrix metalloproteinase-9 in patients with systemic sclerosis. *Arthritis Res Ther*. 2004; 7(1): R71-R79.
  39. Fuzii HT, Yoshikawa GT, Junta CM, Sandrin-Garcia P, Fachin AL, Sakamoto-Hojo ET, et al. Affected and non-affected skin fibroblasts from systemic sclerosis patients share a gene expression profile deviated from the one observed in healthy individuals. *Clin Exp Rheumatol*. 2008; 26(5): 866-874.

# Isolation and Differentiation of Adipose-Derived Stem Cells into Odontoblast-Like Cells: A Preliminary *In Vitro* Study

Saber Khazaei, D.D.S., M.Sc., Ph.D.<sup>1,2</sup>, Abbasali Khademi, D.D.S., M.Sc.<sup>1\*</sup>, Mohammad Hossein Nasr Esfahani, Ph.D.<sup>3</sup>,  
Mozafar Khazaei, Ph.D.<sup>4\*</sup>, Mohammad Hossein Nekoofar, D.D.S., M.Sc., Ph.D.<sup>5</sup>,  
Paul M. H. Dummer, B.D.S., M.Sc.D., Ph.D., D.D.Sc., F.D.S.R.<sup>6</sup>

1. Department of Endodontics, School of Dentistry and Dental Research Centre, Dental Research Institute, Isfahan University of Medical Sciences, Isfahan, Iran
2. Department of Endodontics, School of Dentistry, Kermanshah University of Medical Sciences, Kermanshah, Iran
3. Department of Animal Biotechnology, Reproductive Biomedicine Research Center, Royan Institute for Biotechnology, ACECR, Isfahan, Iran
4. Fertility and Infertility Research Centre, Health Technology Institute, Kermanshah University of Medical Sciences, Kermanshah, Iran
5. Department of Endodontics, School of Dentistry, Tehran University of Medical Sciences, Tehran, Iran
6. School of Dentistry, College of Biomedical and Life Sciences, Cardiff University, Cardiff, UK

\*Corresponding Addresses: P.O.Box: 8174673461, Department of Endodontics, School of Dentistry and Dental Research Centre, Dental Research Institute, Isfahan University of Medical Sciences, Isfahan, Iran  
P.O.Box: 6714869914, Fertility and Infertility Research Centre, Health Technology Institute, Kermanshah University of Medical Sciences, Kermanshah, Iran  
Emails: a\_khademi@dnr.mui.ac.ir, mkhazaei1345@yahoo.com

Received: 15/December/2019, Accepted: 21/January/2020

## Abstract

**Objective:** The aim of present study was to isolate and differentiate human adipose-derived stem cells (ASCs) into odontoblast-like cells.

**Materials and Methods:** In this experimental study, human adipose tissues were taken from the buccal fat pad of three individuals (mean age:  $24.6 \pm 2.1$  years). The tissues were transferred to a laboratory in a sterile culture medium, divided into small pieces and digested by collagenase I (2 mg/mL, 60-90 minutes). ASCs were isolated by passing the cell suspension through cell strainers (70 and 40  $\mu$ m), followed by incubation at 37°C and 5% CO<sub>2</sub> in Dulbecco's modified eagle medium (DMEM) supplemented with fetal bovine serum (FBS 5%) and penicillin/streptomycin (P/S). After three passages, the ASCs were harvested. Subsequently, flow cytometry and reverse transcriptase polymerase chain reaction (RT-PCR) were used to detect expression levels of NANOG and OCT4 to evaluate stemness. Then, a differentiation medium that included high-glucose DMEM supplemented with 10% FBS, dexamethasone (10 nM), sodium  $\beta$ -glycerophosphate (5 mM) and ascorbic acid (100  $\mu$ M) was added. The cells were cultivated for four weeks, and the odontogenic medium was changed every two days. Cell differentiation was evaluated with Alizarin red staining and expressions of collagen I (COL1A1), dentin sialophosphoprotein (DSPP) and dentin matrix protein-1 (DMP1).

**Results:** The ASCs were effectively and easily isolated. They were negative for CD45 and positive for the CD105 and CD73 markers. The ASCs expressed OCT4 and NANOG. Differentiated cells highly expressed DSPP, COL1A1 and DMP1. Alizarin red staining revealed a positive reaction for calcium deposition.

**Conclusion:** ASCs were isolated successfully in high numbers from the buccal fat pad of human volunteers and were differentiated into odontoblast-like cells. These ASCs could be considered a new source of cells for use in regenerative endodontic treatments.

**Keywords:** Mesenchymal Stem Cell, Odontoblast, Regenerative Endodontics

Cell Journal (Yakhteh), Vol 23, No 3, August 2021, Pages: 288-293

**Citation:** Khazaei S, Khademi AA, Nasr Esfahani MH, Khazaei M, Nekoofar MH, Dummer PMH. Isolation and differentiation of adipose-derived stem cells into odontoblast-like cells: a preliminary in vitro study. Cell J. 2021; 23(3): 288-293. doi: 10.22074/cellj.2021.7325.

This open-access article has been published under the terms of the Creative Commons Attribution Non-Commercial 3.0 (CC BY-NC 3.0).

## Introduction

Stem cells (SCs) have self-renewal ability and the potential to differentiate into several kinds of mature cells, including cardiac, nerve and cartilage; they also maintain their survival and do not undergo atrophy and premature hyperplasia (1). In general, SCs are divided into two groups - embryonic and postnatal, depending on their characteristics. Embryonic SCs (ESCs) have a great ability to differentiate, but their application is associated with substantial medical ethics challenges. Postnatal SCs are undifferentiated cells that are located among

differentiated and specialized cells of various tissues (2).

A type of postnatal SC, described as non-hematopoietic SCs that reside in the bone marrow is called mesenchymal SCs (MSCs). These cells are multipotent and can be isolated from several tissues without serious ethical problems; they can also be multiplied *in vitro* (3). Importantly, MSCs derived from various tissues, although having similar general properties, are not exactly alike and vary in terms of proliferation and immune suppression capacity and ability to differentiate into different tissues (4).

Several types of progenitor/SCs specific to dental tissues have been isolated and identified (5). Moreover, there are other oral tissues from which MSCs can be isolated (6, 7). The use of host SCs reduces inflammatory responses and potential problems with cross infection; therefore, progenitor and SCs of adult tissues such as dental pulp SCs (DPSCs) (8), SCs from human exfoliated deciduous teeth (SHEDs) (9), SCs of the apical papilla (SCAPs) (10) and bone marrow SCs (BMSCs) (11) have been used to regenerate pulp tissue. There are various reports that discuss transplantation of MSCs from dental tissue into root canals for endodontic regeneration, and many protocols have been suggested that use the cell-based approach (12, 13). Nevertheless, for most adult patients with a necrotic tooth who are candidates for pulp regeneration, the majority of the MSCs from dental tissues, including DPSCs, SHEDs and SCAPs, are not available. This might open up a new idea of using other sources of MSCs. At the same time, there is a move towards the use of adipose-derived SCs (ASCs) in regenerative medicine (14, 15).

ASCs can be extracted in large volumes and have the capability to grow and proliferate in great numbers. In addition, the efficacy of ASCs, unlike other MSCs (16), does not change with age, and is not affected by gender, obesity and various diseases, such as vascular diseases (17). Several studies have reported that ASCs generate the nerve growth factors that improve remyelination in impaired nerves and are more resistant to apoptosis (18, 19). ASCs can also express specific characteristics of nerve and glial cells (20).

Given the advantages and appropriateness of this available resource of SCs, the present study aimed to assess the isolation and differentiation of ASCs into odontoblast-like cells.

## Materials and Methods

The protocol of the present experimental study was approved by the Regional Bioethics Committee affiliated with Kermanshah University of Medical Sciences (KUMS), Kermanshah, Iran (#3009137 and #IR.KUMS.REC.1398.862).

### Isolation of adipose-derived stem cells

Human adipose tissue was taken from additional unwanted fat from the buccal fat pad of three patients (2 females and 1 male, following their informed consent) who were candidates for maxillary LeFort osteotomies. Their mean age was  $24.6 \pm 2.1$  years. The samples were transferred to a laboratory under sterile conditions using a culture medium. The tissues were chopped and digested by collagenase I (Sigma-Aldrich, Germany, 2 mg/mL, 60-90 minutes). The cell suspension was then centrifuged for 10 minutes at 1500 rpm. Then, the ASCs were isolated by passing the cell suspension through cell strainers (70 and 40  $\mu$ m), and the ASCs were incubated at 37°C and 5% CO<sub>2</sub> in Dulbecco's modified eagle medium (DMEM, Gibco, Germany) supplemented with 5% fetal bovine serum (FBS, Gibco) plus penicillin/streptomycin (P/S, Gibco, Denmark).

### Flow cytometry

Mesenchymal (CD105, CD73) and non-mesenchymal (CD45) markers were used to confirm the stemness of the ASCs. Passage-3 isolated ASCs were washed twice with flow cytometry buffer that contained phosphate-buffered saline (PBS) plus 0.5% bovine serum albumin. Anti-CD105-PE, anti-CD73-PreCP and anti-CD45-FITC were used for identification of the ASCs. The cells were incubated with 10  $\mu$ L of each isotype antibody for 45 minutes at 4°C. The isolated ASCs were washed three times with flow cytometry buffer and fixed with 1% paraformaldehyde.

### Differentiation of adipose-derived stem cells

The ASCs were cultured in differentiation medium that contained high-glucose DMEM supplemented with FBS (10%), dexamethasone (10 nM, Sigma-Aldrich, Germany), sodium  $\beta$ -glycerophosphate (5 mM, Sigma-Aldrich, Germany) and ascorbic acid (100  $\mu$ M, Sigma-Aldrich, Germany) for 4 weeks (Table 1) (21, 22).

**Table 1:** Differentiation protocol

Material*	Company	Concentration
Dexamethasone	Sigma-Aldrich	10 nM
Sodium $\beta$ -glycerophosphate	Sigma-Aldrich	5 mM
Ascorbic acid	Sigma-Aldrich	100 $\mu$ M

\*; Differentiation medium consisted of the above materials added to high-glucose Dulbecco's modified eagle medium (DMEM) supplemented with 10% fetal bovine serum (FBS).

### Reverse transcriptase polymerase chain reaction

After three passages and to ensure that no false positive response was present for expressions of NANOG and OCT4, we compared the ASCs to precharacterised SHEDs (23) in terms of expression levels of NANOG and OCT4 for evaluation of stemness. To analyse differentiation, dentin sialophosphoprotein (*DSPP*), dentin matrix protein (*DMP*) and collagen I (*COL1A1*) gene expressions by using a semi-quantitative polymerase chain reaction (PCR) were performed. One  $\mu$ L of cDNA was used as a template in reverse transcriptase PCR (RT-PCR) and was added to 12.5  $\mu$ L of 2x Master Mix RED (1.5 mM MgCl<sub>2</sub>, Merck, Germany) that included 150 mM Tris-HCl (pH=8.5), 40 mM NH<sub>4</sub>, 3 mM MgCl<sub>2</sub>, 0.2% Tween® 20, 0.4 mM of each dNTP, 0.2 U/ $\mu$ L Amplicon Taq DNA polymerase, an inert red dye and stabilizer, 1  $\mu$ L of each primer (10  $\mu$ M), and up to 25  $\mu$ L nuclease-free water. Amplification was carried out using a thermocycler (Eppendorf AG 22331, Hamburg, Germany). The conditions for RT-PCR amplification were as follows: an initial denaturation at 94°C for 5 minutes, 30 cycles of three-step PCR that consisted of 94°C for 20 seconds, 60°C for 25 seconds and 72°C for 45 seconds, and a final extension at 72°C for 10 minutes. The RT-PCR output was used for the electrophoresis agarose gel (1.5%) along with molecular weight markers. Table 2 lists the primers used in this study.

## Mineralization evaluation

The cells were incubated with 40 mM Alizarin red stain (pH=4.2) for 10 minutes. Then, the cells were washed five times with PBS. After each wash, the cells were centrifuged with PBS to reduce the non-specific Alizarin red stain dye and were analysed to detect calcified nodular deposition.

## Results

After 24 hours of culture, we observed small, spheroid and translucent ASCs. The ASCs were passaged when they became 70-80% confluent; at this stage the ASCs had a spindle morphology (Fig.1).

**Table 2:** Gene primer sequences

Gene	Accession number	Annealing temperature (°C)	Size (bp)	Primer sequence (5'-3')	Reference
<i>DSPP</i>	NM_014208	60	118	F: CAGTACAGGATGAGTTAAATGCCAGTG R: CCATTCCCTTCTCCCTTGTGACC	(24)
<i>DMP1</i>	NM_004407	60	211	F: GAGAGTCAGAGCGAGGAA R: CTTGGCAGTCATTGTCATC	Present study
<i>COL1A1</i>	NM_000088	60	128	F: GTGCTAAAGGTGCCAATGGT R: ACCAGGTTACCGCTGTAC	(25)
<i>NANOG</i>	NM_024865	60	158	F: CAAAGGCAAACAACCCACTT R: TCTGCTGGAGGCTGAGGTAT	(26)
<i>POU5F1 (OCT-4)</i>	NM_002701	60	110	F: AGTGAGAGGCAACCTGGAGA R: ACACTCGGACCACATCCTTC	(27)

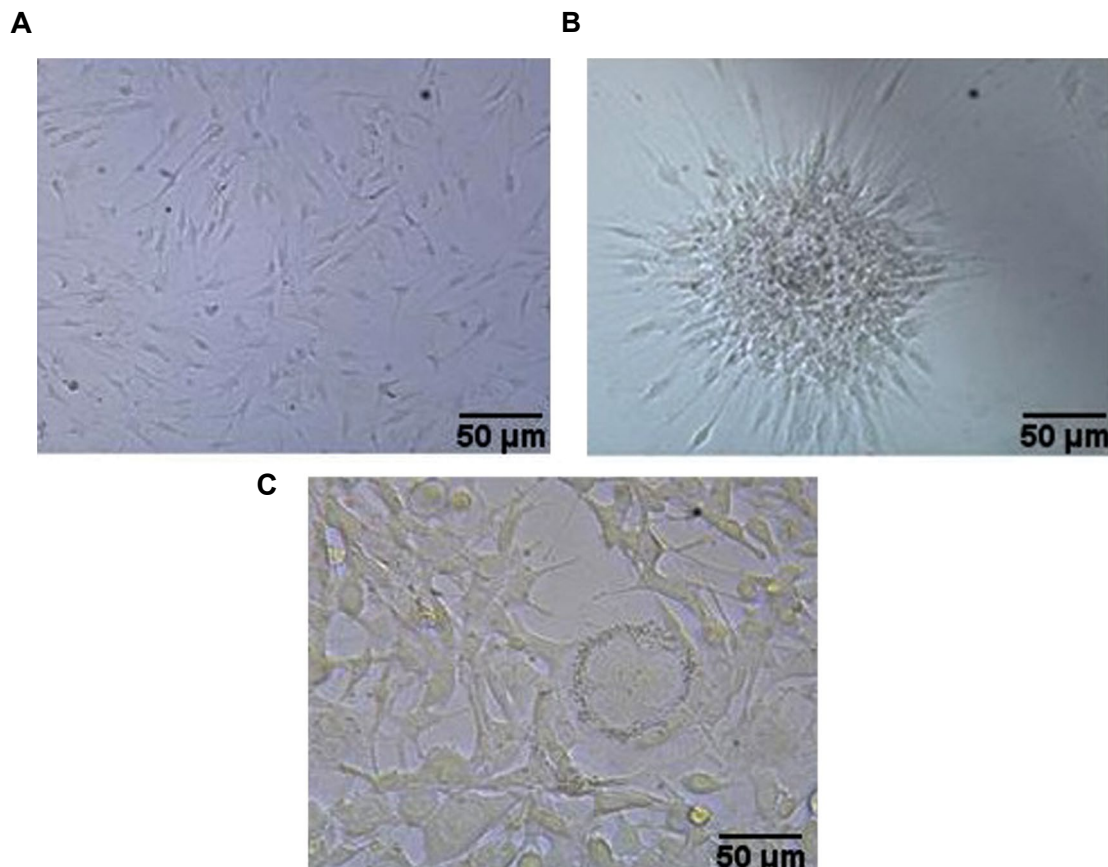


**Fig.1:** *In vitro* culture of isolated adipose-derived stem cells (ASCs) during different culture periods. **A.** After one week, **B.** Cellular sphere at passage three, and **C.** Odontoblast-like cells after 28 days treatment by differentiation medium (scale bar: 50 µm).

At passage three, the ASCs expressed OCT4 and NANOG (Fig.2), similar to precharacterised SHEDs. This showed that there was no false-positive response to the expressions of NANOG and OCT4. The flow cytometry results showed that isolated the ASCs were positive for CD105 and CD73, and negative for CD45 (Fig.3).

The ASCs differentiated into odontoblast-like cells after four weeks incubation in differentiation medium. The cells increased in size, and became nodular with a more

oval and/or round shape (Fig.1C). Expressions of three genes associated with odontoblast-like cell differentiation (*COL1A1*, *DSPP*, and *DMP1* genes) were confirmed (Fig.2).

ASCs that differentiated into odontoblast-like cells after four weeks were analysed for mineralization with Alizarin red staining. There was detectable calcified nodular deposition in these ASCs compared with the control group (Fig.4).

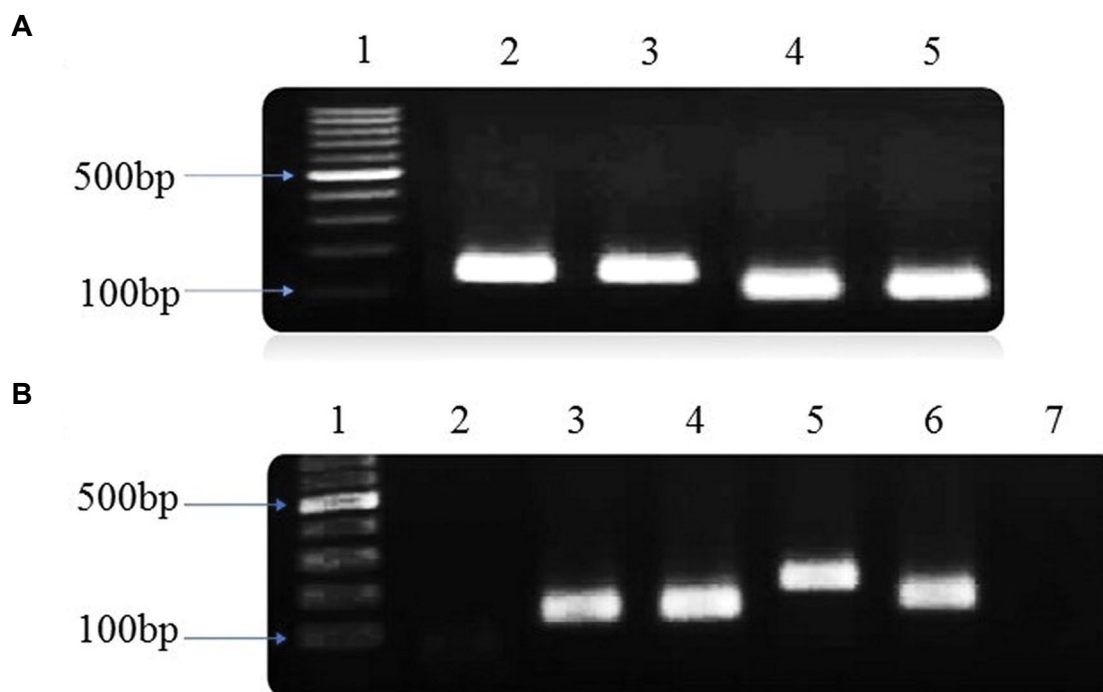


**Fig.2:** Reverse transcriptase polymerase chain reaction (RT-PCR) of stemness genes of adipose-derived stem cells (ASCs) and odontoblast-like cell specific genes. **A.** Representative example of RT-PCR for gene expression analysis. 1; 100 bp DNA ladder (Lad), 2; *NANOG* (SHEDs), 3; *NANOG* (ASCs), 4; *OCT4* (SHEDs), 5; *OCT4* (ASCs). **B.** Representative example of RT-PCR for gene expression analysis. 1; 100 bp DNA ladder (Lad), 2; *DSPP* after 14 days treatment with differentiation medium, 3; *DSPP* after 21 days treatment with differentiation medium, 4; *DSPP* after 28 days treatment with differentiation medium, 5; *DMP1*, 6; *COL1A1*, 7; Control group (ASCs after 28 days treatment with culture medium without the differentiation medium).

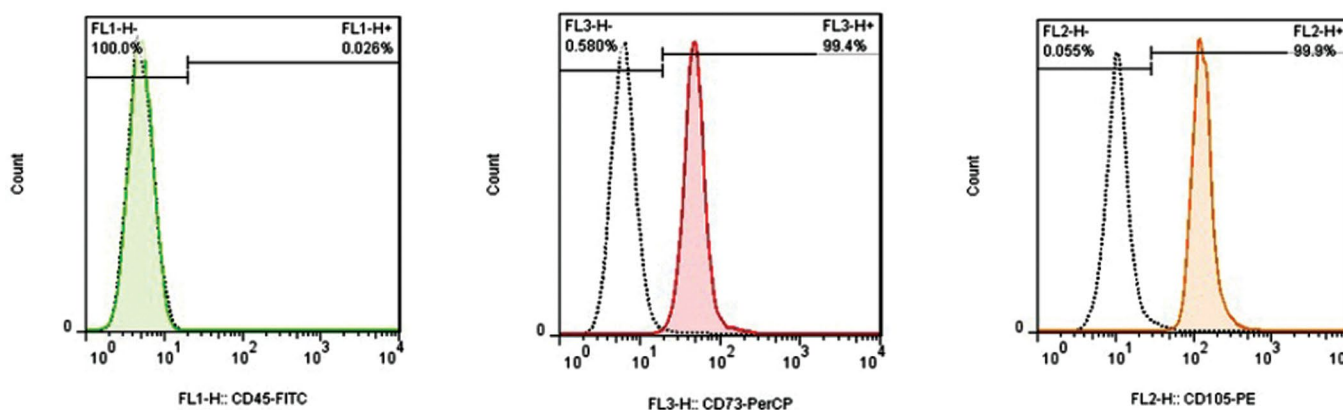


**Fig.3:** Flow cytometry results show that the isolated adipose-derived stem cells (ASCs) were positive for CD105, CD73, and negative for CD45.

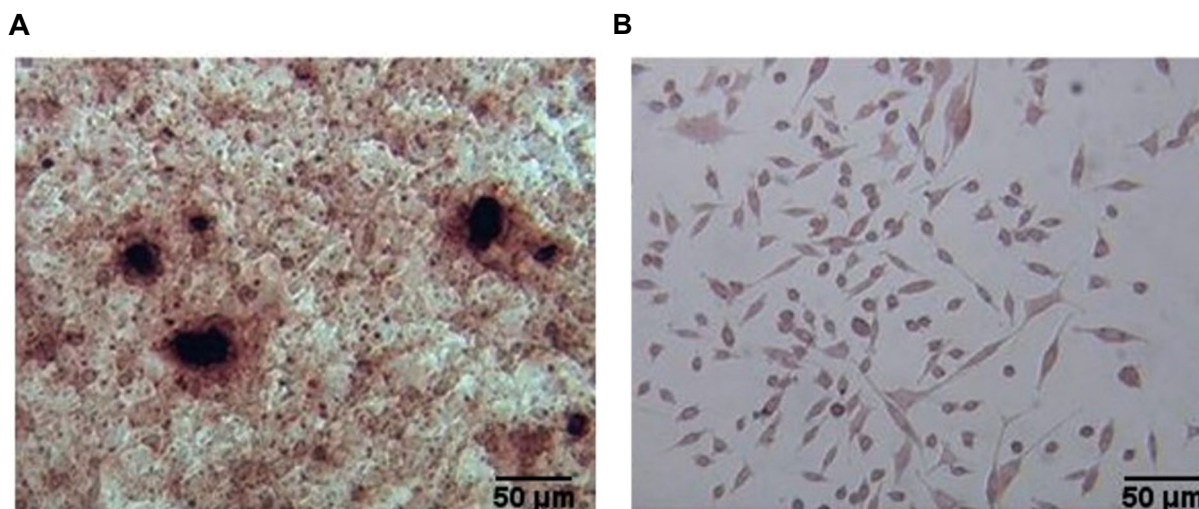


**Fig.4:** Alizarin Red Staining of odontoblast-like cells. **A.** Calcium deposition of odontoblast-like cells using Alizarin red staining after 28 days of treatment with differentiation medium. **B.** Control group (scale bar: 50 µm).

## Discussion

Several types of SCs specific to dental tissues (DPSCs, SCAPs, SHEDs and BMSCs) have been isolated and evaluated for endodontic regeneration (8-11). MSCs that are derived from various tissues are similar in terms of general characteristics; however, they differ in terms of proliferation, immune suppression, and the ability to differentiate into various tissues (7). To date, no study has evaluated the differentiation potential of ASCs from human buccal fat pad into odontoblast-like cells. It has been reported that this adipose tissue may have neural crest origin (28), and the present study supports the concept that differentiation into odontogenic-like cells can occur in ASCs from the human buccal fat pad if sufficient signals are provided.

ASCs have self-renewal ability and potential to differentiate into various lineages of mesenchymal tissue. These cells resemble similar surface antigens such as MSCs, but are not identical to BMSCs (29). *In vitro* studies have shown that they can differentiate into different lineages, including adipocytes, cartilage, bone, muscle, hematopoietic, neural, liver, angiogenic, and epithelial cells (30). ASCs express mesenchymal markers such as CD90, CD44 and CD105, and negative expression of the hematopoietic markers CD14, CD34 and CD45 (31). The results of the present study revealed that ASCs expressed CD90, CD105, OCT4 and NANOG, as do SHEDs.

Several protocols and growth factors have been introduced for differentiation of MSCs into odontoblast-like cells. These include bone morphogenetic proteins (BMPs) (32), transforming growth factor (TGFβ1-3) (32), nerve growth factor (NGF) (33) and fibroblast growth factor (FGF-2) (34). Wu et al. (35) reported that ASCs could differentiate into odontoblast-like cells using the inguinal fat pads of mice as a source for ASCs. In the present study, we used a simple and inexpensive protocol that was composed of dexamethasone, sodium β-glycerophosphate and ascorbic acid. By

altering the composition of these growth factors, the differentiation of these cells was altered and the cells had the capability to express markers of odontoblasts or osteoblasts, depending on their exposure to different combinations of growth factors. Other studies have evaluated growth factors administered alone or in different combinations to enhance differentiation of odontoblast-like cells (36-38).

The results of the present study revealed that these ASCs differentiated into odontoblast-like cells and expressed *COL1A1*, *DMP1* and *DSPP* genes after four weeks of treatment, whereas after two weeks the cells did not express these markers. DSPP is produced by odontoblasts inside the tooth pulp. However, osteoblasts can also produce this protein. DSPP plays a pivotal role in mineral deposition during dentinogenesis (39). Type I collagen is the major protein of dentin and regulates the expression level of DMP1. It has been demonstrated that type I collagen and DMP1 are expressed mainly in active odontoblasts (40).

It has been reported that ASCs could be used for regeneration (15). However, human ASCs, particularly buccal fat pad for complete pulp regeneration, has not been evaluated. Using this line of cells may open new fields of research for endodontic regeneration treatments. They can be extracted in large volumes from the buccal fat pad and can grow and proliferate in large numbers. In addition, the efficacy of ASCs, unlike other MSCs, does not change due to age, gender, or obesity.

## Conclusion

In the present *in vitro* study, high numbers of ASCs were isolated successfully from the human buccal fat pad and were differentiated into odontoblast-like cells. A subsequent *in vivo* study is suggested to evaluate the differentiation potential of ASCs into odontoblast-like cells.

## Acknowledgments

Research reported in this publication was supported by Elite Researcher Grant Committee under award number [977517] from the National Institutes for Medical Research Development (NIMAD), Tehran, Iran. There is no conflict of interest in this study.

## Authors' Contributions

S.Kh.; Contributed to conception and design, analysis, drafted and critically revised the manuscript. A.Kh., M.H.-N.E.; Contributed to conception, interpretation, drafted and critically revised the manuscript. M.Kh.; Contributed to conception and design, acquisition, analysis, interpretation, drafted and critically revised the manuscript. M.H.N., P.M.H.D.; Contributed to interpretation, drafted and critically revised the manuscript. All authors gave their final approval and agree to be accountable for all aspects of this work.

## References

- Rossi DJ, Jamieson CHM, Weissman IL. Stems cells and the pathways to aging and cancer. *Cell*. 2008; 132(4): 681-696.
- Shi Y, Du L, Lin L, Wang Y. Tumour-associated mesenchymal stem/stromal cells: emerging therapeutic targets. *Nat Rev Drug Discov*. 2017; 16(1): 35-52.
- Ding DC, Chang YH, Shyu WC, Lin SZ. Human umbilical cord mesenchymal stem cells: a new era for stem cell therapy. *Cell Transplant*. 2015; 24(3): 339-347.
- Zajdel A, Kalucka M, Kokoszka-Mikolaj E, Wilczok A. Osteogenic differentiation of human mesenchymal stem cells from adipose tissue and Wharton's jelly of the umbilical cord. *Acta Biochim Pol*. 2017; 64(2): 365-369.
- Pisciotta A, Carnevale G, Meloni S, Riccio M, De Biasi S, Gibellini L, et al. Human dental pulp stem cells (hDPSCs): isolation, enrichment and comparative differentiation of two sub-populations. *BMC Dev Biol*. 2015; 15: 14.
- Cao Y, Song M, Kim E, Shon W, Chugal N, Bogen G, et al. Pulp-dentin regeneration: current state and future prospects. *J Dent Res*. 2015; 94(11): 1544-1551.
- Khazaei M, Bozorgi A, Khazaei S, Khademi A. Stem cells in dentistry, sources, and applications. *Dental Hypotheses*. 2016; 7(2): 42-52.
- Nakashima M, Iohara K. Mobilized dental pulp stem cells for pulp regeneration: initiation of clinical trial. *J Endod*. 2014; 40(4 Suppl): S26-S32.
- Cordeiro MM, Dong Z, Kaneko T, Zhang Z, Miyazawa M, Shi S, et al. Dental pulp tissue engineering with stem cells from exfoliated deciduous teeth. *J Endod*. 2008; 34(8): 962-969.
- Iohara K, Imabayashi K, Ishizaka R, Watanabe A, Nabekura J, Ito M, et al. Complete pulp regeneration after pulpectomy by transplantation of CD105+ stem cells with stromal cell-derived factor-1. *Tissue Eng Part A*. 2011; 17(15-16): 1911-1920.
- Murakami M, Hayashi Y, Iohara K, Osako Y, Hirose Y, Nakashima M. Trophic effects and regenerative potential of mobilized mesenchymal stem cells from bone marrow and adipose tissue as alternative cell sources for pulp/dentin regeneration. *Cell Transplant*. 2015; 24(9): 1753-1765.
- Rosa V, Zhang Z, Grande RH, Nor JE. Dental pulp tissue engineering in full-length human root canals. *J Dent Res*. 2013; 92(11): 970-975.
- Ravindran S, Zhang Y, Huang CC, George A. Odontogenic induction of dental stem cells by extracellular matrix-inspired three-dimensional scaffold. *Tissue Eng Part A*. 2014; 20(1-2): 92-102.
- Bajek A, Gurtowska N, Oikowska J, Kazmierski L, Maj M, Drewa T. Adipose-derived stem cells as a tool in cell-based therapies. *Arch Immunol Ther Exp (Warsz)*. 2016; 64(6): 443-454.
- Mazini L, Rochette L, Amine M, Malka G. Regenerative capacity of adipose derived stem cells (ADSCs), comparison with mesenchymal stem cells (MSCs). *Int J Mol Sci*. 2019; 20(10): 2523.
- Iohara K, Murakami M, Nakata K, Nakashima M. Age-dependent decline in dental pulp regeneration after pulpectomy in dogs. *Exp Gerontol*. 2014; 52: 39-45.
- DiMuzio P, Tulenko T. Tissue engineering applications to vascular bypass graft development: the use of adipose-derived stem cells. *J Vasc Surg*. 2007; 45 Suppl A: A99-A103.
- Schipper BM, Marra KG, Zhang W, Donnenberg AD, Rubin JP. Regional anatomic and age effects on cell function of human adipose-derived stem cells. *Ann Plast Surg*. 2008; 60(5): 538-544.
- Lopatina T, Kalinina N, Karagyaur M, Stambolsky D, Rubina K, Revischin A, et al. Adipose-derived stem cells stimulate regeneration of peripheral nerves: BDNF secreted by these cells promotes nerve healing and axon growth de novo. *PLoS One*. 2011; 6(3): e17899.
- Sondell M, Sundler F, Kanje M. Vascular endothelial growth factor is a neurotrophic factor which stimulates axonal outgrowth through the flk-1 receptor. *Eur J Neurosci*. 2000; 12(12): 4243-4254.
- Teti G, Salvatore V, Ruggeri A, Manzoli L, Gesi M, Orsini G, et al. In vitro reparative dentin: a biochemical and morphological study. *Eur J Histochem*. 2013; 57(3): e23.
- Baldion PA, Velandia-Romero ML, Castellanos JE. Odontoblast-like cells differentiated from dental pulp stem cells retain their phenotype after subcultivation. *Int J Cell Biol*. 2018; 2018: 6853189.
- Karbalaie K, Tanhaei S, Rabiei F, Kiani-Esfahani A, Masoudi NS, Nasr-Esfahani MH, et al. Stem cells from human exfoliated deciduous tooth exhibit stromal-derived inducing activity and lead to generation of neural crest cells from human embryonic stem cells. *Cell J*. 2015; 17(1): 37-48.
- Min JH, Ko SY, Cho YB, Ryu CJ, Jang YJ. Dentinogenic potential of human adult dental pulp cells during the extended primary culture. *Hum Cell*. 2011; 24(1): 43-50.
- Makpol S, Jam FA, Yusof YAM, Ngah WZW. Modulation of collagen synthesis and its gene expression in human skin fibroblasts by tocotrienol-rich fraction. *Arch Med Sci*. 2011; 7(5): 889-895.
- Zeng X, Miura T, Luo Y, Bhattacharya B, Condie B, Chen J, et al. Properties of pluripotent human embryonic stem cells BG01 and BG02. *Stem Cells*. 2004; 22(3): 292-312.
- Maki CB, Pacchiarotti J, Ramos T, Pascual M, Pham J, Kinjo J, et al. Phenotypic and molecular characterization of spermatogonial stem cells in adult primate testes. *Hum Reprod*. 2009; 24(6): 1480-1491.
- Billon N, Iannarelli P, Monteiro MC, Glavieux-Pardanaud C, Richardson WD, Kessar N, et al. The generation of adipocytes by the neural crest. *Development*. 2007; 134(12): 2283-2292.
- Pachon-Pena G, Yu G, Tucker A, Wu X, Vendrell J, Bunnell BA, et al. Stromal stem cells from adipose tissue and bone marrow of age-matched female donors display distinct immunophenotypic profiles. *J Cell Physiol*. 2011; 226(3): 843-851.
- Gimble JM, Bunnell BA, Chiu ES, Guilak F. Concise review: adipose-derived stromal vascular fraction cells and stem cells: let's not get lost in translation. *Stem Cells*. 2011; 29(5): 749-754.
- Salehi H, Amirpour N, Niapour A, Razavi S. An overview of neural differentiation potential of human adipose derived stem cells. *Stem Cell Rev Rep*. 2016; 12(1): 26-41.
- Aranha AMF, Zhang Z, Neiva KG, Costa CAS, Hebling J, Nor JE. Hypoxia enhances the angiogenic potential of human dental pulp cells. *J Endod*. 2010; 36(10): 1633-1637.
- Ando Y, Honda MJ, Ohshima H, Tonomura A, Ohara T, Itaya T, et al. The induction of dentin bridge-like structures by constructs of subcultured dental pulp-derived cells and porous HA/TCP in porcine teeth. *Nagoya J Med Sci*. 2009; 71(1-2): 51-62.
- Cavalcanti BN, Zeitlin BD, Nor JE. A hydrogel scaffold that maintains viability and supports differentiation of dental pulp stem cells. *Dent Mater*. 2013; 29(1): 97-102.
- Wu L, Zhu F, Wu Y, Lin Y, Nie X, Jing W, et al. Dentin sialophosphoprotein-promoted mineralization and expression of odontogenic genes in adipose-derived stromal cells. *Cells Tissues Organs*. 2008; 187(2): 103-112.
- Zhang W, Walboomers XF, Jansen JA. The formation of tertiary dentin after pulp capping with a calcium phosphate cement, loaded with PLGA microparticles containing TGF-beta1. *J Biomed Mater Res A*. 2008; 85(2): 439-44.
- Huang GT, Shagrananova K, Chan SW. Formation of odontoblast-like cells from cultured human dental pulp cells on dentin in vitro. *J Endod*. 2006; 32(11): 1066-1073.
- Wei X, Ling J, Wu L, Liu L, Xiao Y. Expression of mineralization markers in dental pulp cells. *J Endod*. 2007; 33(6): 703-708.
- Yamakoshi Y. Dentinogenesis and dentin Sialophosphoprotein (DSPP). *J Oral Biosci*. 2009; 51(3): 134.
- Mizuno M, Miyamoto T, Wada K, Watatani S, Zhang GX. Type I collagen regulated dentin matrix protein-1 (Dmp-1) and osteocalcin (OCN) gene expression of rat dental pulp cells. *J Cell Biochem*. 2003; 88(6): 1112-1119.

# Mir-106b Cluster Regulates Primordial Germ Cells Differentiation from Human Mesenchymal Stem Cells

Sadaf Mahboudi, Ph.D.<sup>1</sup>, Kazem Parivar, Ph.D.<sup>1\*</sup>, Zohreh Mazaheri, Ph.D.<sup>2</sup>, Shiva Irani, Ph.D.<sup>1</sup>

1. Department of Biology, Science and Research Branch, Islamic Azad University, Tehran, Iran

2. Basic Medical Sciences Research Center, Histogenotech Company, Tehran, Iran

\*Corresponding Address: P.O.Box: 14515/775, Department of Biology, Science and Research Branch, Islamic Azad University, Tehran, Iran  
Email: kazem\_parivar@yahoo.com

Received: 13/April/2019, Accepted: 16/February/2020

## Abstract

**Objective:** Numerous evidence indicates that microRNAs (miRNAs) are critical regulators in the spermatogenesis process. The aim of this study was to investigate *Mir-106b* cluster regulates primordial germ cells (PGCs) differentiation from human mesenchymal stem cells (MSCs).

**Materials and Methods:** In this experimental study, samples containing male adipose (n: 9 samples- age: 25-40 years) were obtained from cosmetic surgeries performed for the liposuction in Imam Khomeini Hospital. The differentiation of MSCs into PGCs was accomplished by transfection of a lentivector expressing *miR-106b*. The transfection of *miR-106b* was also confirmed by the detection of a clear green fluorescent protein (GFP) signal in MSCs. MSCs were treated with bone morphogenic factor 4 (BMP4) protein, as a putative inducer of PGCs differentiation, to induce the differentiation of MSCs into PGCs (positive control). After 4 days of transfection, the expression of *miR-106b*, *STELLA*, and *FRAGILIS* genes was evaluated by real-time polymerase chain reaction (PCR). Also, the levels of thymocyte differentiation antigen 1 (Thy1) protein was assessed by the western blot analysis. The cell surface expression of CD90 was also determined by immunocytochemistry method. The cytotoxicity of *miR-106b* was examined in MSCs after 24, 48, and 72 hours using the MTT assay.

**Results:** MSCs treated with BMP4 or transfected by *miR-106b* were successfully differentiated into PGCs. The results of this study also showed that the expression of *miR-106b* was significantly increased after 48 hours from transfection. Also, we showed *STELLA*, *FRAGILIS*, as well as the protein expression of Thy1, was significantly higher in MSCs transfected by lentivector expressing *miR-106b* in comparison with MSCs treated with BMP4 ( $P \leq 0.05$ ). MTT assay showed *miR-106b* was no toxic during 72 hours in 1  $\mu\text{g/ml}$  dose, that this amount could elevated germ cells marker significantly higher than other experimental groups ( $P \leq 0.05$ ).

**Conclusion:** According to this findings, it appears that *miR-106b* plays an essential role in the differentiation of MSCs into PGCs.

**Keywords:** Mesenchymal Stem Cells, MicroRNA, *MIR-106b*

Cell Journal(yakhteh), Vol 23, No 3, August 2021, Pages: 294-302

**Citation:** Mahboudi S, Parivar K, Mazaheri Z, Irani Sh. Mir-106b cluster regulates primordial germ cells differentiation from human mesenchymal stem cells. Cell J. 2021; 23(3): 294-302. doi: 10.22074/cellj.2021.6836.

This open-access article has been published under the terms of the Creative Commons Attribution Non-Commercial 3.0 (CC BY-NC 3.0).

## Introduction

Infertility is a serious physiological problem in human populations, especially in young adults. Epidemiological studies have showed that, male infertility accounts for approximately 50% of all causes of infertility among couples (1). Transplantation of stem cells for infertility has attracted many attention of researchers in recent years. Germ cells are differentiated cells that contribute to the complicated processes of fertilization. To date, many researchers have devoted themselves to reproducing germ cell differentiation, or gametogenesis, *in vitro* (2). It has been established that mesenchymal stem cells (MSCs) which are mainly derived from bone marrow or adipose tissues have great potentials (3) for the repair of various types of tissues. MSCs can differentiate into bone, neurons, adipose, cartilage, muscle, hepatocytes, insulin-producing cells, and skin in proper conditions *in vivo* (3-5). Also it is stated that MSCs have been regarded as an attractive and promising tool for cell-based therapy in immune disorders and inflammatory diseases, as

well as for regenerative medicine, owing to their potent immunomodulatory function, paracrine effects and capacity of multilineage differentiation. Previously, other researcher show that generation of spermatogonial stem cells (SSCs) from MSCs *in vitro* (6).

Furthermore, stem cells can be readily isolated, they have high proliferation rates and high potentials for the differentiation into various types of cells. Based on these features, they could be valuable to be applied for autologous transplantation. Nayernia et al. (7) demonstrated that murine bone marrow stromal cells (BMSCs) are able to differentiate into early germ cells *in vitro* and *in vivo*. Also, Cakici et al. (8) recently demonstrated that adipose tissue-derived mesenchymal stem cells (ASCs) which were probed by green fluorescent protein (GFP) are capable differentiating into sperm-like cells that could lead to the recovery of fertility in a rat model of busulfan-treated azoospermia (9).

It has been shown that BMP4 and retinoic acid are

frequently employed for the differentiation of MSC into spermatogonial cells. However, only a small proportion of cells would be able to differentiate, or in the case of differentiation, they would not be capable of continuing the spermatogenesis process. Recently researchers have been focused on short sequences of micro RNAs for the differentiation of MSCs into different lineages of cells.

MicroRNAs can regulate the expression of the vast majority of proteins at post-translational level by miRNA-induced silencing complex (miRISC). This complex is able to bind their target mRNAs, and then it degrades the synthesized mRNAs, leading to the silencing of a particular gene. The silencing of genes is an essential biological phenomenon by which numerous cellular processes including self-renewal, proliferation, differentiation, and apoptosis could be fine-tuned (10). Moreover, studies have reported that miRNAs are highly expressed and they are involved in the process of spermatogenesis (11-17). In line with this study, the loss of DICER (a protein which facilitates the activation of the RISC activation) could be resulted in a defect in germ cell development (18, 19). Tong et al. (20), characterized the active miRNAs involved in the development of spermatogonial cells by the microarray method. These researchers identified the profile of a number of miRNAs in undifferentiated spermatogonial cells (THY1+-enriched).

Other study showed that Mirlet7 family plays a significant role in the spermatogonial differentiation (19). Also other reports indicated that both *miR-17-92* (miRc1) cluster and its paralog *miR-16b-25* (miRc2) cluster contribute to the self-renewal of SSCs and the promotion of the proliferation of undifferentiated spermatogonial cells. The spermatogonial differentiation depends on several intrinsic and extrinsic signaling proteins, modulate the expression of the leading genes. The downregulation of *LIN28*, *MYC*, *MYCN*, *miR-17-92* (*miRc1*), and *miR-106b-25* (*miRc3*) promotes the differentiation of the undifferentiated spermatogonial cells (16). The field of biotechnology has a tremendous and pivotal contribution to the manipulation of cellular contents to obtain the desired outcomes in biological events. The transfection of cells with miRNAs is one of the exemplary strategies for the overexpression/downregulation of a particular miRNA to alter cellular behaviors. This strategy has become an important tool in miRNA-based therapeutics (21). The goal of the current research has been focused on the role of the *miR-106b* cluster in the differentiation of adipose-derived MSCs (ADMSCs) into PGCs independent of the use of BMP4. The corresponding miRNA was overexpressed in ADMSCs for 4 days to induce the differentiation of these types of cells.

## Materials and Methods

### Ethics statement

In this experimental study, the perusal case-control was approved by the Human Ethics Committees of Azad University (Code number: IR.IAU.SRB.REC.1396.71).

The adipose tissue were removed and transferred under the approved protocols to the research laboratory. All efforts were made under sterile conditions.

### Cell isolation and culture

Samples containing male adipose (n: 9 samples- age: 25-40 years) under local anesthesia were obtained from cosmetic surgeries performed for the liposuction in Imam Khomeini Hospital (all subjects signed an informed consent). Samples were washed several times in phosphate buffered saline (PBS, Gibco, Germany). Then, the tissues were minced and treated with an equal volume of 0.075% type I collagenase (Sigma, Germany) with continuous agitation at 37°C for 1 hour. The enzyme activity was neutralized with Dulbecco's Modified Eagle Medium (DMEM) high glucose without glycerophosphate (Sigma, Belgium) solution containing 10% fetal bovine serum (FBS, Gibco, UK) and then centrifuged at 1200 ×g for 10 minutes to obtain a high-density cell pellet (Clinical Benchtop Centrifuges). The resultant supernatant was discharged, and stromal vascular fraction (SVF) pellet was mixed with 2,000 µl DMEM solution using a pipette. The suspended cells were subsequently passed through 100 µm nylon filter mesh (Falcon Company, USA) and incubated at 37°C in 5% CO<sub>2</sub> in DMEM solution containing 10% FBS. The medium was replaced every 2 days.

### Characterization of adipose-derived stem cells by Flow cytometry

ADSCs were washed three times in PBS and then centrifuged (Hettich, Germany) at 400 g for 5 minutes and resuspended in ice cold PBS. For the blockade of non-specific bindings, the cells were rinsed with 10% bovine serum albumin (BSA, Gibco, UK) in PBS for 30 minutes, washed three times in PBS, and incubated with mouse anti-human CD90 (Abcam, Germany), Rabbit anti-human CD105 (Abcam, Germany), Rabbit anti-human CD34 (Abcam, Germany) and rabbit anti-human CD45 (Abcam, Germany), Mouse anti-human CD44, Mouse anti-human CD73 as a primary antibody at 4°C for 1 hour. Then, the primary antibodies were washed three times in PBS at room temperature and incubated with goat anti-rabbit IgG conjugated with FITC and goat anti-mouse IgG conjugated with phycoerythrin (PE) as a secondary antibody at a ratio of 1:100 at 37°C for 30 minutes in the dark. Afterward, the cells were washed twice in PBS, centrifuged at 400 g for 5 minutes, and evaluated by flow cytometry (Olympus, Japan). The percentage of positive cells was calculated with respect to the negative control. The isotype antibody was applied in negative controls.

### Osteogenic differentiation

To induce the differentiation of ADSCs (at the fourth passage) into osteogenic cells, the culture medium of ADSCs changed to osteogenic maintenance medium containing 10 mM β-glycerophosphate, 0.2 mM ascorbic acid, and 7-10 M dexamethasone for 21 days ( all chemicals

were purchased from Sigma, UK). Cells in a culture medium were nourished every three days throughout the study. To confirm the differentiation of osteogenic cells, Alizarin Red S stain was used. Briefly, the osteogenic medium was removed and washed three times in PBS. The cells were fixed in 70% ethanol at 4°C for 1 hour. After the fixation process, cells were rinsed in deionized water and air-dried. The fixed cells were stained with 2% Alizarin Red S (pH=7.2, Sigma, Belgium) at 37°C for 1 hour, washed in deionized water, and photographed under an inverted microscope (Olympus, Japan).

### Adipogenic differentiation

ADSCs at the fourth passage were incubated for 21 days with adipogenic maintenance medium containing 50 µg/ml indomethacin, 50 µg/ml ascorbic acid, and 100 nM dexamethasone (all chemicals were purchased from Sigma, Germany). The medium changed every three days. The adipogenic differentiation was confirmed using Oil Red O (Sigma, Germany) staining. Briefly, the adipogenic medium was removed and washed three times in PBS. The cells were fixed in 10% formalin for 30-60 minutes at room temperature, washed in distilled water, and treated with 2 mL isopropanol (60%) for 5 minutes. Then, they were removed and stained with Oil Red O (2 mL to each well) at room temperature for 5 minutes. Finally, the cells were rinsed in tap water and photographed under an inverted microscope (Olympus, Japan).

### Study design

The induction of PGCs differentiation was performed based on previously research (22). At the fourth passage, the sub-confluent culture of MSCs maintained in DMEM solution supplemented with 10% FBS. Forty-eight hours prior to the induction of PGCs differentiation, media were replaced with pre-induction media consisting of DMEM, 20% FBS, and 25 ng/ml BMP4 (BME; Sigma, St. Louis, MO, Germany). To induce the PGCs differentiation and enrichment, the pre-induction media were removed, and the cells were washed with PBS. After that, cells were transfected by a lentivector expressing *miR-106b*. The percentage of PGCs-like cells was calculated in 10 randomly chosen fields under an inverted microscope. Each experiment was carried out triplicate.

### MiR-106b transfection

A lentiviral vector expressing *miR-106b* was procured from Gene Copoeia Inc. The lentivirus containing *miR-106b* and its control vector was purchased from Biosettia (USA). The lentivirus was generated regarding the User Manual of the Lenti-Pac™ HIV Expression Packaging Kit (GeneCopoeia, Inc.). For the transfection of ADSCs with lentivirus, 1×10<sup>6</sup> ADSCs were seeded on the plates, and 20 µl of virus suspension (MOI of 50) was added to the plates. The *miR-106b* and its negative control were transfected into pre-induced ADSCs using lipofectamine 3000 (Invitrogen, USA), in accordance with the manufacturer's instructions. The cells were transferred to

a plate, and cultured in 5% CO<sub>2</sub> at 37°C for 4 days.

### Reporter gene assay

Hek293 cells were infected with lentivirus carrying the *miR-106b* for 2 days. The GFP activity was monitored 24 hours after the transfection using the fluorescent microscopy assay system (Labo Med, USA). The GFP activity was considered as an internal control.

### Cell cytotoxicity assay

To determine the cytotoxicity of *miR-106b* transfection in MSCs, the cell viability was measured using MTT (3-(4, 5-Dimethylthiazol-2-yl)-2, 5-diphenyltetrazolium bromide (Atocel, Austria). Briefly, 1× cells were seeded on 96 well-plates and incubated at 37°C overnight to allow the cells to adhere. The cells were then treated with multiple concentrations of *miR-106b* including 0, 0.25, 0.5, and 1 µg of the corresponding miRNA. After the incubation, cells were incubated with MTT solution (5 mg/ml) for 4 hours at 37°C and then the medium was removed to solubilize formazan crystals. Afterward, 100 µl dimethyl sulfoxide (DMSO, Merck, Germany) was added to each well, and the absorbance was measured using an ELISA reader (Bio-Rad Laboratories, USA) at an excitation wavelength of 570 nm. The percentage of viability was evaluated by the comparison of the absorbance of treated cells with the control cells.

### Immunocytochemistry

Cultured PGCs were fixed with 4% paraformaldehyde, incubated with primary antibody, at a dilution of 1:100, against CD90 (Santa Cruz Biotechnology, Santa Cruz, CA, USA) at 4°C overnight. Then, the cells incubated with secondary antibody conjugated with FITC at room temperature for 1 hour. DAPI (Sigma, Germany) was applied for the staining of the cell nucleus. The antibody against CD90 was used at a 1:100 dilution.

### Western blot analysis

Cells were harvested and lysed in lysis buffer (RIPA, Beyotime Institute of Biotechnology, China) supplemented with protease inhibitors (PMSF, Aladdin). The equal amounts of protein (40 µg) were separated by sodium dodecyl sulfate polyacrylamide gel electrophoresis (SDS-PAGE) with 5-12% Tris-Glycine gel (Invitrogen, USA) and subjected to standard western blot analysis. Antibodies against THY1 (Santa Cruz, USA) and β-actin (Santa Cruz, USA) were diluted at 1:1,000. Secondary antibodies used for the western blot analysis were goat anti-mouse IgG-HRP (Santa Cruz, USA) or goat anti-rabbit IgG-HRP (Santa Cruz, USA). Enhanced chemiluminescence was performed according to the manufacturer's instructions (Amersham Life Sciences Inc., Arlington Heights, IL). The results were subjected to densitometry analysis using the ImageJ software. To ensure equal amounts of protein were loaded, the β-actin protein was employed as an internal control. The relative protein expression level was

defined as the ratio of the expression of the target proteins to the GAPDH expression level.

### MiRNA target genes prediction by quantitative real-time polymerase chain reaction analysis

Total RNA, including miRNAs, was extracted using the mirVana miRNA Isolation kit (Ambion, USA) according to the manufacturer's instructions. The *miR-106b* was detected using RT<sup>2</sup> miRNA First Strand Kit (SA Biosciences, USA). The specific miRNA and U6 primers purchased from QIAGEN were used for real-time polymerase chain reaction (PCR). The relative expression was determined using the comparative Ct method ( $2^{-\Delta\Delta C_t}$ ). The expression of mRNAs was determined using SYBR green real-time PCR assay. The levels of mRNA expression were normalized to that of the *GAPDH* expression as the loading control. The relative expression was calculated using the comparative Ct method ( $2^{-\Delta\Delta C_t}$ ). Table 1 shows the primers used for real-time PCR.

**Table 1:** The sequences of primers used for evaluation of relative expression

Gene	Primer sequencing (5'-3')	Accession number
<i>FRAGILIS</i>	F: CATGTCGTCTGGTCCCTGT	NM_003641.4
	R: GTGGAGGCATAGGCCTGG	
<i>GAPDH</i>	F: TTCAGCTCTGGGATGACCTT	NM_002046.7
	R: TGCCACTCAGAAGACTGTGG	
<i>STELLA</i>	F: GGTTCGGAATAAGGCAAAGAG	NM_182489.1
	R: AGGTGAGATACCAAGGGGAGG	

### Statistical analysis

The statistical analysis of the obtained data in quantitative parts was performed using the SPSS software version 16 (SPSS, Chicago, IL). The independent sample t test method or One Way ANOVA were applied for the comparison of the results between groups. The level of significance was set at  $P < 0.05$ . The data was represented by mean  $\pm$  SD. All of data was repeated 3 times. Qualitative data of the cell culture and differentiated part of experiment was described in the text as same as immunostaining and western blot result.

## Results

### Adipose-derived stem cell culture

ADSCs adhered to plastic flask similar to bone marrow MSCs which were characterized by a rapid proliferation. At earlier hours, the cells were floating, and their nucleus was visible (Fig. 1A). After 24 hours, the floated cells were adhered to dish to form fibroblast-like colonies. ADSCs formed spindle-like shape (fibroblast-like) and were loaded

with several lipid granules within those cells. The lipid granules attached to each other and created large droplets; then, released into the cells culture medium. The first was made in 7 days when the cells reached confluence. After the first passage, the cells showed extensive proliferative capacity passage. The four passages were performed in 13 days, and then, the cells were used for the differentiation experiments (Fig. 1B).

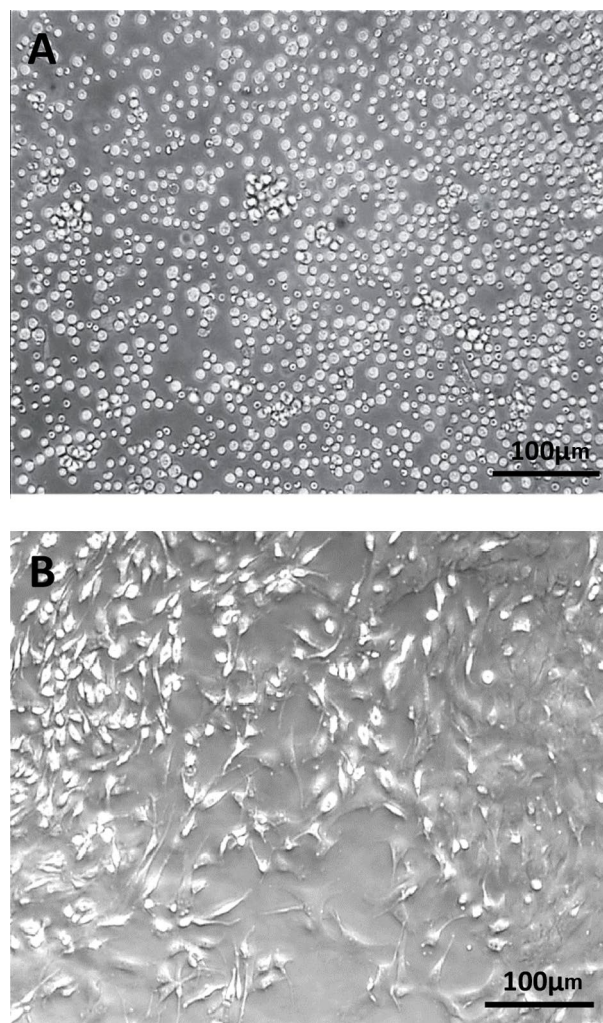


**Fig.1:** The cells isolated from ADSCs. **A.** Isolated stem cells 4 hours after incubation and **B.** ADSCs in the 4<sup>th</sup> passage (scale bar: 100 µm). ADSCs; Adipose-derived stem cells.

### Adipose-derived stem cell characterization and differentiation

As illustrated in Figure 2A, B, ADSCs showed the differentiation potential into adipogenic and osteogenic lineages while they were induced by adipogenic and osteogenic maintenance media, respectively. The adipogenic differentiated cells were visualized with Oil Red O stain. The red arrow in Figure 2A shows adipocytes and the accumulated fat droplets. The osteogenic differentiated cells were visualized with Alizarin Red S stain. The blue arrow in Figure 2B indicates osteoblasts. Furthermore, ADSCs were characterized

by their cell surface antigens. As shown in Figure 2C, a high percentage of the studied cell population were expressing the specific markers of mesenchymal stem cells including CD90 ( $79.1 \pm 5.73$ ), CD105 ( $90.1 \pm 3$ ), CD73 ( $75.8 \pm 3.61$ ), and CD44 ( $89.1 \pm 6.49$ ). The expression of the specific markers for hematopoietic stem cells was detected by few cells (CD34= $5.98 \pm 1.64$ , and CD45= $7.15 \pm 0.26$ ).

### Cell cytotoxicity assessment

In order to investigate the cytotoxicity of *miR-106b* transfection, MTT assay was conducted to examine the viability of ADSCs. According to Figure 3, after 24, 48, and 72 hours incubation time, no significant reduction was observed in the viability of cells expressing *miR-106b* compared with the control cells lacking *miR-106b*.

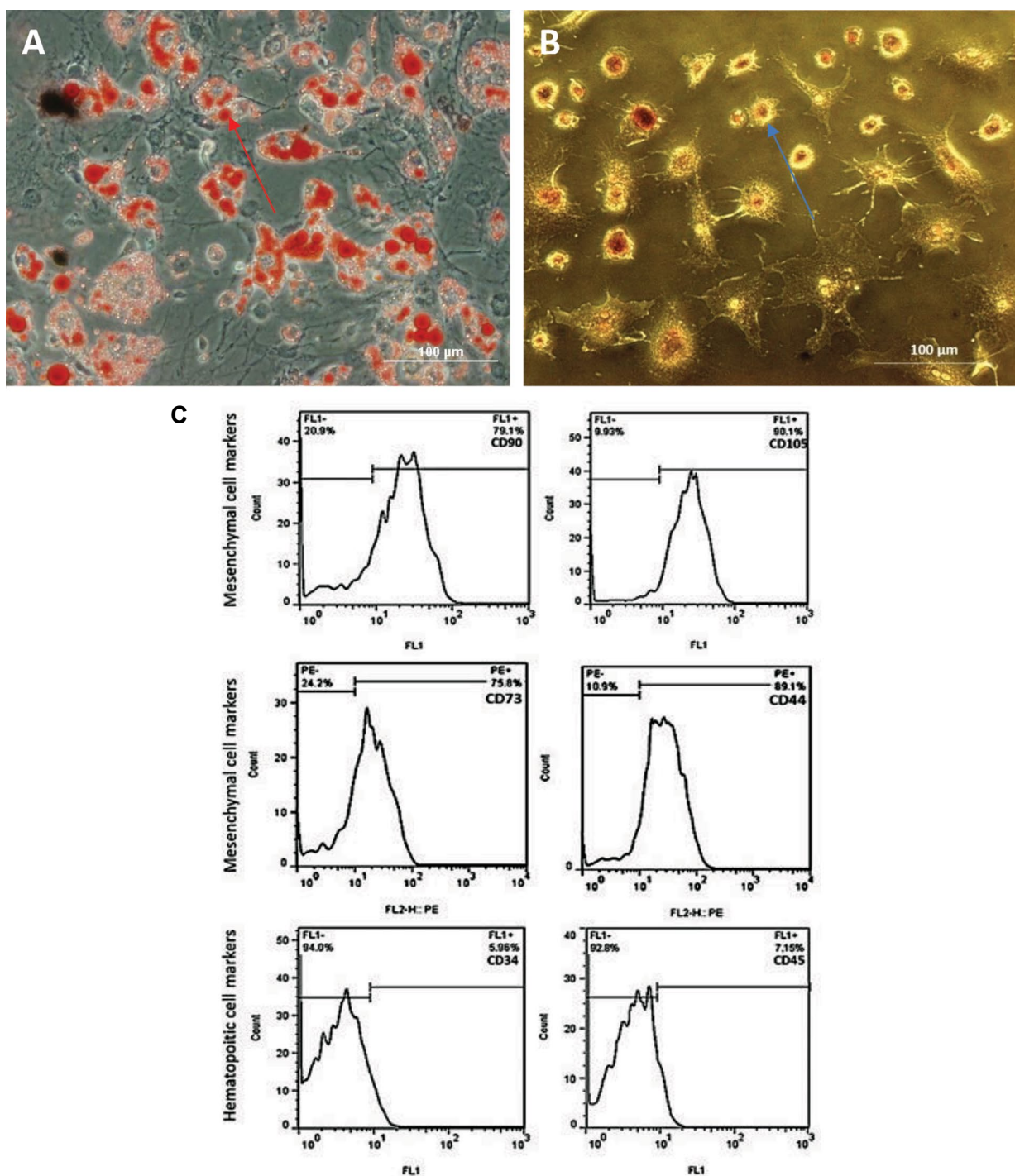


**Fig.2:** The *in vitro* osteogenesis and adipogenic differentiation. **A.** Adipose-derived stem cells (ADSCs) after incubation for 21 days in the adipogenic differentiation medium. The cells were visualized with Oil Red O staining. **B.** ADSCs after incubation for 21 days in the osteogenic differentiation medium. The cells were visualized with Alizarin Red S stain. The blue arrow indicates osteoblasts, and the red arrow shows adipocytes and the accumulated fat droplets (scale bar: 100  $\mu$ m). **C.** Cell surface markers: CD90= $79.1 \pm 5.73$ , CD105= $90.1 \pm 3$ , CD73= $75.8 \pm 3.61$ , CD44= $89.1 \pm 6.49$ , CD34= $5.98 \pm 1.64$ , and CD45= $7.15 \pm 0.26$ . The number of positive cells for each marker was assayed by flow cytometry. The data was presented as mean  $\pm$  SD.

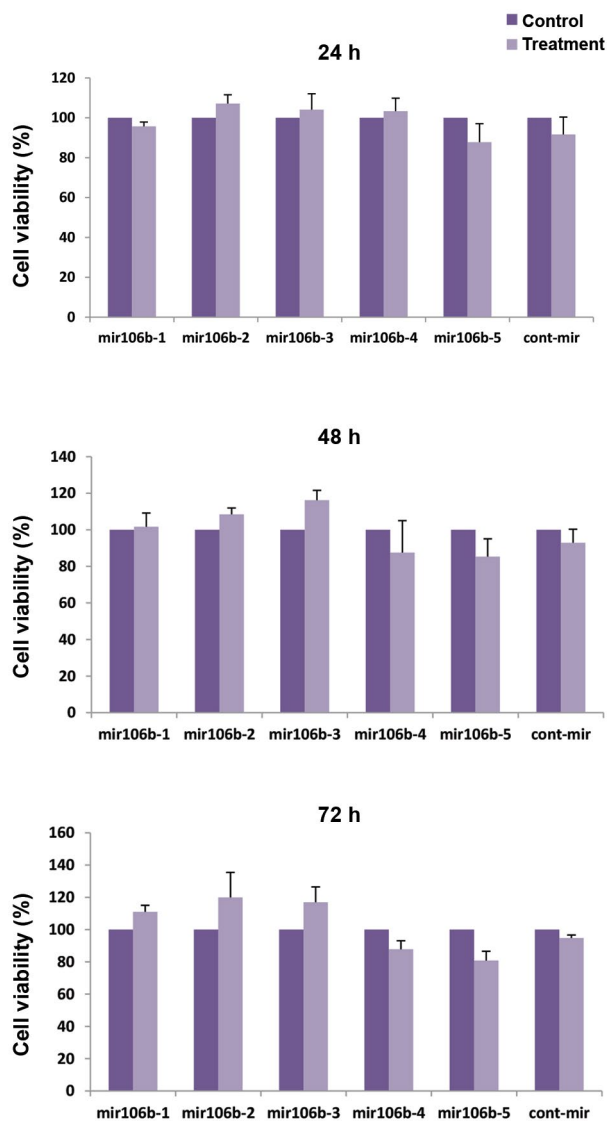


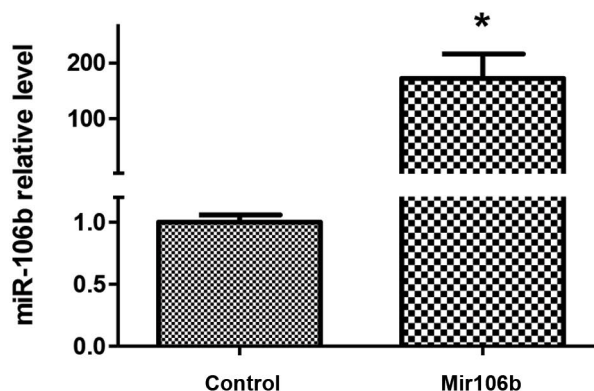
**Fig.3:** Cytotoxicity of *miR-106b* expressing MSCs. The cytotoxicity level of *miR-106b* expressing MSCs was evaluated after 24, 48, 72 hours incubation at various concentrations of *miR-106b*. MSCs; Mesenchymal stem cells and h; Hour.

### Primordial germ cells induction from mesenchymal stem cells

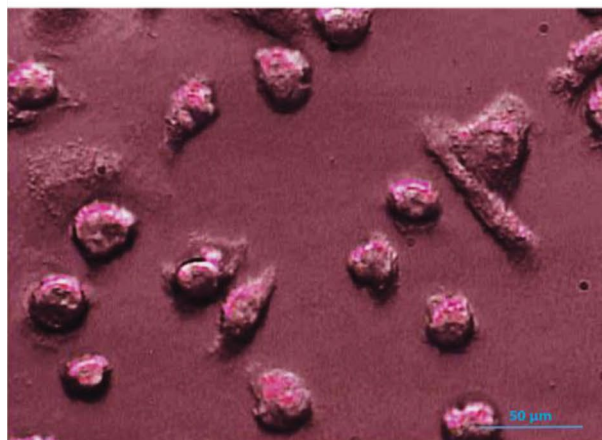
The results showed that three of four specific differentiation markers (FRAGILIS, Thy1, and STELLA) were significantly increased at the levels of gene and protein when the *miR-106b* was overexpressed (Fig.4A). Alkaline phosphatase expression was showed in cells transfected by the *miR-106b* (Fig.4B). Photograph showed positive alkaline phosphatase staining of differentiated cells. A smaller alkaline phosphatase negative cell, possibly a contaminating undifferentiated MSCs. Figure 4C and D indicate the expression levels of *STELLA* and *FRAGLIS* genes were significantly unregulated in BMP4-, and *miR-106b*-treated cells compared to control cells. Moreover as illustrated in Figure 4E, the amount of THY1 protein was significantly increased in *miR-106b*-treated cells compared to BMP4-treated cells and control.

Furthermore, as shown in Figure 5, the expression level of CD90 protein was significantly higher in cells transfected with the *miR-106b* than the cells treated with BMP4. CD90 expression was expressed around the stained nucleus by DAPI (4',6-diamidino-2-phenylindole) in differentiated cell surface. Based on the cells that were stained and non-stained around the nucleus, the results showed over expression of CD90 marker in immunostaining assessment.

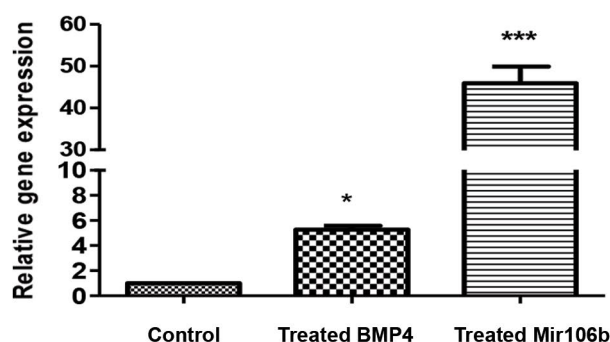
**A**



**B**



**C**



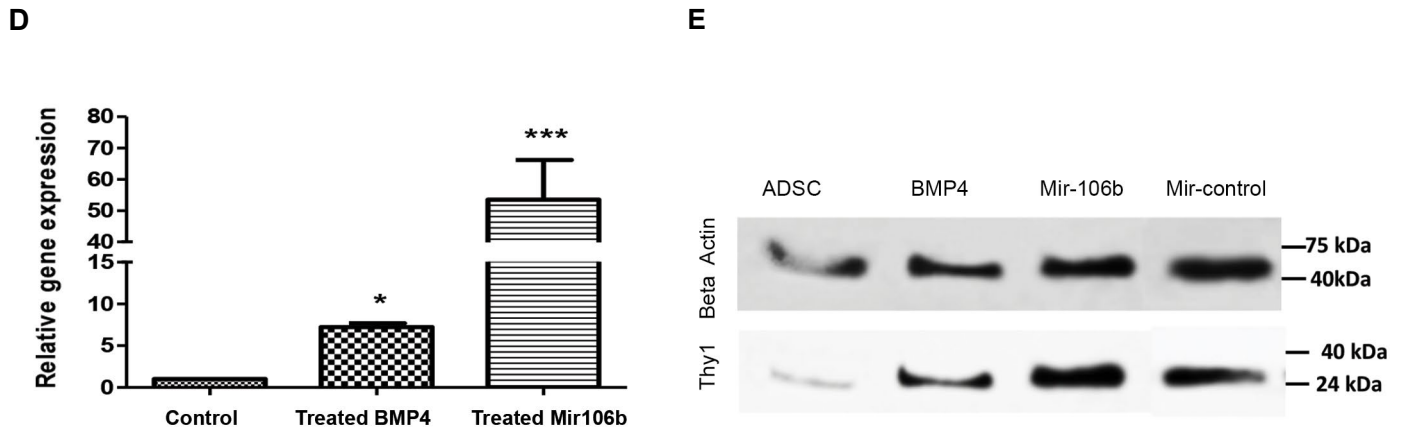


**Fig.4:** The differentiation of ADSCs into PGCs. **A.** The expression of the *miR-106b* measured by real-time PCR after the transfected by lentivector expressing *miR-106b*. **B.** Alkaline phosphatase-positive cells (scale bar: 50  $\mu$ m). **C, D.** The expression of *STELLA* and *FRAGILIS* genes and **E.**Thy1 protein levels were evaluated as specific differentiation markers using real-time PCR and western blot analysis, respectively. ADSCs; Adipose-derived stem cells, PGCs; Primordial germ cells and PCR; Polymerase chain reaction. \* demonstrates the significant changes in comparison to control (\*;  $P \leq 0.05$  and \*\*\*;  $P \leq 0.0001$ ).

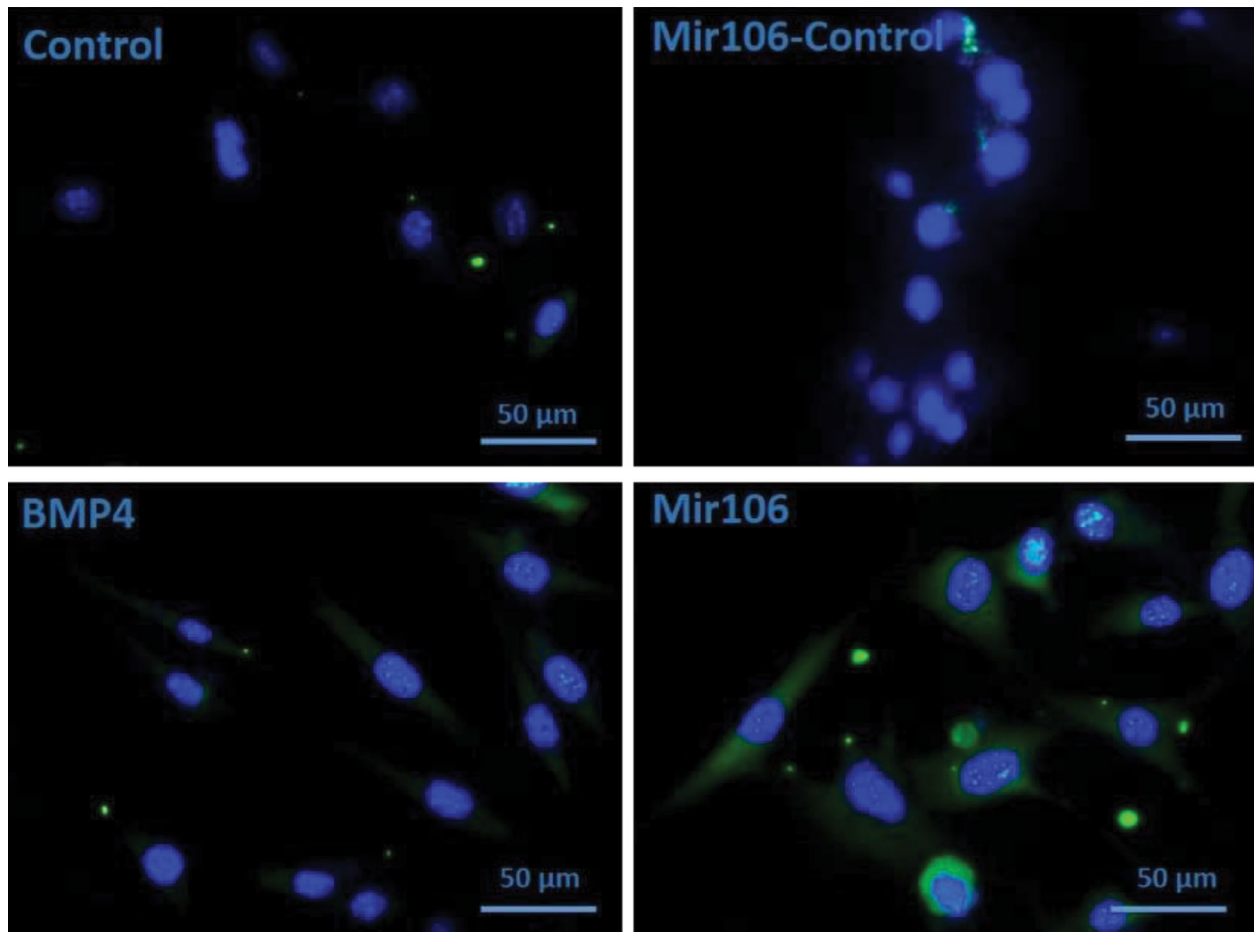


**Fig.5:** CD90 protein level measured as a marker of differentiation on germ cells (ADSCs) (scale bar: 50  $\mu$ m).

## Discussion

The potential capacity of somatic stem cells to differentiate into PGCs, SSCs (23, 24), or advanced spermatids through the meiosis process under appropriate culture conditions has been well-established

in the literature (25, 26). The clinical value of direct differentiation might be more valuable than other strategies as the gene transfection creates an imbalance in the gene contents of genetically modified cells during spermatogenesis. However, the molecular mechanisms

underlying the germ lineage differentiation from MSCs remain elusive.

The miRNAs are known to regulate the development of germ cells (27). To understand the regulatory role of miRNAs in the development of PGCs, ADMSCs were differentiated into PGCs in which *miR-106b* was transfected into ADMSCs to facilitate the differentiation of these cells into PGCs through the upregulation of some target genes responsible for the development of the cell differentiation. Hence, an *in vitro* model of *miR-106b*-transfected ADSCs was employed to induce the differentiation of these cells into PGCs thereby influencing the proliferation, morphogenesis and protein localization of the corresponding cells. Our findings indicate that the transfection of MSCs with *miR-106b* can by itself increase the specific markers of PGCs namely *STELLA* and *FRAGILIS* genes, as well as the expression of Thy1 protein when compared with MSCs treated with BMP4. Moreover, the surface expression of CD90 was higher in cells transfected with *miR-106b* than the cells treated with BMP4. Numerous reports have indicated that miRNAs are potentially able to induce the differentiation of MSCs into various tissues. In line with this, an *in vitro* study performed by Sluijter et al. (28) indicated that a number of miRNAs are involved in the proliferation and differentiation of cardiomyocyte progenitor cells (CMPCs). They showed that *miR-1* and *miR-499* can regulate the proliferation of human CMPCs, as well as their differentiation into cardiomyocytes. Previous studies have also highlighted that miRNAs play critical roles in the process of neurogenesis. Jiao et al. (29) reported that miR-124 promotes the neural differentiation of the subventricular zone, which is the most substantial neurogenic niche in the brain of adult mammalian species. Also, it has been shown that miR-23b induces the chondrogenic differentiation of human MSCs through the suppression of protein kinase A (PKA) signaling (30).

The overall importance of miRNA signaling for the regulation of spermatogenesis has been further elucidated using a conditional knockout of *Dicer* gene in germ cells. The silencing of the *Dicer1* gene in pro-spermatogonia at the early-stage of the birth using *Ddx4* promoter-driven Cre expression resulted in altered meiotic progression increased apoptosis in pachytene spermatocytes, reduced number of round-shape spermatids, and morphological defects in spermatozoa (31). In a study performed by Holt et al. (32), they revealed that nine newly identified miRNAs including miR-10b, -18a, -93, -106b, -126-3p, -127, -181a, -181b, and -301, which are all exclusively expressed in PGCs according to their comparative study, profiling the miRNA expression of PGCs at 12.5 days post-coitum (dpc), gonocytes (GCs) at 15.5 dpc, SSCs at 5 days post-partum (dpp), and testes at four weeks. BMP4 signaling acts through the Smad family proteins and requires a ligand-specific co-receptor TGF- $\beta$  (transforming growth factor-Beta) in murine SSCs (33). In agreement with an indirect mechanism, Okamura et al. (34) have shown that the deficiency of PGCs in

embryos knockout for BMP4 can be compensated by the activation of a sub-type of type I BMP receptor named Activin A Receptor type 1 (ACVR1) in the visceral endoderm, but not the epiblast where PGC precursors are present. It has been implicated that the expression of *FRAGILIS* is elevated in the migratory PGC, stimulating the expression of other germ cell-specific genes such as *VASA* and *STELLA* (35). *STELLA* is considered a crucial marker for murine PGCs, while *DAZZL* and *DDX4* begin their expression in murine PGCs from around the E10.5 stage and last to be expressed afterward (36). It has been reported that *miR-106b* can activate the Wnt/beta-catenin signaling pathway as the loss of *WNT5A* disrupts murine PGCs migration and male sexual development in mice (37).

## Conclusion

*In vitro* model of the spermatogenesis development are noticed by many researchers. This study developed a new approach to gain PGCs from MSCs by the transfection of ADMSCs with the *miR-106b* lentivector. Upregulation of *miR-106b* caused to the specific gene markers of the PGC expression, more efficient than the conventional method used by BMP4. It is thought that finding of pathways governing the meiotic and post meiotic cells would shed light on our understanding about the essential molecules involved in the spermatogenesis and its progression.

## Acknowledgments

We are thankful to the laboratory assistants of the Histogenotech Company for sharing their valuable knowledge and experience to perform this study. There is no financial support and conflict of interest in this study.

## Authors' Contributions

Z.M.; Participated in study design, investigation, and data analyses. S.M.; Performed the experiments and wrote the draft. Sh.I.; Participated in statistical analysis and data curation. K.P.; Participated in the finalization of the manuscript, data validation and approved the final draft. All authors read and approved the final manuscript.

## References

1. Vahdati A, Fathi A, Hajihoseini M, Aliborzi G, Hosseini E. The regenerative effect of bone marrow-derived stem cells in spermatogenesis of infertile hamster. *World J Plast Surg.* 2017; 6(1): 18-25.
2. Huang P, Lin LM, Wu XY, Tang QL, Feng XY, Lin GY, et al. Differentiation of human umbilical cord Wharton's jelly-derived mesenchymal stem cells into germ-like cells in vitro. *J Cell Biochem.* 2010; 109(4): 747-754.
3. Gnecci M, Melo LG. Bone marrow-derived mesenchymal stem cells: isolation, expansion, characterization, viral transduction, and production of conditioned medium. *Methods Mol Biol.* 2009; 482: 281-294.
4. Gimble JM, Katz AJ, Bunnell BA. Adipose-derived stem cells for regenerative medicine. *Circ Res.* 2007; 100(9): 1249-1260.
5. Leatherman J. Stem cells supporting other stem cells. *Front Genet.* 2013; 4: 257.
6. Qu G, Xie X, Li X, Chen Y, De Isla N, Huselstein C, et al. Immunomodulatory function of mesenchymal stem cells: regulation and application. *J Cell Immunother.* 2018; 4(1): 1-3.
7. Nayernia K, Lee JH, Drusenheimer N, Nolte J, Wulf G, Dressel R, et al. Derivation of male germ cells from bone marrow stem cells.

- Lab Invest. 2006; 86(7): 654-663.
8. Cakici C, Buyrukcu B, Duruksu G, Haliloglu AH, Aksoy A, Isik A, et al. Recovery of fertility in azoospermia rats after injection of adipose-tissue-derived mesenchymal stem cells: the sperm generation. *Biomed Res Int.* 2013; 2013: 529589.
  9. Zhang D, Liu X, Peng J, He D, Lin T, Zhu J, et al. Potential spermatogenesis recovery with bone marrow mesenchymal stem cells in an azoospermic rat model. *Int J Mol Sci.* 2014; 15(8): 13151-13165.
  10. Ambros V. The functions of animal microRNAs. *Nature.* 2004; 431(7006): 350-355.
  11. Mishima T, Takizawa T, Luo SS, Ishibashi O, Kawahigashi Y, Mizuguchi Y, et al. MicroRNA (miRNA) cloning analysis reveals sex differences in miRNA expression profiles between adult mouse testis and ovary. *Reproduction.* 2008; 136(6): 811-822.
  12. Ro S, Park C, Sanders KM, McCarrey JR, Yan W. Cloning and expression profiling of testis-expressed microRNAs. *Deve Biol.* 2007; 311(2): 592-602.
  13. Yan N, Lu Y, Sun H, Qiu W, Tao D, Liu Y, et al. Microarray profiling of microRNAs expressed in testis tissues of developing primates. *J Assist Reprod Genet.* 2009; 26(4): 179-186.
  14. Yan N, Lu Y, Sun H, Tao D, Zhang S, Liu W, et al. A microarray for microRNA profiling in mouse testis tissues. *Reproduction.* 2007; 134(1): 73-79.
  15. Buchold GM, Coarfa C, Kim J, Milosavljevic A, Gunaratne PH, Matzuk MM. Analysis of microRNA expression in the prepubertal testis. *PLoS One.* 2010; 5(12): e15317.
  16. Tong MH, Mitchell D, Evanoff R, Griswold MD. Expression of Mirlet7 family microRNAs in response to retinoic acid-induced spermatogonial differentiation in mice. *Biol Reprod.* 2011; 85(1): 189-197.
  17. Niu Z, Goodyear SM, Rao S, Wu X, Tobias JW, Avarbock MR, et al. MicroRNA-21 regulates the self-renewal of mouse spermatogonial stem cells. *Proc Natl Acad Sci USA.* 2011; 108(31): 12740-12745.
  18. Hayashi K, de Sousa Lopes SMC, Kaneda M, Tang F, Hajkova P, Lao K, et al. MicroRNA biogenesis is required for mouse primordial germ cell development and spermatogenesis. *PLoS One.* 2008; 3(3): e1738.
  19. Maatouk DM, Loveland KL, McManus MT, Moore K, Harfe BD. Dicer1 is required for differentiation of the mouse male germline. *Biol Reprod.* 2008; 79(4): 696-703.
  20. Tong MH, Mitchell DA, McGowan SD, Evanoff R, Griswold MD. Two miRNA clusters, Mir-17-92 (Mirc1) and Mir-106b-25 (Mirc3), are involved in the regulation of spermatogonial differentiation in mice. *Biol Reprod.* 2012; 86(3): 72.
  21. Mishima T, Sadovsky E, Gegick ME, Sadovsky Y. Determinants of effective lentivirus-driven microRNA expression in vivo. *Sci Rep.* 2016; 6: 33345.
  22. Mazaheri Z, Movahedin M, Rahbarizadeh F, Amanpour S. Different doses of bone morphogenetic protein 4 promote the expression of early germ cell-specific gene in bone marrow mesenchymal stem cells. *In Vitro Cell Dev Biol Anim.* 2011; 47(8): 521-525.
  23. Xie L, Lin L, Tang Q, Li W, Huang T, Huo X, et al. Sertoli cell-mediated differentiation of male germ cell-like cells from human umbilical cord Wharton's jelly-derived mesenchymal stem cells in an in vitro co-culture system. *Eur J Med Res.* 2015; 20(1): 9.
  24. Latifpour M, Shakiba Y, Amidi F, Mazaheri Z, Sobhani A. Differentiation of human umbilical cord matrix-derived mesenchymal stem cells into germ-like cells. *Avicenna J Med Biotechnol.* 2014; 6(4): 218-227.
  25. Aflatoonian B, Ruban L, Jones M, Aflatoonian R, Fazeli A, Moore H. In vitro post-meiotic germ cell development from human embryonic stem cells. *Hum Reprod.* 2009; 24(12): 3150-3159.
  26. Panula S, Medrano JV, Kee K, Bergström R, Nguyen HN, Byers B, et al. Human germ cell differentiation from fetal and adult-derived induced pluripotent stem cells. *Hum Mol Genet.* 2011; 20(4): 752-762.
  27. Banisch TU, Goudarzi M, Raz E. Small RNAs in germ cell development. *Curr Top Dev Biol.* 2012; 99: 79-113.
  28. Sluijter JPG, van Mil A, van Vliet P, Metz CHG, Liu J, Doevendans PA, et al. MicroRNA-1 and -499 regulate differentiation and proliferation in human-derived cardiomyocyte progenitor cells. *Arterioscler Thromb Vasc Biol.* 2010; 30(4): 859-868.
  29. Jiao S, Liu Y, Yao Y, Teng J. miR-124 promotes proliferation and differentiation of neuronal stem cells through inactivating notch pathway. *Cell Biosci.* 2017; 7: 68.
  30. Ham O, Song BW, Lee SY, Choi E, Cha MJ, Lee CY, et al. The role of microRNA-23b in the differentiation of MSC into chondrocyte by targeting protein kinase A signaling. *Biomaterials.* 2012; 33(18): 4500-4507.
  31. Chen X, Li X, Guo J, Zhang P, Zeng W. The roles of microRNAs in regulation of mammalian spermatogenesis. *J Anim Sci Biotechnol.* 2017; 8: 35.
  32. Holt JE, Stanger SJ, Nixon B, McLaughlin EA. Non-coding RNA in spermatogenesis and epididymal maturation. *Adv Exp Med Biol.* 2016; 886: 95-120.
  33. Jiramongkolchai P, Owens P, Hong CC. Emerging roles of the bone morphogenetic protein pathway in cancer: potential therapeutic target for kinase inhibition. *Biochem Soc Trans.* 2016; 44(4): 1117-1134.
  34. Okamura D, Hayashi K, Matsui Y. Mouse epiblasts change responsiveness to BMP4 signal required for PGC formation through functions of extraembryonic ectoderm. *Mol Reprod Dev.* 2005; 70(1): 20-29.
  35. Toyooka Y, Tsunekawa N, Takahashi Y, Matsui Y, Satoh M, Noce T. Expression and intracellular localization of mouse Vasa-homologue protein during germ cell development. *Mech Dev.* 2000; 93(1-2): 139-149.
  36. Saitou M, Miyauchi H. Gametogenesis from pluripotent stem cells. *Cell Stem Cell.* 2016; 18(6): 721-735.
  37. Chawengsaksophak K, Svingen T, Ng ET, Epp T, Spiller CM, Clark C, et al. Loss of Wnt5a disrupts primordial germ cell migration and male sexual development in mice. *Biol Reprod.* 2012; 86(1): 1-12.

# Neuroprotective Effects of Normobaric Hyperoxia and Transplantation of Encapsulated Choroid Plexus Epithelial Cells on The Focal Brain Ischemia

Maesumeh Eslami, Ph.D.<sup>1\*</sup>, Shahrbanoo Oryan, Ph.D.<sup>1</sup>, Mehdi Rahnema, Ph.D.<sup>2</sup>, Mohammad Reza Bigdeli, Ph.D.<sup>3,4\*</sup>

1. Department of Animal Physiology, Faculty of Biological Sciences, Kharazmi University, Tehran, Iran

2. Biology Research Center, Zanjan Branch, Islamic Azad University, Zanjan, Iran

3. Department of Animal Sciences and Biotechnology, Faculty of Life Sciences and Biotechnology, Shahid Beheshti University, Tehran, Iran

4. Institute for Cognitive and Brain Science, Shahid Beheshti University, Tehran, Iran

\*Corresponding Addresses: P.O.Box: 15719-14911, Department of Animal Physiology, Faculty of Biological Sciences, Kharazmi University, Tehran, Iran

P.O.Box: 193815476, Department of Animal Sciences and Biotechnology, Faculty of Life Sciences and Biotechnology, Shahid Beheshti University, Tehran, Iran

Emails: [masumeeslami@yahoo.com](mailto:masumeeslami@yahoo.com), [bigdelimohammadreza@yahoo.com](mailto:bigdelimohammadreza@yahoo.com)

Received: 09/October/2019, Accepted: 21/December/2019

## Abstract

**Objective:** Choroid plexus epithelial cells (CPECs) have the epithelial characteristic, produce cerebrospinal fluid, contribute to the detoxification process in the central nervous system (CNS), and are responsible for the synthesis and release of many nerve growth factors. On the other hand, studies suggest that normobaric hyperoxia (HO) by induction of ischemic tolerance (IT) can protect against brain damage and neurological diseases. We examined the effect of combination therapy of encapsulated CPECs and HO to protect against ischemic brain injury.

**Materials and Methods:** In this experimental study, six groups of adult male Wistar rats were randomly organized: sham, room air (RA)+middle cerebral artery occlusion (MCAO), HO+MCAO, RA+MCAO+encapsulated CPECs, HO+MCAO+encapsulated CPECs, RA+MCAO+empty capsules. RA/HO were pretreatment. The CPECs were isolated from the brain of neonatal Wistar rats, cultured, and encapsulated. Then microencapsulated CPECs were transplanted in the neck of the animal immediately after the onset of reperfusion in adult rats that had been exposed to 60 minutes MCAO. After 23 hours of reperfusion, the neurologic deficit score (NDS) was assessed. Next, rats were killed, and brains were isolated for measuring brain infarction volume, blood-brain barrier (BBB) permeability, edema, the activity of superoxide dismutase (SOD), and catalase (CAT) and also, the level of malondialdehyde (MDA).

**Results:** Our results showed that NDS decreased equally in HO+MCAO, RA+MCAO+encapsulated CPECs, and HO+MCAO+encapsulated CPECs groups. Brain infarction volume decreased up 79%, BBB stability increased, edema decreased, SOD and CAT activities increased, and MDA decreased in the combination group of HO and transplantation of encapsulated CPECs in the ischemic brain as compared with when HO or transplantation of encapsulated CPECs was applied alone.

**Conclusion:** The combination of HO and transplantation of encapsulated CPECs for stroke in rats was more effective than the other treatments, and it can be taken into account as a promising treatment for ischemic stroke.

**Keywords:** Brain Ischemia, Choroid Plexus, Hyperoxia, Oxidative Stress

Cell Journal (Yakhteh), Vol 23, No 3, August 2021, Pages: 303-312

**Citation:** Eslami M, Oryan Sh, Rahnema M, Bigdeli MR. Neuroprotective effects of normobaric hyperoxia and transplantation of encapsulated choroid plexus epithelial cells on the focal brain ischemia. Cell J. 2021; 23(3): 303-312. doi: 10.22074/cellj.2021.7204.

This open-access article has been published under the terms of the Creative Commons Attribution Non-Commercial 3.0 (CC BY-NC 3.0).

## Introduction

Cerebral ischemia is characterized by an occlusion of blood vessels that leads to interruption of positional blood flow to the brain and the lack of oxygen and glucose (1). Furthermore, in the stroke, depolarization of the neuronal membrane, the release of the neurotransmitter glutamate, and activation of receptor n-methyl-d-aspartate (NMDA), overloading calcium and the apoptosis occur (2). These incidences are related to enhanced reactive oxygen species (ROS) production that disturbs the antioxidant systems and results in an increase of inflammation and brain injury. Moreover, the blood-brain barrier (BBB) loses its integrity due to reperfusion, the sudden increase in oxygen, extra production of ROS, and destruction of proteins of the blood vessel cell membrane (3-5). Therefore, by increasing the antioxidant capacity, it is expected to decrease brain tissue damage due to oxidative

stress in stroke and improve the permeability of the BBB.

The exposure to under-threshold injurious stimuli induces ischemic tolerance (IT), also known as ischemic preconditioning (IP), that activates endogenous neuronal protective processes (6). Various stressors, including anesthetics, cortical spreading depression, ischemia, seizures, inflammatory mediators, and metabolic occlusive, can induce preconditioning in the brain (7). The evidence suggests that ROS mediate brain damage in cerebral mortal and sub-mortal ischemia importantly. Several studies propose that preconditioning with hyperoxia (HO) decreases ischemic brain injury mediated by induction of IT and via the production of ROS (8, 9) and is neuroprotective in experimental ischemic stroke (8-12). Moreover, reports show that HO is applied in the treatment of human stroke, also (13, 14).

There are also many reports of cell therapy for stroke, which demonstrate cell transplantation has good functional

and structural results in animals and humans (15-17). The choroid plexus (CP) is within the brain ventricles and consists of epithelial cells that are involved in the secretion of cerebrospinal fluid (CSF) and surround a weak connective tissue containing penetrable capillaries and cells of lymphoid family. Abundant neurotrophic factors, including nerve growth factor (NGF), brain-derived neurotrophic factor (BDNF), vascular endothelial growth factor (VEGF) neurotrophin 3-4 (NT3-4) and fibroblast growth factor 2 (FGF2) are produced and secreted by the choroid plexus epithelial cells (CPECs) to CSF (18, 19). On the other hand, it has been reported that encapsulation of cells by biomaterials such as alginate allows oxygen and nutrients to nourish the encapsulated cells and provides controlled diffusion of proteins and other therapeutic molecules and at the same time restricts the passage of cytotoxic agents from the host immune defense system (Fig.1) (20). *In vitro* studies show that many active neurotrophic factors such as BDNF and GDNF are secreted by both non-encapsulated and encapsulated CPECs that have a similar model of secretion (21). Therefore, it is expected that CPECs act indirectly by secreting and releasing the trophic substances without the encapsulation effect on the secretory property of cells. The neuroprotective effect of CPECs and conditioned medium of cultured CPECs against ROS-induced oxidative stress has been well shown (22). The previous studies indicated that transplantation of CPECs protected against ischemic brain injury and improved behavioral deficits in animal models of stroke (16, 23).

Although the effect of different monotherapies on stroke has been widely investigated, functional recovery is typically only partial. It seems that applying monotherapies in combination with each other to be an appropriate strategy to achieve a favorable recovery. Hence, in this context, we combined two therapeutic strategies to promote functional recovery after middle cerebral artery occlusion (MCAO) and investigated the effect of this combination on focal brain ischemia. Thus, considering the above reported beneficial effects of both HO and CPECs in the treatment of stroke, and considering that the combination of these two for the treatment of stroke had not been studied, we combined preconditioning by HO and transplants of encapsulated rat CPECs for ischemic stroke in rat for obtaining protective effects.

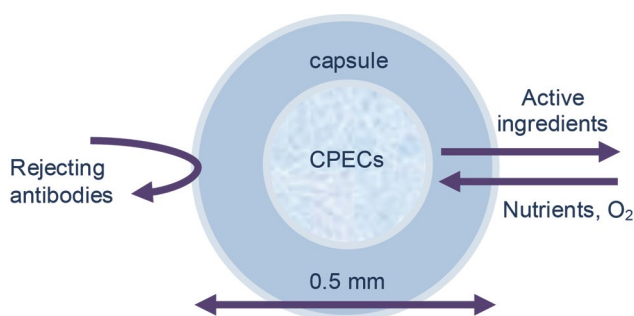


**Fig.1:** Schematic image of the encapsulated CPECs. The capsule prevents the immune system activation against CPECs and provides the interaction of cells with the extracellular environment. The diameter of the microcapsule is 0.5 mm. CPECs; Choroid plexus epithelial cells.

## Materials and Methods

### Experimental animals

In this experimental study, adult male Wister rats weighted from 250 up to 350 g were kept at fixed humidity, the temperature of  $23 \pm 2^\circ\text{C}$  and 12-hour cycle of light-dark (07:00-19:00) for all experiments. Water and food were accessible free. The conduction of all manners was with the approval of the Institutional Animal Ethics Committee of Islamic Azad University (code: IR.IAU.Z.REC.1396, 69). In total, five main groups (in each group, 35 rats) and a sham group (n=21 rats) of rats were randomly formed. HO+MCAO group was put up in an environmental chamber and subjected to 95% oxygen ( $\text{O}_2$ ) periodically, i.e., four sequential hours in each day for continuous six days (8). RA+MCAO group was located in the environmental chamber in the like procedure and subjected to room air (RA) equivalent (21%  $\text{O}_2$ ) for the same intervals. The balance gas when using 95%  $\text{O}_2$  and 21%  $\text{O}_2$ , was nitrogen. Soda-lime, a  $\text{CO}_2$  absorber, was used at the bottom of the container to prevent  $\text{CO}_2$  retention. So with this, we tried to have the rest of nitrogen. The RA+MCAO+encapsulated CPECs group was exposed to RA, and alginate encapsulated CPECs were transplanted in the neck of the rats. The HO+MCAO+encapsulated CPECs group was subjected to HO for the same intervals, and then alginate encapsulated CPECs were implanted in the neck of the rats. The RA+MCAO+empty capsules group was exposed to RA, and free-cell capsules were transplanted in the neck of the rats. At 48 hours after pretreatment by the HO or RA, all the groups were exposed to MCAO for 60 minutes, and then encapsulated CPECs or empty capsules were transplanted in related groups. Each main group was divided randomly into four subgroups to evaluate infarct volume (n=7), brain water content or edema (n=7), the permeability of BBB (n=7), and catalase (CAT) and superoxide dismutase (SOD) activities and malondialdehyde (MDA) level (n=7). In the sham group, three subgroups were designed to evaluate cerebral edema (n=7), the permeability of BBB (n=7), and antioxidant activity (n=7). The neurobehavioral studies were performed by the individual blinded to animal groups before each group was divided randomly into the mentioned subgroups. In a subset of rats, just before removing animals from the environmental chamber, an analysis of arterial blood gas was carried out. Laser Doppler flowmeter (MBF3, Moor Instruments, Axminster, UK) was applied to the record of regional cerebral blood flow (rCBF).

### Choroid plexus epithelial cells isolation and culture

CP tissues were excised from the lateral ventricles of neonatal rats (4-5 day-old), rinsed by phosphate-buffered saline (PBS, Sigma, USA), and next, the incubation with 0.25% trypsin solution (Invitrogen-Gibco, England) was performed for 20 minutes at  $37^\circ\text{C}$ . The next step was the addition of fetal bovine serum (FBS, Invitrogen-Gibco, England) and the centrifuge for 5 minutes. The sediment was transmitted to a culture medium, including Dulbecco's

Modified Eagle's Media (DMEM/F12, Invitrogen-gibco, England), 10% FBS, and 1% pen/strep antibiotic (Sigma, USA). 20  $\mu$ M cytosine arabinoside (Sigma, USA) was used to prevent fibroblast proliferation for one week. The culture medium was changed every 48 hours (22).

### Immunocytofluorescence

Transthyretin (TTR) is the first known protein synthesized solely by the CP and is a marker for CPECs. In this study, for confirmation that cells isolated from the brain are CPECs and not another cell, the immunocytofluorescence was performed to identify the TTR marker. Immunocytofluorescence technique was performed according to the method previously described (22). A 24-well plate was used to CPECs culture. Then, cells were fixed with 4% paraformaldehyde (Sigma, USA). The next steps were the washing with PBS, to be permeable with Triton X-100 (Sigma, USA), and the incubation with the normal goat serum (Abcam, England). Afterward, cells were incubated with the primary antibody against TTR at 4°C. After washing with PBS, the fluorescent secondary antibody (Abcam, England) was used. Finally, the cells were painted by diamidino-2-phenylindole (DAPI) dye (Sigma, USA) and studied by fluorescence microscopy (Olympus, IX 71, Japan).

### Preparing alginate encapsulated choroid plexus epithelial cells

The suspension of CPECs, separated from the bottom of the flask by trypsin, was prepared in a 1.5% alginate solution (Sigma, USA). Then, to the formation of alginate beads, suspension exuded to 60 mM CaCl<sub>2</sub> solution (Merck, Germany). After that, incubation of alginate beads was performed respectively with 0.1% poly-L-lysine solution (Sigma, USA), 0.1% alginate solution, and 55 mM sodium citrate solution (Merck, Germany) each for 5 minutes (24). After washing microcapsules by the normal saline, medium of DMEM/F12 and FBS was used for the culture of microcapsules for seven days prior to implantation. Microcapsules were 0.5 mm in diameter (Fig.1).

### Studying the permeability of alginate microcapsules

For confirmation that the secreted material from the cells and the nutrients for the cells can pass through the microcapsule wall, fluorescent Thioflavin T (ThT, Sigma, USA) color was used. It can pass through the microcapsule wall and observe inside it. For this purpose, cell-free alginate microcapsules were created. Then, alginate microcapsules were incubated for 8 hours in a 0.4 mM ThT solution in the dark. Eventually, the washed microcapsules were studied by a fluorescent microscope (Olympus, IX 71, Japan).

### Environmental chamber

HO treatment (95% O<sub>2</sub>) was initiated in a chamber (65×35×45 cm) with a port of gas entry and exit. Oxygen was delivered at a rate of 3 L/minutes, constantly monitoring its concentration inside the container via

an oxygen meter (Lutron-Do5510, Taiwan). A carbon dioxide absorber, Soda-lime (BDH Limited, Poole, UK), was used in the under of the container. According to the experimental groups, the oxygen concentration was kept at 95% or 21% for HO or RA groups, respectively.

### Focal cerebral ischemia and middle cerebral artery occlusion

For the anesthetization of rats, the 10% chloral hydrate (Merck, Germany, 350 mg/kg, i.p.) was used. According to the previously described method (25), MCAO was done. First, the right common carotid artery (CCA) was represented and separated. A 3-0 silicone-coated nylon suture with a rounded tip by heat was inserted into the internal carotid artery (ICA) and then was moved forward until it occluded the beginning of the middle cerebral artery (MCA). After the advance of approximately 20-22 mm of the suture, calculated from the carotid bifurcation, was created moderate resistance that showed the inhabitanacy of the tip in the anterior cerebral artery (ACA) and the blocking the blood flow to the MCA (Fig.2A). After 60 minutes of ischemia, the suture was pulled out, and reperfusion was created. During surgery, rectal temperature was recorded with a thermometer (Citizen-513w, CITIZEN, UAE) and kept at 37°C by heating and cooling of the surface.

### Transplantation of alginate microcapsules

At one hour after ischemia and immediately after the onset of reperfusion, the encapsulated CPECs or empty capsules were transplanted in the neck of the animal where the carotid artery was exposed to view. Afterward, the surgical site was sutured.

### Biocompatibility of the microcapsule

After 24 hours, microcapsules containing CPECs were regained to study the biocompatibility and stability of them when transplanted in the neck of the animal. Microcapsules were examined after washing with saline buffer under the inverted microscope. Also, to determine the percentage of live cells, decapsulation was initially performed with 55 mM sodium citrate solution. Then, 20  $\mu$ l of cell suspension with 20  $\mu$ l of 0.25% trypan blue dye was mixed. Afterward, 10  $\mu$ l of the above mixture was placed on one side of a hemacytometer counter, and then cells studied by a light microscope. Blue cells are the dead cells, and clear cells are viable. The viable cell percentage was obtained via division of the number of viable cells to the number of total cells and multiplication by 100.

### Neurobehavioral evaluation

At 24 hours after pulling out the suture and while each rat was kept in a separate cage, the neurologic behaviors were assayed by an investigator blind to the experimental groups and endpoint assessment as follows (26): usual locomotion activity=score 0; bend of contralateral forelimb while the animal was suspended by the tail=score 1; contralateral rotational movement but usual state at

relaxation=score 2; absence of righting reflex=score 3; and lack of automatic locomotion function=score 4. The rats that died less than 24 hours after surgery, their brains were colored. If the death was because of the subarachnoid hemorrhage or pulmonary insufficiency and asphyxia, they were omitted from the examination.

### Infarction volume evaluation

At 24 hours after reperfusion, animals were killed with chloral hydrate (Merck, Germany, 700 mg/kg, i.p.), and the decapitation was done. Then, rapid removing of brains and cooling in 4°C normal saline for 15 minutes were performed. Brain, coronal sections were created with a thickness of 2 mm by using Brain Matrix (Tehran, Iran). The sections were soaked in a 2% solution of 2, 3, 5- triphenyl tetrazolium chloride (TTC, Merck, Germany) and immediately held at 37°C for 15 minutes. Then, the photoinitiator of slices was carried out via a digital camera (Canon, DSC-W310). Finally, the infarct volume was calculated using UTHSCSA Image Tools image analysis software and pursuant to the manner of Swanson et al. (27) as follows: measuring of the colorless (infarct area) and colored areas in each hemisphere of the section, multiplying by the thickness 2 mm and then summation all of the sections: (corrected infarct volume)=(left hemisphere volume)–(right hemisphere volume–infarct volume).

### Assessment of brain water amount

First, the decapitation was performed. Then, brains were removed, and after separation of the cerebellum, pons, and olfactory bulb, wet weight (WW) was measured. Dry weight (DW) was assayed after 24 hours and subjected to 120°C. The amount of brain water was obtained as  $[(WW-DW)/WW] \times 100$ .

### Assessment of permeability of the blood-brain barrier

The stability of the BBB was investigated by studying Evans Blue (EB, Sigma Chemicals, USA) ejection (8). Briefly, a 2% EB solution (4 ml/kg) was injected in animal tail vein 30 minutes after MCAO. At 24 hours after reperfusion, anesthesia, and opening the thoracic cavity was done. Then, animals were transcidentally perfused with 250 ml normal saline until the coming out of colorless perfusion fluid from the atrium. In this way, intravascular EB was washed out. Afterward, rats were decapitated, and the brain hemispheres were removed and weighed. 2.5 ml PBS was used for the homogenization of each hemisphere and extraction of EB. For the precipitation of the protein contents, 60% trichloroacetic acid (Merck, Germany, 2.5 ml) was added to the homogenized mixture and then mixed by vortex for 3 minutes. The next steps were included keeping the samples at 4°C for 30 minutes, centrifugation at 1000×g for 30 minutes, and measuring the amount of EB in the supernatant at 610 nm wavelength using spectrophotometry (Genesys 5, USA). The amount of EB was shown as  $\mu\text{g/g}$  of brain tissue for a standard curve.

### Extraction of protein from brain samples

1ml buffer containing 0.32 mol/l sucrose, 1 mmol/l

EDTA, and 10 nmol/l Tris-HCl, pH=7.4 was used for the homogenization of brain right hemisphere tissue (150 to 200 mg). The homogenized mixture was centrifuged at 13600×g for 30 minutes. Then, the supernatant was used for the measurement of SOD and CAT activities, MDA level, and protein contents (28). The measuring protein was done in agreeing to Bradford (29).

### Measuring the activity of superoxide dismutase, catalase and malondialdehyde level

The activity of SOD was determined according to the previous method (30) with some alteration. For obtaining a volume of 1 ml of the final assay mixture, 20  $\mu\text{l}$  enzymatic extract was mixed with 50 mM sodium phosphate buffer (PB), pH=7.0, 0.1 mM EDTA, and 0.48 mM pyrogallol. The blank was a mixture of the above components, except enzymatic extract. The absorbance changes of the final assay mixture were recorded at 420 nm for 1 minute at 25°C versus blank. The results were represented as U/mg protein. For measuring CAT activity, a volume of 1ml of the final assay mixture was prepared. For this purpose, 20  $\mu\text{l}$  enzymatic extract was mixed with 50 mM PB, pH=7.0, and 10 mM hydrogen peroxide. The blank was a mixture of the above components, except enzymatic extract. Then, absorbance decrease was pursued at 240 nm wavelength for 1 minute at 25°C versus blank. The amount of CAT activity was stated as U/mg protein. The level of MDA in homogenates was determined by applying the method described by Uchiyama and Mihara (31). 0.5 ml homogenate was mixed with 1% phosphoric acid solution (3 ml) and 0.6% thiobarbituric acid solution (1 ml). The next steps were included heating the mixture in a bain-marie at 95°C for 45 minutes, cooling, adding n-butanol (4 ml), and mixing the solution by vortex, centrifugation at 3000×g for 10 minutes and measuring the absorbance of the supernatant at 532 nm. The standard was tetraethoxypropane (Merck, Germany). The concentrations of MDA were represented as nmol/mg protein.

### Measuring regional cerebral blood flow

Recording rCBF was performed by Velocitometry Laser Doppler flowmeter (MBF3D, Moor Instrument, Axminster, UK) (32). By placing the probe of laser Doppler flowmeter in the surface, Doppler flux was continually assessed from the 30 minutes before MCAO until 30 minutes after reperfusion.

### Statistical analysis

The data were presented as means  $\pm$  SD and compared via one-way ANOVA followed by LSD. Mann-Whitney U test was used for the analysis of neurologic deficit score (NDS). The level of the statistical significance was set at  $P < 0.05$ .

## Results

### Experimental conditions parameter

The pressure of CO<sub>2</sub> and O<sub>2</sub> analysis in the arterial blood

showed that preclinical HO and RA were rightly created in the pretreatment groups. Any significant difference in pH and pressure of CO<sub>2</sub> in HO and RA groups was not seen ( $P > 0.05$ , pH =  $7.3 \pm 0.09$ ,  $7.4 \pm 0.1$ , pressure of CO<sub>2</sub>:  $39.2 \pm 1.4$ ,  $42.8 \pm 0.8$ ), but the difference in the pressure of O<sub>2</sub> in HO and RA groups was significant ( $P < 0.001$ ,  $335 \pm 24.7$ ,  $95.8 \pm 6.9$ ). rCBF was decreased to less than 24% of the baseline during MCAO in groups exposed to ischemia when compared with rCBF before ischemic damage ( $P < 0.05$ , Fig.2B).

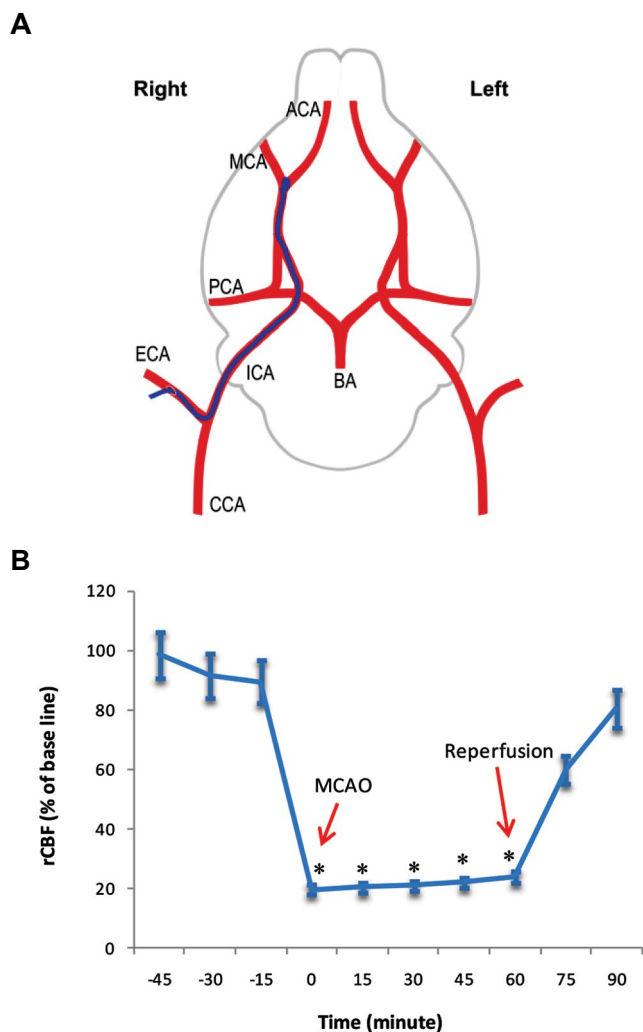


**Fig.2:** Middle cerebral artery occlusion and evaluation of the regional cerebral blood flow. **A.** Schematic presentation of MCAO in the right hemisphere of the rat brain. A nylon suture with the rounded head (blue filament) was inserted into the right ICA via the right ECA and blocked right MCA. **B.** The rCBF in rats undergoing MCAO surgery. The rCBF was characterized by 100% of a baseline before MCAO, but it decreased significantly during MCAO. The rCBF after reperfusion came close to the baseline. \*,  $P < 0.05$  vs. before MCAO ( $n = 7$ ). MCAO; Middle cerebral artery occlusion, CCA; Common carotid artery, ICA; Internal carotid artery, ECA; external carotid artery, BA; Basilar artery, PCA; Posterior cerebral artery, MCA; Middle cerebral artery, ACA; Anterior cerebral artery, and rCBF; Regional cerebral blood flow.

### Culture and identification of choroid plexus epithelial cells

Polygonal cells were observed in the flasks five days after CPECs culture, and their density was 15% (Fig.3A). Two weeks later, the total surface of the flasks was filled with cells that had an epithelial appearance. The

immunocytofluorescence was performed to identify the TTR marker (Fig.3B).

### Alginate microcapsules

The results showed that the alginate microcapsules surface includes three layers of alginate, poly-L-lysine, and alginate (Fig.3C). When the empty alginate microcapsules were incubated with the ThT solution, ThT could permeate them via the pores on the surface of microcapsules (Fig.3D). Also, the surface of microcapsules containing CPECs did not change after 24 hours and was smooth as well as about 75-80% of the cells in the microcapsule were alive. This suggests the biocompatibility and stability of the microcapsules and shows that CPECs indirectly and possibly by releasing trophic factors are effective and do not migrate themselves.

### Neurologic deficit scores

Median NDSs in the RA+MCAO group in comparison with sham was significantly different (2 vs. 0,  $P < 0.05$ ). Median NDSs in the HO+MCAO, RA+MCAO+encapsulated CPECs, and HO+MCAO+encapsulated CPECs groups decreased significantly in comparison with the RA+MCAO and RA+MCAO+empty capsules groups (1 vs. 2,  $P < 0.05$ , Table 1).

### Infarction volume was decreased by hyperoxia and encapsulated choroid plexus epithelial cells

The infarct volume decreased in HO+MCAO, RA+MCAO+encapsulated CPECs, and HO+MCAO+encapsulated CPECs groups compared to the RA+MCAO group after 24 hours MCAO, significantly ( $P < 0.01$ ). Also, a significant difference was not observed between RA+MCAO and RA+MCAO+empty capsules groups in infarct volume ( $P > 0.05$ , Fig.4A, B).

### Hyperoxia and encapsulated choroid plexus epithelial cells decreased brain edema and ameliorated blood-brain barrier permeability

The brain water amount increased in ischemic cerebral tissue (right hemisphere) in the RA+MCAO group compared to the right hemisphere of the sham group, significantly ( $P < 0.01$ ). The edema in the right hemisphere decreased significantly in HO+MCAO ( $P = 0.043$ ), RA+MCAO+encapsulated CPECs ( $P = 0.039$ ), and HO+MCAO+encapsulated CPECs ( $P = 0.014$ ) groups in comparison with a RA+MCAO group ( $P < 0.05$ ). Free-cell capsules had no effect (Fig.4C).

The results showed EB concentration in ischemic cerebral tissue (right hemisphere) in the RA+MCAO group increased and had a significant difference with the sham group ( $P < 0.01$ ). EB leakage in the right hemisphere reduced significantly in HO+MCAO, RA+MCAO+encapsulated CPECs, and HO+MCAO+encapsulated CPECs groups compared with the RA+MCAO group ( $P < 0.01$ ). Changes in BBB permeability in the left hemisphere were not significant. Also, Free-cell capsules had no effect (Fig.4D).

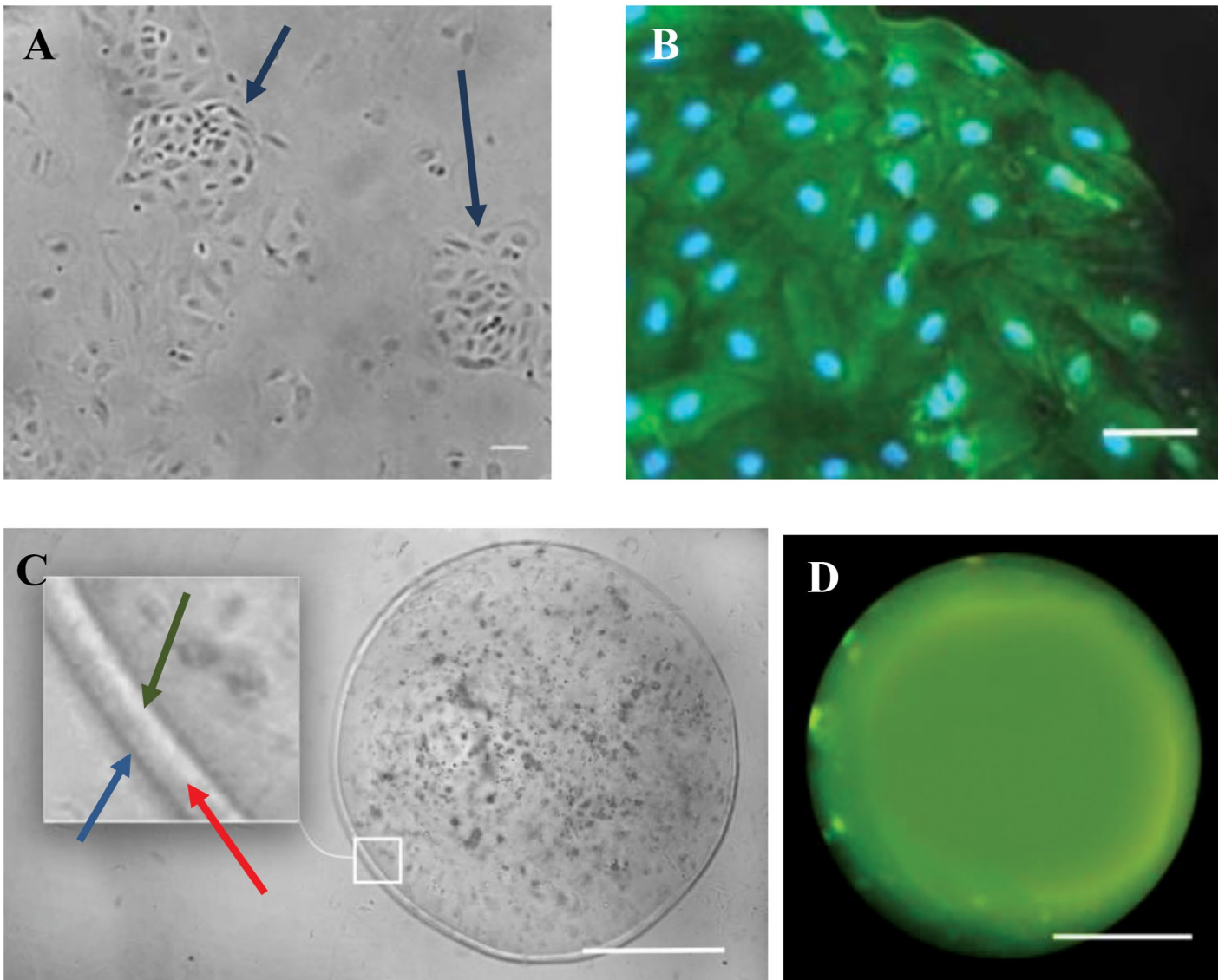


**Fig.3:** Recognition of choroid plexus epithelial cells (CPECs) and image of the microcapsule's surface by fluorescence microscopy. **A.** The appearance of the CPECs 5 days after culturing. Arrows indicate clusters of polygonal cells (CPECs) in culture medium. **B.** The CPECs with maximum confluence (80%). The result of CPECs immunocytochemistry was positive for Transthyretin (TTR, green) (scale bar: 100  $\mu$ m). **C.** Three layers of alginate microcapsule. Inner layer; Alginate (green arrow), Middle layer; Poly-L-Lysine (red arrow), and Outer layer; Alginate (blue arrow). **D.** Free-cell alginate microcapsule was incubated with ThT (scale bar: 200  $\mu$ m).

**Table 1:** Neurologic deficit scores (NDS) in the experimental groups

Number	Groups	NDS in each group					Premature death number	Total	Median	Statistical results
		0	1	2	3	4				
1	Sham	21	0	0	0	0	0	21	0	1 vs. 2= significant
2	RA+MCAO	0	4	13	3	8	6	28	2	3 vs. 2= significant
3	HO+MCAO	9	6	13	0	0	3	28	1	4 vs. 2= significant
4	RA+MCAO+encapsulated CPECs	12	8	8	0	0	2	28	1	5 vs. 2= significant
5	HO+MCAO+encapsulated CPECs	11	12	5	0	0	1	28	1	6 vs. 2= nonsignificant
6	RA+MCAO+empty capsules	0	1	14	4	9	5	28	2	

Results between groups analyzed with a significant level of  $P < 0.05$ .

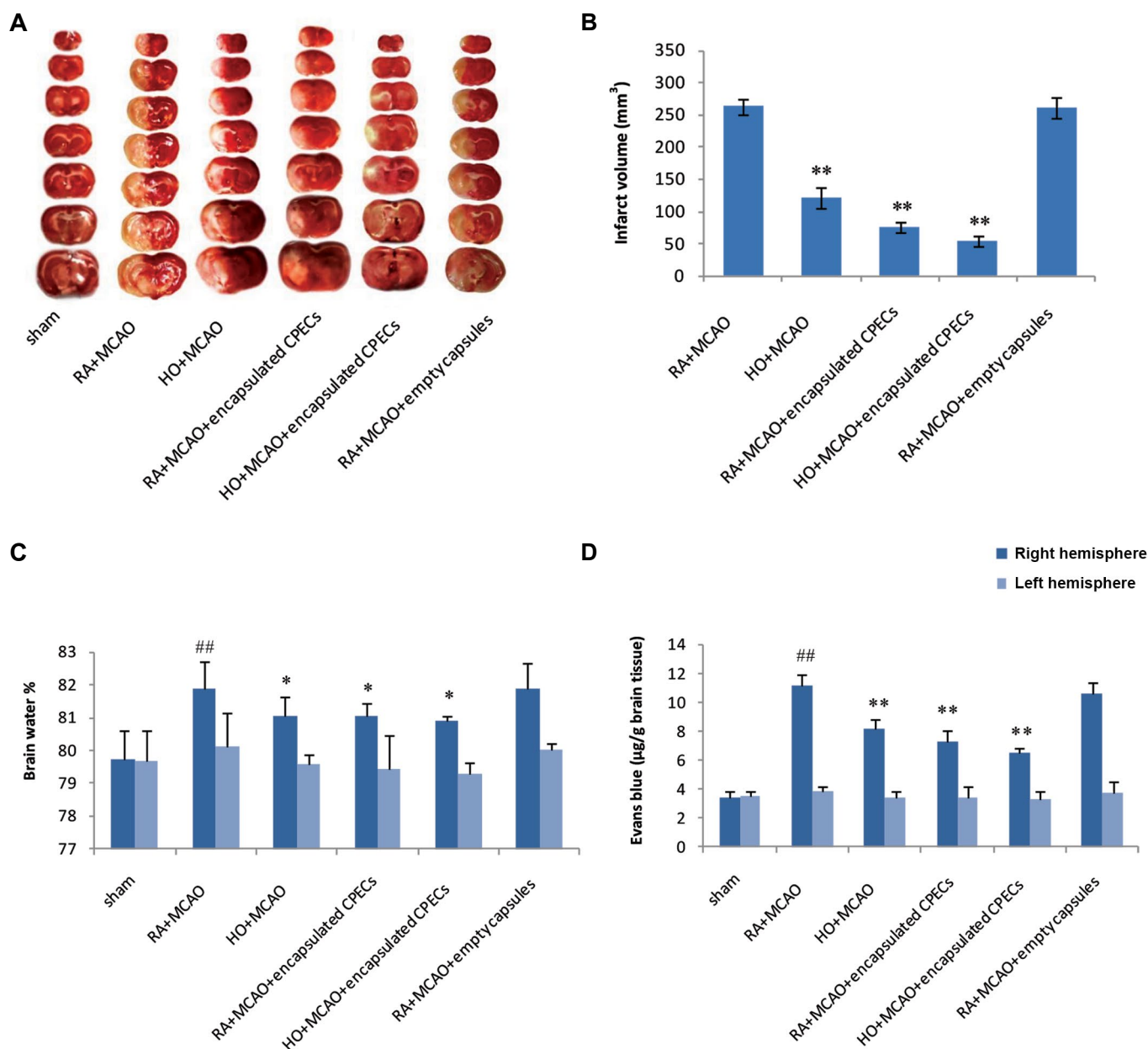


**Fig.4:** The effect of HO and CPECs on brain infarct volume, brain water content, and EB concentration in the experimental groups. **A.** The columns show rat brain coronal sections in the experimental groups. **B, C,** and **D.** ##,  $P < 0.01$  vs. sham, \*,  $P < 0.05$ , \*\*,  $P < 0.01$  vs. RA+MCAO group ( $n=7$ ). RA; Room air, MCAO; Middle cerebral artery occlusion, HO; Hyperoxia, CPECs; Choroid plexus epithelial cells, and EB; Evans blue.

### Hyperoxia and encapsulated choroid plexus epithelial cells increased superoxide dismutase and catalase activity and decreased malondialdehyde level

At 24 hours after ischemia-reperfusion, SOD activity in the right hemisphere showed a decrease in RA+MCAO and RA+MCAO+empty capsules groups compared to the sham group ( $P < 0.01$ ). This value in the RA+MCAO group was 11.14 U/mg protein, whereas, in the HO+MCAO, RA+MCAO+encapsulated CPECs and HO+MCAO+encapsulated CPECs groups showed a significant increase, up to 15, 15.8 and 16.7 U/mg protein, respectively ( $P < 0.01$ , Fig.5A). CAT activity in the right hemisphere decreased in the RA+MCAO and

RA+MCAO+empty capsules groups in comparison to the sham group ( $P < 0.01$ ). But, it increased significantly in HO+MCAO, RA+MCAO+encapsulated CPECs, and HO+MCAO+encapsulated CPECs groups compared to the RA+MCAO group ( $P < 0.01$ , Fig.5B).

Lipid peroxidation was indicated by the MDA content in the brain. MCAO increased the MDA level significantly in the right hemisphere in comparison to the sham group ( $P < 0.01$ ). However, the MDA amount in the right hemisphere lowered significantly in the HO+MCAO, RA+MCAO+encapsulated CPECs, and HO+MCAO+encapsulated CPECs groups compared to the RA+MCAO group ( $P < 0.01$ , Fig.5C).

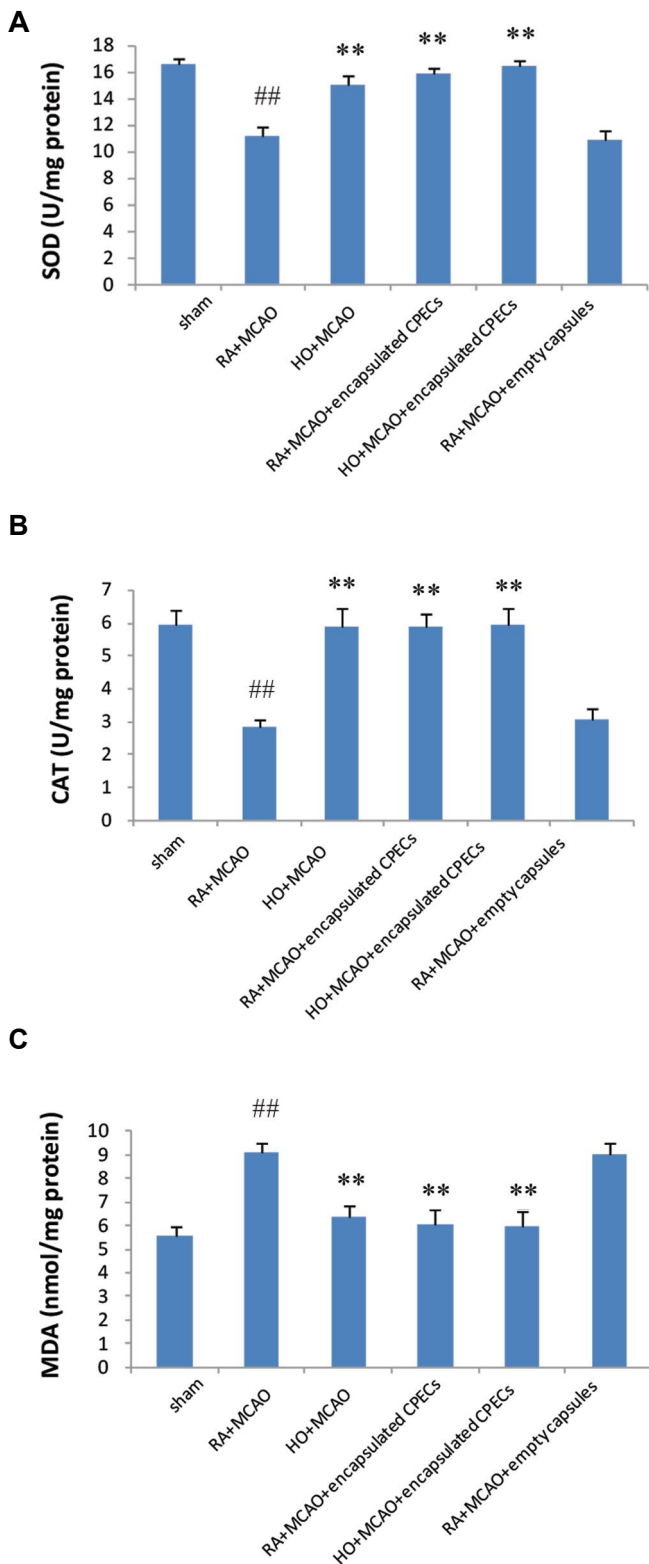


**Fig.5:** Evaluation of antioxidant capacity in the right hemisphere of experimental groups. **A.** The activation of SOD, **B.** CAT, and **C.** MDA level. <sup>##</sup>; P<0.01 vs. sham group, <sup>\*\*</sup>; P<0.01 vs. RA+MCAO group (n=7), SOD; Superoxide dismutase, CAT; Catalase, MDA; Malondialdehyde, RA; Room air, MCAO; Middle cerebral artery occlusion, HO; Hyperoxia, and CPECs; Choroid plexus epithelial cells.

## Discussion

Brain ischemia is one of the outstanding causes of death throughout the world. Despite cerebral ischemia-

associated high costs, there are limited treatment options against ischemic brain damage that most of them have failed to increase recovery rate following the induction of stroke, which proposes an urgent need for the development of new therapies for brain ischemia (1).

Here, for the first time, we applied HO and transplantation of encapsulated CPECs of neonatal rats in combination with each other to enhance recovery and decrease symptoms in an MCAO model of cerebral ischemia in adult rats. In this work, results showed HO and encapsulated CPECs alone and, in combination with each other, had protective effects on oxidative stress-induced ischemia-reperfusion injury in rat brain and reduced brain damage. Also, results showed that HO and encapsulated CPECs alone and in combination with each other due to increasing antioxidant activity (increase SOD and CAT activities and decrease MDA) decreased edema, BBB permeability, neurologic deficits and brain damage in a rat model of MCAO.

Our data showed when HO was combined with encapsulated CPECs for cerebral ischemia, a significant reduction in infarction volume of 79% was achieved. Also, results demonstrated 53% and 70% reductions in total infarction volume by preconditioning with HO alone or transplantation of encapsulated CPECs alone, respectively. Combination therapy was effective than the HO and encapsulated CPECs alone. On the other hand, NDS, a marker of neurological behavior, was improved by HO, encapsulated CPECs, and a combination of HO and encapsulated CPECs, and all three treatments were equally effective as a neuroprotectant based on NDS. This equivalent effect may be explained as perhaps 24 hours is not enough for the effect of encapsulated CPECs on NDS and functional recovery and may increase with time to spare. In an experimental study, was shown normobaric HO decreased infarct volume and NDS in the MCAO model of stroke in rats that is in agreement with our results (33). Also, Borlongan et al. (23) showed improvement in behavioral functions and reduction of infarction volume by CPECs transplants three days after MCAO.

According to experimental reports, transplants of encapsulated CPECs are more effective than the nonencapsulated CPECs transplants, and there is a major immune response to capsule-free CPECs in comparison with encapsulated CPECs. In addition, empty capsules have no effect on the improvement of stroke. Therefore, it may be said that the capsule has no protective effect alone, but it can enhance CPECs effects by reducing the reaction of the host. Our results showed that the viability of encapsulated CPECs after one day was 75-80%, and empty capsules had no therapeutic effect that is in agreement with the work of Borlongan et al. (23).

The interchange between blood and brain tissue is controlled by BBB. Disruption of BBB following the stroke increases edema and causes ischemic injury and mortality. In an experimental stroke, the protection of endothelial cells and the inhibition of MMP activity via

SOD keeps the BBB integrity and decreases brain damage (34). We showed that EB concentration decreased, the stability of the BBB increased, and edema decreased in HO, encapsulated CPECs, and the combination groups when compared with RA+MCAO group, significantly. Moreover, the HO+MCAO+encapsulated CPECs group had more effect in reducing edema than the HO and encapsulated CPECs alone. The previous investigations indicated that reduction of brain edema and decrease of BBB permeability could occur by the HO in rats (8, 35). So far, there has been no report on the effect of the CPECs on edema and the BBB damage caused by stroke.

The evidence proposes that ROS-induced oxidative stress results in the injury of cellular macromolecules, which are linked to the death of neurons induced by ischemia-reperfusion injury (5). We showed that the activity of CAT and SOD increased in HO, encapsulated CPECs, and combination therapy groups when compared with the RA+MCAO group. The lipid peroxidation is determined via the MDA level. The concentration of MDA reverberates that the cause of brain damage is ROS. Extra ROS is scavenged by increasing of SOD and CAT activities and results in a reduction of the lipid peroxidation (12). In this investigation, MDA decreased significantly in HO, encapsulated CPECs, and combination therapy groups in comparison with RA+MCAO group, and combination therapy effect was more than HO and encapsulated CPECs alone.

In one study, it was shown that the pretreatment with HO decreases infarct volume, neurologic deficits scores, and mortality and increases CAT and SOD activities in an animal model of stroke. This shows that HO partly exerts its effects via the increase in antioxidant enzyme activities. It is stated that ROS and HO are compounds that pretreatment via them can increase the activity and expression of SOD (11). Our results showed that HO increased SOD and CAT activities and decreased lipid peroxidation, also. Aliaghaei and colleagues showed that encapsulated CPECs transplants in Alzheimer's disease animal model improved long-term memory, decreased apoptosis, migration microglia, and gliosis and increased neurogenesis, and the SOD activity (24). The view is that CPECs induce the Nrf2/ARE pathway and antioxidant enzymes overactivation in order to protect neurons against oxidative stress (22). In our study, encapsulated CPECs transplants alone and, in combination with HO, could decrease MCAO-induced cerebral infarct volume by increase SOD and CAT antioxidant enzyme activity. Moreover, encapsulated CPECs decreased the MDA amount.

Matsumoto et al. showed that CPECs considerably secreted diffusible factors that repressed ischemic brain injury (16). Previous studies show exogenous BDNF, one of CPECs diffusible factors, decreases brain damage volume, and improves behavioral function significantly after acute ischemia (36, 37). Moreover, decreased expression of BDNF is associated with the sensitivity to stress and enhanced stress responses (38). It is also shown that BDNF heterozygous mice are more vulnerable to stress than control mice, revealing behavioral desperation after mild handling stress (39). In the

other study, was reported when GDNF introduced to the brain following ischemic stroke, showed neuroprotective effects (15). It seems that encapsulated CPECs presumably indirectly by secreting neurotrophic factors decrease oxidative stress occurred by reperfusion and preconditioning with HO in the ischemic brain. However, the precise mechanism linking combination therapy of HO and CPECs to focal ischemia-reperfusion injury still remains an open question. Several limitations of this study are that measurements were made only up to 24 hours after stroke, and the replication in a second species and sex and age differences were not considered. In a study, Lan et al. found that HO did not reduce infarct size in hypertensive Sprague-Dawley rats (40). Thus, it is suggested that the effect of HO and CPECs also be investigated for a period longer and on the ill animals by considering sex and age. Also, in this work, we did not measure the secreted factors of CPECs but suggest that they should be assayed in future studies.

## Conclusion

The result of this study showed the combination therapy of HO and encapsulated CPECs for ischemic brain damage can be more effective than the HO and encapsulated CPECs alone, and signs decrease of ischemic stroke may relate to an increase in antioxidant enzyme activity. Our study introduces a new method of combination therapy for stroke; We hope that with further researches, the arrival of this combination therapy to the clinic more quickly.

## Acknowledgments

This work was performed as a Ph.D. project and financially supported by the Biology Research Center of Islamic Azad University of Zanjan. We should thank the Center of Excellence in Cognitive Neuropsychology in Shahid Beheshti University of Tehran for their supports. The authors declare no conflict of interest.

## Authors' Contributions

M.E., M.R.B., Sh.O., M.R.; Assisted in the study design. M.E., M.R.; Performed the experiments. M.E., M.R.B.; Analyzed the data. M.R., Sh.O.; Drafted the manuscript, which was revised by M.R.B. All authors read and approved the final manuscript.

## References

1. Lee RHC, Lee MHH, Wu CYC, Couto E Silva A, Possoit HE, Hsieh TH, et al. Cerebral ischemia and neuroregeneration. *Neural Regen Res.* 2018; 13(3): 373-385.
2. Suvanish Kumar VS, Gopalakrishnan A, Naziroğlu M, Rajanikant GK. Calcium ion-the key player in cerebral ischemia. *Curr Med Chem.* 2014; 21(18): 2065-2075.
3. Rodriguez F, Bonacasa B, Fenoy FJ, Salom MG. Reactive oxygen and nitrogen species in the renal ischemia/reperfusion injury. *Curr Pharm Des.* 2013; 19(15): 2776-2794.
4. Zhang ZG, Sun X, Zhang QZ, Yang H. Neuroprotective effects of ultra-low molecular-weight heparin on cerebral ischemia/reperfusion injury in rats: involvement of apoptosis, inflammatory reaction and energy metabolism. *Int J Mol Sci.* 2013; 14(1): 1932-1939.
5. Chen H, Yoshioka H, Kim GS, Jung JE, Okami N, Sakata H, et al. Oxidative stress in ischemic brain damage: mechanisms of cell death and potential molecular targets for neuroprotection. *Antioxid*

- Redox Signal. 2011; 14(8): 1505-1517.
6. Iadecola C, Anrather J. Stroke research at a crossroad: asking the brain for directions. *Nat Neurosci*. 2011; 14(11): 1363-1368.
  7. Kirino T. Ischemic tolerance. *J Cereb Blood Flow Metab*. 2002; 22(11): 1283-1296.
  8. Bigdeli MR, Hajizadeh S, Froozandeh M, Rasulian B, Heidarianpour A, Khosbaten A. Prolonged and intermittent normobaric hyperoxia induce different degrees of ischemic tolerance in rat brain tissue. *Brain Res*. 2007; 1152: 228-233.
  9. Zhang X, Xiong L, Hu W, Zheng Y, Zhu Z, Liu Y, et al. Preconditioning with prolonged oxygen exposure induces ischemic tolerance in the brain via oxygen free radical formation. *Can J Anaesth*. 2004; 51(3): 258-263.
  10. Jadhav V, Ostrowski RP, Tong W, Matus B, Jesunathadas R, Zhang JH. Cyclo-oxygenase-2 mediates hyperbaric oxygen preconditioning-induced neuroprotection in the mouse model of surgical brain injury. *Stroke*. 2009; 40(9): 3139-3142.
  11. Bigdeli MR. Preconditioning with prolonged normobaric hyperoxia induces ischemic tolerance partly by upregulation of antioxidant enzymes in rat brain tissue. *Brain Res*. 2009; 1260: 47-54.
  12. Li J, Liu W, Ding S, Xu W, Guan Y, Zhang JH, et al. Hyperbaric oxygen preconditioning induces tolerance against brain ischemia-reperfusion injury by upregulation of antioxidant enzymes in rats. *Brain Res*. 2008; 1210: 223-229.
  13. Singhal AB, Benner T, Roccatagliata L, Koroshetz WJ, Schaefer PW, Lo EH, et al. A pilot study of normobaric oxygen therapy in acute ischemic stroke. *Stroke*. 2005; 36(4): 797-802.
  14. Singhal AB, Ratai E, Benner T, Vangel M, Lee V, Koroshetz WJ, et al. Magnetic resonance spectroscopy study of oxygen therapy in ischemic stroke. *Stroke*. 2007; 38(10): 2851-2854.
  15. Duarte EP, Curcio M, Canzoniero LM, Duarte CB. Neuroprotection by GDNF in the ischemic brain. *Growth Factors*. 2012; 30(4): 242-257.
  16. Matsumoto N, Taguchi A, Kitayama H, Watanabe Y, Ohta M, Yoshihara T, et al. Transplantation of cultured choroid plexus epithelial cells via cerebrospinal fluid shows prominent neuroprotective effects against acute ischemic brain injury in the rat. *Neurosci Lett*. 2010; 469(3): 283-288.
  17. Friedrich MAG, Martins MP, Araujo MD, Klamt C, Vedolin L, Gariochea B, et al. Intra-arterial infusion of autologous bone marrow mononuclear cells in patients with moderate to severe middle-cerebral-artery acute ischemic stroke. *Cell Transplant*. 2012; 21 Suppl 1: S13-S21.
  18. Johanson CE, Palm DE, Primiano MJ, McMillan PN, Chan P, Knuckey NW, et al. Choroid plexus recovery after transient forebrain ischemia: role of growth factors and other repair mechanisms. *Cell Mol Neurobiol*. 2000; 20(2): 197-216.
  19. Stopa EG, Berzin TM, Kim S, Song P, Kuo-LeBlanc V, Rodriguez-Wolf M, et al. Human choroid plexus growth factors: what are the implications for CSF dynamics in Alzheimer's disease? *Exp Neurol*. 2001; 167(1): 40-47.
  20. Emerich DF, Orive G, Thanos C, Tornoe J, Wahlberg LU. Encapsulated cell therapy for neurodegenerative diseases: from promise to product. *Adv Drug Deliv Rev*. 2014; 67-68:131-141.
  21. Huang SL, Wang J, He XJ, Li ZF, Pu JN, Shi W. Secretion of BDNF and GDNF from free and encapsulated choroid plexus epithelial cells. *Neurosci Lett*. 2014; 566: 42-45.
  22. Aliaghaei A, Khodaghali F, Ahmadiani A. Conditioned media of choroid plexus epithelial cells induces Nrf2-activated phase II Antioxidant response proteins and suppresses oxidative stress-induced apoptosis in PC12 cells. *J Mol Neurosci*. 2014; 53(4): 617-625.
  23. Borlongan CV, Skinner SJM, Geaney M, Vasconcellos AV, Elliott RB, Emerich DF. Intracerebral transplantation of porcine choroid plexus provides structural and functional neuroprotection in a rodent model of stroke. *Stroke*. 2004; 35(9): 2206-2210.
  24. Aliaghaei A, Digaleh H, Khodaghali F, Ahmadiani A. Encapsulated choroid plexus epithelial cells actively protect against intrahippocampal A $\beta$ -induced long-term memory dysfunction; upregulation of effective neurogenesis with the abrogated apoptosis and neuroinflammation. *J Mol Neurosci*. 2015; 56(3): 708-721.
  25. Longa EZ, Weinstein PR, Carlson S, Cummins R. Reversible middle cerebral artery occlusion without craniectomy in rats. *Stroke*. 1989; 20(1): 84-91.
  26. Bederson JB, Pitters LH, Tsuji M, Nishimura MC, Davis RL, Bartkowski H. Rat middle cerebral artery occlusion: evaluation of the model and development of a neurologic examination. *Stroke*. 1986; 17(3): 472-476.
  27. Swanson RA, Morton MT, Tsao WG, Savalos RA, Davidson C, Sharp FR. A semiautomated method for measuring brain infarct volume. *J Cereb Blood Flow Metab*. 1990; 10(2): 290-293.
  28. Khalaj R, Hajizadeh Moghaddam A, Zare M. Hesperetin and it nanocrystals ameliorate social behavior deficits and oxido-inflammatory stress in rat model of autism. *Int J Dev Neurosci*. 2018; 69: 80-87.
  29. Bradford MM. A rapid and sensitive method for the quantitation of microgram quantities of protein utilizing the principle of protein-dye binding. *Anal Biochem*. 1976; 72: 248-254.
  30. Genet S, Kale RK, Baquer NZ. Alterations in antioxidant enzymes and oxidative damage in experimental diabetic rat tissues: effect of vanadate and fenugreek (*Trigonella foenum graecum*). *Mol Cell Biochem*. 2002; 236(1-2): 7-12.
  31. Mihara M, Uchiyama M. Determination of malonaldehyde precursor in tissues by thiobarbituric acid test. *Anal Biochem*. 1978; 86(1): 271-278.
  32. Chen SH, Cheung RT. Peripheral and central administration of neuropeptide Y in a rat middle cerebral artery occlusion stroke model reduces cerebral blood flow and increases infarct volume. *Brain Res*. 2002; 927(2): 138-143.
  33. Nasrnia S, Bigdeli MR. Ischemic tolerance induced by normobaric hyperoxia and evaluation of group I and II metabotropic glutamate receptors. *Curr Neurovasc Res*. 2013; 10(1): 21-28.
  34. Li Y, Yang GY. Translational research in stroke, translational medicine research. In: *Pathophysiology of ischemic stroke*. Lapchak PA, Yang GY, editors. 1<sup>st</sup> ed. China: Springer Singapore Press; 2017; 64-65.
  35. Alavian F, Hajizadeh S, Bigdeli MR, Javan M. The role of protein kinase C in ischemic tolerance induced by hyperoxia in rats with stroke. *EXCLI J*. 2012; 11: 188-197.
  36. Ravina K, Briggs DI, Kisilal S, Warraich Z, Nguyen T, Lam RK, et al. Intracerebral delivery of brain-derived neurotrophic factor using HyStem®-C hydrogel implants improves functional recovery and reduces neuroinflammation in a rat model of ischemic stroke. *Int J Mol Sci*. 2018; 19(12): E3782.
  37. Schabitz WR, Sommer C, Zoder W, Kiessling M, Schwaninger M, Schwab S. Intravenous brain-derived neurotrophic factor reduces infarct size and counterregulates bax and BCL-2 expression after temporary focal cerebral ischemia. *Stroke*. 2000; 31(9): 2212-2217.
  38. Tsuru J, Tanaka Y, Ishitobi Y, Maruyama Y, Inoue A, Kawano A, et al. Association of BDNF Val66Met polymorphism with HPA and SAM axis reactivity to psychological and physical stress. *Neuropsychiatr Dis Treat*. 2014; 10: 2123-2133.
  39. Burke TF, Advani T, Adachi M, Monteggia LM, Hensler JG. Sensitivity of hippocampal 5-HT<sub>1A</sub> receptors to mild stress in BDNF-deficient mice. *Int J Neuropsychopharmacol*. 2013; 16(3): 631-645.
  40. Lan J, Esposito E, Ayata C, Singhal AB, Lo EH, Ji X. Different effects of normobaric oxygen in normotensive versus hypertensive rats after focal cerebral ischemia. *Stroke*. 2018; 49(6): 1534-1537.

# Association between rs11614913 Polymorphism of The *MiR-196-a2* Gene and Colorectal Cancer in The Presence of Departure from Hardy-Weinberg Equilibrium

Ali Reza Soltanian, Ph.D.<sup>1,2</sup>, Bistoon Hosseini, Ph.D.<sup>3</sup>, Hossein Mahjub, Ph.D.<sup>1,4</sup>, Fatemeh Bahreini, Ph.D.<sup>5</sup>, Ehsan Nazemalhosseini Mojarad, Ph.D.<sup>6</sup>, Mohammad Ebrahim Ghaffari, M.Sc.<sup>1\*</sup>

1. Department of Biostatistics, School of Public Health, Hamadan University of Medical Sciences, Hamadan, Iran

2. Modeling of Noncommunicable Diseases Research Center, Hamadan University of Medical Sciences, Hamadan, Iran

3. Kermanshah Province Electricity Distribution Company, Kermanshah, Iran

4. Research Center for Health Center, Hamadan University of Medical Sciences, Hamadan, Iran

5. Department of Molecular Medicine and Genetics, Faculty of Medicine, Hamadan University of Medical Sciences, Hamadan, Iran

6. Gastrointestinal (GI) Cancer Department, Gastroenterology and Liver Diseases Research Center, Research Institute for Gastroenterology and Liver Diseases, Shahid Beheshti University of Medical Sciences, Tehran, Iran

\*Corresponding Address: P.O.Box: 6517838736, Department of Biostatistics, School of Public Health, Hamadan University of Medical Sciences, Hamadan, Iran  
Email: m.gh19@yahoo.com

Received: 26/November/2019, Accepted: 02/March/2020

## Abstract

**Objective:** Colorectal cancer (CRC) is the fourth most common and the second most lethal cancer worldwide. CRC mortality is increasing in Iran. In the current study, we aimed to investigate association between rs11614913 polymorphism of the *miR-196-a2* gene and CRC.

**Materials and Methods:** In this case-control study, we assessed association of the rs11614913 polymorphism in 194 patients with CRC (case) and 286 healthy individuals (control). The expectation-maximization (EM) algorithm method was used to adjust deviation from Hardy-Weinberg equilibrium (HWE).

**Results:** There was no significant difference between genotypic frequencies of rs11614913 polymorphism in the control and case groups. Genotypic frequencies differed in the adjusted and unadjusted deviations from the HWE. Analysis of unadjusted and adjusted independent variables showed that age, sex, alcohol consumption, and drug use were statistically significant.

**Conclusion:** Our findings showed that rs11614913 polymorphism was not associated with CRC risk. Deviation from HWE affected the results. It is recommended to perform further studies to establish HWE. Ignoring the equilibrium can cause inconsistencies in the results of studies.

**Keywords:** Association, Colorectal Cancer, Equilibrium, Gene Polymorphism

Cell Journal (Yakhteh), Vol 23, No 3, August 2021, Pages: 313-318

**Citation:** Soltanian AR, Hosseini B, Mahjub H, Bahreini F, Nazemalhosseini Mojarad E, Ghaffari ME. Association between rs11614913 polymorphism of the *miR-196-a2* gene and colorectal cancer in the presence of departure from hardy-weinberg equilibrium. Cell J. 2021; 23(3): 313-318. doi: 10.22074/cellj.2021.7295.

This open-access article has been published under the terms of the Creative Commons Attribution Non-Commercial 3.0 (CC BY-NC 3.0).

## Introduction

Non-communicable diseases (NCDs) are now responsible for most of deaths worldwide (1). Cancer is predicted to be the leading cause of death and the most important obstacle to increase life expectancy in the 21<sup>st</sup> century (2). Increasing the burden of cancer and other NCDs are treats of human development (3). Colorectal cancer (CRC) is the fourth most common cancer type worldwide (2). It is an important public health problem in different populations (4). The World Health Organization (WHO) predicted that by the year 2030 frequency of new cases of CRC and its related deaths will increase by 77 and 80%, respectively. It was shown that frequency of CRC related deaths was increased within the past 10 years in Asia (5). Although it is less prevalent in the Middle East, studies indicated a growing trend. In Iran, as a region in the Middle East, this trend is increasing (6). Although the

exact causes of CRC are yet unknown, it was shown that CRC is influenced by environmental and genetic factors (7).

In recent years, role of predisposing genetic factors in mediating tendency of CRC became more and more apparent (8). Recently, a growing number of studies focused on the association of microRNA (miRNA) polymorphisms with cancer susceptibility, suggesting that accumulation of genetic variants may be involved in cancer progression (9). *miR-196a2* rs11614913, as a definitional miRNA polymorphism, is crucially associated with cancer risk (10). Previous studies showed that *miR-196a2* rs11614913 polymorphism is associated with susceptibility to cancer, especially in lung cancer and hepatocellular carcinoma as well as head and neck cancer. The *miR-196a2* rs11614913 polymorphism may act as a risk factor for cancer patients (9).

Identification of genetic polymorphisms associated with cancer has many diagnostic implications. For example, early detection of high-risk individuals may be possible, which in turn can take different measures to reduce the risk of cancer development or progression (8). There are limited studies on the association of the *miR-196-a2* polymorphism with CRC and the results are inconsistent (11-13). In Iran, only one study with a small sample size was conducted in this regard without Hardy-Weinberg equilibrium (HWE) calculation (14). According to importance of genetic studies in the early detection of CRC and the importance of considering internal validity, the present study was performed to investigate association of rs11614913 polymorphism of the *miR-196-a2* gene and CRC in the presence of departure from HWE.

## Materials and Methods

### Subjects

This hospital-based case-control study was conducted in Taleghani Hospital (Tehran, Iran) from 2014 to 2019. A total of 194 patients with histologically confirmed CRC and without family history of related cancers were enrolled in this study. Two hundred and eighty-six individuals with no colonoscopy signs of CRC were randomly selected from the same residential areas as control group. The study was approved by the Hamadan University of Medical Sciences Ethics Committee (IR.UMSHA.REC.1396.640) and all participants provided a written informed consent. The participants were interviewed and data on gender, age, smoking, alcohol consumption and addiction (opium) were obtained using a structured questionnaire.

### DNA extraction

Genomic DNA was extracted using a standard salt extraction protocol (15, 16). Polymerase chain reaction-restriction fragment length polymorphism (PCR-RFLP) method was used to determine the genotype distributions of *miR-196-2* polymorphism (rs11614913). The specific primers were designed using Primerblast (<http://www.ncbi.nlm.nih.gov/tools/primer-blast/>) and the software Gene Runner. The primers sequences were:

F: 5'-GTCTACTCTCTAGTCCTTAGG-3'  
 R: 5'-TTGAGAGGACGGCATAAAGC-3'

The primers amplified a 383 base pair (bp) fragment. The PCR was done in a final volume of 25 µl with 35 temperature cycles consisting of 45 seconds at 94°C (denaturation), 40 seconds at 55.2°C (annealing) and 45 seconds at 72°C (extension). A final extension step at 72°C was performed for 5 minutes. The PCR products were exposed to restriction enzymes HpyCH4III for 8 hours at 37°C. The enzyme digested products were visualized on 3% agarose gels and stained with DNA green viewer (for visualization under a UV light). Extracted DNA samples

were amplified for the segment that comprised rs11614913 polymorphism. Agarose gel (1%) electrophoresis was done to confirm the PCR product size. The expected product size was 383 bp, which was confirmed by 1% agarose gel electrophoresis. The results of 2% agarose gel electrophoresis on PCR products were digested by restricted endonuclease HpyCH4III.

At this single nucleotide polymorphism (SNP), the nucleotide C is converted to T.



The HpyCH4III enzyme cut site is shown in the above. This enzyme cuts the rare T genotype. In other words, in the normal case, it contains nucleotide C that the enzyme does not recognize and does not cut. In this case, if we have C in one allele and T in the other allele, the condition is heterozygote. To confirm the genotyping results, we selected 10% polymerase chain reaction products for DNA sequencing and the results were 100 % concordant.

### Statistical analyses

#### Method of adjusting the deviation from Hardy-Weinberg equilibrium

Chi-square test was used to evaluate HWE in the control group. Regarding the absence of HWE (P=0.046), the expectation-maximization (EM) algorithm method was used to adjust deviation from HWE (17). For this purpose, the level of deviation was assessed using EM algorithm in the estimation of allele frequency. Then, the genotype frequencies were estimated. For the estimation of allele frequency, disequilibrium coefficient (D) was set for the population deviation from equilibrium. This value is due to the difference between the true value of genotype and the expected value under equilibrium: with the selection of PA(0) for the frequency of allele A in the step E of the algorithm, the expected number of genotypes was obtained from equation 1.

$$n_{AA(m)} = \frac{p_{A(m-1)}^2 + D}{p_{A(m-1)}^2 + 2p_{A(m-1)}(1 - p_{A(m-1)}) - D} n_A$$

In the step M, the new value of the allele frequency was obtained using equation 2.

$$\widehat{p}_{A(m)} = \frac{2n_{AA(m)} + n_{Aa(m)}}{2n}$$

If  $|\hat{p}_{A(m)} - \hat{p}_{A(m-1)}| \leq 0.01$  or  $m \geq 100$  ( $m$  is the repetition of the algorithm) or  $\widehat{p}_{A(m)} = 0$ , the algorithm was stopped and the value of  $\widehat{p}_{A(m)}$  was considered as the final value for the frequency of allele A (17).

### Tests and software

Simple logistic regression analysis was used to determine the effect of each independent variable on CRC and multiple regression analysis was performed for adjusting any confounding variables. Chi-square test and logistic regression analyses were used to investigate the association between rs11614913 polymorphism and CRC. Version 16.0 of the SPSS software (SPSS, Inc., USA) and version 3.4.3 of the R software (to adjust the deviations from equilibrium) were used to perform statistical analysis. A  $P < 0.05$  was considered statistically significant.

### Results

Demographic characteristics of the studied subjects (286 controls and 194 CRC cases) are shown in Table 1.

Results of the simple and multiple logistic regression analyses are shown in Table 2. The odds of CRC in men was 1.82 times more than women. The odds of CRC in subjects with drug (opium) use, alcohol consumption and smoking were also respectively 12.74, 7 and 2.43 times more than those who did not use any of them. Analysis of different age groups revealed that the odds of CRC in subjects with age over 50 years was 12.52 times higher than those with age under 50 years. In adjusted analysis, age and sex groups were significantly associated with CRC, so that the odds of CRC in men was 2.38 times higher than women and in subjects with age over 50 years, it was 13.84 times higher than those with age under

50 years. In addition, the odds of CRC in subjects with alcohol and drug consumption were respectively 3.44 and 2.88 fold higher than those who did not, while the differences were not statistically significant. According to the classification of effect size for the odds ratio, which is 1.5 small, 2 medium and 3 large (18), alcohol and drug use have a significant impact on CRC.

Genotype distribution of the rs11614913 polymorphism for *miR196a2* in patients with CRC was as follows: the homozygous CC genotype was detected in 74 subjects (38.1%), the homozygous TT genotype in 29 subjects (15%) and the heterozygous CT genotype in 91 subjects (46.9%). The genotype distribution of the rs11614913 polymorphism in control group was as follows: the homozygous CC genotype was detected in 108 subjects (37.8%), the homozygous TT genotype in 56 subjects (19.6%) and the heterozygous CT genotype in 122 subjects (42.6%). Regarding the absence of HWE in the control group ( $P = 0.046$ ), the EM algorithm method was used to adjust deviation from HWE. The adjusted genotype distribution of the rs11614913 polymorphism in the control group is shown in Table 3.

T and C allele frequencies were 40.91 and 59.09%, respectively, in the patient group, while they were respectively 38.4 and 61.6% in the control group. Genotype distribution of the rs11614913 polymorphism of the *miR196a2* gene in patients and control groups are shown in Table 3. After adjusting deviation from the equilibrium, frequency of CC, CT and TT genotypes observed in prototype 108 (37.8%), 122 (42.6%) and 56 (19.6%) were changed to 100 (35%), 138 (48.2%) and 48 (16.8%), respectively. The risk of CRC in subjects with CC genotype was higher than those with CT and TT genotype, but the differences were not significant.

**Table 1:** Demographic characteristics of the studied subjects

Variable	Control (n=286)	Case (n=194)
Gender		
Male	121 (52.2)	111 (47.8)
Female	165 (66.5)	83 (33.5)
Age (Y)		
<50	172 (89.1)	21 (10.9)
≥50	104 (39.5)	159 (60.5)
Smoking		
No	263 (62.2)	160 (37.8)
Yes	23 (40.4)	34 (59.6)
Alcohol consumption		
No	282 (62.3)	171 (37.7)
Yes	4 (19)	17 (81)
Opium use		
No	285 (61.4)	176 (38.6)
Yes	1 (11.1)	8 (88.9)

Data are presented as n (%).

**Table 2:** Association of independent variables in unadjusted and adjusted form with dependent variable (CRC=yes, CRC=no)

Variable	Unadjusted <sup>a</sup>		Adjusted <sup>b</sup>	
	OR (CI 95%)	Significance	OR (CI 95%)	Significance
Gender				
Male	1		1	
Female	0.55 (0.38 – 0.79)	0.001	0.42 (0.26 – 0.67)	<0.001
Smoking				
No	1		1	
Yes	2.43 (1.38 – 4.27)	0.002	0.92 (0.40 – 2.13)	0.842
Alcohol consumption				
No	1		1	
Yes	7 (2.32 – 21.17)	0.001	3.44 (0.75 – 15.72)	0.112
Opiumuse				
No	1		1	
Yes	12.74 (1.58 – 102.70)	0.017	2.88 (0.24 – 33.87)	0.401
Age (Y)				
<50	1		1	
>=50	12.52 (7.47 – 20.98)	<0.001	13.84 (8.05 – 23.78)	<0.001

<sup>a</sup>; Simple logistic regression, <sup>b</sup>; Multiple logistic regression, OR; Odd ratio, and CI; Confidence interval.

**Table 3:** The genotype and allele distribution of the rs11614913 polymorphism in the case and control groups by adjusting deviation from the HWE to the control group

Genotype	Case n (%)	Control n (%)	OR, 95% CI (Lower-Upper)	P value ( $\chi^2$ , df)	Adjusted OR, 95% CI (Lower-Upper)	Adjusted P value ( $\chi^2$ , df)	Minimum detectable OR
RS116							
CC	74 (38.1)	100 (35)	Reference group	-	Reference group	-	-
CT	91 (46.9)	138 (48.2)	1.09 (0.73 – 1.63)	0.358 (0.85, 1)	0.89 (0.60 - 1.33)	0.772 (0.08 , 1)	0.57
TT	29 (15)	48 (16.8)	0.76 (0.44 – 1.29)	0.192 (1.70, 1)	0.82 (0.47 – 1.42)	0.591 (0.29 , 1)	0.46
CT+TT	120 (61.9)	186 (65)	0.98 (0.68 – 1.43)	0.980 (0.001, 1)	0.87 (0.60 – 1.27)	0.477 (0.51 , 1)	0.58
Alleles							
C	239 (61.6)	338 (59.09)	Reference group	-	Reference group	-	-
T	149 (38.4)	234 (40.91)	0.90 (0.69 – 1.17)	0.436 (0.61, 1)	0.90 (0.69 – 1.17)	0.436 (0.61, 1)	0.69

HWE; Hardy-Weinberg equilibrium, OR; Odd ratio, and CI; Confidence interval.

## Discussion

In the present study, we found that the genetic variant rs11614913 polymorphism of the *miR-196-a2* was not significantly associated with CRC. This lack of association was obtained either using the raw control genotype data or

the artificially adjusted distribution followed to fit HWE. It is important to consider the degree of deviation from the equilibrium. Based on STrengthening the REporting of Genetic Association studies (STREGA) guideline, if HWE is not maintained, the results will be wrong. Despite

the significance of this equilibrium, there are still many other genetic association studies which do not notice it (19, 20).

Accuracy of the results reported in a variety of studies (e.g. CONSORT, STROBE) depends on the internal validity of the study. In 2009, Little et al. (21) provided an extension of the STrengthening the Reporting of OBservational Studies in Epidemiology (STROBE) guidelines as titled STREGA to assess internal validity of genetic association studies. One of the STREGA items is about HWE. Based on STREGA guideline, if HWE is not maintained, the results will be wrong. The STREGA guideline did not explain a solution when there is deviation from the equilibrium. For this reason, in this paper, we used a new applied method to adjust the deviation from the equilibrium. These results have represented that if the HWE is not balanced in the control group, it can have an impact on the results of the study.

The occurrence of several mutations at tumor suppressor genes or proto-oncogenes is the critical genetic cause of CRC development (22). micro-RNAs can act as an oncogene or oncomiR through inhibition of cancer-related genes. Therefore, micro-RNAs can be studied as possible biomarkers for the diagnosis of cancer. To date, several studies showed association of *miR196a2* rs11614913 polymorphism with various malignancies (9). Hu et al. (23) reported in 2008 that risk of non-small cell lung cancer (NSCLC) is higher in individuals with homozygous CC genotype of rs11614913 polymorphism of the *miR196a2* and the prognosis of NSCLC is worse in these patients. Additionally, it was reported that risk of breast cancer is lower in individuals with the homozygous TT genotype (24). However, results of the previous study, regarding the effect of *miR196a2* rs11614913 polymorphism on CRC are challenging (13). In the present study, allele and genotype frequencies of rs11614913 polymorphism of the *miR196a2* gene were assessed in Iranian patients with CRC to find the possible association between the rs11614913 polymorphism as a genetic factor and CRC. Our results showed that risk of CRC in subjects with CC genotype was higher than subjects with CT or TT genotypes. In addition, risk of CRC in subjects with the C allele was more than subjects with the T allele, but the difference was not significant. Our results are similar to the two other studies that studied CRC. They also did not find any significant association between *miR-196a2* polymorphism and the risk of CRC was found. Hezova et al. (12) investigated 197 patients with non-hereditary CRC and 212 control subject in Europe. They did not find any correlation between the rs11614913 polymorphism of the *miR196a2* gene and the risk of CRC. Their finding was consistent with the data obtained from Chen et al. (11). Previous study obtained in Iran showed a significant association without equilibrium calculation (14).

On the other hand, Zhan et al. (13) reported that the C allele of rs11614913 polymorphism is a risk factor for CRC. However, they did not find any association between

rs11614913 polymorphism and factors such as tumor size, cancer stage and metastasis. Notably, another study reported that risk of gastric cancer in Chinese individuals with the CC genotype of *miR196a2* is higher than those with CT and TT genotype. Therefore, the C allele of rs11614913 polymorphism has a considerable effect on gastrointestinal cancer in China (25).

Our results showed that risk of CRC, with both unadjusted and adjusted form, was higher in subjects with age over 50 years. In 2019, Wong et al. (26) showed that age is a risk factor for CRC. In line with the present study, it was shown that risk of CRC was increased dramatically after age 50 years; 90% of all CRCs were diagnosed after 50 years old. Our results also showed that the risk of CRC in men was 2.38 times higher than women. Previous studies performed by Wong et al. (26) and Kolligs et al. (27) found similar results among the advanced cancer patients. In addition, in the unadjusted analysis, results of the present study showed that risk of CRC was high in subjects who were using alcohol, drug and smoke. In the adjusted analysis, alcohol and drug use had a significant impact on CRC. It was reported that CRC (~30-50%) was affected by lifestyles, such as a high red and processed meat consumption, obesity, diabetes and alcohol overuse (26). It was postulated that smoking is responsible for 12% mortality of CRC. Carcinogenic substances in tobacco smoke increase risk of colorectal cancer. By comparing with non-drinkers, it was shown that higher alcohol consumption was significantly associated with elevated CRC risk (28, 29).

## Conclusion

Our results showed that with and without using EM method, no significant association did exist between rs11614913 polymorphism and CRC risk. Deviation from HWE affected the results. It is suggested that future studies of this polymorphism should investigate HWE. Ignoring the equilibrium can cause inconsistencies in the results of studies.

## Acknowledgements

This work was supported by funding from Hamadan University of Medical Sciences (Hamadan, Iran, Contract No. 9609286037). There is no conflict of interest in this study.

## Authors' Contributions

A.R.S., B. H., M.E.Gh.; Analyzed the data and drafted the manuscript. A.R.S., F.B., M.E.Gh.; Designed the study and directed implementation. B.H.; Designed the study. H.M., E.N.M., F.B.; Edited the manuscript for intellectual content and provided critical comment on the manuscript. E.N.M.; Data gathering. H.M.; Analyzed the data and designed the part of study. All authors read and approved the final manuscript.

## References

1. World Health Organization. Global health observatory. Geneva: World Health Organization. Available from: <http://who.int/gho/data->

- base/en/. (21 June 2018).
2. Bray F, Ferlay J, Soerjomataram I, Siegel RL, Torre LA, Jemal A. Global cancer statistics 2018: GLOBOCAN estimates of incidence and mortality worldwide for 36 cancers in 185 countries. *CA Cancer J Clin.* 2018; 68(6): 394-424.
  3. Global Burden of Disease Cancer Collaboration; Fitzmaurice C, Abate D, Abbasi N, Abbastabar H, Abd-Allah F. Global, regional, and national cancer incidence, mortality, years of life lost, years lived with disability, and disability-adjusted life-years for 29 cancer groups, 1990 to 2017: a systematic analysis for the global burden of disease study. *JAMA Oncol.* 2019; 5(12): 1749-1768.
  4. Moridikia A, Mirzaei H, Sahebkar A, Salimian J. MicroRNAs: potential candidates for diagnosis and treatment of colorectal cancer. *J Cell Physiol.* 2018; 233(2): 901-913.
  5. Arnold M, Sierra MS, Laversanne M, Soerjomataram I, Jemal A, Bray F. Global patterns and trends in colorectal cancer incidence and mortality. *Gut.* 2017; 66(4): 683-6891.
  6. Rezaianzadeh A, Safarpour AR, Marzban M, Mohaghegh A. A systematic review over the incidence of colorectal cancer in Iran. *Ann Colorectal Res.* 2015; 3(1): e25724.
  7. Moossavi M, Parsamanesh N, Mohammadoo-Khorasani M, Moosavi M, Tavakkoli T, Fakharian T, et al. Positive correlation between vitamin D receptor gene FokI polymorphism and colorectal cancer susceptibility in South-Khorasan of Iran. *J Cell Biochem.* 2018; 119(10): 8190-8194.
  8. Tan SC. Low penetrance genetic polymorphisms as potential biomarkers for colorectal cancer predisposition. *J Gene Med.* 2018; 20(4): e3010.
  9. Liu Y, He A, Liu B, Zhong Y, Liao X, Yang J, et al. rs11614913 polymorphism in miRNA-196a2 and cancer risk: an updated meta-analysis. *Oncotargets Ther.* 2018; 11: 1121-1139.
  10. Jiang J, Jia ZF, Cao DH, Wu YH, Sun ZW, Cao XY. Association of the miR-146a rs2910164 polymorphism with gastric cancer susceptibility and prognosis. *Future Oncol.* 2016; 12(19): 2215-2226.
  11. Chen H, Sun LY, Chen LL, Zheng HQ, Zhang QF. A variant in microRNA-196a2 is not associated with susceptibility to and progression of colorectal cancer in Chinese. *Intern Med J.* 2012; 42(6): e115-e119.
  12. Hezova R, Kovarikova A, Bienertova-Vasku J, Sachlova M, Redova M, Vasku A, et al. Evaluation of SNPs in miR-196-a2, miR-27a and miR-146a as risk factors of colorectal cancer. *World J Gastroenterol.* 2012; 18(22): 2827-2831.
  13. Zhan JF, Chen LH, Chen ZX, Yuan YW, Xie GZ, Sun AM, et al. A functional variant in microRNA-196a2 is associated with susceptibility of colorectal cancer in a Chinese population. *Arch Med Res.* 2011; 42(2): 144-148.
  14. Mirtalbi H, Heydari Nasrabadi M, Pourhosseigholi M, Asadzadeh Aghdai H. Association of miR-196a2 (rs11614913) polymorphism with colorectal cancer in Tehran population. *Medical Sciences.* 2014; 23(4 and 1): 11-15.
  15. Miller SA, Dykes DD, Polesky HF. A simple salting out procedure for extracting DNA from human nucleated cells. *Nucleic Acids Res.* 1988; 16(3): 1215.
  16. Sadeghi H, Nazemalhosseini-Mojarad E, Piltan S, Fazeli E, Moradi Y, Amin-Beidokhti M, et al. A candidate intronic CYP24A1 gene variant affects the risk of colorectal cancer. *Biomark Med.* 2020; 14(1): 23-29.
  17. Soltanian AR, Mahjub H, Hosseini B, Bahreini F, Ghaffari ME, Mohagheghi S. Adjusting deviations from Hardy Weinberg equilibrium (HWE) for association study of male infertility and polymorphisms in XRCC1 and LIG4 genes. *JP Journal of Biostatistics.* 2019; 16(1): 103-111.
  18. Sullivan GM, Feinn R. Using effect size—or why the P value is not enough. *J Grad Med Educ.* 2012; 4(3): 279-282.
  19. Li M, Li C. Assessing departure from Hardy-Weinberg equilibrium in the presence of disease association. *Genet Epidemiol.* 2008; 32(7): 589-599.
  20. Preuß Michael H, Ziegler A. Comments on: association study between coronary artery disease and rs1333049 and rs10757274 polymorphisms at 9p21 locus in South-West Iran. *Cell J.* 2016; 17(4): 756.
  21. Little J, Higgins JPT, Ioannidis JPA, Moher D, Gagnon F, von Elm E, et al. Strengthening the Reporting of Genetic Association Studies (STREGA)—an extension of the STROBE statement. *Genet Epidemiol.* 2009; 33(7): 581-598.
  22. Wang WS, Chen PM, Su Y. Colorectal carcinoma: from tumorigenesis to treatment. *CellMol Life Sci.* 2006; 63(6): 663-671.
  23. Hu Z, Chen J, Tian T, Zhou X, Gu H, Xu L, et al. Genetic variants of miRNA sequences and non-small cell lung cancer survival. *J Clin Invest.* 2008; 118(7): 2600-2608.
  24. Hoffman AE, Zheng T, Yi C, Leaderer D, Weidhaas J, Slack F, et al. microRNA miR-196a-2 and breast cancer: a genetic and epigenetic association study and functional analysis. *Cancer Res.* 2009; 69(14): 5970-5977.
  25. Peng S, Kuang Z, Sheng C, Zhang Y, Xu H, Cheng Q. Association of microRNA-196a-2 gene polymorphism with gastric cancer risk in a Chinese population. *Dig Dis Sci.* 2010; 55(8): 2288-2293.
  26. Wong MC, Ding H, Wang J, Chan PS, Huang J. Prevalence and risk factors of colorectal cancer in Asia. *Intest Res.* 2019; 17(3): 317-329.
  27. Kolligs FT, Crispin A, Munte A, Wagner A, Mansmann U, Göke B. Risk of advanced colorectal neoplasia according to age and gender. *PLoS One.* 2011; 6(5): e20076.
  28. Choi YJ, Lee DH, Han K-D, Kim HS, Yoon H, Shin CM, et al. The relationship between drinking alcohol and esophageal, gastric or colorectal cancer: A nationwide population-based cohort study of South Korea. *PLoS One.* 2017; 12(10): e0185778.
  29. Naing C, Lai PK, Mak JW. Immediately modifiable risk factors attributable to colorectal cancer in Malaysia. *BMC Public Health.* 2017; 17(1): 637.

# Astaxanthin Protects Human Granulosa Cells against Oxidative Stress through Activation of NRF2/ARE Pathway and Its Downstream Phase II Enzymes

Mojtaba Eslami, Ph.D.<sup>1</sup>, Sahar Esfandyari, D.V.M.<sup>1</sup>, Marzieh Aghahosseini, M.D.<sup>2</sup>, Zahra Rashidi, Ph.D.<sup>3</sup>, Shirzad Hosseinishental, Ph.D.<sup>1</sup>, Samane Brenjian, Ph.D.<sup>1</sup>, Aligholi Sobhani, Ph.D.<sup>1</sup>, Fardin Amidi, Ph.D.<sup>1\*</sup>

1. Department of Anatomy, School of Medicine, Tehran University of Medical Sciences, Tehran, Iran

2. Department of Infertility, Shariati Hospital, Tehran University of Medical Sciences, Tehran, Iran

3. Fertility and Infertility Research Center, Health Technology Institute, Kermanshah University of Medical Sciences, Kermanshah, Iran

\*Corresponding Address: Department of Anatomy, School of Medicine, Tehran University of Medical Sciences, Tehran, Iran  
Email: famidi@sina.tums.ac.ir

Received: 19/October/2019, Accepted: 17/January/2020

## Abstract

Objective: Astaxanthin (AST) has been introduced as a radical scavenger and an anti-apoptotic factor that acts via regulating the nuclear factor-E2-related factor 2 (NRF2) and related factors. Here, we intended to examine the effect of AST on granulosa cells (GCs) against oxidative stress by examining NRF2 and downstream phase II antioxidant enzymes.

**Materials and Methods:** In this experimental study, we used cultured human primary GCs for the study. First, we performed the 3-(4,5-dimethylthiazol-2-yl)-2,5-diphenyltetrazolium bromide (MTT) test to evaluate cells viability after treatment with hydrogen peroxide (H<sub>2</sub>O<sub>2</sub>) and AST. The apoptosis rate and ROS levels were measured by flow cytometry. To determine NRF2 and phase II enzymes expression, we performed real-time polymerase chain reaction (PCR). Finally, we used western blot to measure the protein levels of NRF2 and Kelch-like ECH-associated protein 1 (KEAP1). Enzyme activity analysis was also performed to detect NRF2 activity.

**Results:** This study showed that AST suppressed ROS generation (P<0.01) and cell death (P<0.05) in GCs induced by oxidative stress. AST also elevated gene and protein expression and nuclear localization of NRF2 and had an inhibitory effect on the protein levels of KEAP1 (P<0.05). Furthermore, when we used trigonelline (Trig) as a known inhibitor of NRF2, it attenuated the protective effects of AST by decreasing NRF2 activity and gene expression of phase II enzymes (P<0.05).

**Conclusion:** Our results presented the protective role of AST against oxidative stress in GCs which was mediated through up-regulating the phase II enzymes as a result of NRF2 activation. Our study may help in improving *in vitro* fertilization (IVF) outcomes and treatment of infertility.

**Keywords:** Astaxanthin, Granulosa Cells, Nuclear Factor-E2-Related Factor 2, Oxidative Stress

Cell Journal (Yakhteh), Vol 23, No 3, August 2021, Pages: 319-328

**Citation:** Eslami M, Esfandyari S, Aghahosseini M, Rashidi Z, Hosseinishental Sh, Brenjian S, Sobhani A, Amidi F. Astaxanthin protects human granulosa cells against oxidative stress through activation of NRF2/ARE pathway and its downstream phase II enzymes. Cell J. 2021; 23(3): 319-328. doi: 10.22074/cellj.2021.7222.

This open-access article has been published under the terms of the Creative Commons Attribution Non-Commercial 3.0 (CC BY-NC 3.0).

## Introduction

Oxidative stress as a result of disruption in reduction-oxidation (redox) homeostasis is an unavoidable threat for different human cells. When a great amount of reactive oxygen species (ROS) is generated, cells become more sensitive to outcomes of oxidative stress including apoptosis and damages to major organic molecules. For a better understanding it should be noted that oxidative stress is caused by an imbalance between the production of ROS and antioxidant scavengers levels (1). In normal states, a complex antioxidant system with several important defense enzymes, protects cells against oxidative stress through scavenging ROS and maintaining the redox homeostasis. Among these endogenous scavengers, nuclear factor-E2-related factor 2 (NRF2)/Kelch-like ECH-associated protein 1 (KEAP1)-antioxidant response element (ARE) pathway and its underlying mechanism involving phase II enzymes including

glutamate-cysteine ligase (GCL), heme oxygenase 1 (HO1), and NAD(P)H quinone dehydrogenase 1 (NQO1), regulate antioxidant responses. GCL holoenzyme is an important antioxidant in glutathione biosynthesis with two different subunits, GCLC as a catalytic subunit and GCLM as a modifier subunit. HO1 cleaves the heme ring and leads to the formation of biliverdin and subsequently, bilirubin as potent antioxidants. Moreover, an excess amount of heme sensitizes cells to apoptosis. NQO1, as a flavoprotein can be produced under different stress conditions particularly oxidative stress in order to reduce quinones to hydroquinones and prevent the formation of subsequent ROS (2). Therefore, when ROS production is increased, NRF2 as a key transcription factor, translocates into the nucleus and enhances the expression of phase II antioxidant enzymes by attaching to ARE region but under normal conditions, KEAP1 binds to NRF2 and facilitates

its degradation through ubiquitination. Any disturbance in the function of this pathway results in an inability to neutralize the oxidative stress and following damages to multiple cells (3).

It is widely known that oxidative stress is highly correlated with chronic inflammation, age-related diseases, cancer, and infertility in both men and women. Over the past years, considerable effort has been made to increase the success rate of infertility treatments. Oxidative stress is regarded as an imperative factor affecting the success rates of *in vitro* fertilization (IVF) especially in granulosa cells (GCs) of women with polycystic ovarian syndrome (PCOS) (4). GCs surround the oocyte within the developing ovarian follicles and are key cells for the production of steroids as well as growth factors required for ovarian follicles growth and function. Although maintenance of normal physiological levels of ROS is important for successful fertilization and regulation of spermatozoa maturation, capacitation, hyperactivation, acrosomal reaction, chemotactic processes, and sperm-oocyte fusion, the overproduction of ROS has been linked to many fertility complications caused by damaging many organic molecules. Since oxidative stress reverses well maturation of GCs and embryo quality, a great attempt must be made for management of ROS generation (5).

Astaxanthin (AST, 3,3'-dihydroxy- $\beta$ , $\beta$ '-carotene-4,4'-dione) is a powerful carotenoid pigment naturally found in orange and red fruits. AST with multiple health benefits has a wide range of biological activities including antioxidant, anti-apoptotic, anti-inflammatory, and neuroprotective effects. AST with a great antioxidant capacity can inhibit oxidative damage and then, protect different cells from most pathological conditions. Previous studies reported that AST shows significant antioxidant activities not only through radical scavenging but also by inducing the expression of NRF2 and its downstream target genes, to promote the antioxidant defense in human cells (6). However, there is no study indicating the protective role of AST in human GCs against oxidative stress. Since oxidative damage is a major cause of GCs and oocytes apoptosis and subsequent infertility in women, we intended to examine the possible role of AST in protecting cultured primary human GCs against hydrogen peroxide ( $H_2O_2$ )-induced oxidative stress through up-regulation of NRF2 pathway and subsequent activation of phase II enzymes including GCL, HO1, and NQO1. Furthermore, trigonelline (Trig) was used as an inhibitor of NRF2 (7) to express the link between NRF2-ARE pathway and AST-induced phase II enzymes expression.

## Materials and Methods

This study was approved by the Ethics Committee of Tehran University of Medical Sciences (IR.TUMS.MEDICINE.REC.1395.730) and written informed consent was obtained from all contributors before initiation of the research.

## Study population and granulosa cells isolation and culture

Our study was an experimental study. GCs used in the current study were provided from follicular fluid of healthy women aged between 20-38 years old, who had a regular menstrual cycle and healthy ovulatory function, were not taking any hormonal drugs and underwent IVF for tubal and male infertility in the Infertility Department of Shariati Hospital affiliated with Tehran University of Medical Sciences (TUMS). A history of PCOS, autoimmune diseases, menstrual disturbance, endometriosis, hirsutism, and hyperprolactinemia was regarded as exclusion criteria.

Purification of GCs was done according to previous studies (8). First, to eliminate the individual's effects, follicular fluids obtained from different participants were pooled and centrifuged at 3000 rpm for 10 minutes. The cell pellet was resuspended in Dulbecco's Modified Eagle Medium F-12 (DMEM/F-12, Gibco, Finland), then layered over Ficoll-Paque (GE Healthcare Biosciences, Uppsala, Sweden) and centrifuged at 3000 rpm for 10 minutes. We collected GCs from the interphase, and washed, and cultured them in a complete medium that contained DMEM/F-12 supplemented with 10% (v/v) heat-inactivated fetal bovine serum (FBS, Gibco, South America), 100 mg/ml of streptomycin (Gibco by Life Technologies, Auckland, New Zealand), 100 U/ml of penicillin (Gibco by Life Technologies, Auckland, New Zealand), 2 mmol/l of glutamax (Sigma, St Louis, MO, USA), and 2 mg/ml of amphotericin B (PAN Biotech, Berlin, Germany) at 37°C in a humidified atmosphere containing 5%  $CO_2$ , for different experiments. The medium was freshly changed every other day. In the present study, we defined the study groups as control, cells treated with dimethyl sulfoxide (DMSO, Sigma, Germany),  $H_2O_2$ , AST, AST+ $H_2O_2$ , and Trig+AST+ $H_2O_2$ .

## Measurement of cell viability

To evaluate the viability of GCs after treatment with  $H_2O_2$  and AST (Sigma, China) and to determine an optimum dose for GCs treatment, 3-(4,5-dimethylthiazol-2-yl)-2,5-diphenyltetrazolium bromide (MTT, Alfa Aesar by Thermo Fisher Scientific, Germany) test was conducted according to previous studies (9, 10). It should be noted that AST was prepared by dissolving in DMSO. The test depends on the ability of viable cells to reduce tetrazolium bromide by mitochondrial dehydrogenase to produce formazan crystals (11). Briefly, GCs were cultured in a 96-well plate at a density of  $1 \times 10^4$  cells per well and treated with  $H_2O_2$  (Fluka, Germany) at concentrations of 100, 150, 200, 300, and 400  $\mu$ M for 2 hours at 37°C, to evaluate the cell viability after oxidative stress. Next, MTT solution at a concentration of 0.5 mg/ml was added to each well and plates were dark incubated at 37°C for 4 hours. DMSO was used for dissolving the produced colorful crystals and the optical density (OD) of samples was estimated at 570 nm by a microplate reader (EONTM, BioTek, USA).

with a background control as the blank. Moreover, GCs were treated with various concentrations of AST (0, 5, 10, and 20  $\mu\text{M}$ ) for 24 hours at 37°C using MTT assay for evaluating the cell viability as described above. Finally, the MTT assay was conducted after pretreating cells with different concentrations of AST (0, 5, and 10  $\mu\text{M}$ ) for 24 hours followed by  $\text{H}_2\text{O}_2$  treatment at a concentration of 200  $\mu\text{M}$  for another 2 hours at 37°C to determine the optimal dose of AST for next steps.

### Measurement of reactive oxygen species levels

The intracellular ROS levels were calculated using 2'-7'-Dichlorodihydrofluorescein diacetate (DCFH-DA, Sigma, Switzerland) fluorescent probe by flow cytometry (12). Briefly, cells were cultured at a density of  $2 \times 10^5$  cells per well in the presence or absence of 5  $\mu\text{M}$  of AST for 24 hours and then, exposed to 200  $\mu\text{M}$   $\text{H}_2\text{O}_2$  for another 2 hours at 37°C. In addition, Trig (Sigma, Switzerland) at a concentration of 0.1  $\mu\text{M}$  was used as an inhibitor of NRF2, 1 hour before treatment with AST. Then, GCs were incubated with 1  $\mu\text{M}$  of DCFH-DA for 30 minutes at 37°C and resuspended in phosphate buffered saline (PBS, Sigma, Germany). Flow cytometry was applied for detecting the fluorescence intensity at the wavelength of 525nm (FL1-H) band-pass filter based on mean fluorescence intensity of 10,000 cells. FlowJo 7.6.1 was applied for analyzing the results.

### Apoptosis assay

The Annexin V FITC-Propidium Iodide (PI) Apoptosis Detection Kit (Invitrogen by Thermo Fisher Scientific eBioscience) was applied to determine the total cell apoptosis according to the manufacturers' protocol. In details, GCs were cultured in a six-well plate at a density of  $1 \times 10^5$  cells per well in the presence or absence of 5  $\mu\text{M}$  of AST for 24 hours and then, treated with 200  $\mu\text{M}$   $\text{H}_2\text{O}_2$  for another 2 hours at 37°C. Moreover, the effect of Trig at a concentration of 0.1  $\mu\text{M}$  on GCs viability was measured. Next, GCs were resuspended in 1X Annexin-Binding buffer and a dark incubation at room temperature for 15 minutes was accomplished after adding Annexin V-FITC and PI. The fluorescence emission was measured by flow cytometry. Staining for apoptosis was performed as described by the manufacturer. Annexin V-negative, PI-negative stained cells: viable cells; Annexin V-positive, PI-negative stained cells: early apoptotic cells; Annexin V-positive, PI-positive stained cells: late apoptotic cells; and Annexin V-negative, PI-positive stained cells: necrotic cells (13). The stained cells were analyzed by FlowJo software.

### Real-time polymerase chain reaction

Total RNA was extracted from cells using TRIzol reagent (Life Technologies, Gaithersburg, MD, USA)

as explained by the manufacturer. Next, 1  $\mu\text{g}$  of total RNA was applicable for cDNA synthesis using a First-Strand cDNA Synthesis Kit (Thermo scientific, Foster City, CA, USA) based on the manufacturer's protocol. Real-time polymerase chain reaction (real-time PCR) was conducted to quantitate mRNA levels by the RealQ plus 5x Master Mix Green (Bio-Rad Laboratories, Hercules, CA, USA) using an Applied Biosystem StepOne real-time PCR, according to the manufacturers' protocol. *GAPDH* was used as an internal standard for normalizing the expression levels of our studied genes using the  $2^{-\Delta\Delta\text{Ct}}$  method in order to obtain the relative fold change results (14). All samples were analyzed in triplicate. The primers used in the present study are shown in Table 1.

**Table 1:** Forward and reverse primers used for real-time polymerase chain reaction

Primer	Primer sequence (5'-3')
<i>NRF2</i>	F: TTCCTTCAGCAGCATCCTCTC R: AATCTGTGTTGACTGTGGCATC
<i>GCLC</i>	F: GGGCGATGAGGTGGAATAC R: GGGTAGGATGGTTTGGGTTTG
<i>GCLM</i>	F: GCGGTATTCCGGTCATTGTG R: GGTAAGTTATGCTCCTAAGTCAG
<i>HO1</i>	F: TGACACCAAGGACCAGAGC R: TAAGGACCCATCGGAGAAGC
<i>NQO1</i>	F: TATCCTGCCGAGTCTGTTCTG R: AACTGGAATATCACAAGGTCTGC
<i>GAPDH</i>	F: AGTCCACTGGCGTCTTCAC R: ATCTTGAGGCTGTTGTCATACTTC

### Western blot analysis

GCs were lysed by a Protein Extraction Kit (Active Motif Inc., Carlsbad, CA, USA) based on the manufacturer's protocol. The insoluble material was removed by centrifugation at  $15000 \times g$  for 10 minutes at 4°C. After collecting supernatants, Bradford reagent (Bio-Rad, Foster City, MI, USA) was used to determine the protein concentrations. Protein lysates at a concentration of 20  $\mu\text{g}/\mu\text{l}$  were subjected to sodium dodecyl sulfate-polyacrylamide gel electrophoresis (SDS-PAGE) and then, transferred to polyvinylidene difluoride membranes (Bio-Rad). After blocking with 5% BSA in TBST buffer at 4°C overnight, the membranes were blotted with primary antibodies including antibody against NRF2 (1:750;

GeneTex, USA), antibody against KEAP1 (1:750; Abcam, Cambridge, MA, USA), and antibody against  $\beta$ -actin (1:500; Santa Cruz Biotechnology, CA, USA), at 4°C overnight. Next, the blots were washed and incubated with corresponding horseradish peroxidase (HRP)-linked secondary antibodies (rabbit anti-mouse IgG, ab97046, 1:5000; Abcam, Cambridge, UK) for 2 hours at room temperature. Protein bands were developed using a chemiluminescence system (ECL-plus, Lumigen, Inc., Southfield, MI, USA) (15).  $\beta$ -actin was used as an internal protein to normalize the expression of target proteins NRF2 and KEAP1. Data were analyzed by the ImageJ software.

**Measurement of NRF2 activity**

We used a TransAM NRF2 Transcription Factor ELISA Kit (Active Motif Inc., Carlsbad, CA, USA) to evaluate the binding activity of NRF2 to DNA according to the manufacturer’s protocol. In detail, we incubated 2.5  $\mu$ g of nuclear extracts in a 96-well plate after ARE oligonucleotides immobilization. By washing and adding an NRF2 antibody, we incubated the plate again and finally used a HRP-linked secondary antibody to provide colorimetric data. A microplate reader was applied for detecting the absorbance at 450 nm.  $A_{450}$  indicated the binding activity of NRF2-ARE.

**Statistical analysis**

The Statistical Package for Social Sciences 22 (SPSS 22, Inc., Chicago, IL, USA) was used for the statistical analysis of all results. The Kolmogorov–Smirnov test was used for testing the normalization of data. For multiple comparisons between groups, Mann-Whitney U-test was used for nonparametric data. Results are shown as mean  $\pm$  standard deviation. Values of  $P < 0.05$  were regarded as significant.

**Results**

**The viability of granulosa cells after H<sub>2</sub>O<sub>2</sub> and Astaxanthin treatments**

To determine the viability of GCs following treatment with various concentrations of AST (0, 5, 10, and 20  $\mu$ M), we used MTT assay which showed a significant cell death at a concentration of 20  $\mu$ M compared to the control group. Moreover, we also used MTT assay for determining the most appropriate concentration of H<sub>2</sub>O<sub>2</sub> for induction of oxidative stress. Thus, we treated GCs with different concentrations of H<sub>2</sub>O<sub>2</sub> (100, 150, 200, 300, and 400  $\mu$ M) for 2 hours. We detected a reduction of cell viability up to 50% at 200  $\mu$ M and higher concentrations after 2 hours ( $P < 0.001$ ). Finally, we pretreated our studied cells with various concentrations of AST (0, 5, and 10  $\mu$ M) for 24 hours followed by an extra treatment with 200  $\mu$ M H<sub>2</sub>O<sub>2</sub> for 2 hours, to find the optimal dose of AST for protecting GCs from oxidative damage as provided in Figure 1. Here, the optimal dose of AST with the best protective effect was 5  $\mu$ M for 24 hours.

**Astaxanthin inhibits reactive oxygen species production**

Intracellular ROS levels were evaluated by a DCFH-DA fluorescent probe. For this purpose, we pretreated cells with 5  $\mu$ M of AST for 24 hours and then, treated them with 200  $\mu$ M of H<sub>2</sub>O<sub>2</sub> for another 2 hours. Here, we observed a significant increase in ROS generation using a DCF fluorescence, in the H<sub>2</sub>O<sub>2</sub>-treated group (mean fluorescence: 215 vs. 93) as shown in Figure 2, which was remarkably reduced to 50% after pretreatment with AST in the AST+H<sub>2</sub>O<sub>2</sub> and Trig+AST+H<sub>2</sub>O<sub>2</sub> groups ( $P < 0.01$  and  $P < 0.001$ , respectively). The fluorescence intensity of GCs was significantly decreased after AST pretreatment in all AST-treated groups.

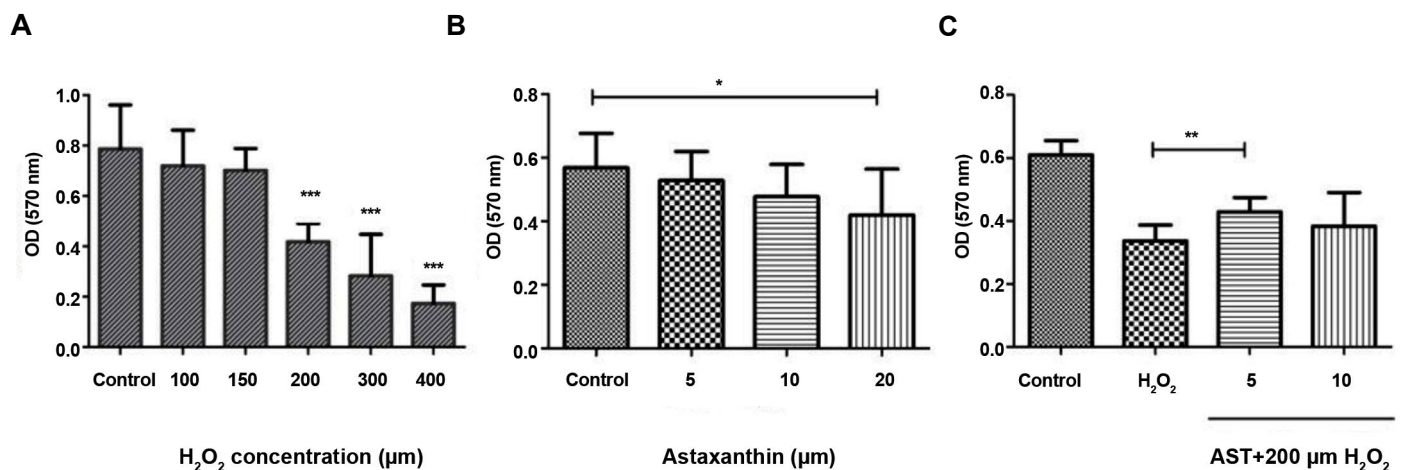


**Fig.1:** H<sub>2</sub>O<sub>2</sub> and AST toxicity measurement and the protective effect of AST against H<sub>2</sub>O<sub>2</sub> in GCs. **A.** To evaluate oxidative stress conditions; GCs were treated with various concentrations of H<sub>2</sub>O<sub>2</sub> (100, 150, 200, 300, and 400  $\mu$ M) for 2 hours. **B.** To determine AST toxicity on GCs, various concentrations of AST (0, 5, 10, and 20  $\mu$ M) were used for 24 hours. **C.** To evaluate the protective effects of AST on oxidative stress conditions, GCs were treated with various concentrations of AST (0, 5, and 10  $\mu$ M) for 24 hours, next treated with 200  $\mu$ M of H<sub>2</sub>O<sub>2</sub> for another 2 hours. Results are demonstrated as the mean  $\pm$  SD. \*,  $P < 0.05$ , \*\*,  $P < 0.01$ , and \*\*\*,  $P < 0.001$ , GCs; Granulosa cells, AST; Astaxanthin, and OD; Optimal density.

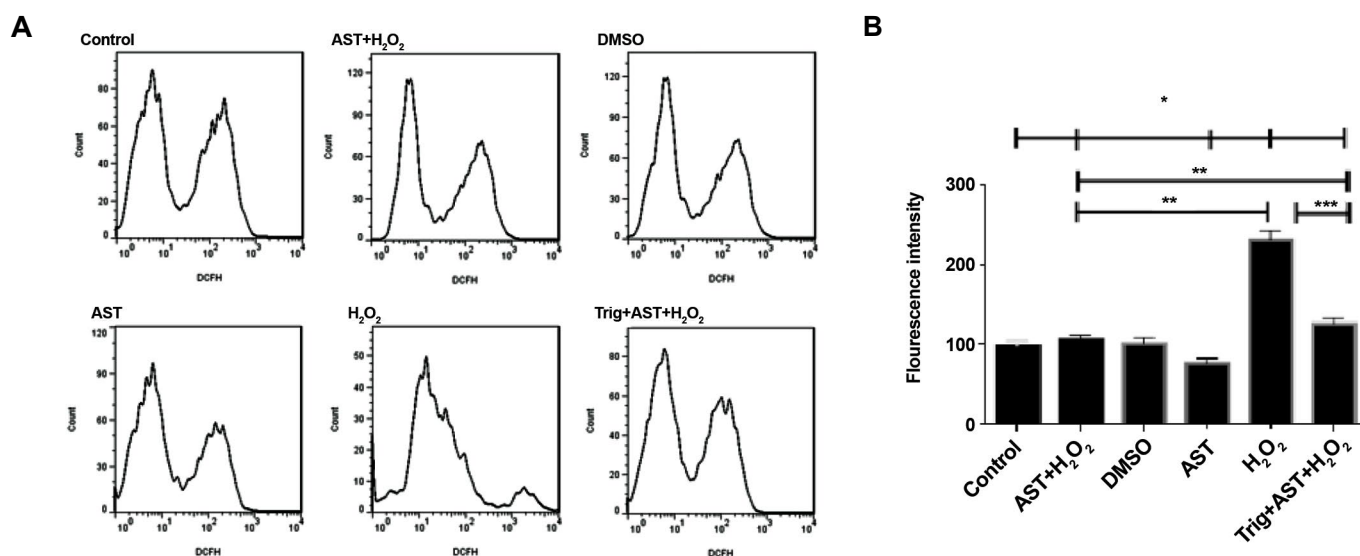


**Fig. 2:** ROS induction. **A, B.** AST protects GCs from H<sub>2</sub>O<sub>2</sub>-mediated ROS generation. GCs were pretreated with 5  $\mu$ M of AST for 24 hours, and then treated with 200  $\mu$ M of H<sub>2</sub>O<sub>2</sub> for another 2 hours. GCs were also treated with 0.1  $\mu$ M of Trig 1 hour before the exposure to AST. Intracellular ROS levels were evaluated by flow cytometry using a DCFH-DA fluorescent probe. Values are presented as the median fluorescence  $\pm$  SD of 3 independent experiments. \*, P<0.05, \*\*, P<0.01, \*\*\*, P<0.001, ROS; Reactive oxygen species, AST; Astaxanthin, GCs; Granulosa cells, DMSO; Dimethyl sulfoxide, and Trig; Trigonelline.

### Astaxanthin prevents granulosa cells from H<sub>2</sub>O<sub>2</sub>-induced apoptosis

H<sub>2</sub>O<sub>2</sub> exposure as a common model used for the induction of oxidative damage, increases cellular apoptosis. To determine the protective effect of AST against H<sub>2</sub>O<sub>2</sub>-induced apoptosis, GCs were pretreated with 5  $\mu$ M of AST as the optimal dose for 24 hours and then, treated with 200  $\mu$ M of H<sub>2</sub>O<sub>2</sub> for 2 hours. The annexin V/PI staining was performed to determine the total GCs apoptosis due to H<sub>2</sub>O<sub>2</sub> treatment with or without pretreatment of AST by using flow cytometry. As provided in Figure 3, annexin V+/PI- as an indicator of early apoptotic cells percentage showed a higher apoptosis rate in the H<sub>2</sub>O<sub>2</sub>-treated GCs in comparison with the control group which was significantly reduced after pretreatment with AST (P<0.05). Moreover, GCs were treated with 0.1  $\mu$ M of Trig as a known inhibitor of NRF2 1 hour before treatment with AST. Remarkably, the apoptosis rate was still significantly lower in the Trig+AST+H<sub>2</sub>O<sub>2</sub> GCs compared to H<sub>2</sub>O<sub>2</sub>-treated GCs (P<0.01) but Trig treatment slightly increased the percentage of early apoptotic cells compared to the AST+H<sub>2</sub>O<sub>2</sub> group (P<0.05).

### Astaxanthin enhances gene and protein expression and nuclear localization of NRF2 while declines KEAP1 protein levels

Firstly, our results indicated that H<sub>2</sub>O<sub>2</sub> treatment resulted in induced expression of NRF2. The protein levels of KEAP1 as an endogenous inhibitor of NRF2, was also increased after H<sub>2</sub>O<sub>2</sub> exposure, however, it was not significant. Moreover, pretreatment with AST significantly induced NRF2 expression at both mRNA and protein levels in cells with or without H<sub>2</sub>O<sub>2</sub> exposure (P<0.01). Moreover, AST increased NRF2 activity and its connection to ARE region in DNA compared to the H<sub>2</sub>O<sub>2</sub>-treated GCs without AST exposure (P<0.05) which was induced by Trig treatment as

an inhibitor of NRF2 (P<0.05). AST also reduced KEAP1 protein levels in cells with or without H<sub>2</sub>O<sub>2</sub> exposure (P<0.05). Furthermore, Trig resulted in a significant decrease in NRF2 gene expression in GCs treated with H<sub>2</sub>O<sub>2</sub> (P<0.01, Fig.4A-C). It also significantly reduced gene and protein expression of NRF2 compared to the H<sub>2</sub>O<sub>2</sub>-treated group after AST pretreatment (P<0.01). The protein levels of KEAP1 were significantly induced in the Trig+AST+H<sub>2</sub>O<sub>2</sub> group in comparison to the H<sub>2</sub>O<sub>2</sub>-treated group with or without AST pretreatment (P<0.01). However, as provided in Figure 4, the higher expression of NRF2 at both mRNA and protein levels and the lower protein levels of KEAP1 were still observed as significant after Trig exposure in the Trig+AST+H<sub>2</sub>O<sub>2</sub> GCs compared to the H<sub>2</sub>O<sub>2</sub>-treated GCs.

### Astaxanthin increases the expression of GCLC, GCLM, HO1, and NQO1 genes

To determine whether the effect of AST on the activation of NRF2/ARE pathway is followed by a higher gene expression of phase II enzymes including GCLC, GCLM, HO1, and NQO1, we conducted real-time PCR. The gene expression of these antioxidant enzymes was increased after exposure to H<sub>2</sub>O<sub>2</sub> in comparison with the control group. Our results demonstrated that pretreatment with 5  $\mu$ M of AST for 24 hours, significantly enhanced the gene expression of phase II enzymes in the H<sub>2</sub>O<sub>2</sub>-treated and untreated groups (Fig.5). Moreover, Trig as an inhibitor of NRF2, significantly attenuated this effect on the mRNA levels of GCLC, GCLM, and HO1 in the H<sub>2</sub>O<sub>2</sub>-treated GCs after pretreatment with AST (P<0.01). Therefore, these findings support the role of phase II antioxidant enzymes in the protective effects of AST through NRF2 up-regulation.

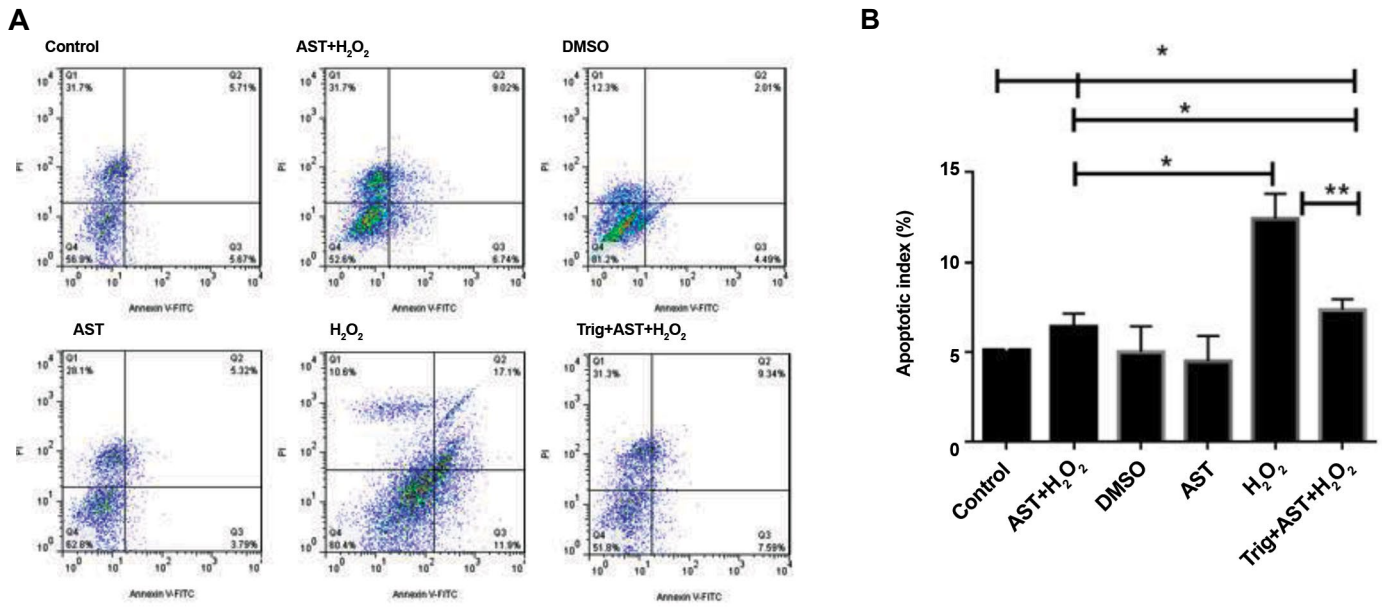


**Fig.3:** AST protects GCs from H<sub>2</sub>O<sub>2</sub>-induced apoptosis. **A.** The apoptosis rate was measured by an annexin V/PI double staining test and flow cytometry. The quadrants on annexin V/PI dot plots classed as: Annexin V-negative, PI-negative staining cells: viable cells; Annexin V-positive, PI-negative staining cells: early apoptotic cells; Annexin V-positive, PI-positive staining cells: late apoptotic cells; and Annexin V-negative, PI-positive staining cells: necrotic cells. **B.** The quantitative data are shown as median ± SD of three independent experiments. \*, P<0.05, \*\*, P<0.01, AST; Astaxanthin, GCs; Granulosa cells, DMSO; Dimethyl sulfoxide, and Trig; Trigonelline.

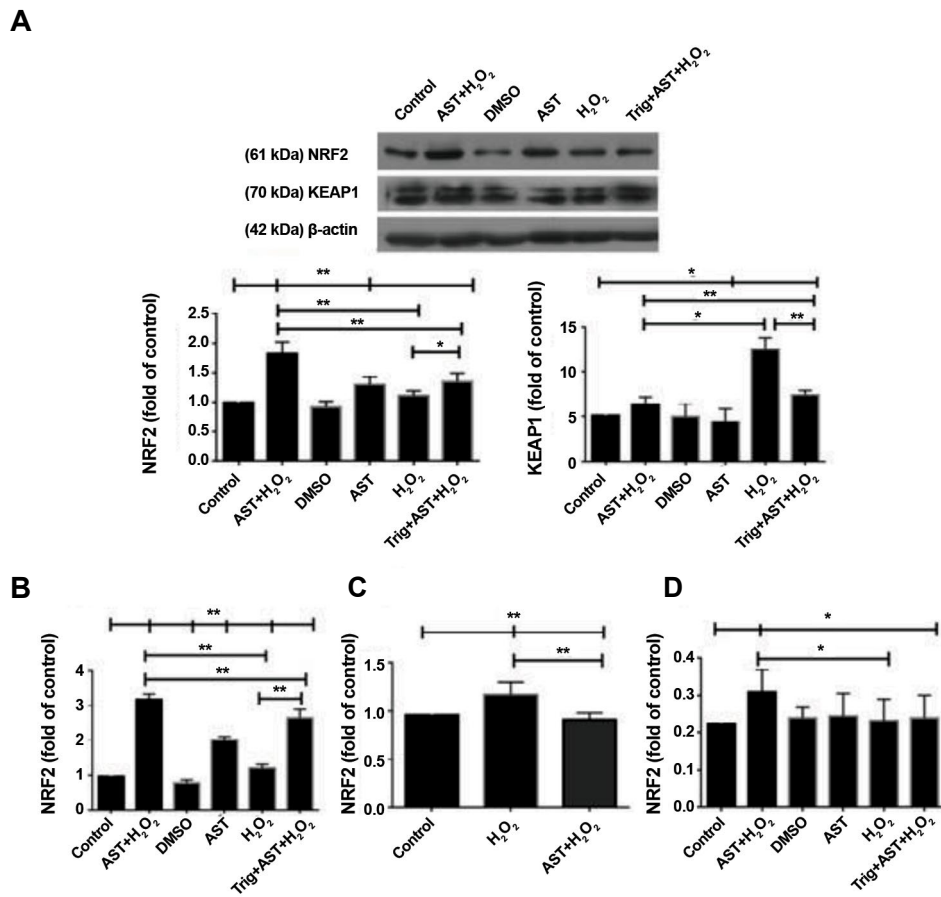


**Fig.4:** Evaluation of NRF2 mRNA, protein, and activity and KEAP1 protein levels after AST and H<sub>2</sub>O<sub>2</sub> treatment in GCs. **A.** NRF2 and KEAP1 protein levels were evaluated by western blot after treatment with 5 μM of AST for 24 hours and then treatment with 200 μM of H<sub>2</sub>O<sub>2</sub> for another 2 hours. The band densities of NRF2 and KEAP1 were normalized against β-actin. **B.** **C.** Real-time PCR was conducted to evaluate the expression of NRF2 mRNA. GAPDH was used as an internal standard for normalization. **D.** Effects of AST on DNA binding activity of NRF2. The molecular weights of NRF2, KEAP1, and β-actin are reported to be 61, 70, and 42 kDa, respectively. The data are indicated as the mean ± SD of 3 independent experiments. \*, P<0.05, \*\*, P<0.01, AST; Astaxanthin, GCs; Granulosa cells, PCR; Polymerase chain reaction, DMSO; Dimethyl sulfoxide, and Trig; Trigonelline.

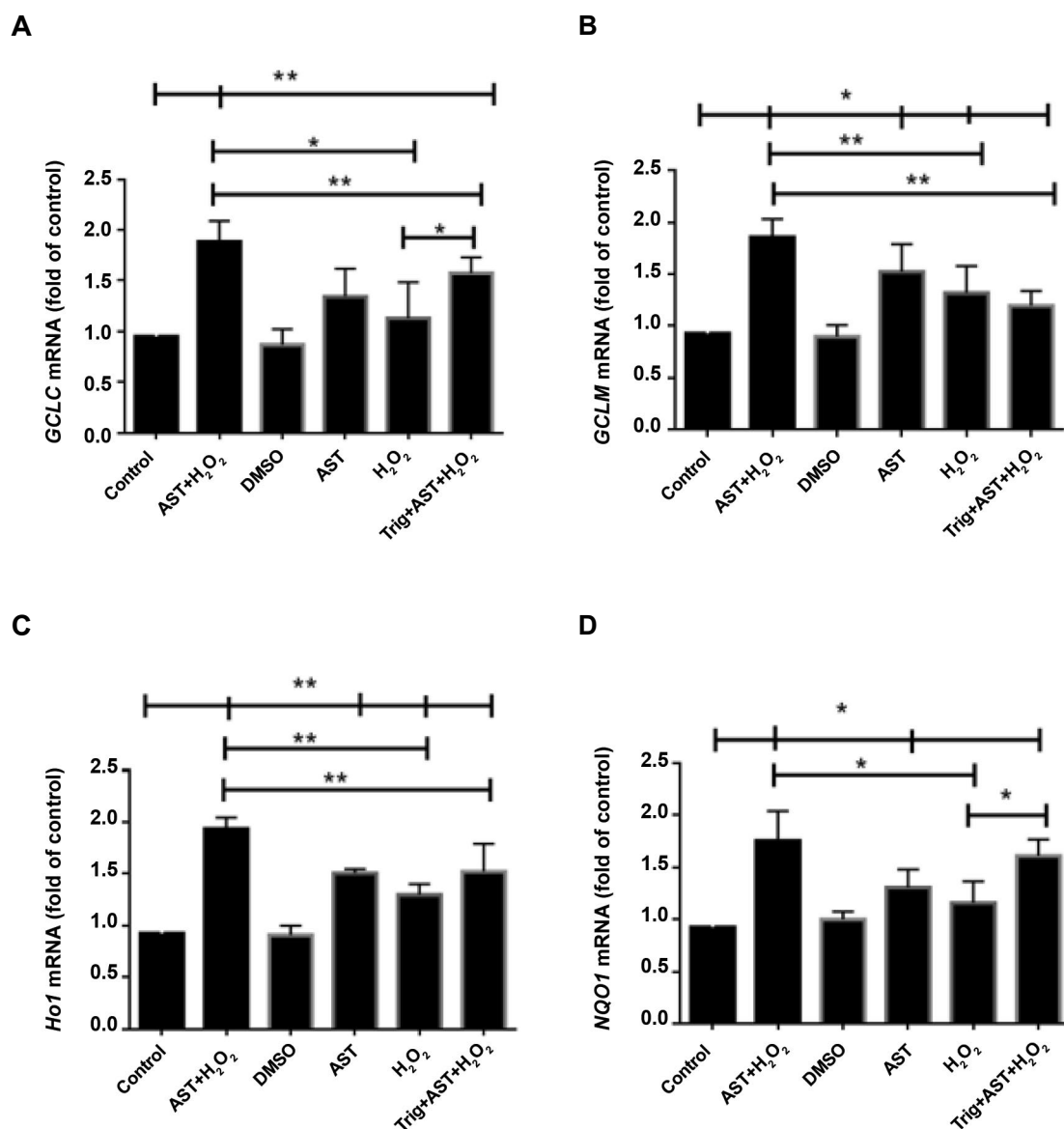


**Fig.5:** Evaluation of *GCLC*, *GCLM*, *Ho1*, and *NQO1* mRNAs after AST and H<sub>2</sub>O<sub>2</sub> treatment in GCs. After treatment with 5  $\mu$ M of AST for 24 hours and then treatment with 200  $\mu$ M of H<sub>2</sub>O<sub>2</sub> for another 2 hours, **A.** *GCLC*, **B.** *GCLM*, **C.** *Ho1*, and **D.** *NQO1* mRNAs were measured using real-time PCR. *GAPDH* was used as an internal standard for normalization. The data are indicated as the mean  $\pm$  SD of 3 independent experiments. \*,  $P < 0.05$ , \*\*,  $P < 0.01$ , AST; Astaxanthin, GCs; Granulosa cells, PCR; Polymerase chain reaction, DMSO; Dimethyl sulfoxide, and Trig; Trigonelline.

## Discussion

In the present study, we intended to examine the effects of AST on H<sub>2</sub>O<sub>2</sub>-induced oxidative stress in primary human GCs through investigating the expression of *NRF2*, *KEAP1* and downstream phase II enzymes including *GCL*, *HO1*, and *NQO1*. The main finding of our study was the stimulatory effect of AST on the gene and protein levels and the nuclear localization of *NRF2* along with its inhibitory effect on *KEAP1* protein levels. Importantly, we indicated that AST pretreatment suppressed ROS generation and cell death in GCs under the conditions of oxidative stress. Moreover, we revealed that using Trig as an inhibitor of *NRF2*, reduced the protective effects of AST by decreasing *NRF2* expression and activity and the gene expression of phase II enzymes. However, its

inhibitory role did not completely remove the protective effects of AST on GCs. Therefore, our study may support a key role of the *NRF2*/*ARE* pathway in stimulating antioxidant enzymes induced by AST pretreatment in GCs.

As mentioned before, oxidative stress plays an important role in GCs related disorders like PCOS and may have a notable influence on IVF outcome. Therefore, developing an accurate model of oxidative stress is essential in different studies. One of the most applicable models used for establishing oxidative stress is the treatment of cultured cells like primary human GCs with H<sub>2</sub>O<sub>2</sub> (4). Here, we used the model of H<sub>2</sub>O<sub>2</sub>-induced oxidative stress in GCs for investigating the antioxidant efficiency against oxidative damage. 200  $\mu$ M of H<sub>2</sub>O<sub>2</sub> for 2 hours was determined to

induce oxidative stress in GCs for the next experiments. In our recent study, we showed that a concentration of 200  $\mu\text{M}$  of  $\text{H}_2\text{O}_2$  for 2 hours, promotes oxidative stress in GCs (16). A recent similar study also used 200, 400, and 600  $\mu\text{M}$  of  $\text{H}_2\text{O}_2$  for 48 hours to induce oxidative stress in GCs and evaluate the expression of *NRF2* and associated antioxidant enzymes (17). In addition, another study used 200  $\mu\text{M}$  of  $\text{H}_2\text{O}_2$  for 24 hours to create the same condition in retinal pigment epithelial cells (18). Furthermore, 400  $\mu\text{M}$  of  $\text{H}_2\text{O}_2$  for 48 hours was used to trigger the model of oxidative stress in GCs (17). Our chosen concentration of  $\text{H}_2\text{O}_2$  for creating the model of oxidative stress was almost supported by other studies too in different cultured cells like human keratinocytes (19).

Antioxidant enzymes are produced more under conditions of excess ROS production to neutralize oxidative stress and return the homeostasis of cells like GCs and then, regulate ovarian follicles growth and function. Earlier studies emphasized the importance of *NRF2* and *KEAP1* in the regulation of GCs condition at several phases of follicles (17). Since the exact mechanisms underlying the interaction between oxidative stress and antioxidant defense in human GCs, are largely unknown and need more comprehensive investigations, here, we intended to explore the role of *NRF2*/*ARE* pathway in protecting GCs against ROS production and apoptosis by using the natural carotenoid pigment, AST.

Recently, AST has been under great attention for its various biological functions including ROS scavenging, anti-inflammatory, anti-apoptotic, and anti-oxidative effects (20). AST is a powerful carotenoid antioxidant having many potential applications in human health protection. Although the exact mechanism of AST in reducing oxidative damage is largely unknown, the role of *NRF2*/*ARE* pathway activation for these anti-oxidative effects was illustrated (21). However, the protective effect of AST on human GCs against oxidative stress is still elusive. Here, we firstly determined the best protective concentration of AST. The optimal dose of AST we used was 5  $\mu\text{M}$  for 24 hours which was also supported by other researches done under similar concentrations. For instance, 5  $\mu\text{M}$  of AST was able to protect keratinocytes and peritoneal mesothelial cells from oxidative damage (22, 23). Likewise, AST at concentrations of 5 and 6.25  $\mu\text{M}$  increased the expression of phase II antioxidant enzymes in other types of cells (24).

One of the most important results of our study is that AST can inhibit ROS production and protect cells from apoptosis. The intracellular ROS levels generated by  $\text{H}_2\text{O}_2$  were significantly lower in GCs after pretreatment with 5  $\mu\text{M}$  AST. Several studies demonstrated that AST acts as a potent free radical scavenger and reduces the amount of intracellular ROS in several types of human cells. For instance, AST at a concentration of 5  $\mu\text{M}$  protected peritoneal mesothelial cells by scavenging glucose-induced ROS (23). Interestingly, another study showed that AST at concentrations of 10 and 20  $\mu\text{M}$  decreased ROS production in retinal pigment epithelial cells (18).

Moreover, 2  $\mu\text{M}$  of AST decreased fatty acid-induced ROS production in human lymphocytes (25). Several studies also reported the preventive effects of AST on ROS production in human neuroblastoma cells (26). AST at concentrations of 10 and 100  $\mu\text{M}$  also scavenged intracellular ROS in retinal ganglion cells (27). Putting these together, we may conclude that AST as a direct scavenger of free radicals like  $\text{H}_2\text{O}_2$ , has beneficial effects on improving viability of primary human GCs.

In our study, flow cytometry analysis showed a possible role of AST in decreasing  $\text{H}_2\text{O}_2$ -induced GCs early and late apoptosis through its anti-oxidative and anti-apoptotic properties. The present study suggests that AST up-regulated *NRF2*/*ARE* pathway and as a result, suppressed the apoptosis rate of GCs induced by intracellular ROS. Along with our data, other studies also suggested the inhibitory role of AST on apoptosis in different human cell types including keratinocytes treated with 5  $\mu\text{M}$  AST (22), alveolar epithelial cells treated with 8  $\mu\text{M}$  AST (28), and human neuroblastoma cells treated with 20  $\mu\text{M}$  AST (29). Therefore, AST can be used for protecting GCs from apoptosis through its scavenging activity and then, to strengthen the ability to reproduce in women. Moreover, as high levels of *NRF2* were observed in the presence of AST followed by a decrease in ROS production and cell damage, we may suggest *NRF2* as a survival protein in follicular development.

Among many endogenous antioxidant components involved in maintaining cellular homeostasis, *NRF2*-*ARE* pathway and its underlying targets phase II enzymes *GCLC*, *HO1*, and *NQO1*, are of great importance (2). They are induced under conditions of oxidative stress when *NRF2* as a key transcription factor, is translocated into the nucleus for binding to *ARE* region leading to enhanced expression of phase II antioxidant enzymes. But until the homeostasis of the cell remains normal, *NRF2* is inactivated by its endogenous inhibitor, *KEAP1* protein (30). As described earlier, the phase II enzymes induced by this pathway consist of several antioxidants. Here, we intended to evaluate the effects of AST treatment on mRNA and protein expression and the activity of *NRF2* as well as the gene expression of *GCLC*, *GCLM*, *HO1*, and *NQO1*. Furthermore, we evaluated the protein levels of *KEAP1* to investigate whether the effects of AST on the *NRF2*-*ARE* pathway is dependent on *NRF2* inhibitor or not. Our study demonstrated that AST pretreatment induced the gene and protein levels of *NRF2* but reduced the protein levels of *KEAP1* in GCs in the presence or absence of  $\text{H}_2\text{O}_2$ . Moreover, measurement of *NRF2* activity showed that AST was able to significantly increase *NRF2* translocation to the nucleus and its connection to the *ARE* consensus site (5'-GTCACAGTGA CT CAGCAGAATCTG-3') compared to  $\text{H}_2\text{O}_2$ -treated GCs without AST. Then, AST stimulates *NRF2*-*ARE* pathway by both enhancing the gene expression and activity of *NRF2* and decreasing *KEAP1* protein levels. Interestingly, a higher level of *NRF2* in the nucleus may result from its up-regulation and lower levels of *KEAP1* protein as its intracellular inhibitor.

We also observed a significant increase in the gene expression of phase II enzymes after AST pretreatment in H<sub>2</sub>O<sub>2</sub>-treated and untreated groups which followed by subsequent protection of GCs against oxidative damage and cell death. Some studies support our findings including a recent study that indicated the potential role of AST in increasing the nuclear localization of NRF2 and subsequent expression of *NQO1* and *HO1* in glomerular mesangial cells (31). Interestingly, AST induced the gene expression of *HO1* followed by the activation of NRF2 nuclear translocation in human umbilical vein endothelial cells which was reduced after using NRF2 specific small interfering RNA (siRNA) for its inhibition (32). Furthermore, AST reduced the levels of KEAP1 protein which triggered its dissociation from NRF2 and increased the nuclear localization of NRF2 in the kidney of diabetic rats (33). Another investigation on the brain after experimental subarachnoid hemorrhage showed that AST can activate NRF2-ARE pathway and subsequent gene expression of *HO1* and *NQO1* enzymes, then ameliorated oxidative stress (34). Moreover, AST at a concentration of 6.25 μM produced the highest gene expression of *NRF2*, *NQO1*, and *HO1* compared to other concentrations of AST in HepG2 cells (24). In another similar study on retinal pigment epithelial cells, researchers reported a higher NRF2 nuclear localization and GCLC, GCLM, HO1, and NQO1 expression after treatment with 5, 10, and 20 μM of AST (18). In view of our findings and the others, we may remark the importance of NRF2-ARE pathway in the activation of its downstream phase II antioxidant enzymes for the protection of ovarian follicles, preventing women from oxidative stress-related disorders, and increasing the success rates of IVF. Here, we pointed towards the activation of NRF2-ARE pathway by AST as well as other antioxidants such as phenolic compounds and carotenoids (35). Finally, we hope to achieve a better pregnancy result by applying AST as an inducer of NRF2/ARE pathway to neutralize oxidative stress and apoptosis in human GCs.

Moreover, Trig as an alkaloid derived from niacin (vitamin B3) was added at a concentration of 0.1 μM to express the importance of NRF2 in the protective effects of AST and describe the link between NRF2-ARE pathway and AST-induced phase II enzymes expression (7). Here, we observed a significant decrease in the expression of *NRF2* at both mRNA and protein levels as well as the gene expression of phase II enzymes by adding Trig to H<sub>2</sub>O<sub>2</sub>-treated and untreated GCs after AST pretreatment. Likewise, Trig treatment induced the levels of endogenous inhibitor of NRF2, KEAP1 protein along with a reduction in NRF2 activity in H<sub>2</sub>O<sub>2</sub>-treated GCs after AST pretreatment. This underlines the remarkable role of AST-induced NRF2/ARE pathway in stimulating phase II enzymes. However, our results revealed that the protective effects of AST on our studied target expression remained significant after Trig treatment compared to H<sub>2</sub>O<sub>2</sub>-treated GCs which highlighted the effectiveness of AST and the inability of Trig to completely erase the protective effects of AST. Furthermore, there are other studies regarding the inhibitory role of Trig on the nuclear

accumulation of NRF2 protein in different types of cells (36). According to our data and those reported by previous studies, it seems likely that Trig inhibits NRF2 pathway and its downstream antioxidant enzymes mostly by inhibition of NRF2 nuclear accumulation. Putting these findings together, our study established the importance of NRF2/ARE pathway in the related antioxidant defense induced by AST regarding the possibility that Trig has an inverse influence on the stimulatory role of AST on GCLC, GCLM, HO1, and NQO1 expression.

Altogether, in this study, we showed that AST as a protective natural factor promotes gene and protein levels of NRF2 and inhibits the protein levels of KEAP1 in primary human GCs. We may consider this mechanism for the inhibition of H<sub>2</sub>O<sub>2</sub>-induced apoptosis and intracellular ROS generation by AST treatment. Hence, here for the first time, we showed that AST inhibits H<sub>2</sub>O<sub>2</sub>-induced apoptosis and intracellular ROS generation through a mechanism by which NRF2 induces the expression of antioxidant enzymes such as GCL, HO1, and NQO1 in GCs. Therefore, the current study provides supporting data considering the possible role of AST in presenting a noble therapeutic strategy for infertility, PCOS and other ovarian diseases related to oxidative damage. These results show that AST as a radical scavenger and an anti-apoptotic factor, probably protects primary human GCs against H<sub>2</sub>O<sub>2</sub>-induced oxidative stress and cell death via regulating NRF2 and related factors and thus, improves the development of the ovarian follicles.

The limitations of the present study included using Trig as an inhibitor of *NRF2*. Because this agent is not capable of completely suppressing *NRF2* as provided in our results, a more applicable and specific material must be applied for complete inhibition of *NRF2* to investigate its role in activating downstream antioxidant defense. Therefore, we suggest the use of a specific siRNA for this propose in future studies related to this topic.

## Conclusion

Our study demonstrated that AST promotes gene and protein levels of *NRF2* and inhibits the protein levels of KEAP1 in primary human GCs. It seems likely that activation of NRF2 by AST may attenuate oxidative stress in human GCs through activation of downstream antioxidant enzymes including GCL, HO1, and NQO1 and may produce better outcomes of IVF and reproduction in women.

## Acknowledgements

This study was supported by Tehran University of Medical Sciences (Grant No. 32156) and it is acknowledged by authors. The authors declare that there is no conflict of interest in this study.

## Authors' Contributions

F.A., A.S.; Contributed to conception and design. M.E., Z.R., S.E.; Contributed to all experimental work, data and

statistical analysis. M.A.; Performed follicle collection. Sh.H., S.B.; Conducted molecular experiments and RT-qPCR analysis. All authors edited and approved the final version of this manuscript for submission, participated in the finalization of the manuscript and approved the final draft.

## References

- Devine PJ, Perreault SD, Luderer U. Roles of reactive oxygen species and antioxidants in ovarian toxicity. *Biol Reprod.* 2012; 86(2): 27.
- McMahon M, Itoh K, Yamamoto M, Hayes JD. Keap1-dependent proteasomal degradation of transcription factor Nrf2 contributes to the negative regulation of antioxidant response element-driven gene expression. *J Biol Chem.* 2003; 278(24): 21592-21600.
- Kaspar JW, Niture SK, Jaiswal AK. Nrf2:INrf2 (Keap1) signaling in oxidative stress. *Free Radic Biol Med.* 2009; 47(9): 1304-1309.
- Karuputhula NB, Chattopadhyay R, Chakravarty B, Chaudhury K. Oxidative status in granulosa cells of infertile women undergoing IVF. *Syst Biol Reprod Med.* 2013; 59(2): 91-98.
- Shkolnik K, Tadmor A, Ben-Dor S, Nevo N, Galiani D, Dekel N. Reactive oxygen species are indispensable in ovulation. *Proc Natl Acad Sci USA.* 2011; 108(4): 1462-1467.
- Heidari Khoei H, Fakhri S, Parvardeh S, Shams Mofarahe Z, Baninameh Z, Vardiani M. Astaxanthin prevents the methotrexate-induced reproductive toxicity by targeting oxidative stress in male mice. *Toxin Reviews.* 2019; 38(3): 248-254.
- Boettler U, Sommerfeld K, Volz N, Pahlke G, Teller N, Somoza V, et al. Coffee constituents as modulators of Nrf2 nuclear translocation and ARE (EpRE)-dependent gene expression. *J Nutr Biochem.* 2011; 22(5): 426-440.
- Boiteux S, Radicella JP. The human OGG1 gene: structure, functions, and its implication in the process of carcinogenesis. *Arch Biochem Biophys.* 2000; 377(1): 1-8.
- Kook D, Wolf AH, Yu AL, Neubauer AS, Priglinger SG, Kampik A, et al. The protective effect of quercetin against oxidative stress in the human RPE in vitro. *Invest Ophthalmol Vis Sci.* 2008; 49(4): 1712-1720.
- Jia Y, Lin J, Mi Y, Zhang C. Quercetin attenuates cadmium-induced oxidative damage and apoptosis in granulosa cells from chicken ovarian follicles. *Reprod Toxicol.* 2011; 31(4): 477-485.
- van Meerloo J, Kaspers GJL, Cloos J. Cell sensitivity assays: the MTT assay. *Methods Mol Biol.* 2011; 731: 237-245.
- Furfaro AL, Traverso N, Domenicotti C, Piras S, Moretta L, Marinari UM, et al. The Nrf2/HO-1 axis in cancer cell growth and chemoresistance. *Oxid Med Cell Longev.* 2016; 2016: 1958174.
- Sawai H, Domae N. Discrimination between primary necrosis and apoptosis by necrostatin-1 in Annexin V-positive/propidium iodide-negative cells. *Biochem Biophys Res Commun.* 2011; 411(3): 569.
- Kubista M, Andrade JM, Bengtsson M, Forootan A, Jonak J, Lind K, et al. The real-time polymerase chain reaction. *Mol Aspects Med.* 2006; 27(2-3): 95-125.
- Mahmood T, Yang PC. Western blot: technique, theory, and trouble shooting. *N Am J Med Sci.* 2012; 4(9): 429-434.
- Rashidi Z, Aleyasin A, Eslami M, Nekoonam S, Zendedel A, Bahramrezaie M, et al. Quercetin protects human granulosa cells against oxidative stress via thioredoxin system. *Reprod Biol.* 2019; 19(3): 245-254.
- Akino N, Wada-Hiraike O, Terao H, Honjoh H, Isono W, Fu H, et al. Activation of Nrf2 might reduce oxidative stress in human granulosa cells. *Mol Cell Endocrinol.* 2018; 470: 96-104.
- Li Z, Dong X, Liu H, Chen X, Shi H, Fan Y, et al. Astaxanthin protects ARPE-19 cells from oxidative stress via upregulation of Nrf2-regulated phase II enzymes through activation of PI3K/Akt. *Mol Vis.* 2013; 19: 1656-1666.
- Wang Xy, He Py, Du J, Zhang Jz. Quercetin in combating H<sub>2</sub>O<sub>2</sub> induced early cell apoptosis and mitochondrial damage to normal human keratinocytes. *Chin Med J (Engl).* 2010; 123(5): 532-536.
- Davinelli S, Nielsen ME, Scapagnini G. Astaxanthin in skin health, repair, and disease: a comprehensive review. *Nutrients.* 2018; 10(4): 522.
- Copple IM. The Keap1-Nrf2 cell defense pathway--a promising therapeutic target? *Adv Pharmacol.* 2012; 63: 43-79.
- Yoshihisa Y, Rehman MU, Shimizu T. Astaxanthin, a xanthophyll carotenoid, inhibits ultraviolet-induced apoptosis in keratinocytes. *Exp Dermatol.* 2014; 23(3): 178-183.
- Hara K, Hamada C, Wakabayashi K, Kanda R, Kaneko K, Horikoshi S, et al. Scavenging of reactive oxygen species by astaxanthin inhibits epithelial-mesenchymal transition in high glucose-stimulated mesothelial cells. *PLoS One.* 2017; 12(9): e0184332.
- Saw CLL, Yang AY, Guo Y, Kong ANT. Astaxanthin and omega-3 fatty acids individually and in combination protect against oxidative stress via the Nrf2-ARE pathway. *Food Chem Toxicol.* 2013; 62: 869-875.
- Campoio TR, Oliveira FA, Otton R. Oxidative stress in human lymphocytes treated with fatty acid mixture: role of carotenoid astaxanthin. *Toxicol In Vitro.* 2011; 25(7): 1448-1456.
- Lee DH, Kim CS, Lee YJ. Astaxanthin protects against MPTP/MPP+ induced mitochondrial dysfunction and ROS production in vivo and in vitro. *Food Chem Toxicol.* 2011; 49(1): 271-280.
- Nakajima Y, Inokuchi Y, Shimazawa M, Otsubo K, Ishibashi T, Hara H. Astaxanthin, a dietary carotenoid, protects retinal cells against oxidative stress in-vitro and in mice in-vivo. *J Pharm Pharmacol.* 2008; 60(10): 1365-1374.
- Song X, Wang B, Lin S, Jing L, Mao C, Xu P, et al. Astaxanthin inhibits apoptosis in alveolar epithelial cells type II in vivo and in vitro through the ROS-dependent mitochondrial signalling pathway. *J Cell Mol Med.* 2014; 18(11): 2198-2212.
- Ikeda Y, Tsuji S, Satoh A, Ishikura M, Shirasawa T, Shimizu T. Protective effects of astaxanthin on 6-hydroxydopamine-induced apoptosis in human neuroblastoma SH-SY5Y cells. *J Neurochem.* 2008; 107(6): 1730-1740.
- Eggle AL, Gay KA, Mesecar AD. Molecular mechanisms of natural products in chemoprevention: induction of cytoprotective enzymes by Nrf2. *Mol Nutr Food Res.* 2008; 52 Suppl 1: S84-S94.
- Xie X, Chen Q, Tao J. Astaxanthin promotes Nrf2/ARE signaling to inhibit HG-induced renal fibrosis in GMCs. *Mar Drugs.* 2018; 16(4): 117.
- Niu T, Xuan R, Jiang L, Wu W, Zhen Z, Song Y, et al. Astaxanthin induces the Nrf2/HO-1 antioxidant pathway in human umbilical vein endothelial cells by generating trace amounts of ROS. *J Agric Food Chem.* 2018; 66(6): 1551-1559.
- Zhu X, Chen Y, Chen Q, Yang H, Xie X. Astaxanthin promotes Nrf2/ARE signaling to alleviate renal fibronectin and collagen IV accumulation in diabetic rats. *J Diabetes Res.* 2018; 2018: 6730315.
- Wu Q, Zhang X-S, Wang H-D, Zhang X, Yu Q, Li W, et al. Astaxanthin activates nuclear factor erythroid-related factor 2 and the antioxidant responsive element (Nrf2-ARE) pathway in the brain after subarachnoid hemorrhage in rats and attenuates early brain injury. *Mar Drugs.* 2014; 12(12): 6125-6141.
- Upadhyay S, Dixit M. Role of polyphenols and other phytochemicals on molecular signaling. *Oxid Men Cell Longev.* 2015; 2015: 504254.
- Sirota R, Gibson D, Kohen R. The role of the catecholic and the electrophilic moieties of caffeic acid in Nrf2/Keap1 pathway activation in ovarian carcinoma cell lines. *Redox Biol.* 2015; 4: 48-59.

# MiR-221 Expression Level Correlates with Insulin-Induced Doxorubicin Resistance in MCF-7 Breast Cancer Cells

Parisa Kheradmand, M.Sc.<sup>1</sup>, Sadeq Vallian Borojeni, Ph.D.<sup>1\*</sup>, Saeed Esmaeili-Mahani, Ph.D.<sup>2</sup>

1. Department of Cellular and Molecular Biology and Microbiology, Faculty of Science and Technology, University of Isfahan, Isfahan, Iran  
2. Department of Biology, Shahid Bahonar University of Kerman, Kerman, Iran

\*Corresponding Address: Department of Cellular and Molecular Biology and Microbiology, Faculty of Science and Technology, University of Isfahan, Isfahan, Iran  
Email: svallian@sci.ui.ac.ir

Received: 22/September/2019, Accepted: 08/January/2020

## Abstract

**Objective:** Insulin induces anti-cancer drugs resistance in tumor cells. However, the mechanism by which insulin induces its drug resistance effects is not clear. In the present study, the expression of miR-221 in insulin-treated MCF-7 cells in response to the anti-cancer drug doxorubicin, was investigated.

**Materials and Methods:** In this experimental study, cell viability was evaluated using MTT (3-[4,5 dimethylthiazol-2-yl]-2,5-diphenyl tetrazolium bromide) assay. The expression level of miR-221 was determined by real time polymerase chain reaction (RT-PCR). Furthermore, the expression of insulin receptor (IR) and cleaved caspase-3 protein was assessed by Western blotting.

**Results:** The results showed that treatment of the MCF-7 cells with insulin reduced the anti-cancer effects of doxorubicin. Viability of naive and insulin-treated cells following doxorubicin (DOX) treatment was  $62.9 \pm 5.7\%$  and  $79 \pm 7.2\%$ , respectively. Furthermore, the expression of miR-221 in insulin-treated cells was significantly increased ( $2.6 \pm 0.37$ -fold change) as compared with the control group. A significant decrease (26%) in the expression of caspase-3 protein and a significant increase (24%) in IR were observed in insulin-induced drug resistant MCF-7 cells as compared to the naive cells.

**Conclusion:** Together, the data showed a positive correlation between the expression of miR-221 and IR expression, but a negative correlation with caspase3 expression, in insulin-induced drug resistant MCF-7 breast cancer cells. This could suggest a new mechanism for the role of miR-221 in cancer drugs resistance induced by insulin.

**Keywords:** Breast Cancer, Doxorubicin, Insulin Receptor, MCF-7 Cells, MiR-221

Cell Journal(yakhteh), Vol 23, No 3, August 2021, Pages: 329-334

**Citation:** Kheradmand P, Vallian Borojeni S, Esmaeili-Mahani S. MiR-221 expression level Correlates with insulin-induced doxorubicin resistance in MCF-7 breast cancer cells. Cell J. 2021; 23(3): 329-334. doi: 10.22074/cellj.2021.7153.

This open-access article has been published under the terms of the Creative Commons Attribution Non-Commercial 3.0 (CC BY-NC 3.0).

## Introduction

Chemotherapy based on doxorubicin (DOX) is one of the most common treatments for breast cancer. DOX belongs to the family of anthracyclines, which functions through two main mechanisms: i. It can intercalate itself into the DNA and inhibit DNA and RNA polymerases and disrupt DNA repair mechanism by topoisomerase enzymes, and ii. DOX can cause the formation of free radicals resulting in damages to proteins, cell membranes and DNA. Despite advances in cancer therapy, drug resistance such as DOX resistance is one of the most important challenges.

Numerous studies showed the association between insulin signaling and tumor metastasis and drug resistance (1, 2). Due to its connection with a network of signaling pathways, insulin signaling has been considered one of the very complicated pathways (2). Upon binding of insulin to the  $\alpha$ -subunit of insulin receptor (IR), conformational changes induce trans-phosphorylation of each  $\beta$ -subunit, resulting in the activation of IR. Subsequently, the activated IR phosphorylates intracellular substrates such as the IR substrate (IRS) family. IRS phosphorylation finally results in the activation of downstream effectors such as AKT (protein kinase B), which mediates several functions that prevent cell death and result in cell survival

like activating protein and glycogen synthesis (2, 3). This cascade of phosphorylation events is commonly known as the PI3K/AKT pathway of insulin signaling which sometimes increases carcinogenicity (3, 4) and induces drug resistance (1, 5, 6). In fact, in many types of cancers, insulin induces resistance to chemotherapy and may even be associated with late diagnosis, especially in patients with obesity and type-2 diabetes.

A significant association between cancer-related mortality and use of exogenous insulin was reported (7). Moreover, the relevance of increased risk of breast cancer and type-2 diabetes in women was demonstrated (8). Furthermore, the association between diabetes and an increased risk of colorectal cancer was reported. In addition, it was reported that the up-regulation of IR can enhance multistage tumor progression and cause intrinsic resistance to insulin-like growth factor-1 receptor (IGF-1R) targeted therapy (9). Moreover, the over-expression of IRs in cancers was shown in different reports (9, 10). However, the mechanism(s) by which insulin induces drug resistance is not fully understood.

miRNAs are small noncoding RNAs (18-23 nucleotide) which are transcribed by RNA polymerase II and play

critical roles in gene regulation (11). Recent studies indicated that more than half of the known human genes are targets for miRNAs and each miRNA can regulate multiple target genes (12). It is believed that more than 50% of miRNAs are located in the genomic regions that were deleted or duplicated in various types of tumors, leading to under regulation of gene expression (13). It was reported that up- or down-regulation of miRNAs expression could lead to variations in chemotherapy susceptibility of cancer cells through various cellular pathways (14, 15). Moreover, it was shown that several miRNAs can regulate cellular response to anti-cancer drugs by modifying drug concentration, survival pathway, apoptotic response and cell cycle (16). It was demonstrated that there is an aberrant expression of miRNAs such as miR-221, miR-21, miR-19, and miR-127, in drug-resistant cancer cells (17-19). Moreover, several reports indicate the involvement of miRNAs such as, miR-221, miR-181b, miR-126 and miR-21, in regulation of expression of genes involved in insulin signal transduction pathway (20, 21).

In this study, the changes in the expression of miR-221, IR and apoptotic components of caspase-3, were evaluated in insulin-induced drug resistant MCF-7 breast cancer cells.

## Materials and Methods

In this experimental study, cell culture reagents, fetal bovine serum (FBS), penicillin-streptomycin solution and trypsin-EDTA, were obtained from Biosera Company (Boussens, France). Cell culture flasks and dishes were purchased from SPL Life Science, Inc. (Gyeonggi-Do, South Korea). MTT (3-[4, 5-dimethyl-2-thiazolyl]-2, 5-diphenyl-2-tetrazolium bromide) and primary monoclonal anti- $\beta$ -actin antibody (A-5316) were obtained from Sigma-Aldrich (St. Louis, MO). Primary polyclonal anti-Insulin R $\beta$  (sc-711), secondary goat anti-rabbit (sc-2004), and secondary goat anti-mouse (sc-2357) antibodies were purchased from Santa Cruz Biotechnology, Inc. (Santa Cruz, CA). Primary polyclonal anti-Caspase-3 (#9662) was purchased from Cell Signaling Technology (Danvers, MA, USA).

The present work was approved by Department of Research and Technology of University of Isfahan as a Ph.D. thesis.

### Cell culture

The MCF-7 cell line was obtained from the National Cell Bank of Iran (Pasteur Institute, Tehran, Iran). The cells were cultured in Dulbecco's modified Eagle's medium (DMEM, Biosera, France) supplemented with 10% FBS, penicillin (100 U/mL), and streptomycin (100  $\mu$ g/mL). They were maintained in 5% CO<sub>2</sub> atmosphere at 37°C. Cells were cultured in 96-well culture plates at initial seeding number of 5 $\times$ 10<sup>3</sup> cells per well.

### Cell viability analysis

Cell viability was assessed by MTT assay (22). In

this method, MTT is reduced to purple formazan by mitochondrial dehydrogenase, revealing the number of living cells. MTT was dissolved in phosphate-buffered saline (PBS) at final 5 mg/ml concentration. In each assay, 20  $\mu$ l of MTT was added to each well containing 5 $\times$ 10<sup>3</sup> MCF-7 cells, and then, incubated for 2 hours at 37°C. In the next step, the culture medium was removed carefully and 100  $\mu$ l dimethyl sulfoxide (DMSO) was added to the cells. The cell plate was gently shaken until formazan crystals were dissolved completely. Absorbance (optical density) was determined at 490 nm by an automatic microplate reader (ELX 8000, Biotek-USA).

In order to determine the antitumor effects of DOX in breast cancer cells, the MCF-7 cells were treated with the increasing concentrations of DOX and their viability was determined by MTT assay. After the initial 24 hours of attachment/growth period, the cells were incubated with DOX 1, 5 and 10  $\mu$ M for 48 and 72 hours. The main studied groups in MTT test were naive cell group and insulin-treated cell group. The naive cells received no insulin treatment. This group included the following subgroups: i. Control cells which were cultured in 200  $\mu$ l complete DMEM growth medium and ii. Three groups of MCF-7 cells that were incubated with different doses of DOX (1, 5 and 10  $\mu$ M).

Treated MCF-7 cells group contained cells which were treated with insulin (48 or 72 hours). This group contained subgroups including control group, which was cultured in 200  $\mu$ l complete DMEM growth medium with 10 nM insulin, and three groups of insulin pretreated MCF-7 cells that were incubated in the presence of different doses of DOX (1, 5 and 10  $\mu$ M) for further 24 hours.

### Total RNA isolation and real time polymerase chain reaction

Total RNA extraction was performed from collected cells using RNX<sup>+</sup> reagent (SinaClone Co., Iran), and then, cDNA was synthesized using a universal cDNA synthesis kit (Exiqon, Copenhagen, Denmark) according to the manufacturer's protocol. U48 small nuclear RNA was used as the internal control. The real-time polymerase chain reaction (PCR) reactions were performed using the specific primers of hsa-miR-221 and U48 (Pars Genome co., Iran). Quantitative PCR (qPCR) was performed using 7500 real-time PCR system (Applied Biosystem-USA). In our experiments for comparing gene expression levels among samples, the 2<sup>- $\Delta\Delta$ CT</sup> method was used (23). The main studied groups for RT-PCR were naive cells group and insulin-treated cells group. In naive cells group, no insulin treatment was done and this group included: control cells which were cultured in 200  $\mu$ l complete DMEM growth medium and a group of MCF-7 cells that was incubated with DOX (10  $\mu$ M).

Insulin-treated cells group contained MCF-7 cells which were treated with insulin. This group contained a control group which was cultured in 200  $\mu$ l complete DMEM growth medium supplemented with 10 nM insulin, and

a group of insulin-pretreated MCF-7 cells that were incubated with DOX (10  $\mu$ M) for 24 hours.

### Western blot analysis

Changes in the expression of caspases could significantly affect resistance to chemotherapy drugs (24, 25). In our study, we assessed the activated caspase-3 (as executive caspases) and IR protein expression, by western blotting.

MCF-7 cells were lysed and homogenized in ice-cold buffer containing 10 mM Tris-HCl (pH=7.4), 0.1% sodium dodecyl sulfate (SDS), 1 mM EDTA, 0.1% Na-deoxycholate, 1% NP-40 with protease inhibitors (1 mM phenylmethylsulfonyl fluoride, 2.5  $\mu$ g/ml leupeptin, and 10  $\mu$ g/ml aprotinin), and 1 mM sodium orthovanadate. The total proteins were extracted by centrifugation at 14,000 $\times$ g for 15 minutes at 4°C. Equal amounts of proteins (40  $\mu$ g) were fractionated by sodium dodecyl sulfate polyacrylamide gel electrophoresis (9% SDS-PAGE) and transferred to polyvinylidenedifluoride (PVDF) membrane (Roche Co, Germany). After blocking at room temperature for 1 hour, the membranes were immunostained with primary antibodies against human IR (dilution, 1:1,000; sc-711; Santa Cruz Biotechnology, Inc., Dallas, TX, USA) and cleaved caspase-3 (1:1000 dilution, cell signaling, USA) at 4°C, overnight. After washing, the membranes were incubated with matched horseradish peroxidase-conjugated secondary antibodies (1:10,000; Santa Cruz Biotechnology, Inc.) at room temperature for 1 hour. Then, the blots were assessed using the ECL system and imaged by Chemi Doc XRS+ imaging system (Bio-Rad Company, USA). The intensity of the bands was determined by Lab Works analyzing software (UVP, UK). In our immunoblot experiments,  $\beta$ -actin (1:10,000) was used as the loading control. Immune detection was recorded using Chemi Doc XRS+ imaging system (Bio-Rad Company, USA).

### Statistical analysis

All tests were performed in triplicate and the data was analyzed using SPSS (version 20) software (IBM, New York, NY, USA). The results are presented as mean  $\pm$  standard error of the mean. For evaluating the differences in mean values among experimental groups, one-way analysis of variance was performed and it was followed by the Tukey test. A  $P < 0.05$  was considered significant.

## Results

### The effects of doxorubicin on naive and insulin-treated MCF-7 cells viability

As shown in Figure 1, DOX had antitumor effects on MCF-7 cells in a dose-dependent manner. A significant effect was observed in the cells treated with 5 ( $P < 0.05$ ) and 10  $\mu$ M ( $P < 0.001$ ) DOX (indicated as naive cells in Fig.1). Furthermore, to examine the effects of insulin treatment on doxorubicin-induced tumor cell death, distinct group of cells were pretreated with 10 nM insulin for 48 (Fig.1A) or 72 hours ( Fig.1B) and then, different

doses of DOX were added for an additional 24 hours. Our data showed that insulin could induce DOX resistance in MCF-7 cells.

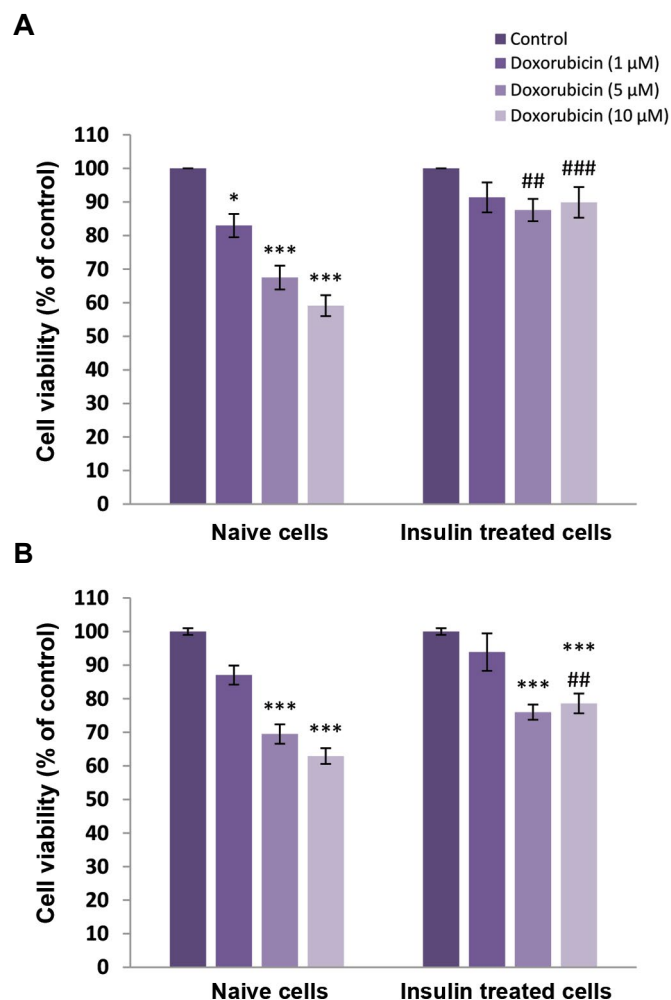


**Fig.1:** Effects of different concentrations of doxorubicin on naive and insulin-treated MCF-7 cells viability. The cells were pretreated with insulin 10 nM and vehicle for **A**, 48 and **B**, 72 hours. Cell viability was determined by MTT assay. Data is expressed as mean  $\pm$  SEM (n=6 wells for each group). \*;  $P < 0.05$ , \*\*\*;  $P < 0.001$  are significantly different versus the control group, ##;  $P < 0.01$ , and ###;  $P < 0.001$  are significantly different versus naive cells at the same dose of doxorubicin.

### MiR-221 expression in naive and insulin-treated cells

To investigate the changes in miR-221 expression following the development of DOX resistance, the expression level of miR-221 was evaluated by qRT-PCR. As shown in Figure 2, miR-221 expression was up-regulated in insulin-treated MCF-7 cells. DOX could significantly decrease miR-221 levels in naive and insulin-treated cells. However, in the presence of doxorubicin, the data showed that the level of miR-221 in insulin-pretreated cells was greater than those in naive cells (Fig.2, Table 1).

As indicated in Figures 1 and 2, MiR-221 expression was evaluated in different situations including control MCF-7 naive cells, DOX- treated MCF-7 naive cells, insulin-treated MCF-7 cells and insulin + DOX-treated MCF-7 cells.

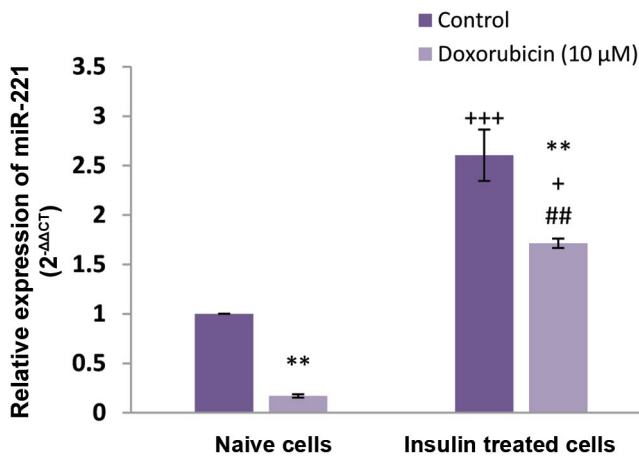


**Fig.2:** The effects of insulin treatment on miR-221 expression in naive (control) and insulin-pretreated MCF-7 cells in the presence of doxorubicin (10 μM) or vehicle. \*\*; P<0.01 is significantly different versus control group, +; P<0.05, +++; P<0.001 are significantly different versus control naive cells, and ##; P<0.01 is significantly different versus doxorubicin-treated naive cells. The data was analyzed by 2<sup>-ΔΔCt</sup>.

**Table 1:** Expression of miR-221 in naive (control) and insulin-pretreated MCF-7 cells in the presence of doxorubicin (10 μM) or vehicle

	naive cell		Insulin-treated cell	
	Control	Doxorubicin	Insulin	Doxorubicin+Insulin
1		0.17 ± 0.03	2.6 ± 0.37	1.71 ± 0.07

**The expression level of caspase-3 protein in naive and insulin-treated MCF-7 cells**

The expression level of activated caspase-3 protein was investigated by Western blotting in naive and insulin-treated MCF-7 cells. The data showed that incubation with 10 μM DOX could significantly increase caspase-3 band density in naive cells. However, in the presence of insulin, the expression of caspase-3 was reduced in comparison with the naive cells (Fig.3A, B).

**The expression level of insulin receptor (subunit β) protein in naive and insulin-treated MCF-7 cells**

To examine the contribution of changes in IR protein density, Western blotting was used to evaluate the level of expression of IR in naive and insulin-treated MCF-7 cells. The results showed that treatment with 10 nM insulin could significantly increase IR band density (Fig.3A, C).

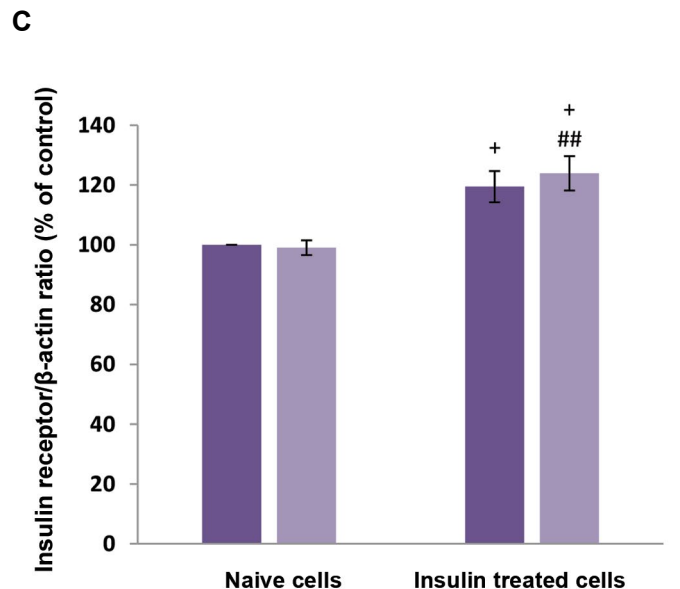
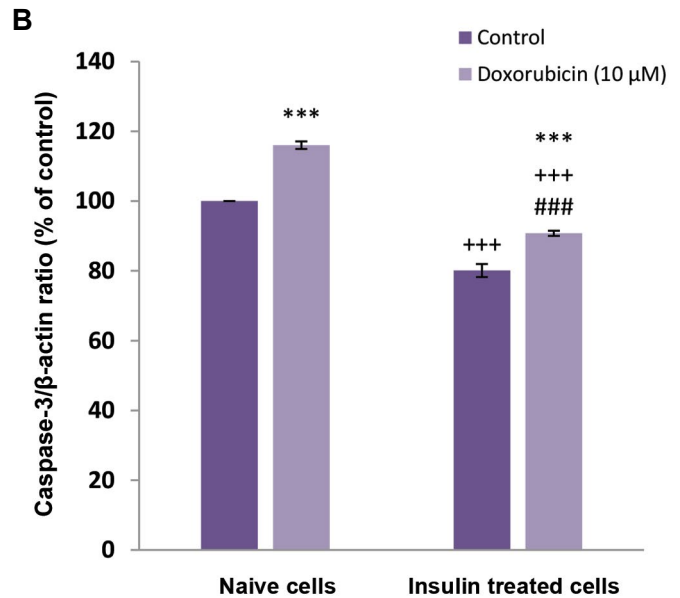
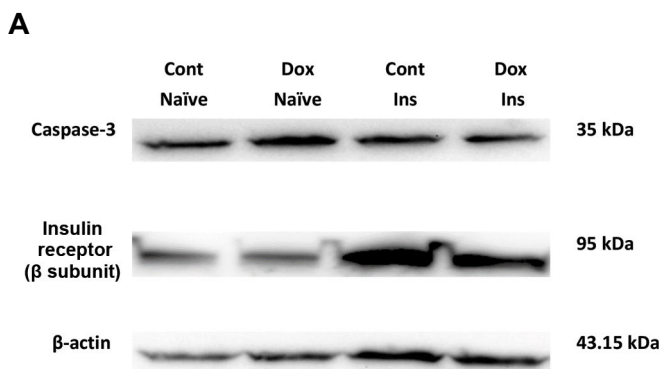


**Fig.3:** The effects of insulin treatment on caspase-3 and insulin receptor protein levels in naive (control) and insulin-pretreated MCF-7 cells in the presence of doxorubicin (10 μM) or vehicle. **A.** Protein bands were detected by Western blot analysis. **B.** Ratio of caspase-3 to β-actin level. **C.** Ratio of insulin receptor to β-actin level. β-actin was used as an internal control. Each value in the graph represents mean ± SEM band density ratio for each group. \*\*\*, P<0.001 is significantly different versus control group, +++; P<0.001 is significantly different versus control naive cells, ###; P<0.001 is significantly different versus doxorubicin-treated naive cells, +; P<0.05 is significantly different versus the control naive cells, ##; P<0.01 is significantly different versus the doxorubicin (DOX)-treated naive cells, Cont; Control, Dox; Doxorubicin, and Ins; Insulin.

**Discussion**

Drug resistance especially to DOX (a commonly used drug), is a major obstacle for breast cancer chemotherapy. Different genes were found to be associated with DOX resistance. Reduced expression of cyclin D2, cyclin B1 and p-ERK1 were shown to cause DOX resistance in breast cancer cell lines (26). Furthermore, decreased expression of miR-298 was found to be significantly correlated with DOX resistance in MDA-MB-231 cells (27).

The results of this study clearly showed that insulin can

cause DOX resistance in MCF-7 breast cancer cell lines. The data suggested that induction of DOX resistance by insulin might be through i. Overexpression of miR-221, ii. Increases in the expression of IR, and iii. Down regulation of caspase-3.

In several studies, a significant association between the risk of cancer and use of exogenous insulin or up regulation of IR was reported (28). Furthermore, it was shown that insulin can cause drug resistance in different types of cancer (29). However, the detailed mechanism (s) has not been fully clarified.

In this study, the data showed that insulin treatment can lead to DOX resistance. Previous studies showed that breast cancer cells were not able to reduce IR sensitivity in the presence of high doses of insulin (30). The overexpression of IR in insulin-treated MCF-7 cells resulted in an increase in insulin signal transduction. It was documented that insulin through its tyrosine kinase receptor, can control proliferation, differentiation, and survival of cells via two signaling pathways including PI3K/AKT and Ras-MAPK (5).

Different studies demonstrated that increased activity of PI3K/AKT pathway is associated with cancer progression, invasion, epithelial-mesenchymal transition and resistance to anti-cancer drugs (28-30). PI3K/AKT signaling pathway is a complex signaling network that can regulate several proteins by multiple mechanisms of regulation. For example, PI3K/AKT activation can phosphorylate glycogen synthase kinase 3  $\beta$  (GSK-3 $\beta$ ), which suppresses GSK-3 $\beta$  (31). This process leads to stabilization of nuclear  $\beta$ -catenin followed by transactivation of slug transcription factor (32). Recent studies showed that slug, a repressor of E-cadherin, has an important role in the epithelial-mesenchymal transition in cancer cells (33). It was reported that miR-221 expression is related to slug as a transcription factor (34) suggesting that over expression of miR-221 in insulin-treated MCF-7 cells may partially result from slug over expression which was induced by the activation of PI3K/AKT signaling. As these studies showed, slug transcription factor silencing by siRNA against slug could significantly decrease miR-221 expression. This finding may lead to the development of therapeutic strategies for overcoming insulin-induced drug resistance in breast cancer.

Recently, several studies indicated that miR-221 has an important role in repressing the expression of caspase-3 as its target gene (24, 25). Moreover, it was indicated that p53, as a tumor suppressor, could play a critical role in tumor cells apoptosis (35, 36) and its activation is one of the important mechanism of antitumor drugs (37, 38). It was demonstrated that DOX induced apoptosis in MCF-7 cells through p53 activation followed by caspase-3 activation and DNA fragmentation (39). Using the MTT assay, we found that DOX reduced viability of naive MCF-7 cells. On the other hand, insulin pretreatment before DOX incubation, could increase viability of MCF-7 cells in comparison with naive DOX-treated cells, and therefore, caused DOX resistance. Our results, as confirmed by Western blotting assay, showed that caspase-3 expression

level increased under DOX treatment in naive cells, and its expression level decreased after insulin treatment. This suggested that miR-221 overexpression through insulin treatment could led to caspase-3 down regulation. In a collaborative project with Dr. Haddadi, in Department of Biology, Shahid Bahonar University of Kerman, the expression of protein levels of Bax and Bcl-2 is under investigation (personal communication, unpublished data). Their preliminary data indicated that insulin induced drug resistance by increasing Bcl-2/Bax ratio and prevention of apoptosis in MCF7 cells.

Taken together, the present data suggested that insulin could induce DOX resistance in breast cancer cells. This happens through, at least in part, miR-221 overexpression as one of the key regulator of both PI3K/AKT, and Ras-MAPK in insulin signaling pathway followed by caspase-3 down regulation. Meanwhile, it would be interesting to investigate, in a new study, the expression of other molecules involved in this signaling pathway. Our observations could help clarifying one of the possible mechanisms of insulin-induced drug resistance in MCF-7 as a well-known breast cancer cell line. Nevertheless, performing the experiments in other cells would be part of our future projects to elucidate the mechanisms by which insulin affects breast cancer drug resistance.

## Conclusion

In the present work, the expression of miR-221 in insulin-treated MCF-7 cells in response to anti-cancer drug DOX was investigated. Furthermore, the expression of cleaved caspase-3 protein and IR was examined. The main findings of this research could be summarized as follows: i. In the presence of DOX, the miR-221 expression level in insulin-pretreated cells was greater than those in naive cells, ii. DOX incubation could significantly increase caspase-3 band density in naive cells. However, in the presence of insulin, the expression of caspase-3 was reduced in comparison with the naive cells, and iii. Insulin treatment could significantly increase IR band density in insulin-treated cells.

## Acknowledgments

This study was financially supported by Department of Research of University of Isfahan and the Pathology and Stem Cell Research Center, Kerman University of Medical Sciences. We are grateful to Prof. Shahriar Dabiri for financial and scientific supports. There is no conflict of interest in this study.

## Authors' Contributions

S.V.B., S.E.-M.; Designed and supervised the study and finalized the manuscript. P.Kh.; Performed the experiments, analyzed the data and drafted the manuscript. All authors read and approved the final manuscript.

## References

1. Li H, Bathth IS, Qu X, Xu L, Song N, Wang R, et al. IGF-IR sign-

- aling in epithelial to mesenchymal transition and targeting IGF-1R therapy: overview and new insights. *Mol Cancer*. 2017; 16(1): 6.
2. Gristina V, Cupri MG, Torchio M, Mezzogori C, Cacciabue L, Danova M. Diabetes and cancer: a critical appraisal of the pathogenetic and therapeutic links. *Biomed Rep*. 2015; 3(2): 131-136.
  3. Pollak M. The insulin and insulin-like growth factor receptor family in neoplasia: an update. *Nat Rev Cancer*. 2012; 12(3): 159-169.
  4. Fruman DA, Chiu H, Hopkins BD, Bagrodia S, Cantley LC, Abraham RT. The PI3K pathway in human disease. *Cell*. 2017; 170(4): 605-635.
  5. Boucher J, Kleinriders A, Kahn CR. Insulin receptor signaling in normal and insulin-resistant states. *Cold Spring Harb Perspect Biol*. 2014; 6(1): a009191.
  6. Hafsı S, Pezzino FM, Candido S, Ligresti G, Spandidos DA, Souza Z, et al. Gene alterations in the PI3K/PTEN/AKT pathway as a mechanism of drug-resistance (review). *Int J Oncol*. 2012; 40(3): 639-644.
  7. Bowker SL, Majumdar SR, Veugelers P, Johnson JA. Increased cancer-related mortality for patients with type 2 diabetes who use sulfonylureas or insulin. *Diabetes Care*. 2006; 29(2): 254-258.
  8. Michels KB, Solomon CG, Hu FB, Rosner BA, Hankinson SE, Colditz GA, et al. Type 2 diabetes and subsequent incidence of breast cancer in the Nurses' Health Study. *Diabetes Care*. 2003; 26(6): 1752-1758.
  9. Ulanet DB, Ludwig DL, Kahn CR, Hanahan D. Insulin receptor functionally enhances multistage tumor progression and conveys intrinsic resistance to IGF-1R targeted therapy. *Proc Natl Acad Sci USA*. 2010; 107(24): 10791-10798.
  10. Forest A, Amatulli M, Ludwig DL, Damoci CB, Wang Y, Burns CA, et al. Intrinsic resistance to cixutumumab is conferred by distinct isoforms of the insulin receptor. *Mol Cancer Res*. 2015; 13(12): 1615-1626.
  11. Bushati N, Cohen SM. MicroRNA functions. *Annu Rev Cell Dev Biol*. 2007; 23: 175-205.
  12. Garzon R, Croce CM. MicroRNAs in normal and malignant hematopoiesis. *Curr Opin Hematol*. 2008; 15(4): 352-358.
  13. Bhatti I, Lee A, Lund J, Larvin M. Small RNA: a large contributor to carcinogenesis? *J Gastrointest Surg*. 2009; 13(7): 1379-1388.
  14. Sethi S, Ali S, Sethi S, Sarkar FH. MicroRNAs in personalized cancer therapy. *Clin Genet*. 2014; 86(1): 68-73.
  15. Khan S, Kumar D, Jaggi M, Chauhan SC. Targeting microRNAs in pancreatic cancer: microplayers in the big game. *Cancer Res*. 2013; 73(22): 6541-6544.
  16. Garajová I, Le Large TY, Frampton AE, Rolfo C, Voortman J, Giovannetti E. Molecular mechanisms underlying the role of microRNAs in the chemoresistance of pancreatic cancer. *Biomed Res Int*. 2014; 2014: 678401.
  17. Song J, Ouyang Y, Che J, Li X, Zhao Y, Yang K, et al. Potential value of miR-221/222 as diagnostic, prognostic, and therapeutic biomarkers for diseases. *Front Immunol*. 2017; 8: 56.
  18. Gong C, Yao Y, Wang Y, Liu B, Wu W, Chen J, et al. Up-regulation of miR-21 mediates resistance to trastuzumab therapy for breast cancer. *J Biol Chem*. 2011; 286(21): 19127-19137.
  19. Singh R, Mo YY. Role of microRNAs in breast cancer. *Cancer Biol Ther*. 2013; 14(3): 201-212.
  20. He Y, Ding Y, Liang B, Lin J, Kim TK, Yu H, et al. A systematic study of dysregulated MicroRNA in type 2 diabetes mellitus. *Int J Mol Sci*. 2017; 18(3): 456.
  21. Chakraborty C, Doss C, Bandyopadhyay S, Agoramoorthy G. Influence of miRNA in insulin signaling pathway and insulin resistance: micro-molecules with a major role in type-2 diabetes. *Wiley Interdiscip Rev RNA*. 2014; 5(5): 697-712.
  22. Denizot F, Lang R. Rapid colorimetric assay for cell growth and survival: modifications to the tetrazolium dye procedure giving improved sensitivity and reliability. *J Immunol Methods*. 1986; 89(2): 271-277.
  23. Livak KJ, Schmittgen TD. Analysis of relative gene expression data using real-time quantitative PCR and the 2(-Delta Delta C(T)) method. *Methods*. 2001; 25(4): 402-408.
  24. Fornari F, Pollutri D, Patrizi C, La Bella T, Marinelli S, Gardini AC, et al. In hepatocellular carcinoma miR-221 modulates Sorafenib resistance through inhibition of caspase-3 mediated apoptosis. *Clin Cancer Res*. 2017; 23(14): 3953-3965.
  25. Ergün S, Öztüzcu S. MiR-221: a critical player in apoptosis as a target of caspase-3. *Cancer Cell & Microenvironment*. 2014; 1: e313.
  26. Bao L, Hazari S, Mehra S, Kaushal D, Moroz K, Dash S. Increased expression of P-glycoprotein and doxorubicin chemoresistance of metastatic breast cancer is regulated by miR-298. *Am J Pathol*. 2012; 180(6): 2490-2503.
  27. Smith L, Watson MB, O'Kane SL, Drew PJ, Lind MJ, Cawkwell L. The analysis of doxorubicin resistance in human breast cancer cells using antibody microarrays. *Mol Cancer Ther*. 2006; 5(8): 2115-2120.
  28. Wei Z, Liang L, Junsong L, Rui C, Shuai C, Guanglin Q, et al. The impact of insulin on chemotherapeutic sensitivity to 5-fluorouracil in gastric cancer cell lines SGC7901, MKN45 and MKN28. *J Exp Clin Cancer Res*. 2015; 34(1): 64.
  29. Chen J, Huang X-F, Qiao L, Katsifis A. Insulin caused drug resistance to oxaliplatin in colon cancer cell line HT29. *J Gastrointest Oncol*. 2011; 2(1): 27-33.
  30. Mountjoy KG, Finlay GJ, Holdaway IM. Abnormal insulin-receptor down regulation and dissociation of down regulation from insulin biological action in cultured human tumor cells. *Cancer Res*. 1987; 47(24 Pt 1): 6500-6504.
  31. Cross DA, Alessi DR, Cohen P, Andjelkovich M, Hemmings BA. Inhibition of glycogen synthase kinase-3 by insulin mediated by protein kinase B. *Nature*. 1995; 378(6559): 785-789.
  32. Saegusa M, Hashimura M, Kuwata T, Okayasu I. Requirement of the Akt/ $\beta$ -catenin pathway for uterine carcinosarcoma genesis, modulating E-cadherin expression through the transactivation of Slug. *Am J Pathol*. 2009; 174(6): 2107-2115.
  33. Adhikary A, Chakraborty S, Mazumdar M, Ghosh S, Mukherjee S, Manna A, et al. Inhibition of epithelial to mesenchymal transition by e-cadherin up-regulation via repression of slug transcription and inhibition of e-cadherin degradation dual role of scaffold/matrix attachment region-binding protein 1 (SMAR1) in breast cancer cells. *J Biol Chem*. 2014; 289(37): 25431-25444.
  34. Lambertini E, Lolli A, Vezzali F, Penolazzi L, Gambari R, Piva R. Correlation between Slug transcription factor and miR-221 in MDA-MB-231 breast cancer cells. *BMC Cancer*. 2012; 12: 445.
  35. Agarwal ML, Taylor WR, Chernov MV, Chernova OB, Stark GR. The p53 network. *J Biol Chem*. 1998; 273(1): 1-4.
  36. Blandino G, Di Agostino S. New therapeutic strategies to treat human cancers expressing mutant p53 proteins. *J Exp Clin Cancer Res*. 2018; 37(1): 30.
  37. Lotem J, Peled-Kamar M, Groner Y, Sachs L. Cellular oxidative stress and the control of apoptosis by wild-type p53, cytotoxic compounds, and cytokines. *Proc Natl Acad Sci USA*. 1996; 93(17): 9166-9171.
  38. Hientz K, Mohr A, Bhakta-Guha D, Efferth T. The role of p53 in cancer drug resistance and targeted chemotherapy. *Oncotarget*. 2017; 8(5): 8921-8946.
  39. Wang S, Konorev EA, Kotamraju S, Joseph J, Kalivendi S, Kalyanaraman B. Doxorubicin induces apoptosis in normal and tumor cells via distinctly different mechanisms intermediacy of H(2)O(2)- and p53-dependent pathways. *J Biol Chem*. 2004; 279(24): 25535-25543.

# The Effect of Contrast Enhanced Abdominopelvic Magnetic Resonance Imaging on Expression and Methylation Level of *ATM* and *AKT* Genes

Amir Hossein Jalali, Ph.D.<sup>1</sup>, Hossein Mozdarani, Ph.D.<sup>1\*</sup>, Hossein Ghanaati, M.D.<sup>2</sup>

1. Department of Medical Genetics, Faculty of Medical Sciences, Tarbiat Modares University, Tehran, Iran  
2. Advanced Diagnostic and Interventional Radiology Research Center, Tehran University of Medical Sciences, Tehran, Iran

\*Corresponding Address: P.O.Box: 14115-111, Department of Medical Genetics, Faculty of Medical Sciences, Tarbiat Modares University, Tehran, Iran  
Email: mozdarah@modares.ac.ir

Received: 06/November/2019, Accepted: 28/December/2019

## Abstract

**Objective:** To evaluate the effect of contrast enhanced abdominopelvic magnetic resonance imaging (MRI), using a 3 Tesla scanner, on expression and methylation level of *ATM* and *AKT* genes in human peripheral blood lymphocytes.

**Materials and Methods:** In this prospective *in vivo* study, blood samples were obtained from 20 volunteer patients with mean age of  $43 \pm 8$  years (range 32-68 years) before contrast enhanced MRI, 2 hours and 24 hours after contrast enhanced abdominopelvic 3 Tesla MRI. After separation of mononuclear cells from peripheral blood, using Ficoll-Hypaque, we analyzed gene expression changes of *ATM* and *AKT* genes 2 hours and 24 hours after MRI using quantitative reverse transcription polymerase chain reaction (qRT-PCR). We also evaluated methylation percentage of the above mentioned genes in before, 2 hours and 24 hours after MRI, using MethySYBR method.

**Results:** Fold change analysis, in comparison with the baseline, respectively showed  $1.1 \pm 0.7$  and  $0.8 \pm 0.5$  mean of gene expressions in 2 and 24 hours after MRI for *ATM*, while the results were  $1.4 \pm 0.6$  and  $1.4 \pm 1$  for *AKT* ( $P > 0.05$ ). Methylation of the *ATM* gene promoter were  $8.8 \pm 1.5\%$ ,  $9 \pm 0.6\%$  and  $9 \pm 0.8\%$  in before contrast enhanced MRI, 2 and 24 hours after contrast enhanced MRI, respectively ( $P > 0.05$ ). Methylation of *AKT* gene promoter in before contrast enhanced MRI, 2 hours and 24 hours after contrast enhanced MRI was  $5.4 \pm 2.5$ ,  $5 \pm 3.2$ ,  $4.9 \pm 2.9$  respectively ( $P > 0.05$ ).

**Conclusion:** Contrast enhanced abdominopelvic MRI using 3 Tesla scanner apparently has no negative effect on the expression and promoter methylation level of *ATM* and *AKT* genes involved in the repair pathways of genome.

**Keywords:** 3 Tesla Magnetic Resonance Imaging, Contrast Media, Gene Expression, Methylation

Cell Journal (Yakhteh), Vol 23, No 3, August 2021, Pages: 335-340

**Citation:** Jalali AH, Mozdarani H, Ghanaati H. The effect of contrast enhanced abdominopelvic magnetic resonance imaging on expression and methylation level of *ATM* and *AKT* gene. Cell J. 2021; 23(3): 335-340. doi: 10.22074/cellj.2021.7258.

This open-access article has been published under the terms of the Creative Commons Attribution Non-Commercial 3.0 (CC BY-NC 3.0).

## Introduction

Magnetic resonance imaging (MRI) is a powerful and relatively safe diagnostic imaging modality, commonly used to visualize internal organs of the human body. In comparison with computed tomography (CT) scan, using static and gradient field combined with radiofrequency (RF), MRI provides higher contrast among the different body tissues such as brain, abdominopelvic and cardiovascular system (1).

Although it is proved that ionizing radiation, such as X-rays or  $\gamma$ -radiation, may cause DNA damage, there are unresolved questions about health risks due to non-ionizing radiation (2). The increased exposure to non-ionizing radiation from wireless communication devices, power lines and MRI caused new safety concerns (3).

Due to the high number of MRI scans performed in the world and the usage of high-field machines operating at high magnet field levels, any evidence of possible genotoxic effects of MRI needs meticulous consideration.

There are contradictory results about the genetic damage of MRI on human blood cells of individuals exposed to different fields of MRI. While some articles

mentioned enhanced DNA damage in human lymphocytes after MRI (4-8), others did not approve these findings (1, 9-16). Besides, radiocontrast agents which are frequently used in diagnostic radiology as well as MRI may cause genotoxicity (17-19). In the studies reporting DNA damage after MRI, the most important finding is DNA-double strand break (DNA-DSB). Knowledge is now incomplete about cytotoxicity due to the complex way of response to genotoxins by evoking cellular processes that may finally lead to DNA repair, damage fixation as mutations or damage removal by different routes of cell death (20, 21).

Many studies showed gene up-regulations involved in signal transduction process, cell cycle, DNA repair and apoptosis after radiation exposure in different cells (22, 23).

It seems that *AKT* activation is an important event in the induction of radiocontrast agent mediating side effects and inhibition of *AKT* activity impairs repair of DNA-DSB (24). As a large number of MRI examinations reformed by contrast media and due to the effect of some contrast agents on *AKT* expression we have considered this repair gene to evaluate the safety of contrast enhanced MRI.

Besides, Ataxia telangiectasia mutated (*ATM*) gene encodes a serine threonine protein kinase activated by sensing DNA-DSB (25).

DSB induced by irradiation, leads to activation and phosphorylation of ATM, cell-cycle checkpoints and DNA repair proteins. Besides, X-irradiation can induce up-regulation of *ATM* gene expression in lymphoblastoid cell lines (26). Halm et al. (27) found that CT scan exposure can alter *ATM* gene expression. One important note about tumor suppressor genes is that they can be inactivated by their promoter methylation and many environmental factors can change DNA methylation patterns of human cells (25).

To the best of our knowledge, there are limited studies about the effect of ionizing radiation on gene expression and DNA methylation. In addition, there is no study about the effect of MRI on gene expression and methylation.

In this study, we aimed to assess the effect of contrast enhanced abdominopelvic MRI using a 3 Tesla scanner on expression and methylation level of *ATM* and *AKT* genes in human peripheral blood lymphocytes.

## Materials and Methods

Written informed consent was obtained from all patients. The study was performed in accordance with the Declaration of Helsinki and approved by Ethics Committee of Tarbiat Modares University (Tehran, Iran, IR.TMU.REC.1396.585). Patients with a history of malignancy, inflammatory or autoimmune diseases, receiving any chemo- or radio-therapy, being smoker and performed medical imaging during the last three months were excluded from the study.

In this prospective *in vivo* study, twenty volunteer patients (15 women and 5 men) referred for abdominopelvic MRI to the imaging center, contributed to this study. The mean age of our studied cases was  $43 \pm 8$  years (range: 32-68 years). The mean body weight of our patients was  $66.5 \pm 13.5$  kilogram (range: 45-90) and their mean height was  $162.4 \pm 6.6$  centimeter (range: 150-175). Final diagnosis of our patients was uterine fibroids in five, ovarian simple cyst in three and liver hemangioma in three cases while nine cases were normal. Sample size was calculated for comparison of two means, considering that type I and II statistical errors were

0.05 and 0.2. All parameters of the formula were extracted from the study performed by Lee et al. (5).

Contrast enhanced abdominopelvic MRI was performed by 3 Tesla MRI machine (Discovery, USA) equipped with a maximum gradient strength amplitude per axis of 50 mT/m and a maximum slew rate per axis of 200 T/m/sec. Pelvic MRI standard sequences were sagittal and coronal T2 fast spin-echo (FSE), axial T2, T2 fat suppression and T1 FSE, axial multi b-value diffusion-weighted imaging (DWI) 50, 400 and 800 seconds/mm<sup>2</sup>, coronal, sagittal and axial T1 FSE FS post contrast injection. The abdomen MRI protocol included coronal and axial T2 single-shot FSE (SSFSE), axial fast imaging employing steady-state acquisition (FIESTA) and 3D T1 GE FS liver acquisition with volume acceleration (LAVA), axial multi b-value DWI 50, 500 and 1000 seconds/mm<sup>2</sup>, coronal and axial post-IV GBCA 3D T1 LAVA FS sequences. Gadoterate meglumine (Dotarem, Guerbet, France, 0.2 mL/kg, 0.1 mmol/kg) was administrated using injector. Using antecubital vein, 5 ml of peripheral blood were drawn from each patient before MRI, 2 hours and 24 hours after MRI.

Blood samples were collected in ethylenediaminetetraacetic acid (EDTA) for the separation of mononuclear cells from whole blood using Ficoll-Hypaque (Lymphodex, Germany).

## Evaluating expression of *ATM* and *AKT* genes

To analyze mRNA expression, we extracted RNA from peripheral blood mononuclear cells (PBMCs) using a total RNA extraction kit (Yekta Tajhiz Azma, Iran) based on the manufacturer's protocol. We quantified concentration of RNA using a NanoDrop (IMPLEN, Germany) and the purity of RNA was evaluated by the 260/280 nanometer absorbance ratio. After RNA extraction, complementary DNA (cDNA) was synthesized by using a synthesis kit based on the manufacturer's protocol. Human  $\beta$ -Actin (*ACTB*) gene was applied as internal control to normalize input RNA amount, reverse transcription efficiency and RNA quality.

mRNA levels of target genes, including *ATM*, *AKT*, as well as housekeeping gene (*ACTB*) were measured by semi-quantitative reverse transcription polymerase chain reaction (PCR) using SYBR Green detection kit (Biofact, South Korea). Primers of the targeted genes are shown in Table 1.

**Table 1:** Primer sequences of the target genes to evaluate gene expression

Gene	Primer sequence (5'-3')	Size (bp)	TM (°C)
<i>ATM</i>	F: GCCTGATTCGAGATCCTGAAAC	22	62.1
	R: GGCTTGTGTTGAGGCTGATAC	21	61.3
<i>AKT</i>	F: AAGAAGCTCCTGCCACCCTT	20	60.5
	R: CAGTAAGCCAGGCTGTCATAG	22	64
<i>BETA ACTIN</i>	F: TGGATGATGATATCGCCG	18	53.9
	R: CACGATGGAGGGGAAGAC	18	58.4

TM; Melting temperature.

Duplicate repeat was performed for each sample in a StepOnePlus™ Real-Time PCR System (Applied Biosystems, USA). The temperatures set was one cycle of 95°C (pre-denaturation) for 10 minutes followed by 40 cycles including 15 seconds of denaturation at 95°C, 30 seconds of annealing at 60°C, and 10 seconds of extension at 72°C.

LinReg software was used for calculation of the PCR efficiency and the relative expression of genes was measured according to the method previously reported by Pfaffl and his colleagues (28).

### Evaluating methylation of *ATM* and *AKT* genes promoter

Genomic DNA was isolated from PBMCs using a DNA extraction Kit (Yekta Tajhiz Azma, Iran) based on the manufacturer's protocol. We assessed the quality of DNA by utilizing an absorbance ratio of 260 nm to 280 nm ( $A_{260/A280}$ ) by a NanoDrop. We considered the samples with the absorbance ratio of 1.8-2.0 as good quality. Sodium bisulfite treatment of genomic DNA was done using the protocol described by Herman et al. (29) with modifications, as reported previously. Sodium bisulfite treatment changes unmethylated cytosine to uracil, whereas methylated cytosines exist unchanged. After bisulfite treatment, we aliquoted DNA samples at 80°C. In this study, we used one-step MethySYBR method to calculate methylation quantitatively. By this method, bisulfite modified DNA was amplified in two concurrent real-time PCR reaction. The primers applied for MethySYBR are presented in Table 2.

In the first reaction, DNA was amplified, regardless of the methylation status and it was used as reference control for normalization of the methylated alleles in the second reaction. In this method, fully methylated DNA is used as a calibrator to measure the methylation percentage.

PCR conditions for *ATM* methylation were 95°C for 10 minutes, followed by 40 cycles of 95°C for 15 seconds, 58°C for 30 seconds and 72°C for 10 seconds. PCR conditions for *AKT* methylation were 95°C for 10 minutes, thereafter followed by 40 cycles of 95°C for 15 seconds, 57°C for 30 seconds and 72°C for 10 seconds.

The cycle threshold ( $C_t$ ) value of amplified DNA was retrieved from the  $C_t$  of amplified methylated DNA to acquire the sample's and calibrator's  $\Delta C_t$  values. For calculation of methylation percent of each sample, fully methylated  $\Delta C_t$  was retrieved from the sample  $\Delta C_t$  to acquire  $\Delta\Delta C_t$  value, which is then applied into the  $2^{(-\Delta\Delta C_t)}$  formula, and multiplied by 100 to show the methylation percentage of samples.

### Statistical analysis

Statistical analyses were performed by SPSS version 16 (SPSS Inc., USA). For normal distributed variables, we used parametric tests (repeated measure ANOVA or paired t test) for comparison of the groups. If variables did not show normal distribution or if data were ordinal, we would use non-parametric tests. We considered  $P < 0.05$  as statistically significant.

**Table 2:** Primer sequences to evaluate methylation in the target genes

Primer	Primer sequence (5'-3')	Size (bp)	TM (°C)
<i>ATM</i> -Methylated	F: GTTTTGGAGTTTGAGTTGAAGGGT	24	55.8
	R: AACTACCTACTCCCCTTCCAA	22	55.1
<i>ATM</i> -Outer	F: GAGGGTGGGTGAGAGTTT	18	50.9
	R: CCCCTACCTACTACTC	17	54
<i>AKT</i> -Methylated	F: GGGTGTTTTTGCGGGTTCG	18	57.5
	R: CGACCGCGACGAATCTTTC	19	56.4
<i>AKT</i> -Outer	F: GGTTTGGAGTTGGGGTT	17	52.4
	R: AAACCCTCCCACAACTTAAAAAC	24	54.2

TM; Melting temperature.

## Results

### Results of gene expression

No statistically significant change was seen in expression of *ATM* and *AKT* genes of the cases after contrast enhanced MRI. Mean of gene expressions were  $1.1 \pm 0.7$  and  $0.8 \pm 0.5$  fold change in 2 and 24 hours after contrast enhanced MRI for *ATM* gene ( $P > 0.05$ , based on paired t test, Fig.1). The results for *AKT* showed that the mean of gene expressions were  $1.4 \pm 0.6$  and  $1.4 \pm 1$  fold change in 2 and 24 hours after contrast enhanced MRI ( $P > 0.05$ , based on paired t test, Fig.2).

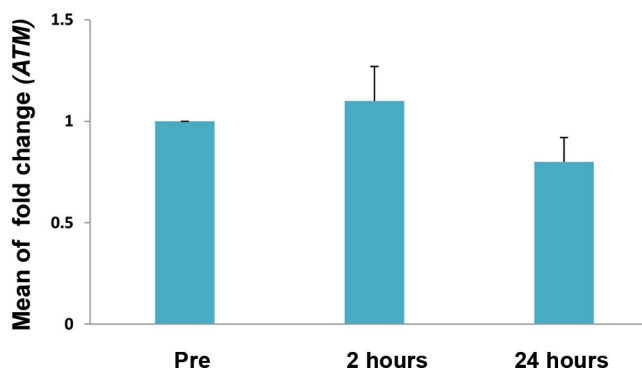


Fig.1: Relative expression (fold change) of mRNA transcripts for *ATM* gene in 20 cases before (Pre), 2 and 24 hours after magnetic resonance imaging (MRI). Error bars represent standard error (SE).

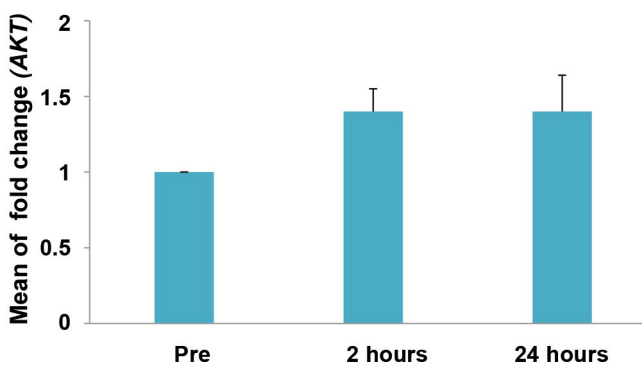


Fig.2: Relative expression (fold change) of mRNA transcripts for *AKT* gene in 20 cases before (Pre), 2 and 24 hours after magnetic resonance imaging (MRI). Error bars represent standard error (SE).

### Results of methylation

There was not statistically significant change in the methylation percent of *ATM* gene after contrast enhanced MRI. Methylation percent of the *ATM* gene promoter were  $8.8 \pm 1.5\%$ ,  $9 \pm 0.6\%$  and  $9 \pm 0.8\%$  in respectively before contrast enhanced MRI, 2 hours and 24 hours after contrast enhanced MRI ( $P > 0.05$ , based on repeated measure ANOVA, Fig.3).

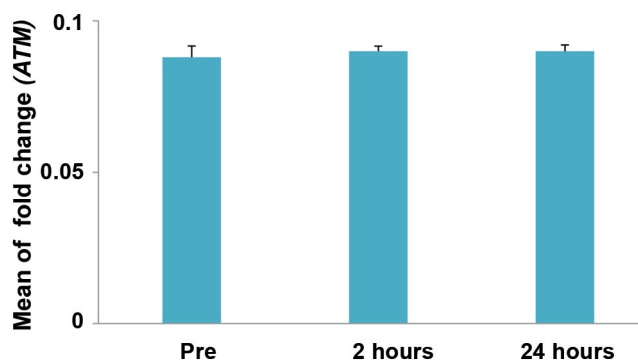


Fig.3: Methylation level of *ATM* gene in 20 cases before, 2 hours and 24 hours after contrast enhanced magnetic resonance imaging (MRI). Error bars represent standard error (SE).

Methylation percent of *AKT* gene promoter in before, 2 hours and 24 hours after contrast enhanced MRI was respectively  $5.4 \pm 2.5$ ,  $5 \pm 3.2$ ,  $4.9 \pm 2.9$  showing no statistically significant change in DNA methylation ( $P > 0.05$ , based on repeated measure ANOVA, Fig.4).

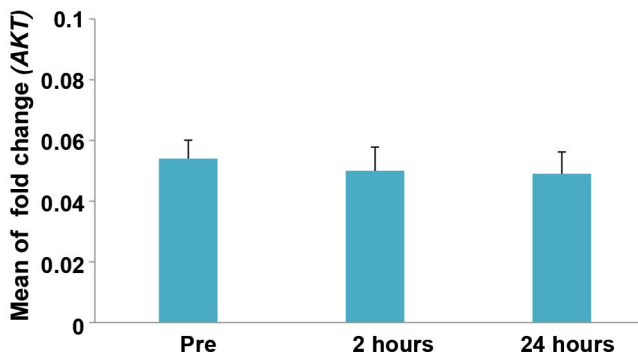


Fig.4: Methylation level of *AKT* gene in 20 cases before, 2 hours and 24 hours after contrast enhanced magnetic resonance imaging (MRI). Error bars represent standard error (SE).

## Discussion

MRI is a non-invasive diagnostic modality in comparison with the other imaging scanners, such as X-ray or CT scan, which have ionizing radiation hazards. However, there are some concerns about the possible MRI risks in recent years which have not been clarified yet.

Despite the ionizing radiation causes DNA damage even at low dosages, energy levels of electromagnetic fields (EMF) applied in MRI are not enough for direct breakage of chemical bonds (30). Besides, we cannot exclude the indirect harmful effects of EMF on DNA integrity. Creation of oxidative stress during MRI might be one possible cause of DNA damage (30, 31).

After careful search, we found that there are only 14

research articles about genotoxic effects of MRI in the literature. The above mentioned studies have a lot of diversity in field strengths (1.5-7 Tesla), exposure factors and genotoxicity evaluation methods. Besides, there is no confirmed hypothesis to explain the possible mechanisms of the molecules significantly affecting this event. Among these reports, five articles mentioned an increase in DSB detected by  $\gamma$ H2AX, enhanced number of micronuclei or increase of comet formation with alkaline single-cell gel electrophoresis (4-8). In contrast, nine studies did not detect any genotoxic effects after MRI using 1.5-7 Tesla machines (1, 9-16).

In our prospective *in vivo* study, we investigated 3 Tesla MRI and the applied MRI sequences were taken from contrast enhanced abdominopelvic protocols used in our routine clinical examinations. To the best of our knowledge, there is no other study in the literature about the evaluation of possible epigenetic changes after abdominopelvic MRI. Our results indicated that MRI has not adverse effects on the gene expression and methylation of *AKT* and *ATM* genes.

Similar to our study, Brand et al. (1) used Dotarem for contrast enhanced cardiac MRI using 1.5 Tesla scanner and they did not find immediate increase in DNA damage of human lymphocytes. A different contrast media (Gadobutrol) was used in Fiechter et al. (7) study for MRI on 1.5 Tesla scanner by using  $\gamma$ H2AX immunofluorescence microscopy and they showed a significant increase of DSB. Reddig et al. (12) also used Gadobutrol for evaluation of H2AX foci formation in patients underwent MRI. They found no evidence of DNA damage after MRI with different magnetic fields (1-7 Tesla).

In the other study performed by Yildiz et al. (6), the authors reported that contrast enhanced MRI, using Omniscan, was associated with an immediate increase in single-strand DNA breakage. Although studies reported that DNA damage may occur in peripheral blood lymphocytes during MRI, the concern was expressed since only a single marker was evaluated and downstream consequences have not been evaluated.

All of the mentioned articles have examined the cytotoxic effects of MRI. The only study evaluating the effects of MRI on DNA repair genes has been performed by McDonald et al. (32), in which the authors found a small significant increase in the DNA repair protein 53BP1 after MRI.

Considering that DNA damage factors engage repair proteins, such as *ATM* or DNA-PK (32), evaluation of changes in downstream DNA repair factors might be considered as additional markers for the evaluation of the effects of MRI on DNA.

*ATM* gene produces a protein kinase playing important role in triggering proper cellular response to DNA damage (33) and similar to the other tumor suppressor genes, promoter methylation is the main epigenetic mechanism

which can prevent *ATM* transcription (25).

Previous studies showed *ATM* expression changes 1 hour after CT scan from very low radiation dosages, as low as 0.1 Gy (27).

Owing to the results of one study suggesting that extremely low-frequency EFM (ELF-EMF) exposure can induce modification in methylation and expression of DNMTs, epigenetic may have vital role in the biological effects of magnetic exposure (34).

Indeed, *AKT* gene has fundamental role in the cytotoxicity effect of radiocontrast media (RCM) (35).

RCM can influence intracellular signaling pathways and can affect PI3K/Akt pathway via suppressing *AKT* phosphorylation and downstream targets (35, 36). Our study has some limitations need to be mentioned. Firstly, only one contrast media (Dotarem) was studied in our research and we should examine the other contrast agents of MRI. Secondly, we examined only two genes. Using microarray and whole genome methylation assessments, other complementary studies composed of panels of whole genes involved in repair and apoptosis are recommended.

## Conclusion

Contrast enhanced abdominopelvic MRI using 3 Tesla scanner has apparently no negative effect on the expression and promoter methylation levels of two genes involved in the repair pathways of the genome, namely *ATM* and *AKT*. Finally, our results should be interpreted cautiously, since it might not indicate exact evidence whether MRI is safe and it has no adverse effect on DNA. Complementary studies, including evaluation of the other DNA damage and repair markers as well as whole genome methylation, are necessary to understand the MRI safety.

## Acknowledgements

This work was supported by Tarbiat Modares University Research Department under the Grant number IG-39711. The authors declare no conflict of interest.

## Authors' Contributions

A.H.J., H.M., H.Gh.; Participated in the study design, data collection and evaluation, drafting manuscript, and statistical analysis. A.H.J., H.M.; Participated in the Q-PCR, methylation techniques, contributed in the data interpretation and conclusion. All authors performed editing and approved the final version of this manuscript for submission. They also participated in the finalization of manuscript and approved the final draft.

## References

1. Brand M, Ellmann S, Sommer M, May MS, Eller A, Wuest W, et al. Influence of cardiac MR imaging on DNA double-strand breaks in human blood lymphocytes. *Radiology*. 2015; 277(2): 406-412.
2. Hietanen M. Health risks of exposure to non-ionizing radiation-myths or science-based evidence. *Med Lav*. 2006; 97(2): 184-188.
3. van Osch MJ, Webb AG. Safety of ultra-high field MRI: what are

- the specific risks? *Curr Radiol Rep.* 2014; 2: 61.
4. Simi S, Ballardin M, Casella M, De Marchi D, Hartwig V, Giovannetti G, et al. Is the genotoxic effect of magnetic resonance negligible? Low persistence of micronucleus frequency in lymphocytes of individuals after cardiac scan. *Mutat Res.* 2008; 645(1-2): 39-43.
  5. Lee JW, Kim MS, Kim YJ, Choi YJ, Lee Y, Chung HW. Genotoxic effects of 3 T magnetic resonance imaging in cultured human lymphocytes. *Bioelectromagnetics.* 2011; 32(7): 535-542.
  6. Yildiz S, Cece H, Kaya I, Celik H, Taskin A, Aksoy N, et al. Impact of contrast enhanced MRI on lymphocyte DNA damage and serum visfatin level. *Clin Biochem.* 2011; 44(12): 975-979.
  7. Fiechter M, Stehli J, Fuchs TA, Dougoud S, Gaemperli O, Kaufmann PA. Impact of cardiac magnetic resonance imaging on human lymphocyte DNA integrity. *Eur Heart J.* 2013; 34(30): 2340-2345.
  8. Lancellotti P, Nchimi A, Delierneux C, Hego A, Gosset C, Gothot A, et al. Biological effects of cardiac magnetic resonance on human blood cells. *Circ Cardiovasc Imaging.* 2015; 8(9): e003697.
  9. Schreiber WG, Teichmann EM, Schiffer I, Hast J, Akbari W, Georgi H, et al. Lack of mutagenic and co-mutagenic effects of magnetic fields during magnetic resonance imaging. *J Magn Reson Imaging.* 2001; 14(6): 779-788.
  10. Schwenzler NF, Bantleon R, Maurer B, Kehlbach R, Schraml C, Claussen CD, et al. Detection of DNA double-strand breaks using gammaH2AX after MRI exposure at 3 Tesla: an in vitro study. *J Magn Reson Imaging.* 2007; 26(5): 1308-1314.
  11. Szerencsi Á, Kubinyi G, Váliczkó É, Juhász P, Rudas G, MesterÁ, et al. DNA integrity of human leukocytes after magnetic resonance imaging. *Int J Radiat Biol.* 2013; 89(10): 870-876.
  12. Reddig A, Fatahi M, Roggenbuck D, Ricke J, Reinhold D, Speck O, et al. Impact of in vivo high-field-strength and ultra-high-field-strength MR imaging on DNA double-strand-break formation in human lymphocytes. *Radiology.* 2017; 282(3): 782-789.
  13. Reddig A, Fatahi M, Friebe B, Guttek K, Hartig R, Godenschweger F, et al. Analysis of DNA double-strand breaks and cytotoxicity after 7 Tesla magnetic resonance imaging of isolated human lymphocytes. *PLoS One.* 2015; 10(7): e0132702.
  14. Fatahi M, Reddig A, Vijayalaxmi, Friebe B, Hartig R, Prihoda TJ, et al. DNA double-strand breaks and micronuclei in human blood lymphocytes after repeated whole body exposures to 7T magnetic resonance imaging. *Neuroimage.* 2016; 133: 288-293.
  15. Friebe B, Wollrab A, Thormann M, Fischbach K, Ricke J, Grueschow M, et al. Sensory perceptions of individuals exposed to the static field of a 7T MRI: a controlled blinded study. *J Magn Reson Imaging.* 2015; 41(6): 1675-1681.
  16. Suntharalingam S, Mladenov E, Sarabhai T, Wetter A, Kraff O, Quick HH, et al. Abdominopelvic 1.5-T and 3.0-T MR imaging in healthy volunteers: relationship to formation of DNA double-strand breaks. *Radiology.* 2018; 288(2): 529-535.
  17. Norman A, Cochran ST, Sayre JW. Meta-analysis of increases in micronuclei in peripheral blood lymphocytes after angiography or excretory urography. *Radiat Res.* 2001; 155(5): 740-743.
  18. Mozdarani H, Fadaei S. Similar cytogenetic effects of sodium-meglumine diatrizoate and sodium-meglumine ioxithalamate in lymphocytes of patients undergoing brain CT scan. *Toxicol Lett.* 1998; 98(1-2): 25-30.
  19. Tao SM, Zhou F, Schoepf UJ, Johnson AA, Lin ZX, Zhou CS, et al. The effect of abdominal contrast-enhanced CT on DNA double-strand breaks in peripheral blood lymphocytes: an in vitro and in vivo study. *Acta Radiol.* 2019; 60(6): 687-693.
  20. Kaina B. DNA damage-triggered apoptosis: critical role of DNA repair, double-strand breaks, cell proliferation and signaling. *Biochem Pharmacol.* 2003; 15; 66(8): 1547-1554.
  21. Fritz G, Kaina B. Rho GTPases: promising cellular targets for novel anticancer drugs. *Curr Cancer Drug Targets.* 2006; 6(1): 1-14.
  22. Fachin AL, Mello SS, Sandrin-Garcia P, Junta CM, Ghilardi-Netto T, Donadi EA, et al. Gene expression profiles in radiation workers occupationally exposed to ionizing radiation. *J Radiat Res.* 2009; 50(1): 61-71.
  23. Rouchka EC, Flight RM, Fasciotto BH, Estrada R, Eaton JW, Patibandla PK, et al. Dataset for dose and time-dependent transcriptional response to ionizing radiation exposure. *Data Brief.* 2019; 27: 104624.
  24. Toulany M, Kehlbach R, Rodemann HP, Mozdarani H. Radiocontrast media affect radiation-induced DNA damage repair in vitro and in vivo by affecting Akt signalling. *Radiother Oncol.* 2010; 94(1): 110-116.
  25. Mehdipour P, Karami F, Javan F, Mehrazin M. Linking ATM promoter methylation to cell cycle protein expression in brain tumor patients: cellular molecular triangle correlation in ATM territory. *Mol Neurobiol.* 2015; 52(1): 293-302.
  26. Hirai Y, Hayashi T, Kubo Y, Hoki Y, Arita I, Tatsumi K, et al. X-irradiation induces up-regulation of ATM gene expression in wild-type lymphoblastoid cell lines, but not in their heterozygous or homozygous ataxia-telangiectasia counterparts. *Jpn J Cancer Res.* 2001; 92(6): 710-717.
  27. Halm BM, Tiirikainen M, Lai JF, Pagano I, Cooney RV, Franke AA. Changes in whole blood gene expression after computed tomography in children: a pilot study. *Gene Express Genet Genom.* 2015; 8: 1-8.
  28. Pfaffl MW. A new mathematical model for relative quantification in real-time RT-PCR. *Nucleic Acids Res.* 2001; 29(9): e45.
  29. Herman JG, Graff JR, Myohanen S, Nelkin BD, Baylin SB. Methylation-specific PCR: a novel PCR assay for methylation status of CpG islands. *Proc Natl Acad Sci USA.* 1996; 93(18): 9821-9826.
  30. Phillips JL, Singh NP, Lai H. Electromagnetic fields and DNA damage. *Pathophysiology.* 2009; 16(2-3): 79-88.
  31. Ghodbane S, Lahbib A, Sakly M, Abdelmelek H. Bioeffects of static magnetic fields: Oxidative stress, genotoxic effects, and cancer studies. *Biomed Res Int.* 2013; 2013: 602987.
  32. McDonald JS, McDonald RJ, Ekins JB, Tin AS, Costes S, Hudson TM, et al. Gadolinium-enhanced cardiac MR exams of human subjects are associated with significant increases in the DNA repair marker 53BP1, but not the damage marker gammaH2AX. *PLoS One.* 2018; 13(2): e0193634.
  33. Brown KD, Barlow C, Wynshaw-Boris A. Multiple ATM-dependent pathways: an explanation for pleiotropy. *Am J Hum Genet.* 1999; 64(1): 46-50.
  34. Liu Y, Liu Wb, Liu KJ, Ao L, Zhong JL, Cao J, et al. Effect of 50 Hz extremely low-frequency electromagnetic fields on the DNA methylation and DNA methyltransferases in mouse spermatocyte-derived cell line GC-2. *Biomed Res Int.* 2015; 2015: 237183.
  35. Andreucci M, Fuiano G, Presta P, Esposito P, Faga T, Bisesti V, et al. Radiocontrast media cause dephosphorylation of Akt and downstream signaling targets in human renal proximal tubular cells. *Biochem Pharmacol.* 2006; 72(10): 1334-1342.
  36. Yano T, Itoh Y, Sendo T, Kubota T, Oishi R. Cyclic AMP reverses radiocontrast media-induced apoptosis in LLC-PK1 cells by activating A kinase/PI3 kinase. *Kidney Int.* 2003; 64(6): 2052-2063.

# MicroRNA and Hemophilia-A Disease: Bioinformatics Prediction and Experimental Analysis

Halimeh Rezaei, Ph.D.<sup>1</sup>, Majid Motovali-Bashi, Ph.D.<sup>1\*</sup>, Seyed Javad Mowla, Ph.D.<sup>2</sup>

1. Department of Cell and Molecular Biology and Microbiology, Faculty of Biological Sciences and Technology, University of Isfahan, Isfahan, Iran

2. Molecular Genetics Department, Faculty of Biological Sciences, Tarbiat Modares University, Tehran, Iran

\*Corresponding Address: P.O.Box: 8174673441, Department of Cell and Molecular Biology and Microbiology, Faculty of Biological Sciences and Technology, University of Isfahan, Isfahan, Iran  
E.mail: mbashi@sci.ui.ac.ir

Received: 17/August/2019, Accepted: 14/December/2019

## Abstract

**Objective:** Hemophilia-A is a common genetic abnormality resulted from decreased or lack of factor VIII (FVIII) pro-coagulant protein function caused by mutations in the *F8* gene. Majority of molecular studies consider screening of mutations and their relevant impacts on the quality and expression levels of FVIII. Interestingly, some of the functions in FVIII suggest a probable involvement of small non-coding RNAs embedded within the sequence of *F8* gene. Therefore, microRNAs which are encoded within the *F8* gene might have a role in hemophilia development. In this study, miRNAs production in the *F8* gene was investigated by bioinformatics prediction and experimental validation.

**Materials and Methods:** In this experimental study, bioinformatics tools have been utilized to seek the novel microRNAs inserted within human *F8* gene. The ability to express new microRNAs in *F8* locus was studied through reliable bioinformatics databases such as SSCProfiler, RNA fold, miREval, miR-FIND, UCSC genome browser and miRBase. Then, expression and processing of the predicted microRNAs were examined based on bioinformatics methods, in the HEK293 cell lines.

**Results:** We are unable to confirm existence of the considered mature microRNAs in the transfected cells.

**Conclusion:** We hope that through changing experimental conditions, designing new primers or altering cell lines as well as the expression of vectors, exogenous and endogenous expressions of the predicted miRNA will be confirmed.

**Keywords:** Bioinformatics, Factor VIII, HEK293 Cells, Hemophilia-A, MicroRNAs

Cell Journal(yakhteh), Vol 23, No 3, August 2021, Pages: 341-348

**Citation:** Rezaei H, Motovali-Bashi M, Mowla SJ. MicroRNA and hemophilia-A disease: bioinformatics prediction and experimental analysis. Cell J. 2021; 23(3): 341-348. doi: 10.22074/cellj.2021.7109.

This open-access article has been published under the terms of the Creative Commons Attribution Non-Commercial 3.0 (CC BY-NC 3.0).

## Introduction

Hemophilia-A is a heterogeneous deficiency in blood coagulation factor VIII (FVIII), which causes increased bleeding and this occurs approximately 1 in almost 5000-10000 male births. This involves problems originated from easy bruising as well as muscle and joint bleeds.

Almost, it is inherited as an X-linked recessive trait and classified into mild (>5% of normal level), moderate (1-5% of normal level) or severe (<1% of normal level) on the basis of circulating levels of clotting FVIII. Plasma concentration of factor VIII is approximately 200 ng/ml and its biological half-life is nearly 12 hours (1).

FVIII is an essential plasma protein for blood coagulation that is bound to a von willebrand factor and circulates in the blood stream in an inactive form. FVIII is activated (FVIIIa) in response to injury and separates from von willebrand factor. Subsequently, activated FVIIIa interacts with FIX which is another coagulation factor. This interaction forms a blood clot with setting off a chain of additional chemical reactions. FVIII is encoded by the *F8* gene with 186 kb length located on Xq28 chromosome. It contains 26 exons and has two variant transcripts called "isoform a" and "isoform b". Many mutations are reported all over the *F8* gene. Inversions especially in the introns 1 and 22 are involved in 50% of total mutations and 1-4%

of severe hemophilia-A patients, respectively. In addition, severe hemophilia-A have been reported from more than 120 large deletions (>50 bp) (1, 2). Other mutations in the *F8* gene include nonsense and missense mutations (point mutations), as well as small deletions and insertions that are diffused in all 26 exonic regions.

Up to now, about 1000 specific mutations with various types of origin have been collected from the global hemophilia database (HAMSTeRs) (3). In the past decade, non-coding RNAs (ncRNAs) were one of the most available biological findings.

microRNAs (miRNAs) are endogenous single-stranded ncRNAs with 18-25 nucleotides-long that mediate transcriptional and post-transcriptional control of the target gene expressions, as a part of complex gene regulatory networks and they are able to regulate some biological pathways (4).

miRNAs can be found in various genomic regions including, introns of coding genes and 3' un-translated region (3' UTR) of coding genes (5), in addition to introns and exons of non-coding genes (6).

In most mammalian, RNA polymerase II transcribes miRNA genes (pri-miRNA), and their characteristics are the same as protein coding transcripts: a poly (A) tail, exons

and a 5' cap (7). The pri-miRNA, is rapidly trimmed into pre-miRNA precursor with about 70 nucleotides-long (8). The pre-miRNA is afterward transferred to the cytoplasm and was further accomplished to its mature shape, placed either at 5' or 3' side of the stem loop (9, 10).

In mammalian cells, mature miRNA mostly act via completing binding to 3'-UTR of its target genes with its seed sequence. This leads to mRNA degradation or protein translation inhibition (11). To date, in miRBase database (<http://www.mirbase.org/>), more than 2000 human miRNAs have been published (12). In the human genome, approximately 55000 miRNA genes are expected to be present (13). Identification of novel miRNAs by numerous bioinformatics tools have been developed to be fast, effective and cheap (14, 15).

A prosperous way to recognize miRNA genes in different plants and animals like human, mouse, *Drosophila*, *C. elegans* and others is using the bioinformatics approaches (16). The software is designed based on phylogenetic diversity and conservation, secondary structure information, thermodynamic parameters, stability of hairpin, sequence conservation in various species, sequence special parameters, similarity to the famous miRNAs and genomic position of the candidate sequences associated to the famous miRNAs (17-19). Since hemophilia-A is a single-gene hereditary disorder, we decided to select *F8* gene for our genomic analysis.

Here, in order to look for hairpin structures within the human *F8* gene, bioinformatics tools were utilized.

The whole suitable bioinformatics characteristics for producing a real miRNA exist in two of the predicted stem loops. These conserved stem loops were experimentally investigated. In the present study, bioinformatics prediction and experimental validation for miRNAs detection in the *F8* gene was analyzed.

## Materials and Methods

### Bioinformatics tools for prediction of miRNAs

RNA fold algorithm (<http://rna.tbi.univie.ac.at/cgi-bin/RNAfold.cgi>), miREval (<http://mimirna.centenary.org.au/mireval/>) and SSC profiler programs (<http://mirna.imbb.forth.gr/SSCprofiler.html>) were employed to seek the probable hairpin structures in the area of interest. Target secondary structures dependent function of Droscha and Dicer enzymes, which have crucial roles in miRNAs biogenesis, inclined us to use the miR-FIND (<http://140.120.14.132:8080/MicroRNAProject-Web/>). Conservation of the predicted miRNAs was examined using UCSC database (<http://genome.ucsc.edu/>), along with blat search for many organisms such as human genome. Furthermore, mature miRNAs in the candidate sequences were predicted by SSCprofiler. Using miRBase, similarity of our sequences was searched between 24,521 miRNAs loci from 206 species. This study approved by Research Assistant, University of Isfahan.

### DNA preparation

Hemophilia-A is a monogenic disorder and a defect in

the *F8* gene resulting in this disease manifestation. On the other hand, most miRNAs directly affect and target their productive genes. Therefore, in order to predict the miRNAs involved in the control and regulation of hemophilia-A, *F8* gene was examined and analyzed only in healthy subjects.

Genomic DNA template was extracted from the person whole blood referring to Isfahan University Health Center (by receiving consent) according to Miller protocol (20). Based on bioinformatics studies, two candidate regions in *F8* gene were identified (we briefly refer them to can-miR-1 and can-miR-2, in this article).

These regions have ability to express the hairpin structure sequences belonging to possible miRNA precursors. Polymerase chain reaction (PCR) was performed with primers designed by Oligo v.7 and PerlPrimer

(can-miR-1-

R: 5'-TTGTGGAGATTGAGTTCTGACC-3',  
F: 5'-TAGAGACTCCCTTACGTGACTG-3',

can-miR-2-

R: 5'-AGCCTCCAAGGTGCTGTATAT-3',  
F: 5'-CCTGCACTGAGCACTCATGAA-3').

We used NCBI/Primer-BLAST to ensure that the primer sequences are unique. The thermocycler program for can-miR-1 consisted of one cycle for 5 minutes at 94°C, 35 cycles for 30 seconds at 94°C, 58°C for 30 seconds and 72°C for 30 seconds, followed by one cycle for 10 minutes at 72°C, and for can-miR-2 it was designed by one cycle for 5 minutes at 94°C, 35 cycles for 30 seconds at 94°C, 62°C for 30 seconds and 72°C for 30 seconds, followed by one cycle for 10 minutes at 72°C. Electrophoresis was performed in 1% agarose gel and the PCR products were analyzed in order to TA cloning (for double strand DNA); DNAs were purified and extracted using a GeNetBio Gel Extraction Kit (GeNetBio, Korea) (21). Segments into the TA vector pTZ57R/T (Thermo scientific, USA) were cloned into *Escherichia coli* strain *TOP10* based on standard protocol transformed (22). The transformed cells were then plated on LB agar improved with x-Gal (20 mg/ml) and ampicillin (75 mg/ml). Colonies were accidentally chosen and DNA was utilized in colony PCR as templates. Positive colonies (transformed *Escherichia coli* strains) were verified in terms of the existence of inserts direction. Plasmid isolation was carried out using GeNetBio Plasmid Extraction Kit (GeNetBio, Korea) (21).

Recombinant TA vectors were digested by KpnI and SacI (at 37°C for 10 minutes) restriction enzymes and they inserted into pEGFP-C1 expression vectors (cutting with the same restriction enzymes) that are downstream of the GFP gene and carrying CMV promoter and KpnI/SacI restriction sites. Competent cells of *Escherichia coli DH5-α* were transformed by pEGFP-C1 contain DNA carrying pre-miRNAs and finally colony PCR was performed for transformation validation and inserts direction. Additionally, the hairpin structure sequence, as scrambled control (23), was cloned into the pEGFP-C1

vectors. As another negative control, the C1-mock (empty vector) was also utilized. For the reliability of correct inserts, all vectors were sequenced (Genfanavarani Co., Iran).

### Cell lines

HEK293 was cultured in DMEM-HG including 100 U/ml penicillin, 100 µg/ml streptomycin and 10% fetal bovine serum (FBS) (all from Gibco, USA). After 24 hours culture in separate flasks, transfection was performed according to the calcium-phosphate protocol (24). In the first flasks, HEK293 was transfected with the main samples, which were recombinant expression vectors with insert fragments containing predicted can-miR-1 and can-miR-2 precursors. In the second flasks, HEK293 was transfected with pEGFP-C1-Scramble, which were recombinant expression vectors containing insert fragments (it should be noted that length of the insert fragments are approximately equal to the insert fragments in main vectors) and in the third flasks, HEK293 was transfected with pEGFP-C1 empty vectors (C1-Mock) to control potential effect of transfection reagent on the cell. In the last flasks, HEK293 was performed without transfection steps, as a control, using a fluorescence microscope. Finally, fluorescence microscopy was used to confirm the cells transfection and GFP expression.

### RNA extraction and preparation

Total RNA was extracted from HEK293 cell lines using Trizol reagent based on the manufacturer's protocol (Sigma, Germany) (25) and treated with RNAase-free DNaseI (Takara, Japan) for 30 minutes at 37°C followed by heat inactivation for 10 minutes at 65°C by adding Ethylenediaminetetraacetic acid (EDTA).

Purity and quality of RNAs were estimated by NanoDropND-1000 (NanoDropTech; Thermo scientific, USA). In order to confirm the integrity of RNAs, 2% agarose gel electrophoresis were performed.

### Synthesis of cDNA

Universal cDNA Synthesis Kit II (Exiqon, USA) (26) was utilized for cDNA synthesis using Oligo-dT primers and Reverse Transcriptase which have a universal tag sequence at the the 5' end. Besides, polyadenylation of the mature miRNAs were applied for their reverse transcription. To confirm the expression of mature miRNAs, each cDNA sample was amplified using PCR.

Thermocycler program included one cycle for 5 minutes at 94°C, 38 cycles at 94°C for 30 seconds, 60°C for 30 seconds and 72°C for 30 seconds, followed by one cycle for 10 minutes at 72°C. In addition, 13 and 14 primer sets for mature miRNAs of can-miR-1 and can-miR-2 were respectively designed according to bioinformatics

analysis. They were used as forward primer and the primer in the buffer of cDNA Synthesis Kit was used as reverse primer. Then, to check PCR products, the samples were run on 12% polyacrylamide gel.

## Results

### Bioinformatics prediction of miRNAs

*F8* gene involves in hemophilia-A and it was observed by reliable bioinformatics databases due to elicit candidate stem-loops that express miRNAs. For this purpose, comprehensive studies were carried out on the related data servers. Regarding the achieved results from data servers, two stem-loop structures servers, two stem-loop structures can-miR-1 with sequence: (5'-CTCACCTGACTTATCTGTTTCACAGAGTCCACATCTGGCCAATGGGAAACACACCTTTTGCTCAGAAAGACCCTGGGAATGTAGGTCAATCATAATGCAGTAG-3') and

can-miR-2 with sequence: (5'-CCTCACCTCTTGCTGCTCAGCTCCAGGTCGTCGTGGGTTTCAGGGCTCAGCTGCACGCTCCTGCCCGCGCCCTGGGCGTGTGGCACCCAGCCCTGCCATT-3')

were eventually qualified and recommended for further experimental confirmations.

### Sequence, structure and conservation profiler web service

This web service identifies stem-loop structures and it assigns a hidden Markov model (HMM) score apiece determined by applying conservation along with structure features (Fig.1A).

### RNA fold web server

The sequence of hairpin structures obtained from SSC profiler were imported to RNA fold web server for more detailed researches on their secondary structures and stabilities (Fig.1B). Calculated minimum free energies (MFE) for these structures are -26.80 Kcal/mol and -33.30 Kcal/mol, respectively.

### miREval

These sequences were also analyzed in miREval and the corresponding results are shown in Figure 1C.

### miR-FIND

Processing sites for Drosha and Dicer ribonuclease enzymes, mature miRNA sequences and the seed regions were determined for our mentioned sequences in this miRNA predictor service (Table 1).

### UCSC genome browser

Evolutionary conservation for the candidate sequences within 100 species, such as rhesus, mouse, dog, elephant and other vertebrates, were measured in the UCSC genome browser data server (Fig.1D).

**Table 1:** Analyzed information in miR-Find

Sequence	can-miR-1		can-miR-2	
Mature-miRNA Drosha/ Dicer processing site	23/46	76/56	15/45	83/62
Mature-miRNA sequence	5'-ACAGAGUCCAC AUCGGCCAAUGG-3'	5'-CUUUUGCUCAG AAAGACCCUG-3'	5'-UGCUCAGCUCCAGGU CGUCGUGGGUUCAGGG-3'	5'-UGCCCGCGCCCU GGGCGUGAUG-3'
Predict seed site	5'-CAGAGUC-3'	5'-UUUUGCU-3'	5'-GCUCAGC-3'	5'-GCCCCGC-3'

Data corresponding to mature miRNA-5p and-3p are presented.

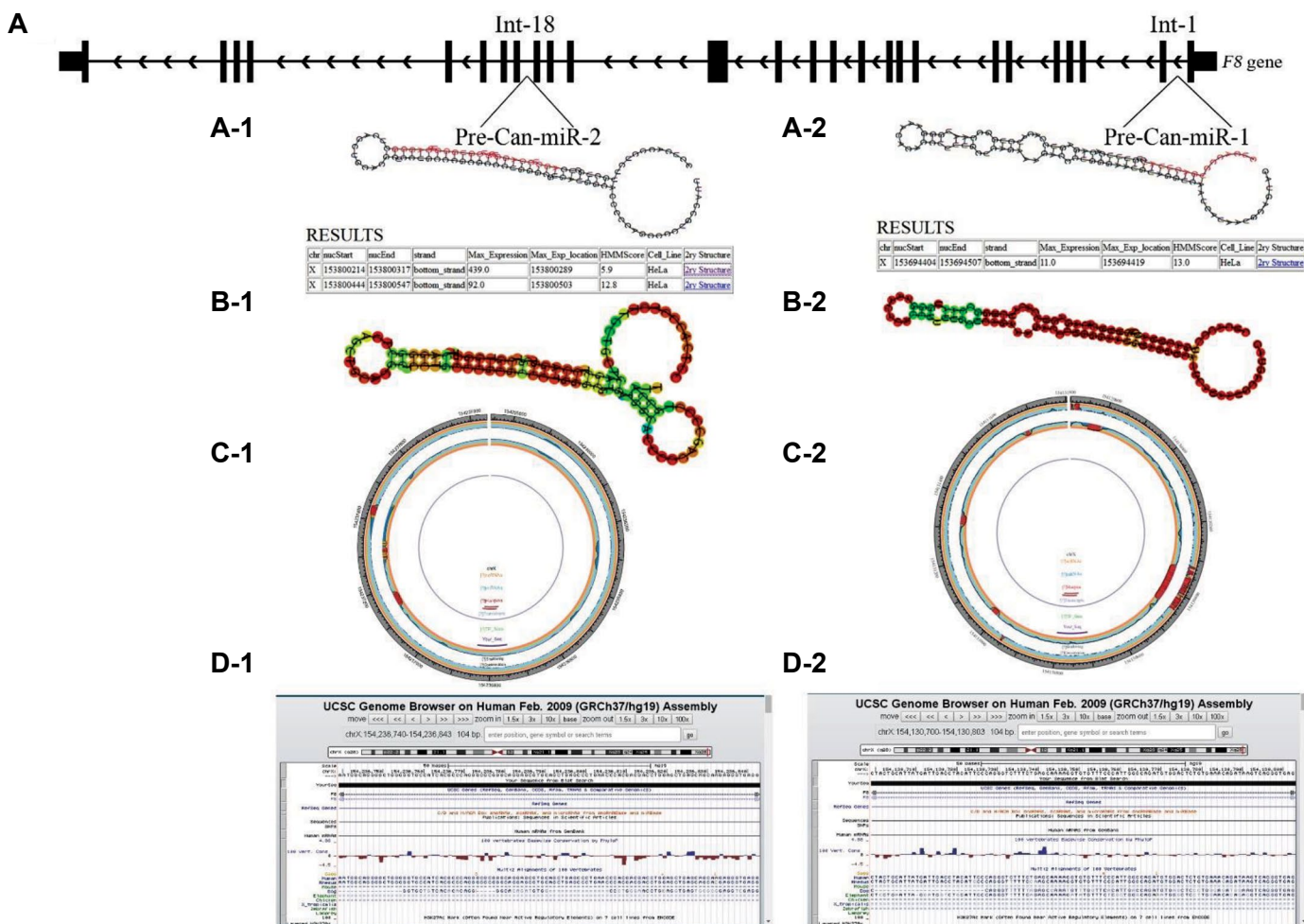


**Fig.1:** Prediction of pre-can-miR-1 and pre-can-miR-2 in the 1<sup>st</sup> and 18<sup>th</sup> introns of human *F8* gene, respectively. **A-1, A-2.** Results of SSC profiler for can-miR-1 and can-miR-2. Hairpin structures containing a probable sequence of mature miR (Red) are shown, and HMM score related to the sestructures are shown in the tables. Furthermore, maximum expression (max-expression) according to a full genome tiling array in HeLa cell line are presented for these sequences. **B-1, B-2.** Secondary structure results of can-miR-1 and can-miR-2 in RNA fold web server are depicted. **C-1, C-2.** About 1000 bp are displayed around our inquiry sequences, as a circle graph by miEVal. **D-1, D-2.** Conservation levels are shown with blue columns in UCSC genome browser.

**MiRBase website**

Ensuring non-registration within the previously identified miRNAs using miRBase was done for these sequences.

**DNA preparation**

After genomic DNA extraction from whole blood, the concentrations and purity of isolated DNA samples were

determined by NanoDrop and the samples were loaded on 1% agarose gel.

The genomic regions containing a sequence of 104 nucleotides putative miRNA precursors were amplified by specific primers and PCR. In addition, by using 100 bp DNA ladder, the bands were determined in the expected locations (370 bp and 679 bp, respectively).

The fragments containing predicted miRNA precursors were cloned into the TA vector. The transformation was carried out in the *TOP10* strains and then cultured in LB agar amended with ampicillin. Additionally, TA vector was cultured on another plate under the same conditions as a negative control sample.

In order to screen the positive colonies, they were randomly selected and colony PCR was performed using primers related to miRNA precursors and vector primers.

In spite of the existence of false bands, the presence of expected bands with ladder pattern confirmed the accuracy of direction of insertions.

In order to clone the fragments containing miRNA precursors in the expressed vector, isolated recombinant TA vectors were double digested by KpnI and SacI. The pEGFP-C1 expression vector by KpnI and SacI was double digested and then the products of this digestion were extracted from the gel.

The fragments containing miRNA precursor sequences were obtained by recombinant TA vector double digestion and inserted into the double digested pEGFP-C1 expression vector.

Then the insertion products transformed into *Escherichia coli* (*DH5- $\alpha$*  strains) and the strains plated on LB agar amended with kanamycin. Colony PCR was performed to select recombinant expression vector colonies containing insertion fragments in accuracy direction and gel electrophoresis confirmed this purpose. Then, plasmid isolation was performed. To verify isolation accuracy, the products were electrophoresed on the agarose gel.

Sequencing was carried out to approve sequence accuracy of the inserts in expression vectors. Sequencing indicated 100% homology between the inserted sequence and the predicted miRNA precursor sequence (Fig.2).

### Cell lines

Transfection efficiency was evaluated by observing the cells during 36 hours after transfection, using fluorescence microscopy (Fig.3) for confirmation of recombinant plasmids expression in HEK293 cells.

### RNA extraction and preparation

About 48 hours after transfection, total RNA was extracted using Trizol. RNA concentration was determined using NanoDrop and RNA quality was assessed by loading samples on 2% agarose gel for confirmation of total RNA isolation accuracy.

### cDNA synthesis and examination of mature miRNAs expression

After cDNA synthesis, using PCR, whereby forward primers attached to the mature miRNAs and reverse primers attached to OligodT, the presence of mature miRNAs were studied. Due to insufficient information on the precise condition and sequences of candidate miRNAs, several forward primers were designed for the candidate miRNAs. These primers were designed according to the sequence recommended by the mentioned bioinformatics servers, for the mature miRNAs in the candidate precursor regions. After PCR, due to the small size of fragments and in order to better identification, PCR products were loaded on polyacrylamide gel. In addition, U6RNA was used as a reference gene. Due to the miRNAs length (about 22 nucleotides) and position of the universal primer on OligodT, 80-100bp fragments were expected.

For can-miR-1, the expected band was not found in any of the designed primers (Fig.4.A-1). Two bands with 80-100 bp were observed for can-miR-2 (primers 2 and 12) in Figure 4A-2. Bands were prepared for sequencing after gel extraction. The sequencing results analysis confirmed existence of two predicted mature miRNAs, but there was not any additional nucleotide between the predicted can-miR-2 sequences and poly-A sequences. To approve the accuracy of mature can-miR-2 in comparison with the probability of error in replication by anchored oligodT, once again two forward primers for the observed sequences were designed by Oligo v.7 software and PerlPrimer (new sequence of primers 2 and 12 with sequences of 5'-GCTGCTCAGCTCCAGGTCG-3' and 5'-TCAGCTGCACGCTCCTGC-3', respectively) and PCR was performed. The samples were loaded on 12% polyacrylamide gel and no band was observed (Fig.4B).



**Fig.2:** Sequencing results. A-1, A-2. When can-miR-1 and can-miR-2 sequences are cloned into the expression vectors must be in direction read the vectors sequence to be properly expressed, also no nucleotide changes were caused by the mutations in these sequences which do not produce defective RNAs. Outputs are confirmed accuracy of work.

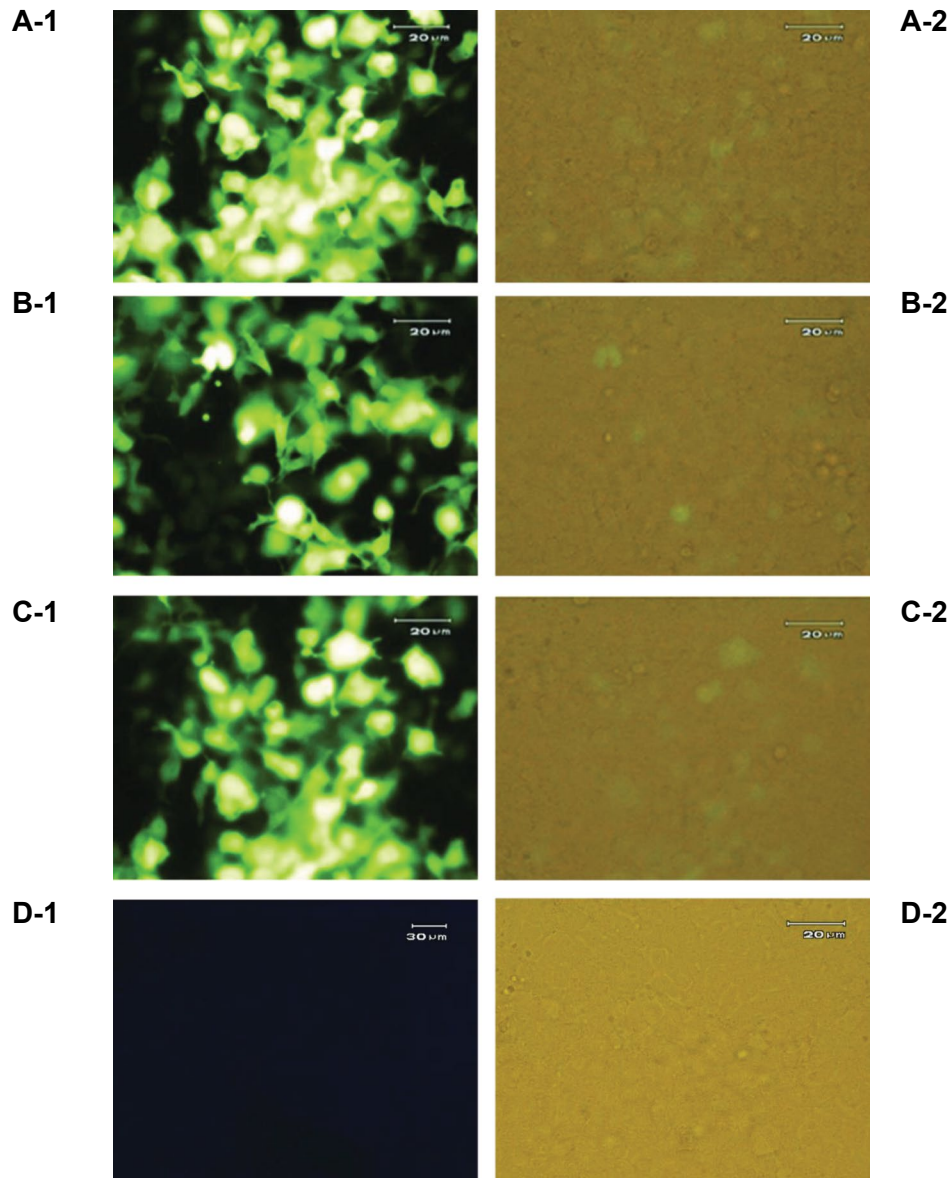


**Fig.3:** Observing GFP protein expression using fluorescence microscopy. GFP expression indicates transfection accuracy in **A-1, A-2**. Pre-miRNA, **B-1, B-2**. Scramble, **C-1, C-2**. Mock and **D-1, D-2**. Untransfected HEK 293 cell lines.

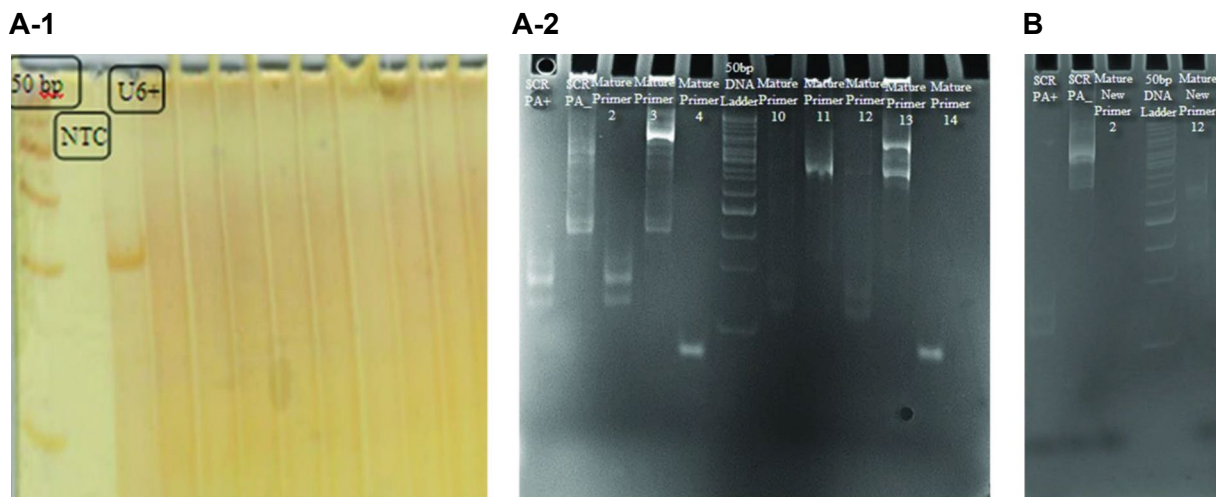


**Fig.4:** Polyacrylamide gel electrophoresis utilization to confirm the mature miRNAs expression. **A-1**. Wells related to negative control (NTC) and positive control (U6+) are indicated in the figure. The subsequent wells are related to polymerase chain reaction (PCR) products with primers designed for mature can-miR-1 at different annealing temperatures. **A-2**. Fragments for primers 2 and 12 with 80-100 bp were observed for can-miR-2 sequence. **B**. Two observed mature miRNAs of can-miR-2 with new sequence of primers loaded on polyacrylamide gel.

## Discussion

Hemophilia-A is a result of a quantitative or qualitative defect in a plasma protein that is involved in blood clotting. It is a common genetic disease and one of the most serious hereditary blood disorders. So far, major molecular researches have focused on a variety of mutations in *F8* gene, particularly the effects of coding region mutation on the rate and quality of FVIII expression (27, 28). Researchers have found increasing evidences based on aberrant expressions of some miRNAs in various diseases by discovering miRNAs and proving their highly significant role in regulating expression of the most important genes.

While clarifying the molecular mechanisms involved in the relevant disorders, discovery of a miRNA associated with a disease helps meet diagnostic and therapeutic needs of the disease (29). So far, most of the miRNA identification has been accomplished by RNA cloning and sequencing. Various protocols have been developed for this purpose and have been successfully used to identify most of the current detected miRNAs.

All of these protocols follow the same rule, but there are differences in details of the method. The major limitation in identifying miRNAs with cloning is difficult to find miRNAs with low expression or in particular stages or limited cell lines. Another problem with these methods is problem to clone some miRNAs due to the physical characteristics, like sequence composition and posttranslational modifications (splicing, methylation). In addition to the above problems, cost and time-consuming will cause restrictions in these methods (30). In this regard, computational algorithms provide quick, efficient and inexpensive methods for predicting novel miRNAs in genomic sequences. Furthermore, predicting the genomic region of miRNA genes facilitates discovery of new genes by limiting the search to specific regions, but predicting the existence of miRNA genes by computational processes is not enough to prove these genes and the presence of predicted miRNA genes should be experimentally confirmed by examining the intrinsic expressions of the mature form of miRNA (31, 32). Although, more than 10 million transcribed loci would increase hairpin structures, not all of them are indeed cleaved to mature miRNAs in the human genome (33). Kim (32) indicated some conditions to mimic a small RNA as a miRNA: first, its expression should be confirmed by some methods like RT-PCR or primer analysis. Second, small RNA sequence should be located in a 60-80 nucleotides hairpin-structure, at either 5' or 3' arm of the hairpin without bulges or internal loops. Third, small RNA sequence should be conserved phylogenetically. Sequence conservation must be seen in the hairpin precursor (pri-miRNA) which is often less than mature miRNA. Finally, increase in miRNA precursor level by reducing Dicer function is a good witness for the existence of miRNA. However, due to problems and technical difficulties that exist in destroying Dicer in some cells, the latter criterion is not used similar to the other criteria.

Considering the conservation factor and the use of RNAfold database to analyze folding and minimum free energy, Yoon and Micheli. (34) predicted the structures of miRNA precursors and identified 38 novel human miRNAs among the structures that were highly similar to the identified miRNAs. Additionally, in the same fashion, Lai et al. (35) confirmed 24 novel miRNA genes by bioinformatics analysis.

By adopting a phylogenetic approach, Berezikov et al. (36) found that nucleotides in the stem sequence of miRNA precursor had significantly higher conservation than the other sequences in stem loop. Considering the matter as well as the other features of known miRNAs, they presented 69 potential candidates for the miRNA and confirmed expression of 16 mature miRNA by Northern blotting; thus 16 novel human miRNAs were identified. Furthermore, by combining bioinformatics predictions with microarray analysis and direct cloning of sequences, Bentwich et al. (37) introduced 89 novel human miRNAs.

Using SSCProfiler, UCSC genome browser and several other databases, Dokanehiifard et al. (38) successfully predicted and validated two novel miRNAs in the *TRKC* gene and hsa-miR-6165 in *NGFR*. They also investigated their possible association with colorectal cancer. Additionally, they predicted and confirmed a new miRNA in *PIK3KCA* human gene with a possible role in colorectal cancer.

By developing a method based on miRDeep, Dokanehiifard et al. (39) discovered 99 putative novel miRNAs that were associated with neurodegenerative diseases. Saleh et al. (40) completely validated the novel hsa-miR-3675b inhibiting proliferation of human breast carcinoma cells. In this work, in order to identify and confirm candidate regions for the expression of miRNAs in *F8* gene bioinformatics methods were utilized. Two candidate regions with appropriate miRNA characteristics and the successful cloning of these areas were determined by the result of the bioinformatics studies. To express these miRNA precursors in human cells, recombinant human vector transfections were performed in a human cell line. It was expected that these cells would create their corresponding mature miRNAs using their processing system by expressing these precursors in the cells. Search for the mature miRNAs were carried out, but no result was achieved after RNA extraction and PCR using the possible mature miRNA primers. It is believed that expression of the predicted miRNA will be detected through altering cell lines and expression vectors or changing the experimental conditions. Another possible recommendation to confirm the candidate miRNA in the transfected cell lines includes PCR conditions, changing cDNA synthesis method or designing different primers.

## Conclusion

Considering the findings obtained from this study, further studies are needed to confirm the presence of candidate miRNAs, in the light of the above points. After

confirmation of the miRNAs at this stage, expression levels should be measured within the transfected and non-transfected cell populations using Real time-PCR. Since the protocols of this study were based on the published articles, bioinformatics prediction of miRNAs in different genes of HEK293 cell line has been experimentally validated. Moreover, expression of the mentioned miRNAs (can-miR-1 and can-miR-2) was confirmed by deep sequencing and RNA sequencing data. Confirmation of the presence of these miRNAs in the *F8* gene and their exogenous expression through the mentioned protocol is the primary goal of this research. We need real-time PCR technique to evaluate endogenous expression of the verified miRNAs. This will be the propsetive objective for future investigations. Changing type of the cell line and experimental conditions according to the recent protocols is considered to resolve the problems of experimentally confirmation of the candidate miRNAs in this article.

## Acknowledgements

We acknowledge contribution of many lab members in this project over the last years. This study was done at the University of Isfahan (Isfahan, Iran), Tarbiat Modares University (Tehran, Iran) and financially supported by Department of Cell and Molecular Biology and Microbiology of University of Isfahan. There is no conflict of interest in this study.

## Authors' Contributions

H.R., M.M.-B.; S.J.M.; Were involved in study design, manuscript preparation and editing. All authors read and approved the final manuscript.

## References

- Salviato R, Belvini D, Radossi P, Tagariello G. Factor VIII gene intron 1 inversion: lower than expected prevalence in Italian haemophilic severe patients. *Haemophilia*. 2004; 10(2): 194-196.
- Lu M, Zhang Q, Deng M, Miao J, Guo Y, Gao W, et al. An analysis of human microRNA and disease associations. *PLoS One*. 2008; 3(10): e3420.
- Kemball-Cook G, Tuddenham EG. The factor VIII mutation database on the world wide web: the haemophilia a mutation, search, test and resource site HAMSTeRS update (version 3.0). *Nucleic Acids Res*. 1997; 25(1): 128-132.
- Aranha MM, Santos DM, Sola S, Steer CJ, Rodrigues CMP. miR-34a regulates mouse neural stem cell differentiation. *PLoS One*. 2011; 6(8): e21396.
- Cai X, Hagedorn CH, Cullen BR. Human microRNAs are processed from capped, polyadenylated transcripts that can also function as mRNAs. *RNA*. 2004; 10(12): 1957-1966.
- Rodriguez A, Griffiths-Jones S, Ashurst JL, Bradley A. Identification of mammalian microRNA host genes and transcription units. *Genome Res*. 2004; 14(10A): 1902-1910.
- Lee Y, Kim M, Han J, Yeom KH, Lee S, Baek SH, et al. MicroRNA genes are transcribed by RNA polymerase II. *EMBO J*. 2004; 23(20): 4051-4060.
- Ambros V. The functions of animal microRNAs. *Nature*. 2004; 431(7006): 350-355.
- Krol J, Loedige I, Filipowicz W. The widespread regulation of microRNA biogenesis, function and decay. *Nat Rev Genet*. 2010; 11(9): 597-610.
- Wang Z. MicroRNA: a matter of life or death. *World J Biol Chem*. 2010; 1: 41-54.
- Wang Y, Lee CG. MicroRNA and cancer—focus on apoptosis. *J Cell Mol Med*. 2009; 13(1):12-23.
- Griffiths JS, Grocock RJ, van DS, Bateman A, Enright AJ. miR-Base: microRNA sequences, targets and gene nomenclature. *Nucleic Acids Res*. 2006; 34: 140-144.
- Miranda KC, Huynh T, Tay Y, Ang YS, Tam WL. A pattern-based method for the identification of MicroRNA binding sites and their corresponding heteroduplexes. *Cell*. 2006; 126(6): 1203-1217.
- Yoon BJ, Vaidyanat PP. Computational identification and analysis of noncoding RNAs. *IEEE Signal Processing Magazine*. 2007; 24(1): 64-74.
- Oulas A, Reczko M, Poirazi P. MicroRNAs and cancer—the search begins! *IEEE Trans Inf Technol Biomed*. 2009; 13(1): 67-77.
- Lopez IdON, Schliep A, Carvalho ACPdLd. The discriminant power of RNA features for pre-miRNA recognition. *BMC Bioinformatics*. 2014; 15: 124.
- Berezikov E, Cuppen E, Plasterk RHA. Approaches to microRNA discovery. *Nat Genet*. 2006; 38 Suppl: S2-S7.
- Berezikov E, Guryev V, van de Belt J, Wienholds E, Plasterk RHA, Cuppen E. Phylogenetic shadowing and computational identification of human microRNA genes. *Cell*. 2005; 120(1): 21-24.
- Li L, Xu J, Yang D, Tan X, Wang H. Computational approaches for microRNA studies: a review. *Mamm Genome*. 2010; 21(1-2): 1-12.
- Miller SA, Dykes DD, Polesky HF. A simple salting out procedure for extracting DNA from human nucleated cells. *Nucleic Acids Res*. 1988; 16(3): 1215.
- Available from: <http://www.genetbio.com> (22 Jun 2019).
- Hana H. TOP10 E. coli competent cells (chemical transformation). *Methods Enzymol*. 1991. Available from: <http://www.k-state.edu> (02 Jul 2019).
- Xu N, Papagiannakopoulos T, Pan G, Thomson JA, Kosik KS. MicroRNA-145 regulates OCT4, SOX2, and KLF4 and represses pluripotency in human embryonic stem cells. *Cell*. 2009; 137(4): 647-658.
- O'Brien P, Elahipanah S, Rogozhnikov D, Yousaf M. Bio-orthogonal mediated nucleic acid transfection of cells via cell surface engineering. *ACS Cent Sci*. 2017; 3(5): 489-500.
- Available from: <https://www.sigmaaldrich.com/IR/en/technical-documents/protocol/protein-biology/protein-lysis-and-extraction/tri-reaquent> (11 Aug 2019).
- Redshaw N, Wilkes T, Whale A, Cowen S, Huggett J, Foy CA. A comparison of miRNA isolation and RT-qPCR technologies and their effects on quantification accuracy and repeatability. *BioTechniques*. 2013; 54: 155-164.
- Friedman RC, Farh KKH, Burge CB, Bartel DP. Most mammalian mRNAs are conserved targets of microRNAs. *Genome Res*. 2009; 19(1): 92-105.
- Kumar MS, Lu J, Mercer KL, Golub TR, Jacks T. Impaired microRNA processing enhances cellular transformation and tumorigenesis. *Nat Genet*. 2007; 39(5): 673-677.
- Hogeweg P. The roots of bioinformatics in theoretical biology. *PLoS Comput Biol*. 2011; 7(3): e1002021.
- John B, Enright AJ, Aravin A, Tuschl T, Sander C, Marks DS. Human microRNA targets. *PLoS Biol*. 2004; 2(11): e363.
- Jima DD, Zhang J, Jacobs C, Richards KL, Dunphy CH, Choi WW, et al. Deep sequencing of the small RNA transcriptome of normal and malignant human B cells identifies hundreds of novel microRNAs. *Blood*. 2010; 116(23): e118-127.
- Kim VN. MicroRNA biogenesis: coordinated cropping and dicing. *Nat Rev Mol Cell Biol*. 2005; 6(5): 376-385.
- Kang W, Friedlander MR. Computational prediction of miRNA genes from small RNA sequencing data. *Front Bioeng Biotechnol*. 2015; 3: 7-13.
- Yoon S, Micheli GD. Computational identification of microRNAs and their targets. *Birth Defects Res C Embryo Today*. 2006; 78(2): 118-128.
- Lai EC, Tomancak P, Williams RW, Rubin GM. Computational identification of *Drosophila* microRNA genes. *Genome Biol*. 2003; 4(7): R42.
- Berezikov E, Guryev V, van de Belt J. Phylogenetic shadowing and computational identification of human microRNA genes. *Cell*. 2005; 120(1): 21-24.
- Bentwich I, Avniel A, Karov Y, Aharonov R, Gilad S, Barad O, et al. Identification of hundreds of conserved and nonconserved human microRNAs. *Nat Genet*. 2005; 37(7): 766-772.
- Dokanehiifard S, Soltani BM, Parsi S, Hosseini F, Javan M, Mowla SJ. Experimental verification of a conserved intronic microRNA located in the human *TrkC* gene with a cell type-dependent apoptotic function. *Cell Mol Life Sci*. 2015; 72(13): 2613-2625.
- Dokanehiifard S, Yasari A, Najafi H, Jafarzadeh M, Nikkhal M, Mowla SJ, et al. A novel microRNA located in the *TrkC* gene regulates the Wnt signaling pathway and is differentially expressed in colorectal cancer specimens. *J Biol Chem*. 2017; 292(18): 7566-7577.
- Saleh AJ, Soltani BM, Dokanehiifard S, Medlej A, Tavalaei M, Mowla SJ. Experimental verification of a predicted novel microRNA located in human *PIK3CA* gene with a potential oncogenic function in colorectal cancer. *Tumour Biol*. 2016; 37(10): 14089-14101.

# Spermatozoa Induce Maternal Mononuclear Cells for Production of Antibody with Cytotoxic Activity on Paternal Blood Mononuclear Cells

Nasrin Sereshki, Ph.D.<sup>1,2\*</sup>, Alireza Andalib, Ph.D.<sup>1</sup>, Mohadeseh Toghiani, M.Sc.<sup>1</sup>,  
Hossein Motedayyen, Ph.D.<sup>3</sup>, Mohammad Sadegh Hesamian, Ph.D.<sup>1</sup>,  
Abbas Rezaei, Ph.D.<sup>1</sup>, David Wilkinson, M.A.<sup>4</sup>

1. Department of Immunology, School of Medicine, Isfahan University of Medical Sciences, Isfahan, Iran  
2. Asadabad School of Medical Science, Asadabad, Iran  
3. Autoimmune Diseases Research Centre, Kashan University of Medical Sciences, Kashan, Iran  
4. University of Aberdeen, Scotland, UK

\*Corresponding Address: Postal code: 6541743897, Asadabad School of Medical Science, Asadabad, Iran  
Email: sereshki55@gmail.com

Received: 13/September/2019, Accepted: 20/January/2020

## Abstract

**Objective:** The maternal immune response to paternal antigens is induced at insemination. We believe that pregnancy protective alloantibodies, such as anti-paternal cytotoxic antibody (APCA), may be produced against the paternal antigens in the context of stimulated immunity at insemination and that they increase during pregnancy. APCA is necessary for pregnancy. It is directed towards paternal human leucocyte antigens (HLAs) and has cytotoxic activity against paternal leucocytes. The present study aims to determine whether APCA is produced by the maternal peripheral blood mononuclear cells (PBMCs) in contact with the husband's spermatozoa and to evaluate the relation of APCA production with HLA class I and II expressions by spermatozoa in fertile couples.

**Materials and Methods:** This cross-sectional study included 30 fertile couples with at least one child. The maternal PBMCs were co-cultured with the husband's spermatozoa and the supernatant was assessed for the presence of IgG by ELISA. Cytotoxic activity of the supernatant on the husband's PBMCs was assessed by the complement-dependent cytotoxicity (CDC) assay.

**Results:** IgG was produced in all co-cultures, and the mean level of supernatant IgG was 669 ng/ml. The cytotoxic activity of the supernatant was observed in all the supernatant obtained from the co-cultures. The mean percentage of APCA in supernatant was 73.93%.

**Conclusion:** Based on the results of this study it can be concluded that APCA may be a natural anti-sperm antibody (ASA), which can be produced during exposure to spermatozoa and may have some influence before pregnancy. Further research is required to determine the role of APCA before pregnancy.

**Keywords:** Antibodies, Antigen, Cell Cytotoxicity, Spermatozoa

Cell Journal (Yakhteh), Vol 23, No 3, August 2021, Pages: 349-354

**Citation:** Sereshki N, Andalib A, Toghiani M, Motedayyen H, Hesamian MS, Rezaei A, Wilkinson D. Spermatozoa induce maternal mononuclear cells for production of antibody with cytotoxic activity on paternal blood mononuclear cells. *Cell J.* 2021; 23(3): 349-354. doi: 10.22074/cellj.2021.7157.  
This open-access article has been published under the terms of the Creative Commons Attribution Non-Commercial 3.0 (CC BY-NC 3.0).

## Introduction

Studies suggest that the maternal immune response to paternal antigens is induced prior to conception and possibly during insemination. After sexual intercourse, the infiltration of neutrophils, macrophages and lymphocytes in the female reproductive tract (FRT) due to the presence of immune stimulating factors in semen has been clearly shown. The consequence of this inflammation is the adaptation of maternal-innate and adaptive immune responses for the occurrence of pregnancy (1-3). In immunity against semen, the immune effector response and the regulatory response (regulatory T cells or Tregs) are induced. Evidence suggests a delicate balance between the effector and regulatory responses, and this may be required for pregnancy to occur. One of the roles of the immune effector response could be preparation of tissue destruction factors such as metalloproteinase enzymes and inflammatory cytokines needed for embryo implantation. A role of the regulatory response is prevention of an excessive effector response (4). Disruptions in balance

between the effector and regulatory response results in pregnancy aberrations, such as recurrent spontaneous abortion (RSA) (5). These findings suggest that induction of both effector and regulatory responses against semen antigens is essential for pregnancy occurrence.

Despite many studies on the induction of the maternal immune response to semen, we could not find any study that has addressed beneficial humoral immunity (antibody production) against semen or spermatozoa. We believe that pregnancy-protective alloantibodies against the paternal antigen may be produced in the context of stimulated immunity at insemination and they increase in pregnancy due to the increase of paternally-derived foetal antigens in the maternal blood circulation. Therefore, any destruction of semen or spermatozoa antigenicity may result in disturbed production of alloantibodies and pregnancy complications. This supposition, the production of pregnancy-protective alloantibody at insemination, was presented when we observed that absence of pregnancy-protective alloantibodies resulted

in RSA (6, 7). Thus, pregnancy-protective alloantibodies must be present before pregnancy and are necessary for pregnancy occurrence; otherwise, RSA occurs.

Anti-paternal cytotoxic antibody (APCA) is one of the pregnancy alloantibodies which belongs to the IgG class and is directed to paternal human leucocyte antigens (HLAs) (8). There is scant information about its function and mechanism of action. The absence of APCA is related to RSA. There is a relationship between APCA development after lymphocyte therapy and the success of this treatment in improving live birth rates in RSA women (6, 9). This suggests that APCA may be produced upon contact with HLAs in semen and spermatozoa. Although there is considerable controversy surrounding HLA class I and II expression by spermatozoa (10-19), we recently demonstrated that these antigens were expressed by spermatozoa (20). Given this description, it is very likely that APCA would be produced in contact with spermatozoa in the context of stimulated immunity at insemination and help pregnancy to occur. We hypothesize that APCA production in contact with spermatozoa may benefit humoral immunity following insemination.

As mentioned, we have not found any study that assessed beneficial humoral immunity against spermatozoa. Thus, to commence the study about maternal humoral immunity against spermatozoa, we aim to determine: i. Whether antibody is produced by the female's peripheral blood mononuclear cells (PBMCs) in the presence of the husband's spermatozoa, ii. Whether APCA is produced by the female's PBMCs in contact with the husband's spermatozoa, and iii. The correlation of APCA and antibody production with HLA class I and II expressions by spermatozoa. To the best of our knowledge, no study has addressed these topics.

## Materials and Methods

### Subjects

In this cross-sectional study, we included 30 fertile couples aged 28-41 years who had at least one child. The anti-sperm antibody (ASA) test was negative in these couples. The maternal participants denied any history of pregnancy complications (e.g., ectopic pregnancy, preterm and post-term labour or preeclampsia), blood transfusion or organ transplantation. The husband of each woman had normal semen status according to the criteria from 2010 guidelines of the World Health Organization. None of the male partners had any history of genital tract disorders such as infections, undescended testis, inguinoscrotal surgery, genital trauma or testicular torsion.

Five women, aged 28-42 years, who were virgins and had no history of semen contact, blood transfusion or organ transplantation were recruited to this study as the uncontacted negative control. Because they had no history of alloantigen contact, we expected that PBMCs obtained from these women would not produce antibodies in the presence of spermatozoa. We chose an age and sex matched control to remove the effect of age and sex related confounding factors such as hormonal factors, variation of microbiota with age and other factors that have important

effects on the immune system. More reliable results could be acquired when the only difference between virgin women (uncontacted control) and the maternal women (with partners) was the lack of semen contact.

Informed consent was obtained from all subjects. The Ethics Committee of Isfahan University of Medical Sciences (Isfahan, Iran) approved this protocol (approval letter: IR.MUI.REC.1395.3.480).

### Purification of spermatozoa

Semen samples were collected by masturbation after 2-3 days of sexual abstinence. Sampling was performed under sterile conditions to prevent false results due to a change of spermatozoa antigenicity induced by toll-like receptors on the spermatozoa in response to microbial antigens. After liquefaction, semen quality was assessed according to WHO standard guidelines (WHO, 2010) and couples were excluded if the husband had an abnormal semen quality. We added 2 ml of AllGrad Wash (LifeGlobal® Group, Canada) to the liquefied semen sample, and centrifuged the sample at 350 g for 10 minutes. The pellet was re-suspended in 1 ml of AllGrad Wash® and 2 gradient solutions (95% and 45%) prepared from AllGrad 100% (LifeGlobal® Group, Canada). In each tube, 1 ml of AllGrad 90% gradient, followed by 1 ml of AllGrad 45% gradient and then 1 ml of the spermatozoa suspension were carefully layered. The tubes were centrifuged at 400 g for 18 minutes. The spermatozoa pellet at the bottom of the centrifuge tubes was washed with AllGrad Wash® and then re-suspended in Ham's F-10 medium (Dacell, Iran) with 1% bovine serum albumin (CMG, Iran). Ham's F-10 medium was used because of its antioxidant properties, which makes it a suitable medium for spermatozoa (21).

### Flow cytometry assay

We added  $1 \times 10^6$  spermatozoa per 100  $\mu$ l medium was added to two tubes of each purified spermatozoa sample. One tube was incubated with phycoerythrin (PE) mouse anti-human HLA-ABC (clone: G46-2.6, BD Pharmingen, USA) and the other was incubated with PE mouse anti-human HLA-DR (clone: G46-6, BD Pharmingen, USA) at room temperature for 30 minutes. After two washes with AllGrad Wash® (400 g for 5 minutes), the spermatozoa were run through a flow cytometer (BD FACSCalibur, USA). Data from at least 100000 events were collected using forward scatter (FSC) and side angle of light scatter (SSC), a logarithmic amplifier. Fluorescence data were obtained with the logarithmic amplifier. To determine background fluorescence (auto-fluorescence and non-specific binding of antibodies), we used two isotype controls (mouse IgG1,  $\kappa$  [clone: G46-2.6, BD Pharmingen, USA] and mouse IgG2a,  $\kappa$  [clone: G46-6, BD Pharmingen, USA]). An antibody titration was performed and we selected the optimal titre that displayed the minimum background to eliminate any background fluorescence. FSC versus SSC gating was used to identify spermatozoa and remove debris. To determine the percentage of HLA class I and II positive spermatozoa, SSC versus logarithmic FL2 (PE) gating was used. The cell viability test was not performed because abnormal and dead spermatozoa were removed by AllGrad solution before staining. The data

were analysed using FlowJo version10 software.

### **Isolation of peripheral blood mononuclear cells and performing co-culture**

After taking 5 ml of heparinized venous blood, the PBMCs were separated by centrifugation on a Ficoll-Hypaque (Lymphoprep, Sigma, USA) density gradient. Cells at the interface were harvested, washed twice and suspended in complete RPMI 1640 medium supplemented with HEPES, L-glutamine, penicillin (100 U/ml), streptomycin (10 mg/ml), 2-mercaptoethanol ( $2 \times 10^{-5}$  M) and 20% autologous serum. In this suspension, we adjusted the cell concentration to  $1 \times 10^6$  cells/ml. A 2 ml suspension ( $2 \times 10^6$  PBMCs) was transferred to 24-well plates and cultured in the presence of  $5 \times 10^6$  spermatozoa. As the negative control,  $2 \times 10^6$  maternal PBMCs without spermatozoa were cultured in parallel to the co-cultures. Cells were then incubated at  $37^\circ\text{C}$  in a humidified 5%  $\text{CO}_2$  atmosphere. After four days, cells were washed three times and the pellet was re-suspended in 2 ml complete RPMI 1640 medium in which autologous serum was replaced by 20% foetal calf serum (FCS). After incubation for eight days at  $37^\circ\text{C}$  in a humidified 5%  $\text{CO}_2$  atmosphere, the supernatants were harvested, aliquoted and kept at  $-80^\circ\text{C}$  for future use.

For the uncontacted negative control, blood was taken from the women volunteers who were virgins. The PBMCs were separated and these cells were co-cultured with the pooled spermatozoa obtained from five normal donors. The culture procedure was similar to that mentioned above. There were two controls: i. Negative control (culture of PBMC alone from the maternal women) and ii. Uncontacted negative control (co-culture PMBC from virgin women with pooled spermatozoa). The first control was run to ensure that any unknown factors did not lead to the production of antibodies, and that the production of antibodies in the co-cultures was because of the presence of spermatozoa. The second control was performed to ensure that antibodies produced in the presence of spermatozoa indicated that sensitization had previously occurred. In other words, the uncontacted negative control was run to confirm that the female humoral immune response (antibody production) was induced by spermatozoa at the time of insemination.

### **Enzyme-linked immunosorbent assay analysis**

The concentration of IgG in the supernatant was measured using an enzyme-linked immunosorbent assay (ELISA) kit in accordance with the manufacturer's protocol [IgG (Total) Human Uncoated ELISA Kit, Invitrogen, USA]. Normal serum samples that contained IgG were used as the positive control.

### **Complement-dependent cytotoxicity assay for determining the anti-paternal cytotoxic antibody titre in the supernatants**

We assessed the APCA percentage by cross-matching between supernatants (1:64 dilution) and freshly prepared paternal PBMCs. The test was performed in triplicate in Terasaki plates covered with light paraffin oil. We mixed one  $\mu\text{l}$  of paternal PBMCs suspension (density:  $2 \times 10^3$  cells/ml)

with 1  $\mu\text{l}$  supernatant. For quality control of the complement-dependent cytotoxicity (CDC) assay and to ensure accuracy of the assay, two control samples – a negative control (antibody without cytotoxic antibody) and positive control (antibody with cytotoxic activity) were used. The positive control was the serum of the women at the third trimester of pregnancy because it contained a high level of APCA. APCA increases to detectable levels from the 28<sup>th</sup> week of pregnancy until four weeks after delivery, after which it decreases to an undetectable level (22). The serum of these women was mixed with their male partner's PBMCs. The negative control consisted of supernatants obtained from co-culturing PBMCs from virgin women with pooled spermatozoa, which lacked any antibodies. After one hour at room temperature, we added 5  $\mu\text{l}$  of rabbit complement (Inno-Train, Germany). One  $\mu\text{l}$  eosin dye was added to the wells after one hour of incubation at room temperature, followed by 5  $\mu\text{l}$  of formalin (37%). The test plates were left overnight to allow the cells to settle. The plates were read using a phase contrast microscope (Olympus, Japan). The number of dead cells among 1000 PBMCs was determined and reported as the percentage of APCA.

### **Statistical analysis**

Descriptive analysis of the percentage of HLA class I and II expression by spermatozoa, IgG concentration and percentage of APCA in supernatant included the mean and standard deviation (SD). A Pearson product-moment correlation coefficient was used to assess the relationship between variables. All data analysis was performed using IBM SPSS statistics 25 software. A  $P \leq 0.05$  was considered statistically significant.

## **Results**

### **Evaluation of human leucocyte antigen class I and II on the surface of spermatozoa**

Flow cytometric results showed that  $25.77 \pm 9.9\%$  of spermatozoa expressed HLA class I on their surface and that  $29.95 \pm 10.10\%$  of spermatozoa expressed HLA class II. Figure 1 presents a representative flow cytometry dot plot and histogram overlay.

### **IgG concentration in the supernatant**

Supernatant IgG levels were measured by ELISA. IgG was detected in all of the supernatants. The mean  $\pm$  SD of the IgG concentration in supernatants was  $669 \pm 132$  ng/ml. The IgG concentration in the negative control was  $3.20 \pm 2.31$  ng/ml and in the uncontacted negative control, it was  $3.2 \pm 2.90$  ng/ml.

### **Percentage of anti-paternal cytotoxic antibody in the supernatant**

CDC results showed that all supernatants were positive for APCA. The percentage of APCA in the supernatant was  $73.93 \pm 16.01\%$ . The percentage of dead cells in the negative controls was  $3.12 \pm 2.96\%$ . Figure 2 shows phase contrast microscope images of PBMCs after the CDC assay.

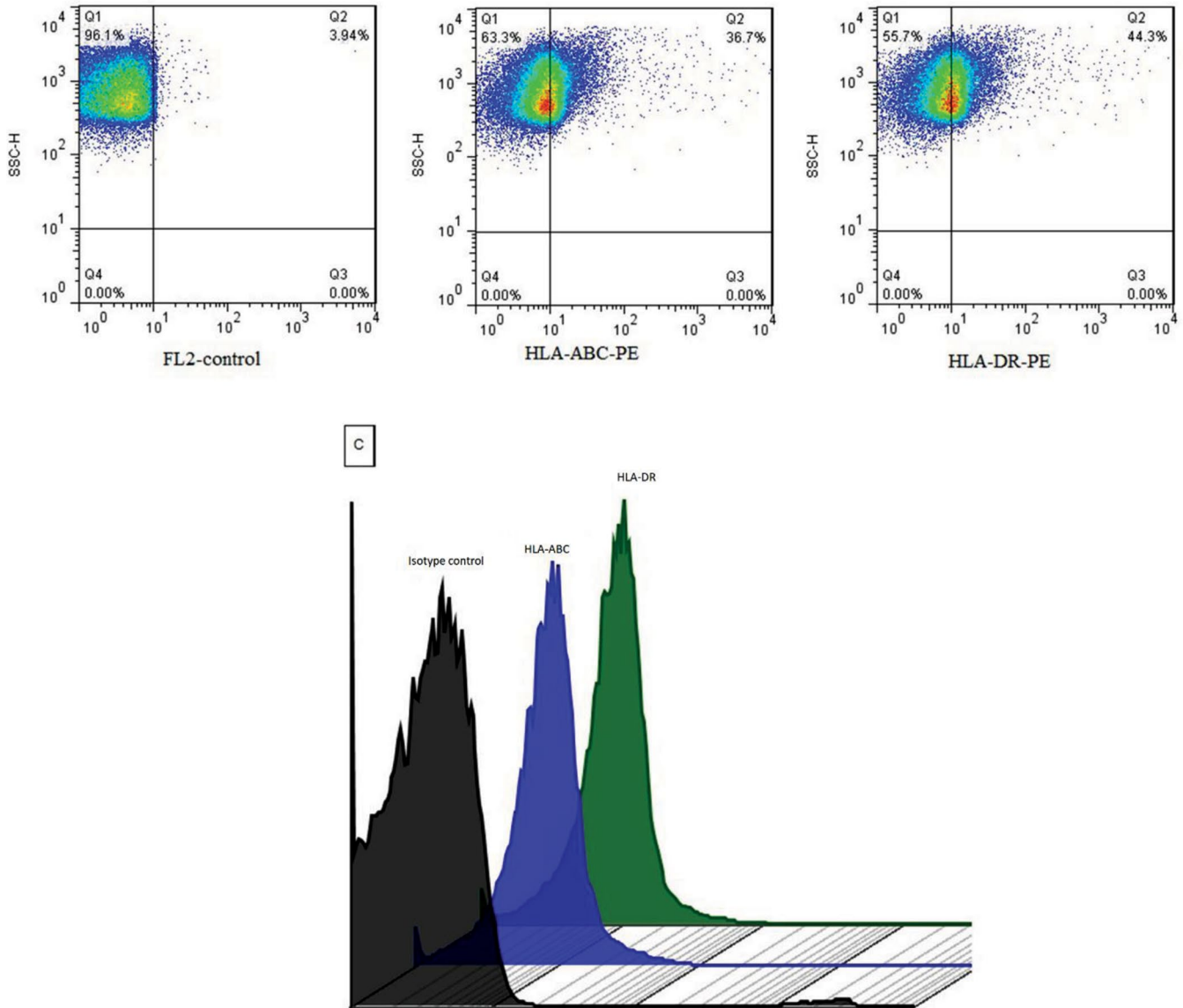


**Fig.1:** Representative of the flow cytometry dot plot and histogram overlay. Purified spermatozoa were assessed for expression of human leucocyte antigen (HLA) class I and II by flow cytometry. The dot plot is used to show the percentage of HLA class I and HLA class II positive spermatozoa. C is a representative stagger histogram overlay of the isotype control with the experimental sets to show the background level after minimizing background auto-fluorescence.

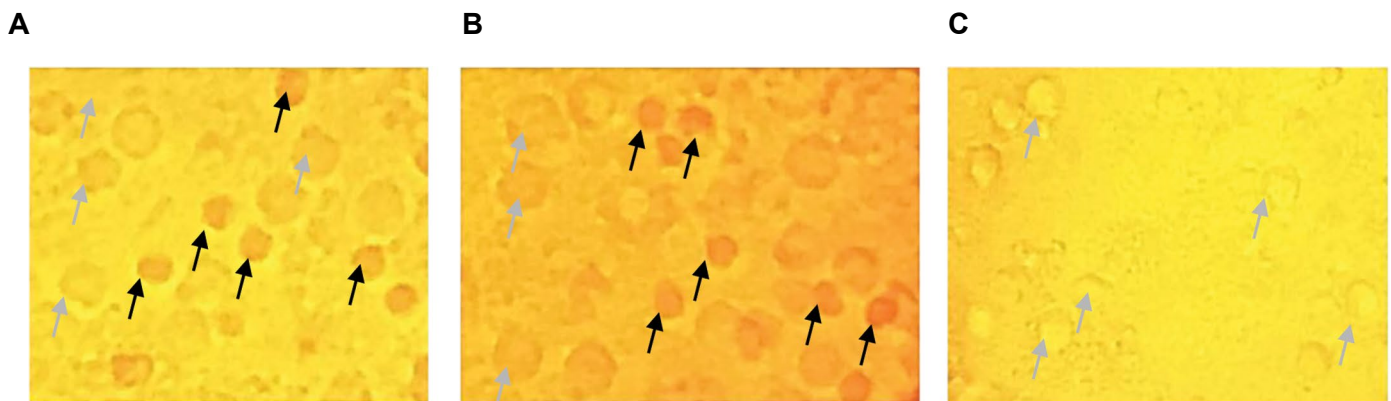


**Fig.2:** Phase contrast microscope images of the husbands' peripheral blood mononuclear cells (PBMCs) after the complement-dependent cytotoxicity (CDC) assay. Eosin dye was taken up by the dead cells and they became a dark colour. **A.** Positive control, **B.** Test (cytotoxic activity of supernatant on paternal PBMCs, and **C.** Negative control. Black arrow; Dead cells and Gray arrow; Live cells.

## Correlation assessments

A Pearson product-moment correlation coefficient was computed to assess the relationship between APCA production and HLA class I and II expression by spermatozoa. There was a positive correlation between these factors [ $P=0.011$  (HLA-I) and  $P=0.013$  (HLA-II), Table 1].

**Table 1:** Correlation results

Pearson correlation		IgG (ng/ml)	APCA (%)
HLA-I %	r	0.459*	0.509**
	P value	0.011	0.004
	n	30	30
HLA-II %	r	0.449*	0.499**
	P value	0.013	0.005
	n	30	30

\*; Correlation is significant at the 0.05 level (2-tailed), \*\*; Correlation is significant at the 0.01 level (2-tailed), n; Number; HLA; Human leucocyte antigens, APCA; Anti-paternal cytotoxic antibody, and r; Correlation coefficient.

## Discussion

Despite numerous studies about the cellular immunity that is induced in FRT at insemination, the humoral immunity and the production of useful antibodies against spermatozoa (ASA) has not been assessed. In this study, we show, for the first time, that IgG and APCA are produced by the wife's PBMCs in the presence of the husband's spermatozoa. Furthermore, we show a positive correlation between HLA expression by spermatozoa and antibody production. To the best of our knowledge, this is the first study that has investigated the ability of spermatozoa to induce the production of IgG and APCA. We could not find any study that investigated the correlation between HLA expression on spermatozoa and the induction of immunity (e.g., antibody production) by spermatozoa.

The production of antibodies (IgG) against an antigen in vitro by PBMCs is indicative of the stimulation of the immune response against the antigen and development of memory B lymphocytes that respond to the presence of the antigen in the body. In this study, we have shown that the antibody (IgG) was produced ASA when the wife's PBMCs were co-cultured with the husband's spermatozoa. This result suggested development of memory humoral immunity ASA in the wife (or maternal) body.

Regarding these produced antibodies, the question arises as to which antigens of spermatozoa have the capability to cross-react with paternal lymphocyte antigens. One of the most likely antigens are the HLA molecules. This study showed a positive correlation between HLA class I and II and APCA production. It is possible that APCA, which is originally developed through exposure to paternally derived foetal antigens during pregnancy, can cross-

react with the same antigens on spermatozoa. However, it should be noted that the immune system is exposed to semen antigen before foetal antigen.

Our results show that fertile women produce antibodies against spermatozoa (ASA). In contrast to our results, many studies have shown that ASA in serum or in FRT secretions results in infertility. Also, numerous studies have sought to determine the antigen specificity of ASA. Despite the large number of studies on the pathogenicity of ASA for pregnancy, the presence of this antibody was reported in a very small percentage of fertile women. Accordingly, the results of our study showed that fertile women have immunological memory of antibody production in the presence of the husband's spermatozoa (23-25). However, the question is raised as to why APCA, a type of ASA, is not detectable in most normal parous women. Two possible reasons can be suggested. First, under normal conditions, APCA producing plasma cells migrate in the FRT and locally produce a small amount of antibody so that the release of antibody into the blood is very limited, and often not identifiable by current methods. Second, APCA may be produced when first encountering spermatozoa, after which it may bind to spermatozoa and be eliminated by cells in the FRT. Consequently, the amount of unbound antibody is very low and cannot be detected in serum and cervical secretion or blood.

The question arises as to why APCA with cytotoxic activity does not lead to infertility. We believe that, in addition to not leading to infertility, APCA has some major roles for supporting pregnancy. These possible roles for APCA before pregnancy include:

- i. Oponizing senescent and damaged spermatozoa for phagocytosis,
- ii. Assisting in promoting a proper immune response required for implantation and tolerance induction,
- iii. Because the cytotoxic activity of immune cells (Natural killer cells and cytotoxic T lymphocytes) is essential for implantation (26-28), it is probable that APCA also has a role in this cytotoxicity process. This role of APCA may occur through the antibody-dependent cell-mediated cytotoxicity (ADCC) that is intermediated by NK cells.

Therefore, it seems logical that the APCA in normal women (which we named natural ASA) has a different function and features compared to the pathogenic ASA in infertile women. We believe that natural and pathogenic ASA may have different properties, such as antigenic specificity, glycosylation type and isotype. Further studies should be performed to assess this supposition.

Determination of the level of APCA in the serum by the CDC assay is a diagnostic test for RSA. However, the sensitivity of this method is low because of the decreased level of APCA in the serum. We intend to use APCA production in the presence of spermatozoa as a diagnostic test for RSA. To achieve this purpose, a study should be performed on a large number of fertile and RSA couples to determine a cut-off value and the normality of APCA.

## Conclusion

Based on the results of this study it can be concluded that APCA can be a natural ASA, which might be produced during exposure to spermatozoa and might have some influence before pregnancy. Further research is required to determine the role of APCA before pregnancy.

## Acknowledgments

The authors would like to thank Dr. Raziye Alipour and Dr. Mitra Rafiee for their valuable insights and recommendations, and for their contribution in conducting some of the experiments for the research. This work did not receive any specific grant from funding agencies in the public, commercial or not-for-profit sectors. The authors declare that there is no conflict of interest regarding the publication of this article.

## Authors' Contributions

N.S.; Contributed to conception and design, experimental work, data and statistical analysis, and interpretation of data manuscript writing and editing. A.A., M.T., H.M., M.S.H.; Contributed to all experimental work, data and statistical analysis, and interpretation of data. A.R., D.W.; Data and statistical analysis, interpretation of data manuscript writing and editing. All authors read and approved the final manuscript.

## References

- Johansson M, Bromfield JJ, Jasper MJ, Robertson SA. Semen activates the female immune response during early pregnancy in mice. *Immunology*. 2004; 112(2): 290-300.
- Bromfield JJ. Seminal fluid and reproduction: much more than previously thought. *J Assist Reprod Genet*. 2014; 31(6): 627-636.
- Schjenken JE, Robertson SA. Seminal fluid signalling in the female reproductive tract: implications for reproductive success and offspring health. *Adv Exp Med Biol*. 2015; 868: 127-158.
- Robertson SA, Sharkey DJ. The role of semen in induction of maternal immune tolerance to pregnancy. *Semin Immunol*. 2001; 13(4): 243-254.
- Saito S, Nakashima A, Shima T, Ito M. Th1/Th2/Th17 and regulatory T-cell paradigm in pregnancy. *Am J Reprod Immunol*. 2010; 63(6): 601-610.
- Chaichian S, Shoaee S, Saremi A, Pedar S, Firouzi F. Factors influencing success rate of leukocyte immunization and anti-paternal antibodies in spontaneous recurrent miscarriage. *Am J Reprod Immunol*. 2007; 57(3): 169-176.
- Kishore R, Agarwal S, Halder A, Das V, Shukla BRK, Agarwal SS. HLA Sharing, anti-paternal cytotoxic antibodies and MLR blocking factors in women with recurrent spontaneous abortion. *J Obstet Gynaecol Res*. 1996; 22(2): 177-183.
- Pandey MK, Rani R, Agrawal S. An update in recurrent spontaneous abortion. *Arch Gynecol Obstet*. 2005; 272(2): 95-108.
- Orgad S, Loewenthal R, Gazit E, Sadetzki S, Novikov I, Carp H. The prognostic value of anti-paternal antibodies and leukocyte immunizations on the proportion of live births in couples with consecutive recurrent miscarriages. *Hum Reprod*. 1999; 14(12): 2974-2979.
- Martin-Villa JM, Longás J, Arnáiz-Villena A. Cyclic expression of HLA class I and II molecules on the surface of purified human spermatozoa and their control by serum inhibin B levels. *Biol Reprod*. 1999; 61(6): 1381-1386.
- Chiang MH, Steuerwald N, Lambert H, Main EK, Steinleitner A. Detection of human-leukocyte antigen class-I messenger-ribonucleic acid transcripts in human spermatozoa via reverse transcription-polymerase chain-reaction. *Fertil Steril*. 1994; 61(2): 276-280.
- Martin-Villa JM, Luque I, Martínez-Quiles N, Corell A, Regueiro JR, Timon M, et al. Diploid expression of human leukocyte antigen class I and class II molecules on spermatozoa and their cyclic inverse correlation with inhibin concentration. *Biol Reprod*. 1996; 55(3): 620-629.
- Rodríguez-Córdoba S, Regueiro JR, Villena AA. HLA-A, -B, -C, -Bw4, Bw6 and -DR antigens are expressed on purified seminal cells other than spermatozoa. *Scand J Immunol*. 1986; 24(5): 545-548.
- Paradisi R, Neri S, Pession A, Magrini E, Bellavia E, Ceccardi S, et al. Human leukocyte antigen I expression in spermatozoa from infertile men. *Int J Androl*. 2001; 24(1): 8-14.
- Paradisi R, Neri S, Pession A, Magrini E, Bellavia E, Ceccardi S, et al. Human leukocyte antigen II expression in sperm cells: comparison between fertile and infertile men. *Arch Androl*. 2000; 45(3): 203-213.
- Haas GG, Nahhas F. Failure to identify hla abc and dr antigens on human-sperm. *Am J Reprod Immunol Microbiol*. 1986; 10(2): 39-46.
- Castilla JA, Gil T, Rodríguez F, Molina J, Samaniego F, Vergara F, et al. Lack of expression of HLA antigens on immature germ-cells from ejaculates with antisperm antibodies. *Am J Reprod Immunol*. 1993; 30(1): 9-14.
- Law HY, Bodmer WF. Use of microimmobilization and microagglutination assays for attempted detection of HLA antigens and beta 2 microglobulin on human sperm. *Tissue Antigens*. 1978; 12(4): 249-269.
- Schaller J, Glander HJ, Ladusch M, Westhoff U, Grosse-Wilde H. Lack of HLA-molecules on human spermatozoa and in seminal plasma. *Andrologia*. 1993; 25(2): 77-81.
- Sereshki N, Andalib A, Ghahiri A, Mehrabian F, Sherkat R, Rezaei A, et al. The expression of human leukocyte antigen by human ejaculated spermatozoa. *Mol Genet Genomic Med*. 2019; 7(12): e1005.
- Chi HJ, Kim JH, Ryu CS, Lee JY, Park JS, Chung DY, et al. Protective effect of antioxidant supplementation in sperm-preparation medium against oxidative stress in human spermatozoa. *Hum Reprod*. 2008; 23(5): 1023-1028.
- Regan L, Braude PR, Hill DP. A prospective study of the incidence, time of appearance and significance of anti-paternal lymphocytotoxic antibodies in human pregnancy. *Hum Reprod*. 1991; 6(2): 294-298.
- Bronson RA. Antisperm antibodies: a critical evaluation and clinical guidelines. *J Reprod Immunol*. 1999; 45(2): 159-183.
- Vazquez-Levin MH, Marin-Briggiler CI, Veaute C. Antisperm antibodies: invaluable tools toward the identification of sperm proteins involved in fertilization. *Am J Reprod Immunol*. 2014; 72(2): 206-218.
- Chiu WWC, Chamley LW. Clinical associations and mechanisms of action of antisperm antibodies. *Fertil Steril*. 2004; 82(3): 529-535.
- Scaife PJ, Bulmer JN, Robson SC, Innes BA, Searle RF. Effector activity of decidual CD8(+) T lymphocytes in early human pregnancy. *Biol Reprod*. 2006; 75(4): 562-567.
- Saito S, Nakashima A, Myojo-Higuma S, Shiozaki A. The balance between cytotoxic NK cells and regulatory NK cells in human pregnancy. *J Reprod Immunol*. 2008; 77(1): 14-22.
- Yamanova MV, Salmina AB, Svetlakov AV, Ellinidi VN, Anikeeva NV, Serebrennikova OA, et al. Cytotoxic activity of endometrial immunocompetent cells determines the outcome of embryo implantation. *Bull Exp Biol Med*. 2004; 137(1): 82-85.

# Neuroprotective Effects of Isoquercetin: An *In Vitro* and *In Vivo* Study

Qingxiao Yang, M.M.<sup>1</sup>, Zhichen Kang, M.D.<sup>2</sup>, Jingze Zhang, M.M.<sup>1</sup>, Fuling Qu, M.M.<sup>2</sup>, Bin Song, M.M.<sup>1\*</sup>

1. Neurosurgery Department, Second Hospital of Jilin University, Changchun City, Jilin Province, 130000, China  
2. Rehabilitation Department, Second Hospital of Jilin University, Changchun City, Jilin Province, 130000, China

\*Corresponding Address: Neurosurgery Department, Second Hospital of Jilin University, Changchun City, Jilin Province, 130000, China  
Email: 15526859189m0@sina.cn

Received: 21/August/2019, Accepted: 26/November/2019

## Abstract

**Objective:** Alzheimer's disease (AD) is considered a neurodegenerative disease that affects the cognitive function of elderly individuals. In this study, we aimed to analyze the neuroprotective potential of isoquercetin against the *in vitro* and *in vivo* models of AD and investigated the possible underlying mechanisms.

**Materials and Methods:** The experimental study was performed on PC12 cells treated with lipopolysaccharide (LPS). Reactive oxygen species (ROS), antioxidant parameters, and pro-inflammatory cytokines were measured. In an *in vivo* approach, Wistar rats were used and divided into different groups. We carried out the Morris water test to determine the cognitive function. Biochemical parameters, antioxidant parameters, and pro-inflammatory parameters were examined.

**Results:** The non-toxic effect on PC12 cells was shown by isoquercetin. Isoquercetin significantly reduced the production of nitrate and ROS, along with the altered levels of antioxidants. Isoquercetin significantly ( $P < 0.001$ ) down-regulated proinflammatory cytokines in PC12 cells treated with LPS. In the *in vivo* approach, isoquercetin-treated groups considerably showed the up-regulation in the latency and transfer latency time, as compared with AD groups. Isoquercetin significantly reduced A $\beta$ -peptide, protein carbonyl, while enhanced the production of brain-derived neurotrophic factor (BDNF) and acetylcholinesterase (AChE). Isoquercetin significantly ( $P < 0.001$ ) reduced pro-inflammatory cytokines and inflammatory mediators, as compared with AD groups.

**Conclusion:** Based on the results, we may infer that, through antioxidant and anti-inflammatory systems, isoquercetin prevented neurochemical and neurobehavioral modifications against the model of colchicine-induced AD rats.

**Keywords:** A $\beta$  Peptide, Alzheimer's Disease, Antioxidant, Inflammation, Isoquercetin

Cell Journal (Yakhteh), Vol 23, No 3, August 2021, Pages: 355-365

**Citation:** Yang Q, Kang Zh, Zhang J, Qu F, Song B. Neuroprotective effects of isoquercetin: an in vitro and in vivo study. Cell J. 2021; 23(2): 355-365.  
doi: 10.22074/cellj.2021.7116.

This open-access article has been published under the terms of the Creative Commons Attribution Non-Commercial 3.0 (CC BY-NC 3.0).

## Introduction

Research suggests that age is the key factor for the development of acute and chronic neurodegenerative disorders, such as Alzheimer's (AD), stroke, and Parkinson's (PD) diseases (1). As we know that the aging process occurs on a global scale, the incidence of early mentioned diseases would be expectable in the near future (2, 3). Moreover, the available therapies only decelerate disease progression (2). Basic molecular science suggests that neuronal damage and death are both involved in the molecular mechanism of AD. *In vitro*, *in vivo*, and post-mortem investigations show neuronal death as a result of the activation of common cell death programs, such as apoptosis (3). Previous research suggests that the genetic manipulation or pharmacological interventions of underlying molecular pathways can protect neurons from deadly insults (4). The strategies for the treatment of neurodegenerative disorders are mainly focused on interrupting, antagonizing, or slowing the molecular events, leading to the irreversible injury or death of neurons in neurodegenerative diseases, which are commonly called neuroprotection (5). Nevertheless, poor translation of rodent investigations into clinical

trials has overturned neurologists and provoked hot debates on the reasons for the apparent failure of neuroprotection against neurodegenerative diseases (4).

AD is considered a wide spread neurodegenerative disease, which affects the cognitive function of elderly individuals (6). In the course of AD, cortical neuron damage and disintegration of the hippocampal region cause memory impairment and alter the cognitive capability (4, 6). The 1<sup>st</sup> clinical symptoms of AD is characterized by the demolition of the short-term memory. The pathological hallmark of AD is the presence of senile plaques, triggering the accumulation of  $\beta$ -amyloid proteins, through the deterioration of neurofibrillary tangles and neuronal and other proteins (6).

Amyloid  $\beta$  peptide (A $\beta$ ) has been considered a possible source of oxidative stress during AD (6, 7). It can generate free radicals that contribute to the expansion of toxic effects. Previous studies suggested that A $\beta$ -induced cytotoxicity stimulates the accumulation of intracellular reactive oxygen species

(ROS), finally leading to the peroxidation of membrane lipids and induced cell death. While the mechanism of A $\beta$ -induced cytotoxicity is still unknown, previous investigations indicate that targeting A $\beta$  would be regarded as a significant neuroprotective approach for the treatment and prevention of the onset of AD. Several lines of evidence suggest that antioxidant therapy has beneficial roles in the treatment of the toxic effects related to A $\beta$ -induced oxidative stress (6, 8). Due to the lack of effective treatment for AD, researchers have focused their research on neuroprotective drugs, having antioxidant and anti-inflammatory properties.

Various efforts have been made in the world to explore the possible treatment for AD; however, there is no effective therapy for the cure of AD. Clinical research suggests that most of the AD patients over the age of 65 suffer from the disease; nevertheless, the symptoms can occur at the early stages (6). The aetiology of AD is very complex, and various pathways of neuronal injury have been proposed (9). According to previous studies, the cortex, hippocampus, and limbic system are considered susceptibility regions for the injury (6, 10). Studies showed that A $\beta$  peptide might be a possible source for the induction of oxidative stress in the brain of AD patients (2, 6). It is now known that it can generate free radical agents that participate in the expansion of its side/toxic effects. Research suggests that A $\beta$ -induced cytotoxicity stimulates the intracellular accumulation of neuronal plaques as a result of the generation of oxidative stress, ultimately leading to the peroxidation of lipids and induction of cell death (2, 6). However, the precise mechanism underlying the role of A $\beta$ -induced neurotoxicity is still unclear. The prevention of A $\beta$  accumulation within the brain is one of the significant targets for the potential therapy of AD, as numerous drugs are screened for this ability as to whether they can halt the onset of the disease (4, 9). Consequently, the antioxidant therapy is the best approach for reducing the pathological conditions and side/toxic effects linked with A $\beta$ -induced oxidative stress. Due to the beneficial effects of antioxidant compounds, researchers have devoted themselves to discovering novel phytochemical agents having antioxidant potential to modulate the detrimental effects of A $\beta$ -induced neurotoxicity.

Isoquercetin (quercetin-3-O-b-D-glucopyranoside) is found in various medicinal and culinary crops, including fruits, herbs, and vegetables (11). The anti-allergic, antioxidant, and anti-inflammatory activities of isoquercetin against different rodent models are well documented (12, 13). Paulke et al. (14) showed higher bioavailability of isoquercetin in comparison with quercetin. To the best of our knowledge, the impact of isoquercetin on the prevention of cognitive defects occurring in AD patients has not been studied.

In the current experimental study, we aimed to assess the neuroprotective potential of isoquercetin against the *in vitro* and *in vivo* models of AD to explore the possible mechanism.

## Materials and Methods

### Chemicals

Dulbecco's modified Eagle's medium (DMEM) was procured from the Thermo Fisher Scientific, Inc, Waltham, MA, USA.

### *In vitro* study

#### Cell culture

In this experimental study, the PC12 (phaeochromocytoma) cell line was purchased from the Shanghai Biochemistry Co., Ltd (Shanghai, China). High-glucose DMEM was used for the culture of the cells containing streptomycin (10 U/ml), fetal bovine serum (10%), and penicillin (100 U/ml). The cells were incubated in an incubator at 37°C in a humidified 95% air, 5% CO<sub>2</sub> atmosphere. When the cells reached 80% confluency, they were treated with the trypsin (0.25%) and passaged.

#### Cytotoxicity assay

The method used for the determination of MTT assay was based on a method, as previously described with minor modifications (15). Briefly, the cells were seeded on to the 96-well plate at a density of  $1 \times 10^4$  cells/plate and further incubated at 37°C for 24 hours in a CO<sub>2</sub> chamber. After 24 hours, the medium was changed with a new medium, containing different doses of isoquercetin and incubated for 24 hours. After the incubation period, the medium (containing isoquercetin) was replaced with the MTT (200  $\mu$ l) solution and incubated at 37°C for the next 4 hours. After that the MTT solution was changed with dimethyl sulfoxide (DMSO) to solubilize the formazan crystals and incubation for 20 minutes at 37°C with occasional shaking, the absorbance of samples was read at 570 nm using a microplate reader (Thermo Scientific Multiscan GO, USA) and the cell viability was calculated (%).

#### Nitrite assay

The Griess assay was used for the determination of nitrite in accordance with a previously described method with minor modifications (16). Briefly, the cell supernatant (100  $\mu$ L) was mixed with the Griess reagent (100  $\mu$ L), containing naphthylethylenediamine (0.01%), p-aminobenzenesulphonamide (1%) in phosphoric acid (2.5% v/v) and kept the reaction mixture in the darkroom for 20 minutes. Finally, the optical absorbance was recorded at 570 nm using a microplate reader.

### Estimation of reactive oxygen species generation

The Nitro Blue Tetrazolium (NBT) assay was applied for the measurement of ROS (16). Briefly, the cells were incubated with NBT and various concentrations of isoquercetin for 2 hours in the 96-well plates. The formazan crystals were solubilised using 2 M KOH (freshly prepared) in DMSO, and finally, the absorbance of specimens was monitored at 630 nm using a microplate reader.

### The concentration of malondialdehyde

The concentration of malondialdehyde (MDA) was assayed, as previously described, with minor modifications (17). Briefly, the cells were seeded in a 6-well plate at a density of  $4 \times 10^5$  cells/well and treated with different concentrations of isoquercetin for 24 hours. Next, the cells were washed with the ice-cold phosphate buffer saline phosphate buffer saline (PBS) and scrapped in a sodium phosphate solution containing Triton-X (0.1%). The cells were lysed and finally centrifuged at 10,000 g for 10 minutes. Afterward, the resulting pellet was discarded, and the supernatant was collected. The cell supernatant (100  $\mu$ L) was mixed with trichloroacetic acid (TCA, 10% w/v) and thiobarbituric acid (TBA, 0.67% w/v) and kept at 95°C for 1 hour. Then, the solution was quickly cooled and mixed with n-butanol-pyridine (15:1) and centrifuged for 10 minutes at 400 g. The upper layer (pink) was collected, and the absorbance was read at 532 nm using a microplate reader.

### Determination of glutathione

Indirect estimation of oxidative injury, reduced glutathione (GSH) level was determined (17). Briefly, PC12 cells at a density ( $4 \times 10^5$  cells/well) were propagated into 6-well plates and incubated at 37°C for 24 hours in the CO<sub>2</sub> chamber. Afterward, the cells were treated with the different concentrations of isoquercetin and washed with the ice-cold PBS and scrapped in sodium phosphate buffer containing Triton-X (0.1%). For the removal of proteins, the cells were lysed (100  $\mu$ L) via adding trichloroacetic acid (10%) and again incubated at 4°C for 1 hours and finally centrifuged at 5000g rpm for 5 minutes. After that, PBS (100  $\mu$ l) and DTNB (50  $\mu$ l) were mixed in the above supernatant (75  $\mu$ l) and finally estimated the absorbance at 412 nm after the 10 minutes.

### Catalase estimation

The method employed for the measurement of the catalase (CAT) enzyme activity was previously described, with minor modifications (17, 18). Briefly, the cell lysate was mixed into the hydrogen peroxidase (H<sub>2</sub>O<sub>2</sub>) phosphate buffer solution in an Eppendorf tube, which was further vortexed and incubated at 37°C for 3-5 minutes. After that, the resulting solution was

mixed with the dichromic acetate solution and kept for 10 minutes at 100°C. After that, the reaction mixture was cooled down using the tap water and centrifuge at 2500 g rpm for 5 minutes and the absorbance of specimens was read at 570 nm.

### Superoxide dismutase activity

The method employed for the measurement of the superoxide dismutase (SOD) enzyme activity was previously described, with minor modifications (16-18). Briefly, cell lysates (100  $\mu$ M) was mixed with Tris buffer (1 ml). After that, pyrogallol was mixed, and the absorbance of the samples was read at 420 nm using a microplate reader for 5 minutes at a time interval of 1 minute. Finally, the activity of the SOD enzyme was reported as the percentage of inhibition of pyrogallol auto-oxidation.

### *In vivo* study

#### Experimental animals

Swiss Wistar rats (150-180 g, either both sex) were used for the current protocol. The rats were kept in the polyethylene cages and kept standard laboratory conditions, such as temperature ( $22 \pm 2^\circ\text{C}$ ), relative humidity (45-75%), and light/dark cycle (12/12 hours). The rats received the standard food pellets and water ad libitum. All the protocol was approved by The Institutional Ethical Committee (SHJU/19/01/05).

#### Experimental protocols

For the AD, the rats were grouped into the following groups, and each group had 12 animals as follows;

Normal control group rats (received vehicle only): group I

AD control received colchicine (15  $\mu$ g/5  $\mu$ l icv): group II

AD control received colchicine (15  $\mu$ g/5  $\mu$ l icv) and Isoquercetin (10 mg/kg): group III

AD control received colchicine (15  $\mu$ g/5  $\mu$ l icv) and Isoquercetin (20 mg/kg): group IV

AD control received colchicine (15  $\mu$ g/5  $\mu$ l icv) and Isoquercetin (40 mg/kg): group V

AD control received colchicine (15  $\mu$ g/5  $\mu$ l icv) and Memantine HCL (10 mg/kg): group VI

The rats were intracerebroventricularly infused with either artificial cerebrospinal fluid. Post-operative procedures or colchicine (15 Ig) mixed in the ACSF. After that, the animals were further used for the determination of neurobehavioral and neuro-chemical parameters (19).

#### Post-operative procedures

After the surgery, the rats were kept in the aseptic condition and received the standard diet (water and food), and the animals were treated with 5 mg/kg

gentamicin (intraperitoneal injection) for the next three days to prevent the sepsis.

### Morris maze test

Morris maze test was used for the estimation of behavioural effect using the previous method with minor modifications (19). Briefly, a circular pool (180 cm in diameter and 60 cm in height) was used for the Morris maze test. The circular pool filled with the water and the entire experimental animal put into quadrants during the acquisition and retention phase (19, 20).

### Probe trial

For the probe trial, on the last day of training, the platform was removed from the pool, and experimental rats were left free to swim in the pool for the next 2 minutes (19). The time interval of the experimental animal reached the target quadrant was compared to other groups, and the data were shown as the latency time  $\pm$  standard error means (SEM).

### Passive avoidance paradigm

The main purpose of the passive avoidance paradigm is determination the learning and memory capacity of the experimental animals (19). Briefly, the experimental rats were kept in the shuttle box, having 2 compartments (one for the light, while another for the dark) and unglued with a guillotine door. During the experiment, the rodent kept for 30 seconds in the light chamber and the next open a guillotine door and finally the experimental rodent were transferred into the dark chamber, and finally, closed the door for the next 10 seconds.

### Neurochemical parameters

At the end of the experimental study, the neurochemical parameters, including protein carbonyl, acetylcholine esterase were estimated using the previously published literature with minor modifications (19).

### Antioxidant parameters

Antioxidant enzymes viz., CAT, GSH, lipid peroxidation (LPO) and SOD were estimated in the hippocampus via using the previously reported literature (19, 21).

### Inflammatory mediators

Pro-inflammatory cytokines like interleukin-1 $\beta$  (IL-1 $\beta$ ), IL-6 and tumour necrosis factor- $\alpha$  (TNF- $\alpha$ ) and inflammatory mediator including nuclear transcription factor (NF- $\kappa$ B), was estimated using standard kits.

### Statistical analysis

One-way analysis of variance (ANOVA) was used for the determination of statistical significance. The difference between the examined and control cells was analysed

using the post hoc Newman-Kuels test, and the values are presented as mean  $\pm$  SEM.  $P < 0.05$  was considered as a statistically significant value.

## Results

### Effect of isoquercetin on cell viability

Figure 1 exhibited the effect of isoquercetin on cell viability. Figure 1 exhibited that the isoquercetin 100  $\mu$ M was found to be non-toxic as they did not induce any considerable alteration in the growth of PC12 cells. Moreover, isoquercetin dose up to 100  $\mu$ M exhibited a sign of cytotoxicity with considerable change. Accordingly, isoquercetin at a dose range of 25-100  $\mu$ M is a safe drug and can be used for further experimental analyses.

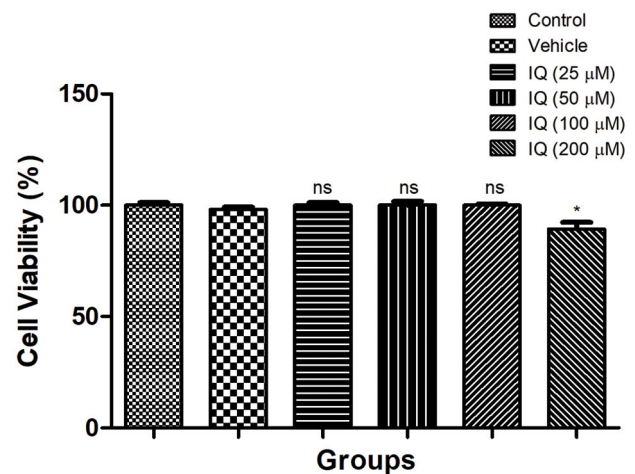


**Fig.1:** The cell viability effect of isoquercetin on P12 cells. ns; Non significant, IQ; Isoquercetin, and \*,  $P < 0.05$ .

### Effect of isoquercetin on lipopolysaccharide induced nitrosative stress

It is well known that during the oxidative stress increased the nitrosative stress due to the generation of free radicals. A similar result was found in the current experimental study. PC12 cells were treated with lipopolysaccharide (LPS, 100 ng/mL) and showed the increased level of nitrite released into the supernatant (24 hours) as compared to the control. Isoquercetin treatment significantly ( $P < 0.05$ ) reduced the release of nitrite into the supernatant in a dose-dependent manner as compared to the LPS-stimulated cells (Fig.2A).

### Effect of isoquercetin on lipopolysaccharide induced reactive oxygen species level

During AD, the ROS level considerably increased due to the generation of free radicals. PC12 cells treated with the LPS (100 ng/mL) considerably ( $P < 0.001$ ) boosted the production of ROS as compared to the normal cells. The concentration-dependent

treatment of isoquercetin significantly ( $P < 0.001$ ) down-regulated the production of ROS as compared to the LPS treated cells (Fig.2B).

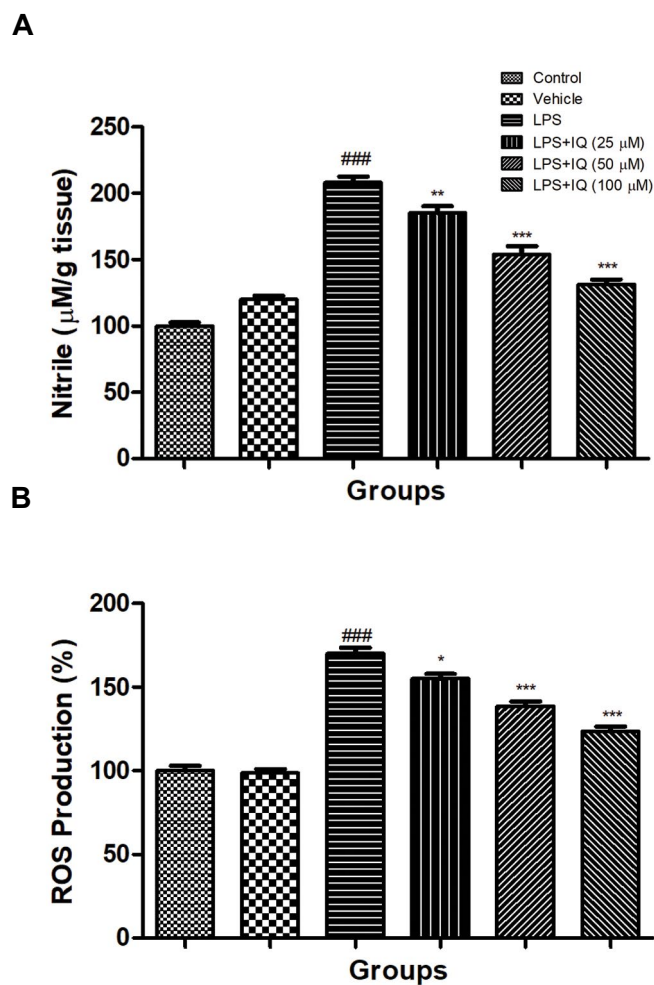


**Fig.2:** Effect of isoquercetin on the LPS induced nitrite and ROS activity in PC12 cells. **A.** Nitrite and **B.** ROS as described in the material and methods. Values are presented as mean  $\pm$  SEM. ### showed the significance as compared to the control group ( $P < 0.001$ ). \* demonstrates the significance as compared to LPS-induced group (\*;  $P < 0.05$ , \*\*;  $P < 0.01$ , and \*\*\*;  $P < 0.001$ ). LPS; Lipopolysaccharide, IQ; Isoquercetin, and ROS; Reactive oxygen species.

**Effect of isoquercetin on lipopolysaccharide induced antioxidant enzymes**

LPS (100 ng/mL) treatment demonstrated the increased level of MDA as compared to healthy control cells. Isoquercetin treatment significantly ( $P < 0.001$ ) decreased the level of MDA as a dose-dependent manner as compared to LPS control cell lines (Fig.3A).

In the level of SOD, CAT and GSH, LPS (100 ng/mL) treatment significantly ( $P < 0.001$ ) showed the reduced level as compared to normal cell lines, and the concentration-dependent treatment of isoquercetin exhibited the increased level of SOD (Fig.3B), CAT (Fig.3C) and GSH (Fig.3D) as compared to the LPS control cell lines.

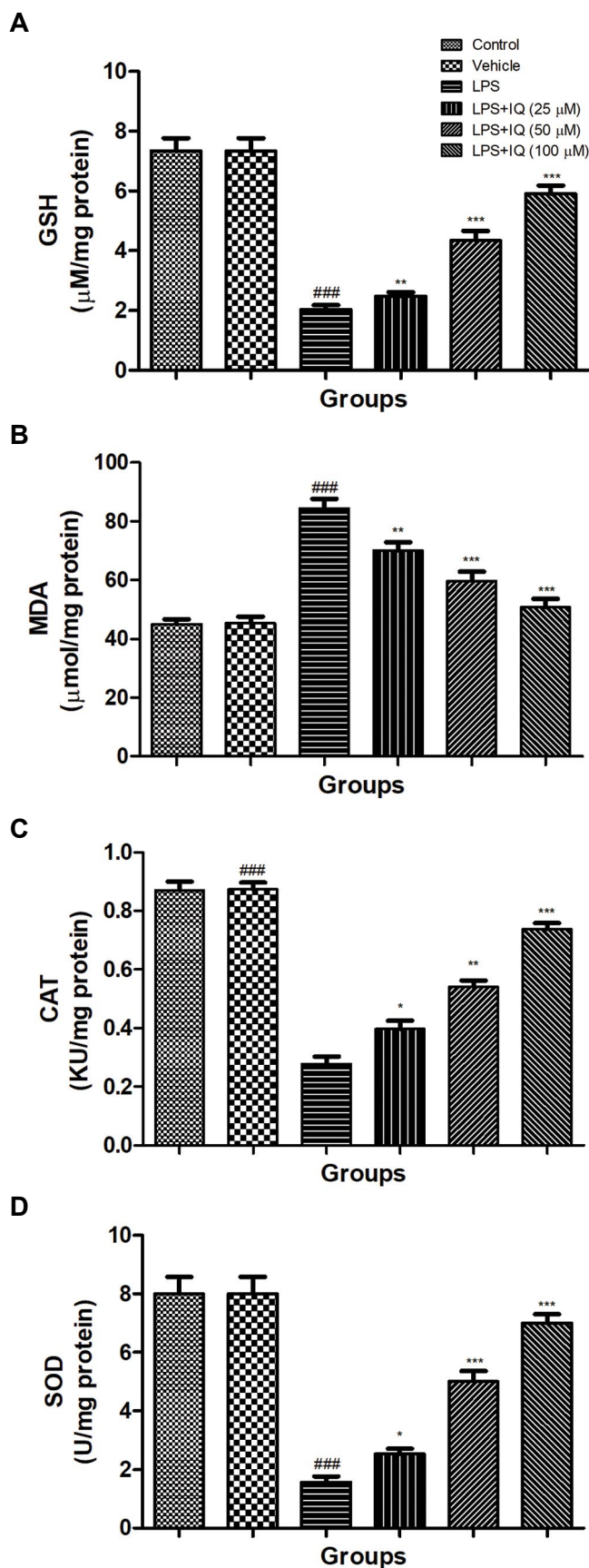


**Fig.3:** Effect of isoquercetin on the LPS induced antioxidant activity in PC12 cells. **A.** GSH, **B.** MDA, **C.** CAT and **D.** SOD as described in the material and methods. Values are presented as mean  $\pm$  SEM. ### showed the significance as compared to the control group ( $P < 0.001$ ). \* demonstrates the significance as compared to LPS-induced group (\*;  $P < 0.05$ , \*\*;  $P < 0.01$ , and \*\*\*;  $P < 0.001$ ). LPS; Lipopolysaccharide, GSH; Glutathione, MDA; Malondialdehyde, CAT; Catalase, SOD; Superoxide dismutase, and IQ; Isoquercetin.

### Effect of isoquercetin on lipopolysaccharide induced pro-inflammatory cytokines

Figure 4 showed the effect of isoquercetin and LPS on the pro-inflammatory cytokines on the PC12 cells. LPS (100 ng/mL) showed the significantly ( $P < 0.001$ ) increased the level of pro-inflammatory cytokines such as IL-1 $\beta$ , IL-6, IL-8, and TNF- $\alpha$  as compared to the control cell lines. The dose-dependent treatment of isoquercetin significantly ( $P < 0.05$ ) reduced the level of pro-inflammatory cytokines, including IL-1 $\beta$  (Fig.4A), IL-6 (Fig.4B), IL-8 (Fig.4C) and TNF- $\alpha$  (Fig.4D) as compared to the LPS induced control cell lines.

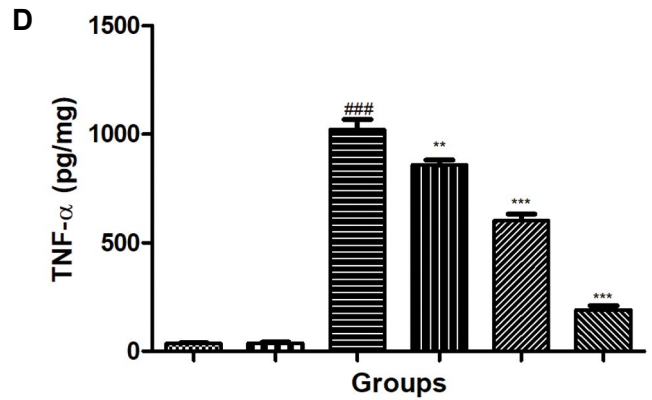
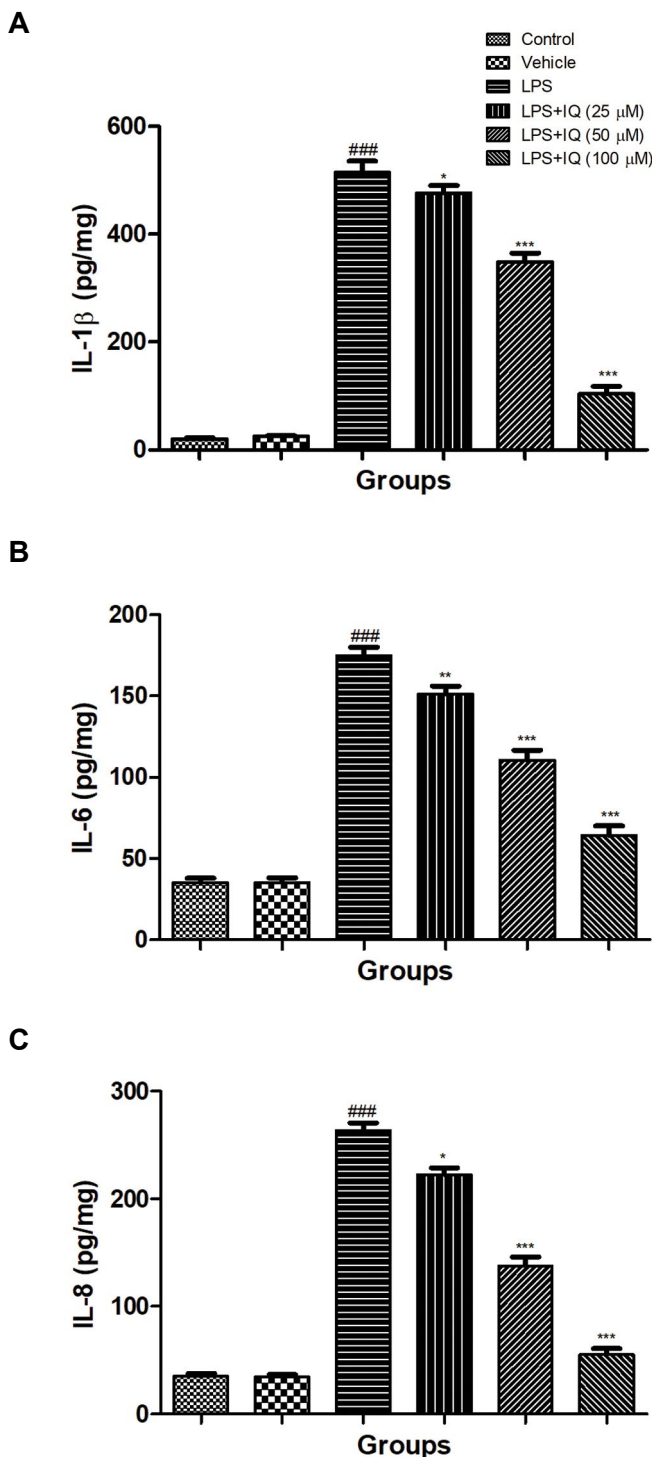


**Fig.4:** Effect of isoquercetin on the LPS induced pro-inflammatory cytokines parameter in PC12 cells. **A.** IL-1 $\beta$ , **B.** IL-6, **C.** IL-8 and **D.** TNF- $\alpha$  as described in the material and methods. Values are presented as mean  $\pm$  SEM. ### showed the significance as compared to the control group ( $P < 0.001$ ). \* demonstrates the significance as compared to LPS-induced group (\*;  $P < 0.05$ , \*\*;  $P < 0.01$ , and \*\*\*;  $P < 0.001$ ). LPS; Lipopolysaccharide, IQ; Isoquercetin, IL-8; Interleukin-8, and TNF- $\alpha$ ; Tumor necrosis factor- $\alpha$ .

### Time spent in the platform quadrant

The probe trial data analysis was performed in experimental rats. Colchicine-treated rats exhibited a significantly decreased latency towards the target quadrant as compared with the spend time by the control group. Moreover, such down-regulation in the time spent in the quadrant was enhanced upon the treatment with isoquercetin in a dose-dependent manner. A similar results were obtained in the memantine-treated group (Fig.5).

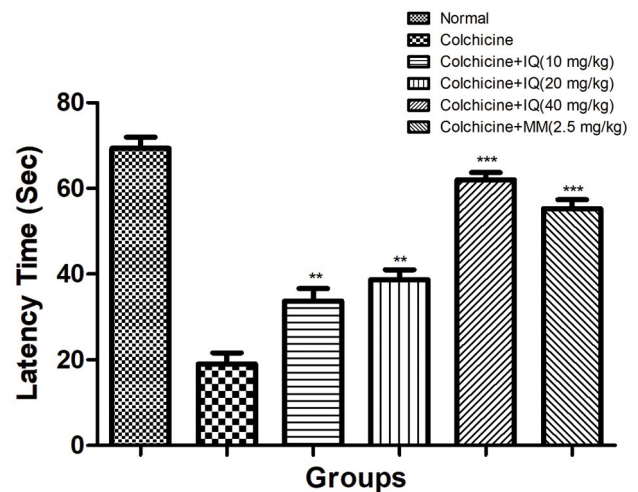


**Fig.5:** Effect of isoquercetin on the colchicine impaired spatial memory and learning in rats appraises via probe trial in water maze; data shows mean  $\pm$  SEM of 6 rats in each group. Significant difference represent as compared to colchicine control group rats (\*\*;  $P < 0.01$  and \*\*\*;  $P < 0.001$ ). IQ; Isoquercetin and MM; Memantine.

### Effect of isoquercetin on memory and learning via passive avoidance paradigm

The passive avoidance paradigm was used for the estimated effect of isoquercetin on the memory and

learning capacity of the rats. Colchicine induced rats exhibited brain damage as compared to the control group rats. Figure 6 showed that the reduced transfer latency time as compared to the acquisition trial transfer latency time from the control group to the colchicine-treated group (3<sup>rd</sup> retention trial). The isoquercetin-treated group exhibited the increased transfer latency time as compared with the acquisition trial. On the other hand, the standard drug-treated group showed the increased transfer latency time as compared to the acquisition trial. Moreover, instantaneous isoquercetin received rats exhibited a significant enhance in TLT in retention trials in comparison with the acquisition trial transfer latency time.

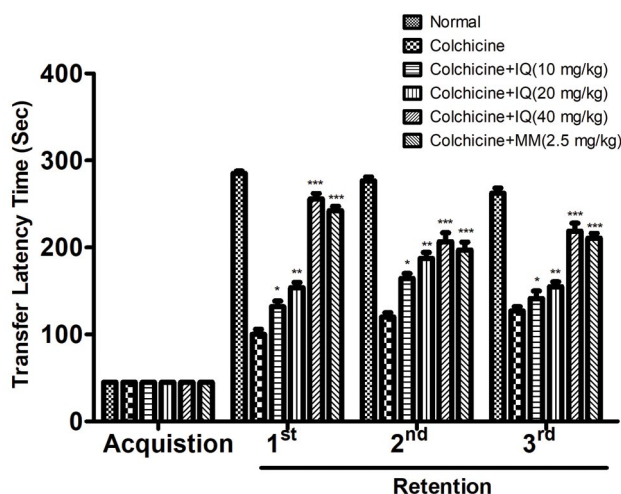


**Fig.6:** showed the effect of isoquercetin and colchicine on passive avoidance response; data shows mean  $\pm$  SEM of 6 rats in each group. Significant difference represent as compared to colchicine control group rats (\*,  $P < 0.05$ , \*\*,  $P < 0.01$ , and \*\*\*,  $P < 0.001$ ). IQ; Isoquercetin and MM; Memantine.

### Effect of isoquercetin on brain-derived neurotrophic factor

Figure S1 (See Supplementary Online Information at [www.celljournal.org](http://www.celljournal.org)) showed the effect of isoquercetin on the level of brain-derived neurotrophic factor (BDNF) in colchicine induced group rats. Colchicine induced group rats exhibited a reduced level of BDNF in comparison to normal control. Colchicine-induced group exhibited a significantly ( $P < 0.001$ ) increased level of BDNF in a dose-dependent manner. On the contrary, Memantine significantly ( $P < 0.001$ ) enhanced the level of BDNF, but the level was slightly lower as compared to the isoquercetin (40 mg/kg) treated drugs.

### Effect of isoquercetin on A $\beta$ peptide activity

During the colchicine induced AD, the level of A $\beta$  peptide activity considerably boosted and reached almost 2-3 times as compared to the normal control. A similar result was obtained in the colchicine induced treated group rats. The level of A $\beta$  peptide activity reached almost 4 times more as compared to normal control. The dose-dependent treatment of isoquercetin treatment significantly ( $P < 0.001$ ) down-

regulated the level of A $\beta$  peptide activity as compared to the colchicine induced group rats. Standard drug (memantine) treated group rats showed the reduced level of A $\beta$  peptide activity as compared to the colchicine induced group rats (Fig.S2) (See Supplementary Online Information at [www.celljournal.org](http://www.celljournal.org)).

### Effect of isoquercetin on acetylcholinesterase activity

Figure S3 (See Supplementary Online Information at [www.celljournal.org](http://www.celljournal.org)) demonstrated the effect of isoquercetin on the level of acetylcholinesterase (AChE) on the colchicine induced group rats. Colchicine-induced group showed the reduced activity of AChE, while the dose-dependently treatment of isoquercetin and standard drug (memantine) significantly ( $P < 0.001$ ) increased the activity of AChE.

### Effect of isoquercetin on P. carbonyl activity

Figure S4 (See Supplementary Online Information at [www.celljournal.org](http://www.celljournal.org)) illustrated the effect of isoquercetin on the level of P. carbonyl activity. Colchicine induced group rats showed the increased activity of P. carbonyl activity and dose-dependently treatment of isoquercetin and standard drug (memantine) significantly ( $P < 0.001$ ) decreased the activity of P. carbonyl activity.

### Effect of isoquercetin on pro-inflammatory cytokines

Figure S5 (See Supplementary Online Information at [www.celljournal.org](http://www.celljournal.org)) showed the effect of isoquercetin on the level of pro-inflammatory cytokines in the colchicine induced AD rats. Colchicine induced group rats showed an increased level of pro-inflammatory cytokines, such as TNF- $\alpha$ , IL-1 $\beta$ , and IL-6 and dose-dependent treatment of isoquercetin significantly ( $P < 0.001$ ) reduced the level of pro-inflammatory cytokines.

### Effect of isoquercetin on NF- $\kappa$ B activity

The level of NF- $\kappa$ B considerably boosted during AD. A similar result was obtained in the colchicine induced AD control group rats. The dose-dependent treatment of isoquercetin significantly ( $P < 0.001$ ) reduced the level of NF- $\kappa$ B as compared to the colchicine induced AD control group rats (Fig.S6) (See Supplementary Online Information at [www.celljournal.org](http://www.celljournal.org)).

## Discussion

In the year of 1976, PC12 cell lines have been considered as the significant model system for neurochemical and neurobiological investigations, as its adaptability, comfort culture, and huge information of their differentiation and proliferation (19). In the current investigation, we used the PC12 cells to investigate the neuroprotective effect of isoquercetin. In an *in vitro* model, PC12 cells were treated with the LPS, which is commonly present in the Gram-Negative bacteria membrane (22). By scrutinizing the apoptosis, cell viability, antioxidant and pro-inflammatory cytokines, we established the cell model of LPS was successfully constructed (23). It is well defined that

oxidative stress plays an important mechanism underlying PC12 induced neurotoxicity during AD (24). Consequently, targeting oxidative stress is the best approach to treat AD. In the current experimental study, we established the LPS induced oxidative model in the PC12 cells. LPS significantly increased the level of MDA (LPO parameter) and intracellular formation of ROS and reduced the levels of SOD, CAT in the PC12 cells as compared with the non-stimulated cells, approaching the pathophysiological condition of oxidative stress during the central nervous system (CNS) disorders. Isoquercetin treatment significantly reduced the intracellular ROS generation, MDA level, and nitrite release and increased the activity of SOD, GSH, and CAT, suggesting the antioxidant role and maintain the intracellular oxidative stress and consequent neuroprotection. On the basis of the results, isoquercetin could be useful for the treatment of neuro-inflammatory diseases like AD, multiple sclerosis, PD etc.

Neurodegenerative disease such as AD is considered as the age-related disease (25). It is related to the early phase of cognitive dysfunction linked with behavioural and social deterioration. The feature of AD is extracellular senile plaques, loss of neurons, intracellular neurofibrillary in the region of brain, such as hippocampus region (6). Previous research suggests that the hippocampus region of the brain is the primary target, which involved in AD pathophysiology (6, 9). It is well known that the accumulation of  $\beta$  amyloid and the generation of amyloid plaques are the hallmarks of AD (6, 26). In the current protocol, we made an attempt to scrutinize the neuroprotective effect of isoquercetin against the *in vitro* and *in vivo* model of AD and explore the possible mechanism of action.

For the learning and memory impairment, colchicine induced AD model is commonly used (27). Colchicine induced the dysfunction in various parts of the brain, especially when inducing the severity into the hippocampus region of the brain. It is well known that the level of AChE was reduced during the impaired learning and memory capacity of rodents (28). A similar result was found in the colchicine-induced group; a marked reduced AChE content was observed, while the dose-dependent treatment of isoquercetin significantly increased the AChE content and suggests the memory and learning improvement. Previous research suggests that the marked increase in the activity of AChE and decrease the activity of choline acetyltransferase showed a reduced level of Ach (29). Various experimental study suggests that the decreased level of AChE activity, indicating the impairment of cognitive function and improved the activity of AChE suggests the increase cognitive function (27). Other parameters such as A $\beta$  start the deposition during the AD in the cerebral area of the brain, and it induces the memory dysfunction with marked cholinergic function (30) bisdemethoxycurcumin and demethoxycurcumin. During AD, the accumulation of A $\beta$  considerably increased and induced memory dysfunction. In the current experimental study, the content of A $\beta$  was

considerably boosted and dose-dependent treatment of isoquercetin significantly reduced the content of A $\beta$ . A similar momentum was observed in the memantine induced group rats.

Previous research suggests that the colchicine administration exhibit the dose- and time-dependent behavioural, neurochemical, anatomical changes, and the changes reached up within 2-3 weeks (27). Colchicine (tubulin inhibitor), avoids microtubule assembly inducing synaptic loss and neurofibrillary degeneration that take part in the diminishing of intracellular trafficking of neurotrophic factors, oxidative stress, inflammation, and axonal excitotoxicity (31). Colchicine also disrupts the cytoskeleton that has to be linked with the neurodegeneration in AD and also executing a deadly effect on the activity and persistence of neurons (19). Meanwhile, colchicine administration does not produce a significant alteration in the gross locomotor and behavioural activities in rats. The current experimental study showed that the open field did not show higher scores for the locomotor and behavioural activities in each rat.

Previous research suggests that the BDNF is the main target in the pathophysiology of various neurodegenerative diseases (19). BDNF is considering as the prognostic and diagnostic biomarker of AD. During the AD, the level of BDNF considerably reduced in the rodent model when treated with colchicine, and it might take part in the reduction of the hippocampus region of the brain linked with the age-related memory decline in the late adulthood (32). Studies suggest that the BDNF gene is related to the late onset of AD. To identify the pathophysiology of the neurodegenerative disease, the rodent model is the crucial tool, and most of researchers used the animal models for elucidation of the neurological disease pathophysiology (33, 34). One of these experimental models, central injection of colchicine, was injected into the lateral ventricles, which is measured as appropriate cases of sporadic dementia of Alzheimer's in humans. During the AD, the level of BDNF was considerably reduced in the hippocampal tissue as compared to the untreated rats and dose-dependently treatment of isoquercetin significantly increased the level of BDNF suggesting the neuroprotective effect via neurotrophin induction. Therefore, the ultimate goal of the current study was elucidating the possible neuroprotective effect of isoquercetin in the animal model of AD disease and explore the possible underlying mechanism.

During the inducing the colchicine intracerebroventricular (icv), its start the reduction of BDNF level into the hippocampal tissue, decreased the level of A $\beta$  peptide level into the hippocampal tissue as well as down-regulated the antioxidant enzymes, these parameter suggesting that the colchicine injection deteriorates the memory and learning ability (34, 35) and its also induces the oxidative stress, boost the inflammatory reaction as well as induces the injury in the central neuronal. Restoration of these enzymes and parameters via isoquercetin suggesting

the neuroprotective effect via enhancing the cognitive function. Definitely, this current experimental study showed the significant memory dysfunction in the Morris water maze test, as confirmed by considerably enhanced the initial acquisition latency, as well as 1<sup>st</sup> and 2<sup>nd</sup> retention latencies.

Previous research suggests that the oxidative stress play a significant role in the expansion of AD (34, 35). Various studies suggest that oxidative stress related to ROS generation and take widely precipitation during the neurological and psychiatric disorder. During the induction of oxidative stress, frequently observed the imbalance between the pro-oxidant and endogenous antioxidant and its can be estimated via measured the redox state in the plasma. Endogenous antioxidant parameters such as SOD, CAT and GSH play a significant role to scavenge the free radicals (35, 36). During the colchicine induced AD, the level of free radical increase due to the induction of oxidative stress and reduced the level of endogenous antioxidant mechanism via increased the peroxidation (36, 37). CAT and SOD are considered as the first line antioxidant and both endogenous antioxidants scavenge the free radical especially the hydroxyl radicals (37, 38). Another antioxidant malonaldehyde (MDA) is the marker of lipid peroxidation and its take part in the oxidative stress and its also consider as the end product of the polyunsaturated fatty acid (PUFA) lipid peroxidation. The level of MDA significantly increased during the oxidative stress and its consider as the significant marker to estimate the oxidative stress throughout the body (37). During the experimental protocol, colchicine induced AD rats showed the increased level of MDA and isoquercetin significantly reduced the level of MDA at dose dependent manner. In the current protocol, the up-regulation of MDA and protein carbonyls level and down-regulation of CAT, GSH and SOD level were observed and dose dependent treatment of isoquercetin significantly reduced the level of MDA, protein carbonyls and increased the level of CAT, GSH and SOD, which suggest the reduction of oxidative stress in the brain. Result suggests the neuroprotective effect of isoquercetin via antioxidant nature.

Another factor of AD pathogenesis, inflammatory, and oxidative stress may take part in the expansion of the disease. The presence of the NF- $\kappa$ B was the first time recognized in the nuclear B cell. NF- $\kappa$ B is the significant transcription factor, which contributes to the activation of genes that are involved in the generation of pro-inflammatory cytokines and induces neuroinflammation in AD. Several references suggest that the NF- $\kappa$ B, having the ability to merge the sequence-specific enhances of the immunoglobulins K light chain gene. During the generation of AD, the NF- $\kappa$ B level was increased in the senile plaques. Various research suggests that the activation of NF- $\kappa$ B and NF- $\kappa$ Bp65 either directly or indirectly associated with the severity of AD and targeting the NF- $\kappa$ B is the best approach to treat AD. Isoquercetin already reported to reduce the NF- $\kappa$ B activation in the tumour cells and also induce the anti-inflammatory effect

via suppressing the NF- $\kappa$ B activation in the lymphocytes (32). NF- $\kappa$ B activates pro-inflammatory cytokines such as IL-1 $\beta$ , IL-6, and TNF- $\alpha$ , which take part in the expansion or progression of inflammatory disease. It is well documented that neuro-inflammation play a crucial role in the expansion of neurodegenerative diseases, such as AD. Neuro-inflammation is involved in the microglial cells activation and also takes part in the participation of astrocytes and neurons. Recent research suggests that the pro-inflammatory cytokines such as IL-1 $\beta$ , IL-6, and TNF- $\alpha$  activate neuroinflammation and start the cognitive function destruction (27). Previous research suggests that the continuous generation of pro-inflammatory cytokines leads to the impairment of cognitive function in the brain. TNF- $\alpha$ , secrete from the plaques during the AD disease and also boost the secretion of IL-1 $\beta$  from the central nervous system. The up-regulation of IL-1 $\beta$  level in the hippocampus region showed the interfering of long-term potentiating that induce cognitive impairment (21, 26, 27). It also induced the suppression of the long-term potentiating, inducing the synaptic plasticity dysfunction in the hippocampus region of the brain. IL-1 $\beta$  also reduces the level of BDNF, which is indirectly reduced by LTP and also causes cognitive dysfunction. It is well documented that enhanced levels of pro-inflammatory cytokines, such as TNF- $\alpha$  and IL-1 $\beta$  in the hippocampus region of the brain are responsible for the dysfunction of postoperative cognitive (8). In the current protocol, isoquercetin significantly reduced the level of pro-inflammatory cytokines and suggestion the anti-inflammatory effect.

Previous research suggests that oxidative stress plays a significant role in the expansion of AD. Various studies suggest that oxidative stress and ROS generation are evident during the neurological and psychiatric disorders. Continuous generation of oxidative stress can induce apoptosis and cell death. During the induction of oxidative stress, frequently observed the imbalance between the pro-oxidant and endogenous antioxidants, and it could be estimated via measuring the redox state in the plasma. CAT and SOD are considered the first-line antioxidants, and the both endogenous antioxidants scavenge the free radicals, especially hydroxyl radicals (37, 38). The endogenous antioxidants, such as SOD, CAT, and GSH play a significant role in scavenging the free radicals (39, 40). During colchicine-induced AD, the level of the free radicals are increased due to the induction of oxidative stress and reduced the level of the endogenous antioxidant mechanism via increasing the peroxidation (38, 39). Another antioxidant MDA is the marker of lipid peroxidation, and it participates in oxidative stress, and it is also considered the end-product of the polyunsaturated fatty acid (PUFA) lipid peroxidation. The level of MDA significantly increased during the oxidative stress and it is considered a significant marker to estimate oxidative stress throughout the body (27). During the experimental protocol, colchicine-induced AD showed an increased level of MDA, while isoquercetin significantly reduced the level of MDA in a dose-dependent manner. In the current protocol, the up-regulation of MDA and protein

carbonyls level and down-regulation of CAT, GSH, and SOD level were observed. The dose-dependent treatment of isoquercetin significantly reduced the level of MDA, protein carbonyls, and it increased the level of CAT, GSH, and SOD, suggesting the reduction of oxidative stress in the brain. The results suggest the neuroprotective effect of isoquercetin via antioxidant nature.

## Conclusion

Isoquercetin did not demonstrate the impact of cell viability on the PC12 cells. PC12 cells treated with LPS had increased nitrile, and ROS levels, and the dose-dependent isoquercetin treatment reduced the level of oxidative stress. The dose-dependent treatment of isoquercetin significantly altered the antioxidant, and pro-inflammatory parameter. Colchicine decreased the latency period and significantly increased the latency time and dose-dependent treatment of isoquercetin in the *in vivo* experimental study. Colchicine-induced group rats decreased levels of BDNF and AchE, while significantly increased levels of A $\beta$ -peptide, P. carbonyl and dose-dependent isoquercetin treatment increased levels of BDNF, AchE and decreased levels of A $\beta$ -peptide, P. carbonyl. Colchicine-induced group rats increased the level of pro-inflammatory cytokines and inflammatory mediators and significantly reduced the level of pro-inflammatory cytokines and inflammatory mediators through dose-dependent isoquercetin treatment. The result showed that isoquercetin significantly altered cognitive function and prevented neurochemical and neurobehavioral alteration against colchicine by inducing rats of AD through the antioxidant and anti-inflammatory mechanism.

## Acknowledgments

This work was financially supported by the Second Hospital of Jilin University, Changchun City, China. The authors declare no conflict of interest.

## Authors' Contributions

Q.Y., Z.K.; Performed the experimental study. Q.Y., Z.K., J.Z., F.Q., B.S.; Analyzed the biochemical data. All the authors equally contributed to the proof reading of the manuscript.

## References

1. Staekenborg SS, Koedam ELGE, Henneman WJP, Stokman P, Barkhof F, Scheltens P, et al. Progression of mild cognitive impairment to dementia contribution of cerebrovascular disease compared with medial temporal lobe atrophy. *Stroke*. 2009; 40(4): 1269-1274.
2. Alzheimer's Association. 2016 Alzheimer's disease facts and figures. *Alzheimer's Dement*. 2016; 12(4): 459-509.
3. Kalaria RN. The role of cerebral ischemia in Alzheimer's disease. *Neurobiol Aging*. 2000; 21(2): 321-330.
4. Wyss-Coray T, Mucke L. Inflammation in neurodegenerative disease - A double-edged sword. *Neuron*. 2002; 35(3): 419-432.
5. Xiang HF, Cao DH, Yang YQ, Wang HQ, Zhu LJ, Ruan BH, et al. Isoflurane protects against injury caused by deprivation of oxygen and glucose in microglia through regulation of the toll-like receptor 4 pathway. *J Mol Neurosci*. 2014; 54(4): 664-670.
6. Barragán Martínez D, García Soldevilla MA, Parra Santiago A, Tejero Martínez J. Alzheimer's disease. *Med*. 2019; 12(74): 4338-4346.
7. Hardy JA, Higgins GA. Alzheimer's disease: The amyloid cascade hypothesis. *Science*. 1992; 256(5054): 184-185.
8. Wang L, Jin G, Yu H, Li Q, Yang H. Protective effect of Tenuifolin against Alzheimer's disease. *Neurosci Lett*. 2019; 705: 195-201.
9. Frank H, Zilker T, Kirchmair M, Eyer F, Haberl B, Tuerkoglu-Raach G, et al. Acute renal failure by ingestion of cortinari species confounded with psychoactive mushrooms: a case series and literature survey. *Clin Nephrol*. 2009; 71(5): 557-562.
10. Rao AT, Degnan AJ, Levy LM. Genetics of Alzheimer disease. *AJNR Am J Neuroradiol*. 2014; 35(3): 457-458.
11. Zhang R, Yao Y, Wang Y, Ren G. Antidiabetic activity of isoquercetin in diabetic KK -Ay mice. *Nutr Metab (Lond)*. 2011; 8: 85.
12. Jayachandran M, Zhang T, Ganesan K, Xu B, Chung SSM. Isoquercetin ameliorates hyperglycemia and regulates key enzymes of glucose metabolism via insulin signaling pathway in streptozotocin-induced diabetic rats. *Eur J Pharmacol*. 2018; 829: 112-120.
13. Wang CP, Li JL, Zhang LZ, Zhang XC, Yu S, Liang XM, et al. Isoquercetin protects cortical neurons from oxygen-glucose deprivation-reperfusion induced injury via suppression of TLR4-NF-kB signal pathway. *Neurochem Int*. 2013; 63(8): 741-749.
14. Paulke A, Eckert GP, Schubert-Zsilavecz M, Wurglics M. Isoquercitrin provides better bioavailability than quercetin: Comparison of quercetin metabolites in body tissue and brain sections after six days administration of isoquercitrin and quercetin. *Pharmazie*. 2012; 67(12): 991-996.
15. Dos Santos GC, Mendonça LM, Antonucci GA, Dos Santos AC, Antunes LMG, Bianchi M de LP. Protective effect of bixin on cisplatin-induced genotoxicity in PC12 cells. *Food Chem Toxicol*. 2012; 50(2): 335-340.
16. Gaire BP, Jamarkattel-Pandit N, Lee D, Song J, Kim JY, Park J, et al. Terminalia chebula extract protects OGD-R induced PC12 cell death and inhibits LPS induced microglia activation. *Molecules*. 2013; 18(3): 3529-3542.
17. Pavlica S, Gebhardt R. Protective effects of flavonoids and two metabolites against oxidative stress in neuronal PC12 cells. *Life Sci*. 2010; 86(3-4): 79-86.
18. Li L, Sun HY, Liu W, Zhao HY, Shao ML. Silymarin protects against acrylamide-induced neurotoxicity via Nrf2 signalling in PC12 cells. *Food Chem Toxicol*. 2017; 102: 93-101.
19. Bhatt PC, Pathak S, Kumar V, Panda BP. Attenuation of neurobehavioral and neurochemical abnormalities in animal model of cognitive deficits of Alzheimer's disease by fermented soybean nanonutraceutical. *Inflammopharmacology*. 2018; 26(1): 105-118.
20. Bhatt PC, Verma A, Al-Abbasi FA, Anwar F, Kumar V, Panda BP. Development of surface-engineered PLGA nanoparticulate-delivery system of Tet1-conjugated nattokinase enzyme for inhibition of A $\beta$ <sub>40</sub> plaques in Alzheimer's disease. *Int J Nanomedicine*. 2017; 12: 8749-8768.
21. Jiang X, Kumar M, Zhu Y. Protective Effect of hyperforin on  $\beta$  Amyloid protein induced apoptosis in PC12 Cells and colchicine induced alzheimer's disease: an anti-oxidant and anti-inflammatory therapy. *J Oleo Sci*. 2018; 67(11): 1443-1453.
22. Dai Xj, Li N, Yu L, Chen Zy, Hua R, Qin X, et al. Activation of BV2 microglia by lipopolysaccharide triggers an inflammatory reaction in PC12 cell apoptosis through a toll-like receptor 4-dependent pathway. *Cell Stress Chaperones*. 2015; 20(2): 321-331.
23. Park KS, Lim JW, Kim H. Inhibitory mechanism of omega-3 fatty acids in pancreatic inflammation and apoptosis. *Ann N Y Acad Sci*. 2009; 1171: 421-427.
24. Lu S, Lu C, Han Q, Li J, Du Z, Liao L, et al. Adipose-derived mesenchymal stem cells protect PC12 cells from glutamate excitotoxicity-induced apoptosis by upregulation of XIAP through PI3-K/Akt activation. *Toxicology*. 2011; 279(1-3): 189-195.
25. Weintraub S, Wicklund AH, Salmon DP. The neuropsychological profile of Alzheimer disease. *Cold Spring Harb Perspect Med*. 2012; 2(4): a006171.
26. Lee YJ, Han SB, Nam SY, Oh KW, Hong JT. Inflammation and Alzheimer's disease. *Arch Pharm Res*. 2010; 33(10): 1539-1556.
27. Kumar A, Dogra S, Prakash A. Neuroprotective effects of Centella asiatica against intracerebroventricular colchicine-

- induced cognitive impairment and oxidative stress. *Int J Alzheimers Dis.* 2009; 2009: 972178.
28. Nazem A, Sankowski R, Bacher M, Al-Abed Y. Rodent models of neuroinflammation for Alzheimer's disease. *J Neuroinflammation.* 2015; 12: 74.
  29. Nazem A, Sankowski R, Bacher M, Al-Abed Y. Rodent models of neuroinflammation for Alzheimer's disease. Vol. 12, *Journal of Neuroinflammation.* 2015. Repeat of reference 28.
  30. Ahmed T, Gilani AH. Inhibitory effect of curcuminoids on acetylcholinesterase activity and attenuation of scopolamine-induced amnesia may explain medicinal use of turmeric in Alzheimer's disease. *Pharmacol Biochem Behav.* 2009; 91(4): 554-559.
  31. Kumar A, Seghal N, Naidu PS, Padi SS, Goyal R. Colchicines-induced neurotoxicity as an animal model of sporadic dementia of Alzheimer's type. *Pharmacol Rep.* 2007; 59(3): 274-283.
  32. Cheignon C, Tomas M, Bonnefont-Rousselot D, Faller P, Hureau C, Collin F. Oxidative stress and the amyloid beta peptide in Alzheimer's disease. *Redox Biol.* 2018; 14: 450-464.
  33. Nagahara AH, Tuszynski MH. Potential therapeutic uses of BDNF in neurological and psychiatric disorders. *Nat Rev Drug Discov.* 2011; 10(3): 209-219.
  34. Lu B, Nagappan G, Guan X, Nathan PJ, Wren P. BDNF-based synaptic repair as a disease-modifying strategy for neurodegenerative diseases. *Nat Rev Neurosci.* 2013; 14(6): 401-416.
  35. Castrén E, Kojima M. Brain-derived neurotrophic factor in mood disorders and antidepressant treatments. *Neurobiol Dis.* 2017; 97(Pt B): 119-126.
  36. Lu B, Nagappan G, Lu Y. BDNF and synaptic plasticity, cognitive function, and dysfunction. *Handb Exp Pharmacol.* 2015; 220: 223-250.
  37. Chen Z, Zhong C. Oxidative stress in Alzheimer's disease. *Neurosci Bull.* 2014; 30(2): 271-281.
  38. Padurariu M, Ciobica A, Lefter R, Serban IL, Stefanescu C, Chirita R. The oxidative stress hypothesis in Alzheimer's disease. *Psychiatr Danub.* 2013; 25(4): 401-409.
  39. Pfeiffer RF, Wszolek ZK, Ebadi M. *Parkinson's disease.* 2<sup>nd</sup> ed. London: United Kingdom; 2012; 1-1287.
  40. Zhao Y, Zhao B. Oxidative stress and the pathogenesis of Alzheimer's disease. *Oxid Med Cell Longev.* 2013; 2013: 316523.
-

# Anti-Atherosclerotic Effect of Afrocyclamin A against Vascular Smooth Muscle Cells Is Mediated via p38 MAPK Signaling Pathway

Yan Gu, M.M.<sup>1</sup>, Zhanzhan Xiao, B.Sc.<sup>2</sup>, Jianlie Wu, M.M.<sup>3</sup>, Mingjin Guo, M.D.<sup>3</sup>, Ping Lv, B.Sc.<sup>4</sup>, Ning Dou, M.M.<sup>5\*</sup>

1. Department of Vascular Surgery, Tianjin First Center Hospital, Tianjin, China

2. Department of Emergency Services, The Fourth People's Hospital of Jinan City, Jinan, Shandong Province, China

3. Department of Vascular Surgery, The Affiliated Hospital of Qingdao University, Qingdao City, China

4. Department of Hematology, The Fourth People's Hospital of Jinan City, Jinan, Shandong Province, China

5. Department of General Surgery, Shanghai Fourth People's Hospital Affiliated to Tongji University School of Medicine, Shanghai, China

*\*Corresponding Address: Department of General Surgery, Shanghai Fourth People's Hospital Affiliated to Tongji University School of Medicine, Shanghai, 200081, China  
Email: 18991318392@sina.cn*

---

This article published in Cell J (Yakhteh), Vol 23, No 2, 2021, on pages 191-198, corresponding author and corresponding address were changed based on authors' request.

The authors would like to apologies for any inconvenience caused.

---

**Citation:** Gu Y, Xiao Zh, Wu J, Guo M, Lv P, Dou N. Anti-atherosclerotic effect of afrocyclamin a against vascular smooth muscle cells is mediated via p38 MAPK signaling pathway. Cell J. 2021; 23(2): 366. doi: 10.22074/cellj.2021.8128.

This open-access article has been published under the terms of the Creative Commons Attribution Non-Commercial 3.0 (CC BY-NC 3.0)

---